Richard F. Kossik
Philip S. Gschwend
E. Eric Adams

Tracing and Modeling Pollutant Transport in Boston Harbor

Tracing and Modeling
Pollutant Transport
in Boston Harbor

Richard F. Kossik
Philip S. Gschwend
E. Eric Adams

AUTHORS

Richard F. Kossik   MS candidate at time of contribution,
                                   Department of Civil Engineering, MIT

Philip M. Gschwend   Assistant Professor,
                                   Civil Engineering, MIT
                                   Ralph M. Parsons Laboratory

E. Eric Adams   Lecturer,
                                   Department of Civil Engineering, MIT
                                   Ralph M. Parsons Laboratory

RELATED REPORTS

Cafe-1: A Two-dimensional Finite Element Circulation Model.
George C. Christodoulou, et al. MITSG 76-11 116 pp. $5.00.

A User's Manual for "Cafe-2": A Two-Layer Finite Element Circulation
Model. James R. Pagenkopf et al. MITSG 77-6 81 pp. $5.00.

Modeling of Coastal Processes: Circulation, Dispersion and Waves:
Opportunity Brief # 38. MIT Marine Industry Collegium.
MITSG 84-4 18 pp. $4.00.

ABSTRACT

A harmonic finite element circulation model and an Eulerian-Lagrangian transport model have been modified and applied with high spatial resolution to Boston Harbor. The applicability of volatile halogenated organic compounds (VHOC) (present in municipal sewage discharges) as tracers has been examined with the intent of using these compounds to calibrate the transport model. The source function of the chlorinated solvents are too complicated to facilitate their use as tracers. However, the trihalo-methanes, especially bromodichloromethane and chlorodibromomethane, appear well suited to serve as tracers in coastal waters. Model simulations agree well with measurements, and calibrated parameters have physically realistic values, indicating that the models adequately represent the major processes acting in the system. Further validation efforts are therefore recommended. Model calibrations are used to investigate the processes of volatilization and physical mixing in the harbor. Solution of the inverse problem to determine piston velocities and dispersion coefficients is somewhat limited by inadequate calibration data. Calibrated piston velocities for bromodichloromethane and chlorodibromomethane range from 2 to 5 cm/hr, corresponding to stagnant film thicknesses of 80 to 200 µm. These results fall between those found for open ocean sites and small lakes and agree well with empirical relationships based on wind speed. Calibrated dispersion coefficients indicated a harbor flushing time of one to two weeks.
An attempt is made to elucidate volatilization mechanisms acting in the harbor by comparing calibrated piston velocities of two compounds. Due to a lack of calibration data, results are inconclusive. Nevertheless, this technique for investigating the process of volatilization is illustrated and shown to be applicable to complex systems which cannot be studied using traditional methods. Effective use of this method in the future will require synoptic observations in both the intermediate and far fields as well as a detailed knowledge of the source strength.

ACKNOWLEDGMENTS

TABLE OF CONTENTS

LIST OF FIGURES

LIST OF TABLES

Chapter 1

Introduction

1.1 Motivation and Goals

The disposal of municipal and industrial wastes into coastal waters such as Boston Harbor is widespread. Sewage, industrial, and stormwater releases can introduce a large variety of hazardous compounds, infectious microorganisms, suspended solids, and oxygen-consuming organic matter into the surrounding waters. The resulting contamination not only diminishes the ability of the area to support recreational activities such as swimming, boating, and fishing, but may also seriously restrict commercial fishing and have adverse ecological effects.

Fortunately, programs are beginning to be implemented to clean up these coastal waters and better manage and utilize their resources in the future. Such programs involve engineering and management decisions which must ultimately be based on a good understanding of the complex physical, chemical, and biological processes occurring in the region. The application of an accurate mathematical simulation model, coupled with complementary current measurements and tracer experiments, can be used to gain this understanding.

Unfortunately, present predictive techniques regarding the physical mixing of contaminants in coastal waters are generally inadequate. Previous modeling efforts in Boston Harbor, for example, have been limited, to a large extent, by the computational expense of existing models. Morever, calibration of these models is typically based on only sparse current

measurements and small-scale tracer experiments. Hence, our knowledge of the long-term physical transport of contaminants in coastal environments is quite limited. The chemical and biological processes affecting the fate of contaminants released into coastal waters are also poorly understood. Such processes include volatilization across the air-sea interface, interaction with particulate matter, and biologically and chemically mediated degradation and removal. Although these processes have been studied in the laboratory, the extrapolation of this information to the coastal environment is oftentimes difficult.

In light of the above, there has been ongoing research at MIT into 1) the development, application, and validation of cost-effective, yet accurate, mathematical models for simulating circulation and pollutant transport in tidal embayments such as Boston Harbor, and 2) the description and quantification of the chemical and biological processes affecting the fate of chemicals in aquatic environments. The present work is multidisciplinary in nature and contributes to both of these efforts. It represents the initial steps of a model calibration and verification study. The immediate goals of this work were to use a combined measurement/modeling approach in Boston Harbor to: 1) validate newly developed mathematical simulation models, 2) begin to quantitatively evaluate large-scale (kilometers) pollutant transport in the region, and 3) specifically investigate the process of volatilization in the harbor. The ultimate goal of this study is to combine hydrodynamic circulation and transport modeling with complementary current velocity measurements and large-scale tracer experiments in order to develop a flexible modeling framework which can be used as an efficient predictive tool for coastal zone management.

1.2 Specific Objectives

Based on these general goals, the present work had the following specific objectives: 1) identify and quantify a number of halogenated hydrocarbons in municipal sewage effluent in order to assess the suitability of these compounds as large-scale tracers of sewage-related contamination; 2) determine the spatial distribution of concentration of these tracers in Boston Harbor during different seasons and use this information to qualitatively evaluate pollutant transport in the region; 3) modify previously developed mathematical circulation and transport models and apply them to Boston Harbor in order to predict two-dimensional contaminant concentrations; 4) calibrate predicted concentrations to observed tracer concentrations in the harbor in order to evaluate the predictive capablilities of the models and quantitatively investigate pollutant transport in the region; 5) utilize the previous results to evaluate the usefulness of the chosen compounds as tracers; and 6) use the results of the tracer experiments and the model calibrations to determine the volatilization rates and mechanisms operating in this coastal region. Through the successful completion of these tasks, we will not only develop the basis on which to predict the physical mixing of chemicals introduced at any point throughout the region, but will also gain a better understanding of an important process, volatilization.

1.3 Overview

Each of these topics is treated at various levels of detail in the following chapters. Due to the multidisciplinary nature of this work, an

effort has been made to present the material at a level that can be followed by chemists and modelers alike.

Chapter 2 provides the necessary background information regarding the chemical aspects of the study. This includes both a discussion of the chemistry of the tracers and a brief presentation of chemical volatilization theory. Chapter 3 describes the mathematical models that were used to simulate circulation and pollutant transport in the harbor. Chapter 4 presents the results of tracer measurements in the effluent and the harbor, from which some qualitative information regarding harbor mixing is inferred. Chapter 5 describes the application of the mathematical models to Boston Harbor. Calibration of the models to measurements is described in Chapter 6, and the results are discussed. Finally, Chapter 7 presents the conclusions of our study and identifies areas for future work and improvements.

Chapter 2

Chemical Aspects of the Tracers

The physical mixing of natural waters and the concurrent volatiliza-
tion mechanisms affecting the fate of many chemicals discharged into these
waters can be extremely complex. This is particularly the case in hydrody-
namically complex coastal waters such as Boston Harbor. The present work
utilized a chemical tracer study to gain valuable insights into both of
these processes. Tracers were used to study both large-scale mixing in the
region and the process of volatilization across the air-water interface.
This was accomplished by calibrating a mathematical model to tracer mea-
surements made in the region. The physical mixing and volatilization
processes acting in the region were then evaluated based on the calibrated
values of the model parameters representing these processes. This chapter
presents the necessary background information regarding the chemistry of
the tracers that were used in this study. It also addresses the topic of
volatilization, and how one can use tracers to study this process.

2.1 Choice of Tracer

Chemical tracers have been used for some time to study water movements
and mixing characteristics of inland and coastal waters (Stewart et al.,
1971; Huang, 1971; Bowden and Lewis, 1973; Murthy, 1974). A great deal of
knowledge regarding the advective and dispersive processes acting in a
system can be inferred from the results of a tracer experiment. Such
experiments consist essentially of determining the concentration of a trac-
er at its source(s), subsequently observing the tracer at a number of loca-

tions throughout the water body, and finally deducing the flow field and dispersion characteristics necessary to explain the spatial and temporal tracer distribution patterns. Tracer experiments have also been used to some extent to investigate volatilization rates in natural water bodies (e.g., Broecker and Peng, 1974; Emerson, 1975; Schwarzenbach et al., 1979; Hesslein et al., 1980; Duran and Hemond, 1984). These studies have used either a mass balance approach or have made inferences from isotopic fractionation in order to quantify volatilization rates, and have been typically restricted to simple lakes, streams, or open ocean systems.

Tracer experiments can utilize either continuous or instantaneous sources and can be based on natural (e.g., CO_2), artifically introduced (e.g., dye), or ongoing (continuous) anthropogenic (e.g., industrial and municipal discharges) inputs. Continuous input experiments are better suited to study long-term, large-scale phenomena. Morevoer, effective natural tracers are inadequate for most applications and artificially introduced tracers are constrained by cost and practicality (especially for large-scale continuous experiments), as well as environmental acceptabilty (e.g., radioactive tracers). In light of these considerations, we chose to utilize existing anthropogenic inputs for our tracer experiments.

A good chemical tracer must satisfy three criteria: 1) it should have an understandable source function; 2) it should be readily measurable without background interferences after dilution to levels several orders of magnitude below its source concentration; and 3) it should be physically, chemically, and biologically conservative or at worst transform or react in an easily predictable manner (Helz, 1980). Based on a consideration of

these criteria, as well as the fact that we were interested not only in tracing large-scale water movement, but also in simultaneously studying the volatilizaton process, a suite of low-molecular-weight halogenated hydrocarbons appeared well suited to serve as our tracers.

The compounds that we chose belong to a group of chemicals known as the volatile halogenated organic compounds (VHOC). These compounds, along with some of their physiochemical properties, are listed in Table 2.1. The sources of these compounds will be discussed in Section 2.2. Primarily due to the recent interest in a subclass of these compounds (the trihalomethanes), the available analytical methods have become highly developed. For example, Dyrssen and Fogelquist (1981), using gas chromatography with electron capture detection, were able to achieve part-per-trillion detection limits with a relatively quick and simple analytical technique.

The VHOCs are not conservative tracers. Nevertheless, they do not exhibit a strong tendency to sorb to particulate matter (Helz and Hsu, 1978) and are essentially chemically and biologically inert over time scales of interest (NAS, 1978). The mechanism primarily responsible for their removal from natural waters is volatilization. The process of volatilization is well studied and a good deal of literature exists on the subject (Section 2.4). Therefore, the nonconservative behavior of these compounds does not pose any serious difficulties. In fact, one may be able to use this nonconservative behavior advantageously to 1) infer something about the mixing characteristics of the system; and 2) simultaneously elucidate information regarding volatilization mechanisms and reaeration rates. This will be expanded upon in Section 2.3.

Table 2.1

Physiochemical Properties of Selected Tracers

Compound	Formula	MW	BP[a] (°C)	solu-bility[b,c,d] (mol/L)	vapor press.[b,e] (atm)
1,1,1-trichloroethane	CH_3CCl_3	133.41	74.1	$10^{-2.07}$	$10^{-0.78}$
tetrachloroethylene	$CCl_2=CCl_2$	165.83	121.0	$10^{-3.04}$	$10^{-1.60}$
trichloroethylene	$CHCl=CCl_2$	131.39	87	$10^{-2.04}$	$10^{-1.01}$
carbon tetrachloride	CCl_4	153.82	76.54	$10^{-2.20}$	$10^{-0.82}$
chloroform	$CHCl_3$	119.38	61.7	$10^{-1.19}$	$10^{-0.59}$
bromodichloromethane	$CHBrCl_2$	163.83	90	$10^{-1.52}$	$10^{-1.20}$
chlorodibromomethane	$CHBr_2Cl$	208.29	120	$10^{-1.65}$	$10^{-1.59}$
bromoform	$CHBr_3$	252.75	149.5	$10^{-1.91}$	$10^{-2.13}$

a Weast (1975)
b at 25°C
c distilled water values shown for sake of compound-to-compound comparison; ionic strength effect should be approximately the same for all compounds (Hunter-Smith et al., 1983)
d from Weast (1975), Mackay and Shiu (1981), or estimated from K_{ow} according to Hansch and Leo (1979) and Chiou and Freed (1977)
e from Weast (1975) or estimated from solubility and Henry's Law constant (Nicholson et al., 1984)

2.2 Sources of VHOCs

There are four major pathways by which VHOCs can enter coastal waters. These are : 1) atmospheric transfer; 2) in situ biosynthesis; 3) industrial and municipal discharge; and 4) accidental spills (Helz and Hsu, 1978). Although atmospheric transfer (e.g., Liss and Slater, 1974) and biosynthesis (e.g., Gschwend et al., 1985) have been demonstrated for some compounds, Helz and Hsu (1978) conclude that these are of minor importance in coastal waters compared to municipal and industrial discharges. Likewise, it is reasonable to assume that accidental spills will only have temporary local effects. On the other hand, the effects of non-point sources such as groundwater leaching of hazardous waste sites has not been sufficiently investigated to determine whether or not this source is negligible. Certainly such a source could have a prominent local effect. Helz (1980) concluded that the major municipal and industrial sources would be sewage treatment plants, waste heat discharges, and major chemical manufacturers, shippers, and users.

It is convenient to divide the compounds in Table 2.1 into two groups, based on their major sources. These two groups are the "solvents" and the "trihalomethanes" (THM). The solvents include tetrachloroethylene, trichloroethylene, 1,1,1-trichloroethane, and carbon tetrachloride. The trihalomethanes include chlorodibromomethane, bromodichloromethane, and bromoform. Chloroform is a member of both groups.

The solvents are compounds used in such activities as degreasing, dry cleaning, stain removal, and as media for chemical processes. Table 2.2 details some of the uses of each of the solvents. These compounds are

Table 2.2

Uses and Ultimate Sources of Selected Solvents

Compound	Applications
1,1,1-trichloroethane	degreasing agent; dry cleaning agent; propellant
trichloroethylene	degreasing agent; dry cleaning agent; solvent; heat exchange liquid; fumigant; organic reagent; anesthetic
tetrachloroethylene	dry cleaning agent; degreasing agent; chemical reagent and intermediate; heat exchange liquid; solvent
carbon tetrachloride	all-purpose solvent; dry cleaning agent; fumigant; drying agent; extractant; degreasing agent
chloroform	all purpose solvent; chemical reagent; insecticide

(from Verschueren, 1977; and Sittig, 1979)

released into the environment in large quantities primarily through munici-
pal sewage discharges and local industrial outfalls. Estimated production
and release rates are presented in Table 2.3 and Table 2.4 to illustrate
the order of magnitude of the quantities involved.

The trihalomethanes have a quite different source history. These
compounds are primarily the products of reactions between chlorine and
naturally occuring organic material. That is, they result from the chlori-
nation of discharge water. The reactions leading to the formation of the
trihalomethanes are illustrated in Figure 2.1. Rook (1974, 1975) first
reported on the occurrence of these compounds in chlorinated water
supplies. Since then there has been a plethora of literature on the
subject (e.g., Jolley, 1978; Jolley et al., 1978; Jolley et al., 1980;
Jolley et al., 1983).

Various formation mechanisms have been suggested (e.g., Rook, 1977;
Morris and Baum, 1978; Gurol et al., 1983). However, due to the complexity
of the organic precursors and the variety of reaction pathways, the chemis-
try of the trihalomethane reaction is not completely understood. Neverthe-
less, it has been demonstrated (Kavanaugh et al., 1978) that the reaction
is strongly dependent on, among other things, both the chlorine dosage and
the total organic carbon loading. Furthermore, it has been noted that the
relative abundances of the bromo-substituted THMs to the chloro-substituted
THMs is a direct function of salinity. That is, chlorination of freshwater
results in a THM distribution favoring chloro-substituted compounds while
chlorination of seawater results almost exclusively in the production of
bromoform (e.g., Helz and Hsu, 1978; Minear and Bird, 1980; Oliver, 1980).

Table 2.3

Estimated World Production Capacities
of Selected Solvents (1973)

Compound	Production capacity $(10^6$ lbs/yr)
tetrachloroethylene	2315
trichloroethylene	2227
1,1,1-trichloroethane	1058
chloroform	540
carbon tetrachloride	2205

(from Pearson and McConnell, 1975)

Table 2.4

Estimated U.S. Release Rates
of Selected Solvents (1975)

Compound	Release rate $(10^6$ lbs/yr)
tetrachloroethylene	388
trichloroethylene	430
1,1,1-trichloroethane	274
chloroform	168
carbon tetrachloride	105

(from Nelson and Van Duuren, 1975)

$$Cl_2 + H_2O \longrightarrow HOCl + H^+ + Cl^-$$

(HYDROLYSIS OF CHLORINE)

$$HOCl + Br^- \longrightarrow HOBr + Cl^-$$

(FORMATION OF OXIDIZING BROMINE)

ORGANIC
PRECURSOR

+

3 HOCl
2 HOCl + HOBr
HOCl + 2 HOBr
3 HOBr

$\longrightarrow$

$CHCl_3$
$CHCl_2Br$
$CHClBr_2$
$CHBr_3$

+ BYPRODUCTS
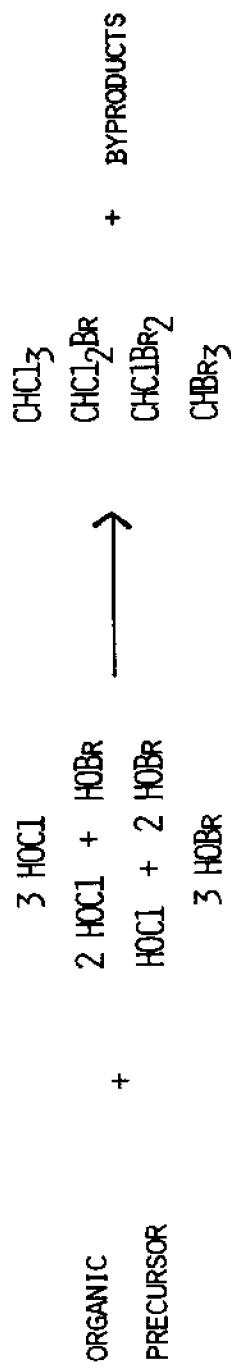
(TRIHALOMETHANE REACTION)

Figure 2.1   Reactions Leading to the Formation of Trihalomethanes

This is a result of the fact that: 1) oxidizing chlorine is converted quickly to oxidizing bromine in the presence of bromide ion (Morris, 1978) and 2) chlorine is preferentially consumed in reactions involving ammonia, organic amines, and amino acids (Rook, 1974; Helz and Hsu, 1978). The kinetics of the THM reaction will be discussed in Chapter 4.

In contrast to the solvents, the THMs are introduced into a discharge system just prior to release. (A small amount of these compounds would also be expected to be present in a sewage system prior to chlorination as a result of the chlorination of drinking water. This, however, is probably small compared to the quantities created upon chlorination at the sewage treatment plant.) As a result, the primary sources of THMs to surface waters are: a) chlorinated sewage discharges, and b) waste heat discharges, in which cooling water is chlorinated to control biofouling.

Hence, we have reason to believe that both the solvents and the tri-halomethanes should be quite common in coastal regions near population centers. Table 2.5 documents the widespread presence of these VHOCs in surface waters near populated regions. However, as pointed out by Helz (1980), it remains to be seen whether the sources of these compounds to a system such as Boston Harbor are sufficiently characterizable in terms of both location and strength to facilitate the use of these VHOCs as chemical tracers.

2.3 Advantages of Using Multiple Tracers

VHOCs volatilize at different rates due to their differing physiochem-ical properties. This can be readily seen in Table 2.6. By using the

Table 2.5

Occurrence of Chosen Tracers in Surface Waters
Near Industrial Sites

Compound	frequency* (%)
trichloroethylene	43
tetrachloroethylene	38
1,1,1-trichloroethane	9
carbon tetrachloride	3
chloroform	87
bromodichloromethane	12
chlorodibromomethane	5
bromoform	3

(from Ewing et al., 1977)

*204 samples collected

Table 2.6

Volatilization Half-Lives Assuming 5 m Mean Depth
as Determined Using Stirred Laboratory Beakers

Compound	Half-life (in hours)
trichloroethylene	30
tetrachloroethylene	34
1,1,1-trichloroethane	30
carbon tetrachloride	33
chloroform	30
bromodichloromethane	39
chlorodibromomethane	51
bromoform	85

(from Helz and Hsu, 1978)

VHOCs as multiple non-conservative tracers, each with unique volatilization removal rates, we may be able to discern system mixing and/or quantify their water-air exchange rates. Such an approach consists of observing two or more tracers simultaneously and taking advantage of the fact that they are subjected to the same advective and dispersive processes. Helz (1980) first illustrated this using the following simple example. Suppose the rate of change with time of the halocarbon distribution within a water parcel can be represented as:

$$\frac{dC}{dt} = -\frac{k}{L}C - D'(t)C \qquad (2.3.1)$$

where C   is concentration (mol/m^3)

   t   is time (sec)

   k   is a volatilization constant (m/sec)

   L   is water mixing depth (m)

   $D'(t)$ is the instantaneous dilution rate (1/sec)

Assuming at $t = 0$ the water parcel contains a concentration of C_A^0, then equation (2.3.1) can be integrated to give

$$\ln(C_A/C_A^0) = -k_A \frac{t}{L} - D(t) \qquad (2.3.2)$$

where $D(t)$ is a dilution function (dimensionless). Repeating the same procedure for halocarbon B with rate constant k_B results in

$$\ln(C_B/C_B^0) = -k_B \frac{t}{L} - D(t) \qquad (2.3.3)$$

Since mixing must affect both compounds identically, we can eliminate $D(t)$ between the two equations, resulting in the following expression:

$$\ln(C_A/C_B) = \ln(C_A^o/C_B^o) - (k_A - k_B)\frac{t}{L} \qquad (2.3.4)$$

Thus, if C_A, C_B, C_A^o, and C_B^o can be measured and k_A and k_B can be determined theoretically, then $\frac{t}{L}$ can be computed. This quantity can then be used in equation (2.3.3) to determine $D(t)$. In this way the dilution function could be mapped. If the mixing depth, L, is known, the age of the water parcel, t, could also be computed. On the other hand, if $\frac{t}{L}$ could be determined independently (i.e., if the flow system was very simple), the difference $k_A - k_B$ could be obtained and this could be used to infer information regarding volatilization. As pointed out by Helz (1980), such an approach is not possible using conservative tracers.

Unfortunately, this simple approach cannot be applied to a system as hydrodynamically complex as Boston Harbor. In such a system it is difficult to separate the effect of mixing from the effect of decay (e.g., volatilization) on the concentration distribution. Hence, a one-dimensional equation as simple as (2.3.1) does not adequately represent the physics of the highly complex multi-dimensional system. (In particular, equation (2.3.1) assumes mixing with "clean" water, a situation that does not apply to our system.) Nevertheless, a more complex model can be used to represent the hydrodynamics, and measurements of multiple nonconservative tracers can then be used to elucidate information that is otherwise difficult to obtain.

In the present work, by calibrating a mathematical model to simultaneous measurements of a number of VHOCs discharged from the same source(s), one can infer a volatilization rate for each compund. By comparing the calibrated volatilization rates for a number of compounds, it may be possible to elucidate the mechanisms of volatilization in the harbor. Such information would improve our ability to predict volatilization rates for dissolved gases such as oxygen, as well as other pollutants of interest. The remaining three sections of this chapter deal specifically with the process of volatilization, and discuss in detail how we can make use of the VHOCs to investigate the mechanism of this important transport process.

2.4 Volatilization

Volatilization is an important environmental pathway for many compounds of interest. For the chlorinated solvents and haloforms in this study, volatilization is the dominant loss mechanism.

The transport of a compound from water across the air-water interface into the atmosphere is a very complex process, depending both on environmental conditions and physiochemical properties of the compound. The modeler would like to apply a quantitative expression in which the rate of chemical transfer across an air-water interface is a function of a few easily measurable or estimated environmental and physiochemical parameters. Unfortunately, despite a long history of interest in the subject, no completely reliable theory yet exists (Broecker and Peng, 1984).

Nevertheless, a number of empirical relationships have been developed (e.g., Wolff and van der Heijde, 1982; Mackay and Yeun, 1983) which are useful for general modeling purposes and contain the dominant determinants of the volatilization rate. Brutsaert and Jirka (1984) provide an excellent review of the volatilization process. What follows is a brief overview of the most commonly used and accepted models along with some general experimental observations.

All of the common models use the piston velocity concept. This arises from the assumption that the concentration of the chemical in the upper few molecular layers of the water is equal to the partial pressure of the gas in the overlying air divided by the compound's Henry's Law constant (Broecker and Peng, 1984). The ratio between the net flux and the concentration difference between the upper few molecular layers and the bulk fluid has the dimensions of a velocity:

$$k_L = F/(C_L - C_S) \qquad (2.4.1)$$

where k_L is a piston velocity (m/sec)

$\quad$ F is the net flux (mol/m^2·sec)

$\quad$ C_S is the concentration in the upper few molecular layers of water (mol/m^3)

$\quad$ C_L is the bulk water concentration (mol/m^3)

The oldest, simplest, and most common model for chemical exchange across the air-water interface is the stagnant film model (Lewis and

Whitman, 1924; Liss and Slater, 1974). This model assumes that the bulk regions of the two fluid phases are homogeneously mixed while interfacial transport is hindered by the presence of a laminar boundary layer on each side of the interface (Figure 2.2a). Transport through these interfaces is by molecular diffusion. This leads to the following formulation:

$$F = k \ (C_L - P/H) \tag{2.4.2}$$

where

$$k = \left[\frac{1}{k_L} + \frac{RT}{Hk_G}\right]^{-1} \tag{2.4.3}$$

and

$$k_L = \frac{D_L}{Z_L} \tag{2.4.4}$$

$$k_G = \frac{D_G}{Z_G} \tag{2.4.5}$$

where k   is the overall piston velocity (m/sec)

k_L is the liquid film piston velocity (m/sec)

k_G is the gas film piston velocity (m/sec)

D_L is the chemical diffusivity in water (m^2/sec)

D_G is the chemical diffusivity in air (m^2/sec)

Z_L is the thickness of the water boundary layer (m)

Z_G is the thickness of the air boundary layer (m)

F   is the mass flux (mol/m^2·sec)

(A) STAGNANT BOUNDARY LAYER MODEL
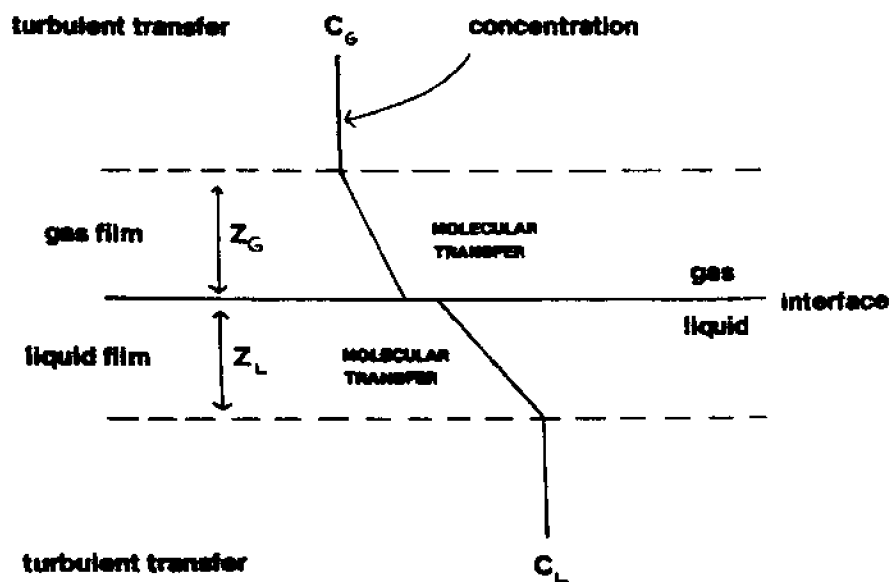
(B) SURFACE RENEWAL MODEL
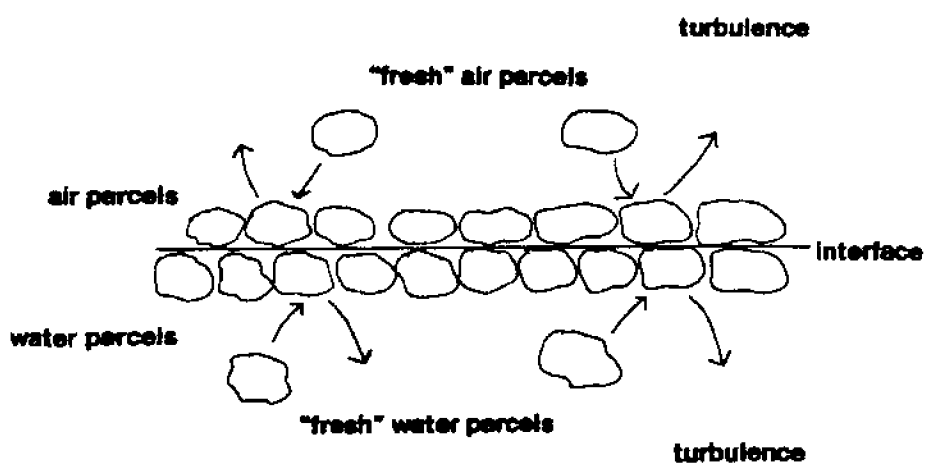
Figure 2.2 Two Simple Models for Chemical Exchange Across the Air-Water Interface

C_L is the bulk water concentration (mol/m^3)

P is the partial pressure of the gas in air (atm)

H is the Henry's Law constant $(atm \cdot m^3/mol)$

T is the temperature $(^\circ K)$

R is the gas constant $(m^3 \cdot atm/mol \cdot {}^\circ K)$

Z_L and Z_G will, in general, be functions of the turbulence level as deter-
mined by water currents and wind. Obviously, this simple model with its
sharp discontinuities and uniform boundary layers is physically unrealis-
tic. Nevertheless, the film model is quite useful for visualizing gas
exchange and greatly simplifies calculations. Its formulation embodies
both chemical and environmental factors, and considers both air-side and
water-side resistance to mass transfer. Furthermore, predictions of chemi-
cal exchange rates using the film model are comparable to those found using
more complex models (Liss and Slater, 1974).

Another commonly accepted model is the surface renewal model (Higbie,
1935; Danckwerts, 1970). This model assumes that parcels of water at the
air-water interface (or parcels of air on the other side of the boundary)
are periodically replaced from below (or above) by fresh parcels. These
parcels then exchange volatile substances by molecular diffusion through
the interface until they are in turn replaced (Figure 2.2b). This replace-
ment of fluid at the surface by fresh water or air from the bulk is brought
about by turbulent motions. This treatment results in an expession for k_L
and k_G of the form:

$$k_L = R_L (D_L)^{\frac{1}{2}} \qquad\qquad (2.4.6)$$

$$k_G = R_G(D_G)^{\frac{1}{2}} \qquad\qquad (2.4.7)$$

where R_L and R_G are related to the rate of renewal of the fluid parcels (i.e., a function of the turbulence).

Both the stagnant film model and the surface renewal model can be written in the form:

$$k = AD^n \qquad\qquad (2.4.8)$$

where D is a molecular diffusivity (m^2/sec)

     k is a piston velocity (m/sec)

     A is an environmental parameter

     n = 1 for film model or n = ½ for surface renewal

Other models have been proposed that show different diffusivity dependencies. For example, Witting (1971) and Deacon (1977) have each proposed different models that predict that k should vary as $D^{2/3}$. O'Connor (1984) has presented a resistance-in-series model that incorporates both film and surface renewal theory. For a smooth water surface, laboratory experiments (e.g., Ledwell, 1982; Jahne et al., 1984a;) tend to suggest a value of n ranging from 0.4 to 0.7. In any case, from a practical point of view, knowledge of the exact dependency of k on D is not essential. Although it is of scientific interest, the uncertainty in the value of n is not going to drastically affect predictions. Furthermore, the proposed models describe mass transfer through a smooth surface, a condition generally not

found in the environment. Hence, the uncertainty in the value of A in equation (2.4.8) is much more important than the uncertainty in the value of n for predicting k.

It is therefore necessary to focus on the functionality of the environmental parameter A. Wind/wave-tunnel experiments show a strong wind-speed dependence of the mass exchange rate. However, oceanic field data do not necessarily verify this effect (Hasse and Liss, 1980). It is very difficult to extrapolate laboratory results to natural systems since the decisive environmental parameters have not yet been fully elucidated. This is illustrated in Figure 2.3, which shows results from recent wind/wave tunnel experiments (Broecker et al., 1978; Jahne et al., 1979; Liss et al., 1981; Merlivat and Memery, 1983; Jahne et al., 1984a). Piston velocities are plotted versus wind-derived friction velocity. The line represents predictions for a smooth water surface. The corresponding lab data in which a smooth water surface was present agree well with theory (Deacon, 1977). The remaining data points (falling well above the line) represent observations in the presence of water surface waves. From the figure, we can conclude: 1) the piston velocity is considerably enhanced in the presence of surface waves; 2) both in the smooth surface regime and the surface wave regime, the piston velocity is approximately proportional to the friction velocity; and 3) in the surface wave regime, the scatter around a straight line drawn through the points is much greater than in the case of the smooth surface regime (i.e., different piston velocities are observed at the same friction velocity). This implies that although k is strongly dependent on the friction velocity, it also has a secondary dependence on the wave environment. It is unclear how to correlate this secondary depen-
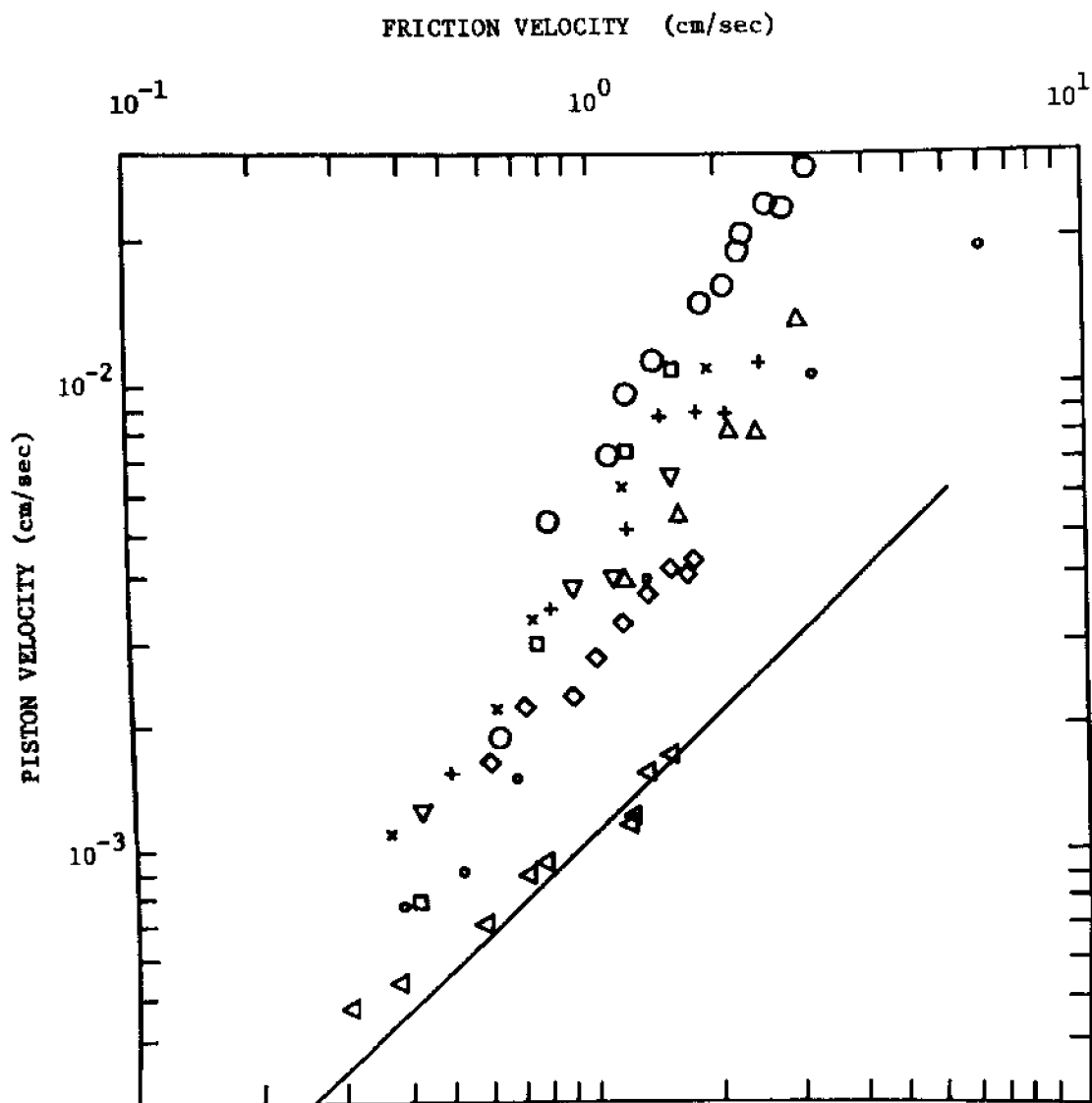
Figure 2.3 Summary of Recent Wind Tunnel Volatilization Experiments:
□ , Liss et al., 1981; + , Merlivat and Memery, 1983; ◇ and ○ ,
Broecker et al., 1978; remaining symbols, Jahne et al., 1984a (piston
velocities normalized to Schmidt Number of 600)

dence with an easily measurable environmental parameter. Nevertheless, it appears that a simple model in which k is proportional to friction velocity contains at least the major determinants of the volatilizaton rate *for low-to-moderate windspeeds* (up to ~10 m/s).

It is generally observed that at a critical wind speed, the piston velocity increases abruptly and above this critical value, appears to increase approximately quadratically with windspeed (Kanwisher, 1963; Liss, 1973; Merlivat and Memery, 1983). Various mechanisms have been proposed to account for this phenomenon (Hasse and Liss, 1980). It is commonly suggested that this enhanced chemical flux at higher windspeeds is a result of bubble entrainment by breaking waves (e.g., Kanwisher, 1963; Kerman, 1984; Broecker and Siems, 1984; Memery and Merlivat, 1984). Laboratory studies have shown that bubbles from breaking waves can lead to increased piston velocities (Merlivat and Memery, 1983; Broecker and Siems, 1984). It is also commonly accepted that gas bubbles of different sizes are present in the oceans at depths down to at least 40 m, and in the coastal region the main source of these bubbles is breaking waves (Blanchard and Woodcock, 1957; Kolovayev, 1976; Medwin, 1977; Johnson and Cooke, 1979).

Monahan and Spillane (1984) have pointed out that there is a significant correlation between piston velocites in the North Atlantic and whitecap cover. They present a model in which whitecaps act as low impedance vents punched through the laminar surface layer. This would result in a reduction of the effective boundary layer thickness. In this respect, this model can be seen as a modification of a film model.

An alternative and intuitively more appealing bubble injection model perceives the bubbles not only as stirring devices, but also as gas transport elements. That is, a bubble is entrained in the water column, reaches equilibrium (or near equilibrium) with the dissolved species, is transported back to the surface, and releases its modified gaseous load to the atmosphere (Kanwisher, 1963; Memery and Merlivat, 1984; Broecker and Siems, 1984; Kerman, 1984). Memery and Merlivat (1984) and Jahne et al. (1984b) have proposed detailed theoretical models to compute gas transfer with bubbles acting as transport elements. They conclude that the solubility of the gas plays an important role in determining the contribution of bubble injection to gas transfer. We present below a very simple bubble injection model which contains the dominant determinants of gas transfer via bubbles (e.g., the solubility effect observed with more complex models), while still retaining analytical simplicity.

2.5 A Simple Bubble Injection Model

We will assume that the total mass transfer rate is a combination of both mass transfer through a water surface and mass transfer via bubbles:

$$k = k_F + k_B \qquad\qquad (2.5.1)$$

where k is the total piston velocity

k_F is the piston velocity for traditional film models

k_B is the bubble injection piston velocity

Consider first a single bubble of surface area S_B which has a residence time of t_r in the water column. While submerged, a chemical may diffuse from the water across a bubble boundary layer into the bubble. When the bubble returns to the surface, it releases all of its internal gases to the atmosphere. We will make the following assumptions: 1) the water column is well mixed and the concentration of the compound of concern is at steady state in the water; and 2) during the bubble's lifetime, its radius does not change due to hydrostatic pressure or significant dissolution of its contents (primarily N_2 and O_2).

Assuming stagnant film theory, the mass flux of an individual chemical into the bubble can be described as:

$$\frac{dn_B}{dt} = \frac{DS_B}{Z_B}(C_L - P_B/H) \tag{2.5.2}$$

where n_B is the mass of chemical in the bubble (mol)

D is chemical diffusivity in water (m^2/sec)

S_B is the surface area of the bubble (m^2)

Z_B is the water-side bubble boundary layer thickness (m)

C_L is the constant bulk water concentration (mol/m^3)

H is Henry's Law constant (atm·m^3/mol)

P_B is the partial pressure of the gas inside the bubble (a function of the age of the bubble) (atm)

The flux is water-side controlled because the stagnant film thickness on the air side of the bubble is on the same order as the size of a bubble.

Assuming the ideal gas law,

$$P_B = n_B RT / V_B \qquad (2.5.3)$$

where V_B is the volume of the bubble (m^3)

R is the gas constant ($m^3 \cdot atm/mol \cdot °K$)

T is the temperature ($°K$)

We can substitute (2.5.3) into (2.5.2) to obtain

$$\frac{dn_B}{dt} = \frac{DS_B}{Z_B}\left[C_L - \frac{RT}{HV_B}n_B\right] \qquad (2.5.4)$$

Equation (2.5.4) can be solved with the initial condition

$$n_B = \frac{P_g^o V_B}{RT} \quad \text{at } t = 0 \qquad (2.5.5)$$

where P_g^o is the initial partial pressure in the bubble (i.e., atmospheric partial pressure) and $t = 0$ corresponds to the birth of the bubble.

The solution is:

$$n_B = \frac{V_B}{RT}[HC_L + (P_g^o - HC_L)e^{-wt}] \qquad (2.5.6)$$

where $w = \dfrac{RTDS_B}{HZ_B V_B} \qquad (2.5.7)$

-42-

n_B is the number of moles of gas in the bubble when the bubble is t seconds old (as $t \to \infty$, equilibrium is reached and $n_B = V_B H C_L / RT$).

Assuming all of the bubbles injected are the same size and G is the number of bubbles injected per unit area of sea surface per unit time, the effective mass flux due to bubble injection is

$$F = n_B G \qquad (2.5.8)$$

where F is the mass flux ($mol/m^2 \cdot sec$).

Substituting (2.5.6) into (2.5.8) we find:

$$F = \frac{G V_B}{RT}[HC_L + (P_g^o - HC_L)e^{-wt}] \qquad (2.5.9)$$

Finally, defining the bubble injection piston velocity as in equation (2.4.1) and assuming spherical bubbles of radius r_B results in the following expression:

$$k_B = \left[\frac{G V_B}{RT}\right] \frac{HC_L + (P_g^o - HC_L)\exp\left[\frac{-3RTDt}{HZ_B r_B}\right]}{(C_L - P_g^o/H)} \qquad (2.5.10)$$

As can be seen, as opposed to gas transfer through a surface film, for gas transfer via bubble injection, the piston velocity is not, in general, independent of the concentration gradient because bubbles come appreciably near Henry's Law equilibrum with the water.

We can make several more assumptions that further simplify equation (2.5.10). For organic contaminants, it is generally quite reasonable to assume that $C_L \gg P_g^0/H$. This results in:

$$k_B = \frac{GV_B H}{RT}\left[1 - \exp\left[\frac{-3RTDt}{HZ_B r_B}\right]\right]$$ (2.5.11)

Defining Q as the fractional approach to equilibrium.

$$Q = 1 - \exp\left[\frac{-3RTDt}{HZ_B r_B}\right]$$ (2.5.12)

(2.5.11) reduces to:

$$k_B = \frac{GV_B HQ}{RT}$$ (2.5.13)

Defining $E = GV_B$, where E is the volume of bubbles injected per unit surface area per unit time and replacing H by the dimensionless Henry's Law constant H' (H' = H/RT), (2.5.13) becomes

$$k_B = EQH'$$ (2.5.14)

Whether or not the bubble reaches equilibrium (i.e., Q approaches 1) with respect to a given compound depends primarily on the size, boundary layer thickness, and residence time of the bubble, as well as the chemical's diffusivity and Henry's Law constant. A typical bubble residence time can be computed using Stoke's Law (which should be considered a mini-

mum since bubbles can be trapped temporarily by the breaking wave). Assuming a typical bubble radius of 150 μm (Broecker and Siems, 1984) and a bubble injection depth of approximately one wave height (Hsu et al., 1984), say 50 cm, a characteristic residence time of about 2.4 seconds is calculated. The fractional approach to equilibrium under these conditions for our particular tracers can be calculated by assuming a stagnant film thickness of about 100 μm (Wolff and van der Heijde, 1982) and using values of D and H from Table 2.7. The results are given in Table 2.8. As can be seen by comparing Tables 2.7 and 2.8, the Henry's Law constant of each compound controls the kinetics, with a small Henry's law constant resulting in a very quick approach to equilibrium. (The larger the Henry's Law constant, the greater the mass of chemical that must diffuse into the bubble to achieve equilibrium.)

We have assumed that the radii of the bubbles remain constant. Bubbles can shrink and dissolve due to pressure increases as a result of hydostatic pressure and surface tension effects. However, the majority of bubbles are probably not injected deep enough to be significantly affected by hydrostatic pressure effects, and surface tension effects will only become important for very small bubbles. It therefore seems reasonable to neglect these effects for the purposes of our simple model. Furthermore, it is an obvious oversimplification to assume that all of the bubbles are the same size. In reality, a spectrum of bubbles is present (e.g., Broecker and Siems, 1984; Hsu et al., 1984) with most of the bubbles being between 100 and 1000 μm in diameter (Blanchard and Woodcock, 1957). However, this fact will simply affect the values of E and Q in (2.5.14), which

Table 2.7

Solution Diffusivities and Henry's Law Constants for Halocarbons

Compound	D^a (cm^2/sec)	H^b $\left[\dfrac{\text{moles/liter air}}{\text{moles/liter water}}\right]$
1,1,1-trichloroethane	1.01×10^{-5}	1.13
trichloroethylene	1.07×10^{-5}	0.36
tetrachloroethylene	0.99×10^{-5}	0.93
bromodichloromethane	1.12×10^{-5}	0.085
chlorodibromomethane	1.11×10^{-5}	0.047
bromoform	1.09×10^{-5}	0.025

a estimated as Hayduck and Laudie (1974)
b values for eqilibrium with distilled water at
   25°C taken from Mackay and Shiu (1981) and Nichloson
   et al. (1984) to show anticipated range in variation
   for equilibrium with seawater

Table 2.8

Fractional Approach to Equilibrium of Selected Tracers
Assuming 2.4 sec Bubble Residence Time*

Compound	Approach to equilibrium (%)
1,1,1-trichloroethane	34.9
trichloroethylene	76.0
tetrachloroethylene	40.0
$CHBrCl_2$	97.4
$CHBr_2Cl$	99.8
$CHBr_3$	>99.9

*bubble radius = 150 μm;
 stagnant film thickness = 100 μm

are only fitting parameters for our model. It should not significantly affect the dependency of k_B on H'.

As a final result, we now rewrite (2.5.1) as

$$k = k_f + EQH' \tag{2.5.15}$$

2.6 Determination of Volatilizaton Mechanisms

One can now evaluate the mechanism of volatilization in the environment by observing the simultaneous volatilization of several compounds. Different compounds will volatilize at different rates according to their physiochemical parameters (namely D and H') and the actual mechanism controlling the volatilization process. For example, based on the surface renewal model, the relative volatilization rate of compound A to compound B can be expressed as

$$\frac{k_A}{k_B} = \left[\frac{D_A}{D_B}\right]^{\frac{1}{2}} \tag{2.6.1}$$

Assuming the film model, the relative volatilization rate of A to B becomes

$$\frac{k_A}{k_B} = \frac{\left[\frac{Z_L}{D_L} + \frac{Z_g}{HD_g}\right]^{-1}_A}{\left[\frac{Z_L}{D_L} + \frac{Z_g}{HD_g}\right]^{-1}_B} \tag{2.6.2}$$

And assuming the bubble injection model (with bubbles acting as transport elements), this ratio can be expressed as

$$\frac{k_A}{k_B} = \frac{H'_A}{H'_B} \frac{Q_A}{Q_B} \qquad\qquad (2.6.3)$$

Hence, if bubble injection is the dominant transfer mechanism, the piston velocities of the various compounds should be closely related to their Henry's Law constants. It is generally true that H' varies widely while D varies over a narrow range between compounds. For the halocarbons, this is particularly the case (see Table 2.7). Thus, bubble injection should result in greater geochemical fractionation (larger difference in volatilization rates). Table 2.9 illustrates this for several halocarbons. Although Model 1 and Model 2 predict relative volatilization rates which are, for all practical purposes, indistinguishable and essentially equal to unity, Model 3 predicts relative volatilization rates significantly greater than one.

Hence, if we obtain estimates of the overall piston velocities for several compounds with different Henry's Law constants, we can compare the results to (2.5.15), where k_f is represented by an empirical surface transfer model (e.g., Mackay and Yeun, 1983). If the observations can be explained entirely by k_f (i.e., $E \approx 0$), then we can conclude for that particular case that either 1) volatilization is controlled by simple surface transfer models and bubbles are unimportant; or 2) if bubble injection is important, the bubbles are primarily acting as mixing devices as opposed to transport devices. On the other hand, if the observations can only be explained by assuming a significant value of E, then bubble injection with bubbles acting as transport elements does play a role, and its relative

Table 2.9

Predicted Relative Volatilization Rates for Representative Halocarbons Based on Three Distinctly Different Air-Water Exchange Models

Relative volatilization ratio of	Model 1 (surface renewal)	Model 2 (stagnant boundary layer)	Model 3* (bubble injection)
$\dfrac{CH_2CCl_2}{CHBr_3}$	0.93	1.12	15.8
$\dfrac{CHBrCl_2}{CHBr_3}$	1.01	1.17	3.4

---

*using values of Q given in Table 2.8

importance is equal to EH'/k_f. This novel approach is only made possible through the use of multiple nonconservative tracers with unique volatilization rates.

Chapter 3

Description of Mathematical Models

The tracer studies which were mentioned in Chapter 2 and will be described in detail in Chapter 4 were complemented by a concurrent modeling study. This chapter presents background information regarding the modeling aspects of this work. After first presenting the general modeling approach, the mathematical models used to simulate pollutant transport in the harbor are described, and some of their advantages and limitations are discussed. The application of these models to Boston Harbor will be presented in Chapter 5.

3.1 General Modeling Approach

The tools utilized to simulate pollutant transport in Boston Harbor consisted essentially of two separate mathematical models which were run in series. The first predicts fluid flow or circulation. That is, if one wants to predict where a contaminant will move when input into a water body, one must first know were the water itself moves. There are alternatives to using a numerical model to produce this advective flow field. These include representing the field by an analytical description (usually a gross simplification such as unidirectional flow) or by interpolating or extrapolating a flow field from observations. However, these alternatives are generally unsatisfactory when dealing with a domain as complex as Boston Harbor.

Once information regarding the advective velocity field has been obtained, one can attempt to simulate the second process, contaminant advection and dispersion. This process represents the transport and mixing of a contaminant within a water body.

The two models used in this research numerically solve equations that mathematically represent the governing conservation laws. These models are known by the acronyms of TEA and ELA. TEA (Tidal Embayment Analysis) simulates water circulation in embayments in which the circulation pattern is predominantly tidally driven. ELA (Eulerian-Langrangian Analysis) uses the results of TEA as input in order to simulate the transport of a contaminant released into the embayment. A simplified computational structure for the TEA/ELA modeling system is shown in Figure 3.1.

Both models were developed at the Ralph Parsons Laboratory for Water Resources and Hydrodynamics at MIT. For a detailed presentation of the models, the reader is referred to Westerink (1984a), Westerink et al. (1984), Westerink et al. (1985), Baptista (1984), Baptista et al. (1984), and Kossik et al. (1986). For the present purposes, a brief description of each model follows.

3.2 Circulation Model (TEA)

TEA is a two-dimensional harmonic finite element circulation model. The finite element method (FEM) facilitates the use of an irregular grid to better represent the complex geometry of many tidal embayments. TEA solves
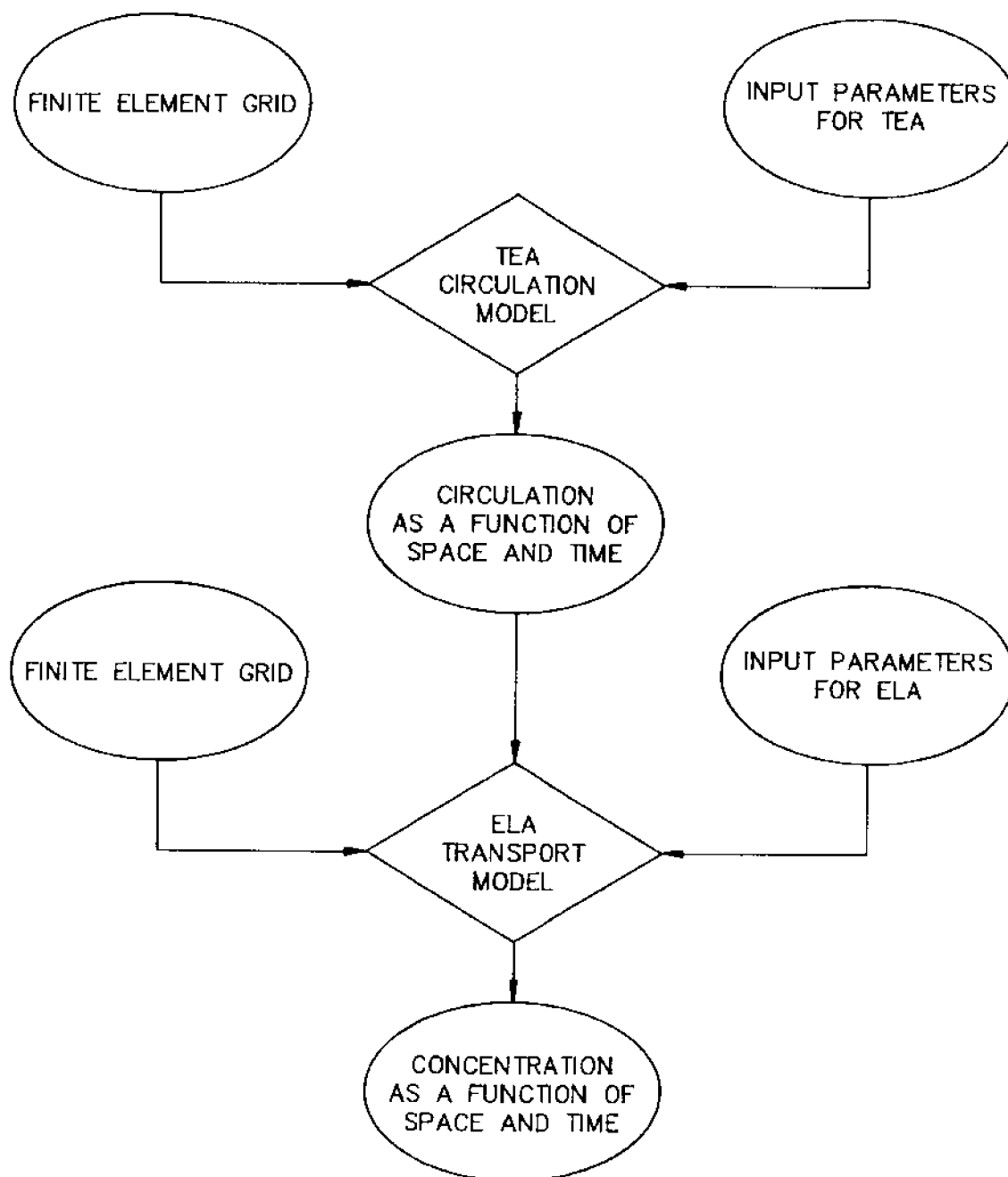
Figure 3.1 Computational structure for TEA/ELA modeling system (diamonds represent computer programs, ovals represent input/output files)

the depth-averaged forms of the Navier-Stokes and continuity equations. These equations are of the form (Dronkers, 1964):

$$\frac{\partial \eta}{\partial t} + \frac{\partial [u(h+\eta)]}{\partial x} + \frac{\partial [v(h+\eta)]}{\partial y} = 0 \qquad (3.2.1)$$

$$\frac{\partial u}{\partial t} + g\frac{\partial \eta}{\partial x} - fv - \tau_x^s/\rho(h+\eta) + \tau_x^b/\rho(h+\eta) + \left[u\frac{\partial u}{\partial x} + v\frac{\partial u}{\partial y}\right] = 0 \qquad (3.2.2)$$

$$\frac{\partial v}{\partial t} + g\frac{\partial \eta}{\partial y} - fu - \tau_y^s/\rho(h+\eta) + \tau_y^b/\rho(h+\eta) + \left[u\frac{\partial v}{\partial x} + v\frac{\partial v}{\partial y}\right] = 0 \qquad (3.2.3)$$

where

$u(x,y,t)$ is the x component of the depth-averaged velocity

$v(x,y,t)$ is the y component of the depth-averaged velocity

$\eta(x,y,t)$ is the surface elevation relative to the mean sea level

h is the mean sea level

ρ is the water density

τ_x^s and τ_y^s are applied surface stresses

τ_x^b and τ_y^b are bottom stresses

g is the gravitational acceleration

f is the Coriolis factor

The boundary conditions associated with these equations are of two types: elevation prescribed and/or normal flux prescribed. Elevation prescribed boundaries are typically open ocean boundaries where tidal forcing exists while flux prescribed boundaries are generally land (zero normal flux) or river (finite normal flux) boundaries.

It is critical to stress the limitations imposed on the model by the assumptions made in deriving the governing equations. Since the equations are depth averaged, strongly stratified estuaries or wind-induced circulation in deep water, which are three-dimensional in nature, cannot be adequately modeled. Also, lateral viscosity has been ignored. Hence, flow separation near land boundaries is not properly modeled. Furthermore, an assumption of constant density has been made which obviously precludes simulation of density-driven currents. Finally, short and intermediate length waves cannot be modeled due to a hydrostatic pressure assumption. Hence, the model should only be applied to well-mixed, tidally dominated coastal embayments.

A somewhat more restrictive assumption is made when the equations are subsequently linearized. This is done by approximating $h + \eta \approx h$, neglecting the convective acceleration terms in the momentum equations, and linearizing bottom friction, yielding the following three linearized equations:

$$\frac{\partial \eta}{\partial t} + \frac{\partial(uh)}{\partial x} + \frac{\partial(vh)}{\partial y} = 0 \qquad (3.2.4)$$

$$\frac{\partial u}{\partial t} + g\frac{\partial \eta}{\partial x} - fv - \frac{1}{\rho h}(\tau_x^s - \tau_x^{b,\ell}) = 0 \qquad (3.2.5)$$

$$\frac{\partial v}{\partial t} + g\frac{\partial \eta}{\partial y} - fu - \frac{1}{\rho h}(\tau_y^s - \tau_y^{b,\ell}) = 0 \qquad (3.2.6)$$

where $\tau_x^{b,\ell}$ and $\tau_y^{b,\ell}$ are linearized bottom stresses.

This procedure can introduce significant error, depending on the magnitude of the nonlinear terms. Open ocean tides can be described accu-

rately by the simple superpositioning of a series of harmonic components since nonlinear effects tend to be neglibigle. In shallow water, however, nonlinear effects can become significant and shallow water tides are generated that play a very important role in producing the residual circulation in a tidal embayment (Westerink et al., 1985). This residual circulation pattern, in turn, determines the flushing efficiency of the embayment (Section 5.3).

TEA does not include these nonlinear terms. A nonlinear version of TEA has been developed, however, that accounts for these nonlinearites by iterative superpositioning of several frequencies (Westerink et al., 1985). Nevertheless, the linear version of TEA was used in this research. This choice was primarily based on the lack of validation data available to justify the expense of using nonlinear TEA and is discussed in more detail in Section 5.3. In any case, linear TEA provided a reasonable representation of the general tidal circulation pattern in Boston Harbor and was quite useful for our application.

TEA takes advantage of the periodic nature of the tidal phenomenon and operates in the frequency domain rather than the time domain. This is valid so long as the forcings on the system have the same periodicity as the responses of the system. This so-called harmonic method offers a number of advantages over traditional time stepping techniques, perhaps the most important being the ability to apply much finer spatial resolution without the expense of small timesteps. As a result, TEA is much cheaper than timestepping models for predominantly tidal flow. Comparing linear TEA (TEA-L) and nonlinear TEA (TEA-NL) to a traditional timestepping model

(CAFE, Wang and Connor, 1975), we find, qualitatively, in terms of computational expense, that:

TEA-L < TEA-NL < CAFE

Computational expense (for both TEA and ELA) will be discussed in more detail in Section 5.5.

The model solves for the spatial variation of elevation and velocity using a Galerkin FEM with piecewise-linear polynomial basis functions. The solution procedure generates six values at each (corner) node of a triangular finite element grid: A_1, A_2, A_3, ϕ_1, ϕ_2, ϕ_3. These six values define the elevation and velocity at each node as follows:

$$u = A_1 \cos(\omega t + \phi_1) \tag{3.2.4}$$

$$v = A_2 \cos(\omega t + \phi_2) \tag{3.2.5}$$

$$\eta = A_3 \cos(\omega t + \phi_3) \tag{3.2.6}$$

where u and v are the x and y components of the depth-averaged velocity at the given node, η is the water elevation, ω is the forcing frequency, and t is time.

Using these equations one can generate the entire time history of the velocity field. Furthermore, any number of solutions can be linearly superimposed to simulate several simultaneous forcing functions. For exam-

ple, a steady current (zero frequency) can be generated by applying a steady wind field or by using the boundary conditions to define a mean slope. The zero frequency solution can then be superimposed on a semidiurnal tide generated by forcing the system at a frequency of $2\pi/T$ (where $T = 12.4$ hrs). The input and output for TEA are summarized in Table 3.1.

3.3 Transport Model (ELA)

ELA is a two-dimensional Eulerian-Lagrangian finite element transport model. By applying the principle of mass conservation to a passive pollutant dissolved in a turbulent flow, one can mathematically describe the physics of transport in the advection-diffusion equation. ELA numerically solves the depth-averaged form of this equation (Daily and Harleman, 1966):

$$\frac{\partial c}{\partial t} + u\frac{\partial c}{\partial x} + v\frac{\partial c}{\partial y} = \frac{1}{h}\frac{\partial}{\partial x}\left[hD_{xx}\frac{\partial c}{\partial x} + hD_{xy}\frac{\partial c}{\partial y}\right]$$

$$+ \frac{1}{h}\frac{\partial}{\partial y}\left[hD_{yx}\frac{\partial c}{\partial x} + hD_{yy}\frac{\partial c}{\partial y}\right] + Q \qquad (3.3.1)$$

where

$c(x,y,t)$ is the depth-averaged concentration

$u(x,y,t)$ is the x component of the depth-averaged velocity

$v(x,y,t)$ is the y component of the depth-averaged velocity

$h(x,y,t)$ is the depth

D_{xx}, D_{xy}, D_{yx}, and D_{yy} are dispersion coefficients

Q represents sources, sinks, and vertical boundary fluxes

Table 3.1

Input/Output for Circulation Model TEA

Input

  — geometry and bathymetry of domain

  — forcing functions (tide, wind, steady currents)

  — bottom friction factor, wind drag coefficient

  — boundary conditions

Output

  — circulation as a function of space and time

    *6 values at each node $(A_1, A_2, A_3, \phi_1, \phi_2, \phi_3)$

    $u = \underline{A}_1 \cos(\omega t + \underline{\phi}_1)$

    $v = \underline{A}_2 \cos(\omega t + \underline{\phi}_2)$

    $\eta = \underline{A}_3 \cos(\omega t + \underline{\phi}_3)$

Associated boundary conditions can be concentration prescribed and/or normal flux prescribed.

An Eulerian-Lagrangian method is employed to solve this transport equation. Essentially, this consists of decoupling the equation into a pure-advection component and a pure-diffusion component. The advection component is solved with a backwards method of characteristics, while the diffusion component is solved using finite elements.

The general procedure is outlined in Figure 3.2. At time t_n, parcels of water are identifed with each node of the numerical grid. These parcels are then tracked backward in time along a particle pathline until the previous time, t_{n-1}, is reached. Since all nodal concentrations are known at t_{n-1} (either from initial conditions, boundary conditions, or from the previous timestep), the concentrations of the fluid parcels at t_{n-1} can be found by spatial interpolation. These concentrations are then directly associated with the nodal concentrations at t_n (Baptista, 1984). This is illustrated in Figure 3.2a.

A fourth-order Runge-Kutta method with constant timestepping is used to solve the set of ordinary differential equations associated with the backward tracking of the fluid parcels. Having solved the advection component of the equation, the diffusion component is then solved using Galerkin FEM with quadratic Lagrange polynomial basis functions (Figure 3.2b). (These same polynomials are used for the spatial interpolation during the advection calculations.) An implicit timestepping scheme is used to solve for the temporal variation in the diffusion equations.
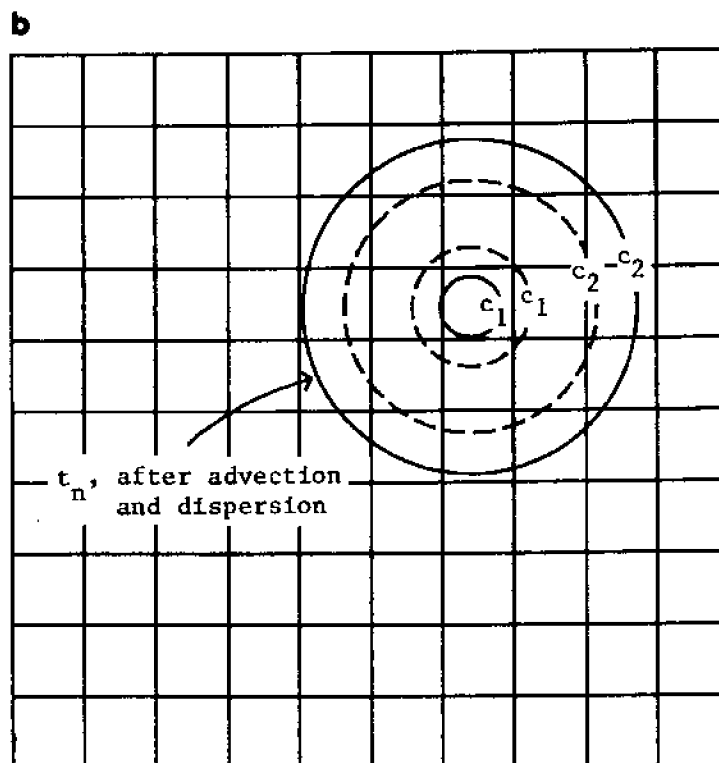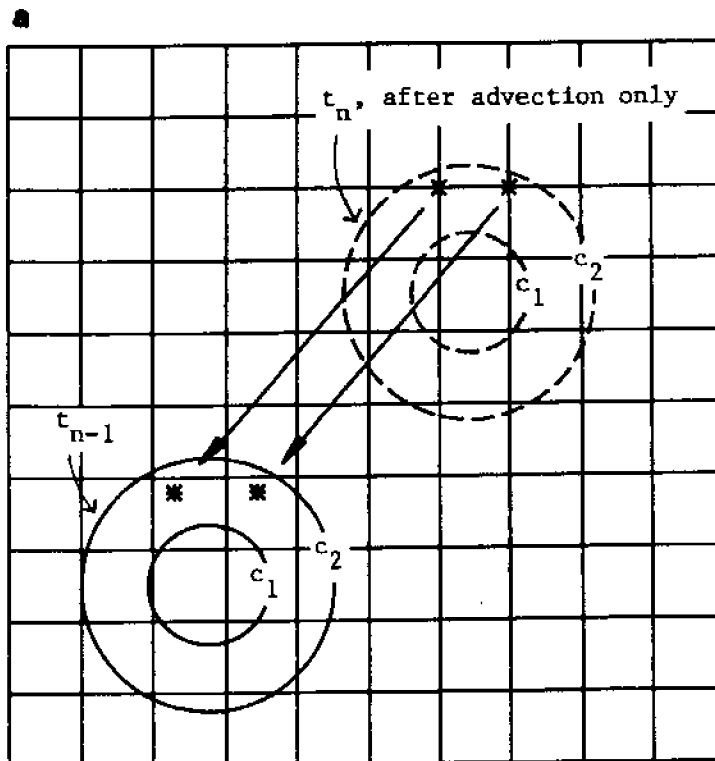
Figure 3.2 Schematic for Eulerian-Lagrangian transport model

The application of ELA to a system as complex as Boston Harbor required a number of refinements and modifications of the original model. These refinements, in and of themselves, constituted a major portion of the research effort. As a result, a number of improvements were incorporated into ELA, including:

a) An algorithm to simulate pollutant concentration near the source before the plume is large enough to be resolved on the finite element grid. This algorithm simulates a continuous source by tracking a series of Gaussian "puffs" forward in time. The technique is general and can be incorporated into other transport models. The procedure is described in detail in Appendix I.

b) Addition of a spatially dependent decay term to represent volatilization. The decay term is defined by a piston velocity and a nodal depth:

$$k_i^n = k/h_i^n \tag{3.3.2}$$

where k_i^n is the first-order decay constant associated with node i at time n, h_i^n is the depth at node i and time n, and k is a piston velocity as defined in Section 2.4.

c) Incorporation of various procedures to more efficiently facilitate long-term simulations (Section 5.1).

The computational procedure for ELA can be summarized as follows:

1) Input appropriate amount of mass, M, into harbor using "puff" algorithm at one or more locations (M = mΔt, where M = mass, m = mass input rate, and Δt = timestep);

2) Advect mass using backward method of characteristics;

3) Diffuse mass using FEM;

4) Decay mass as follows:

$$C_i^n = C_i^* \exp(-k_i^n \Delta t) \qquad (3.3.3)$$

where C_i^n is the final concentration at node i and time n after advection, dispersion, and decay, C_i^* is the concentration at node i and time n after only advection and dispersion, and k_i^n and Δt are as defined above;

5) Repeat steps 1 through 4 for desired length of simulation.

ELA offers a number of advantages over other available transport models (e.g., DISPER, Leimkuhler, 1974). Most significantly, numerical diffusion is greatly reduced. Also, increased resolution near the source is made possible by the "puff" algorithm. Furthermore, ELA offers considerable computational savings for both periodic flows (Section 5.3) and aperiodic flows (since large timesteps can be used). Although the length of timestep does not affect the expense incurred in the advection calculation, it linearly affects the expense incurred in the diffusion calculation (Baptista, 1984).

Not unlike TEA, ELA has some inherent limitations imposed by both the assumptions made in deriving the governing equation, and the particular numerical solution technique used, the most important being 1) the assumption of two-dimensionality; and 2) the unavoidable errors incurred as a result of the spatial discretization of the domain.

While it is important to keep these in mind, it is very likely that the inaccuracies in the circulation model when applied to a complex system such as Boston Harbor will overshadow the inaccuracies in the transport model. This is certainly the case when using the linear version of TEA and likely to still be the case even when the nonlinear version of TEA is applied. (That is, circulation is more difficult to simulate than transport.)

ELA outputs concentrations at each node of a triangular quadratic finite element grid (3 corner nodes and 3 side nodes per element). Concentrations can be saved and output every timestep. The input and output for ELA are summarized in Table 3.2.

Table 3.2

Input/Output for Transport Model ELA

Input

    — geometry and bathymetry of domain

    — advective velocity field (output from TEA)

    — dispersion coefficients, decay rate

    — source location and strength, initial dilution

    — boundary conditions

    — timestep, length of simulation

Output

    — concentration as a function of space and time

       *concentration at every node each timestep

Chapter 4

Tracer Experiments in Boston Harbor

The compounds described in Chapter 2 were used in tracer experiments to gain insight into large-scale mixing and volatilization processes in Boston Harbor. This chapter describes these experiments and presents the results. After first describing the Boston Harbor system, the sampling methods and analytical techniques that were used are discussed. The actual measurements of the tracers at the source and in the harbor are then presented, and based on the observed concentration distributions, some qualitative conclusions regarding pollutant transport are drawn.

4.1 The Boston Harbor System

Boston Harbor is located on the western edge of Massachusetts Bay, a semi-enclosed coastal embayment approximately 100 km long and 40 km wide in the western Gulf of Maine (Figure 4.1). A detailed map of the harbor is presented in Figure 4.2. As can be seen, the system is geographically complex and a number of small islands are scattered throughout the harbor. The bathymetry of the harbor is further complicated by the presence of two shipping channels, President Roads and Nantasket Roads, both of which are indicated on the figure. The harbor is rather shallow (1-10 m), although depths of 20 m are reached in the channels. The topographic complexity of the system results in correspondingly complex circulation patterns.

Tidal flows dominate the water exchange, with nearly half of the volume of the harbor leaving on the outgoing tide. Riverine inputs and

PORTSMOUTH

71°W

70°W

43°N

43°N

GULF
OF
MAINE

0   10
Nautical Miles

GLOUCESTER

↑N

BOSTON

M A S S A C H U S E T T S   B A Y

RACE POINT

42°N

42°N

SANDWICH

71°W

70°W
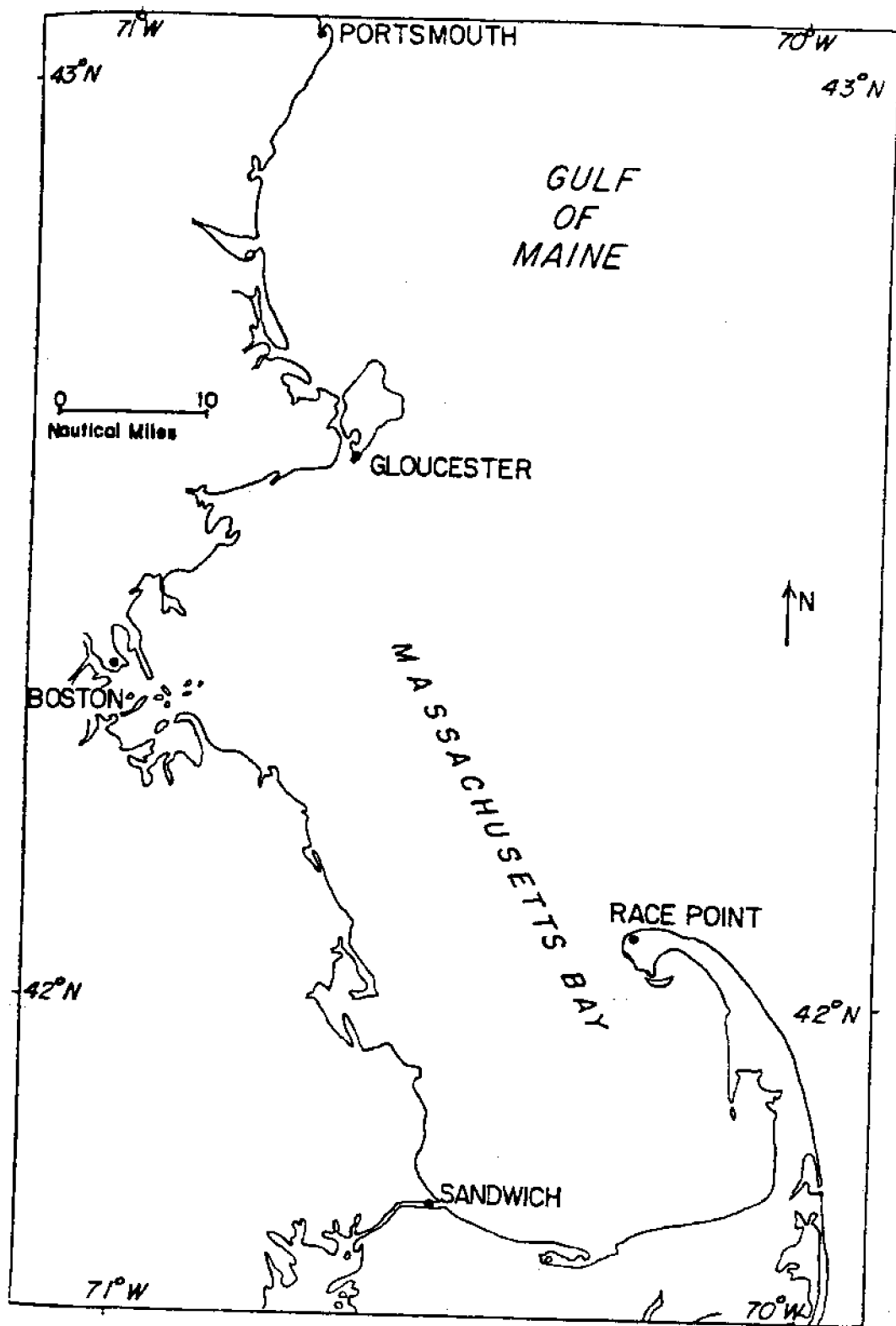
Figure 4.1   Map of Massachusetts Bay
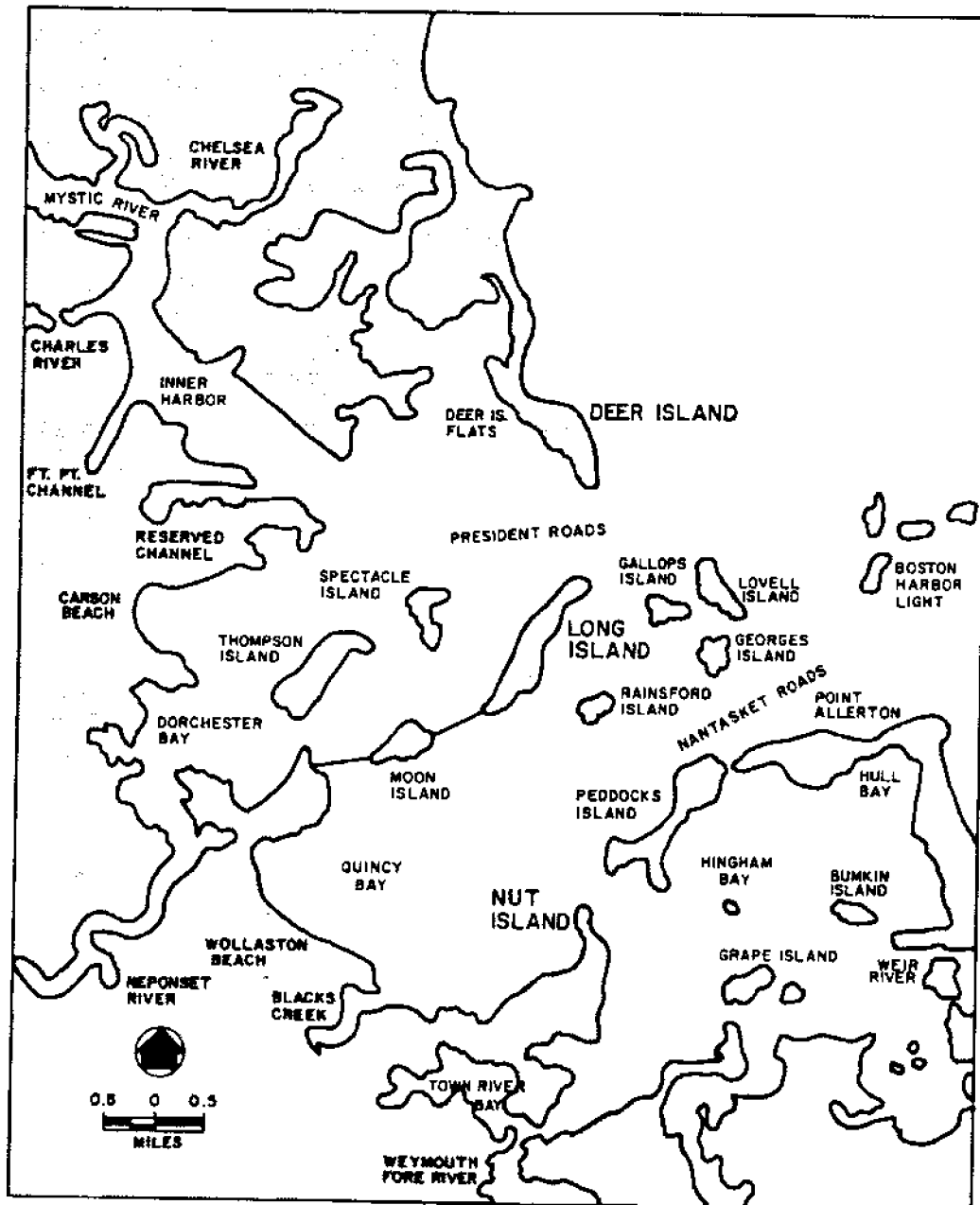
Figure 4.2 Map of Boston Harbor

effluent flows are negligible in comparison. This is evidenced by comparing annual average riverine inputs ($\sim 1.7 \times 10^6$ m^3/day) and effluent flows ($\sim 1.5 \times 10^6$ m^3/day) into the northern part of the harbor to the volume exchanged each tidal cycle (1.1×10^8 m^3) (Metcalf and Eddy, 1984). Flow enters and leaves the harbor primarily through the two channels, where maximum tidal velocities of nearly 1 m/sec occur (NOAA, 1974). The generalized harbor circulation pattern, showing both flood and ebb currents, is illustrated in Figure 4.3.

Figure 4.4 illustrates the major sources of pollution (and potential sources of VHOCs) to the harbor. The primary sources of contaminants are the wastewater treatment facilities at Deer Island and Nut Island, where effluent currently receives primary treatment and chlorination before discharge. The combined outfall discharges from these two plants varies from approximately 15 to 20 m^3/sec. In addition, there are over 100 combined stormwater and sewer overflows (CSOs), some of which discharge to the harbor under both wet and dry conditions. (Dry weather inputs result both from equipment malfunctions and a general overloading of the sewage system.) The CSO input is quite variable, with the average daily flow being approximately 0.7 m^3/sec (Kaltofen and Lax, 1985). This figure may increase by an order of magnitude during severe rain events (Metcalf and Eddy, 1984). There also exist numerous industrial shoreline discharges, particularly in the Inner Harbor region. The larger industrial outfalls discharge up to 0.2 m^3/sec of effluent into the harbor (Kaltofen and Lax, 1985).
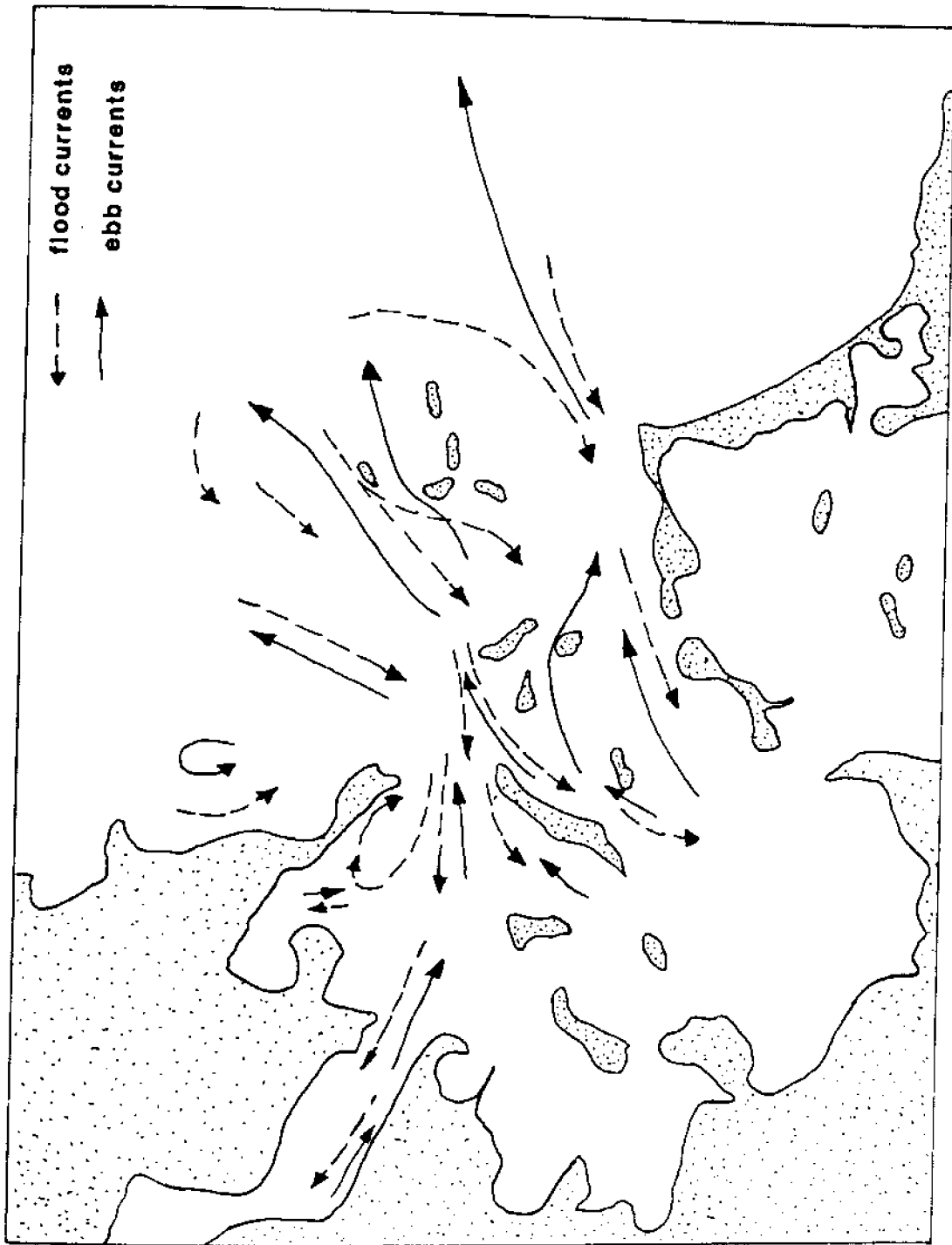
Figure 4.3 Generalized circulation pattern in Boston Harbor (EG&G, 1984a)

flood currents

ebb currents

MYSTIC RIVER

CHARLES RIVER

DEER ISLAND

NEPONSET RIVER

NUT ISLAND

⊗ SEWAGE OUTFALL

● COMBINED SEWER OUTLETS

○ STORM WATER OVERFLOW

1 MILE
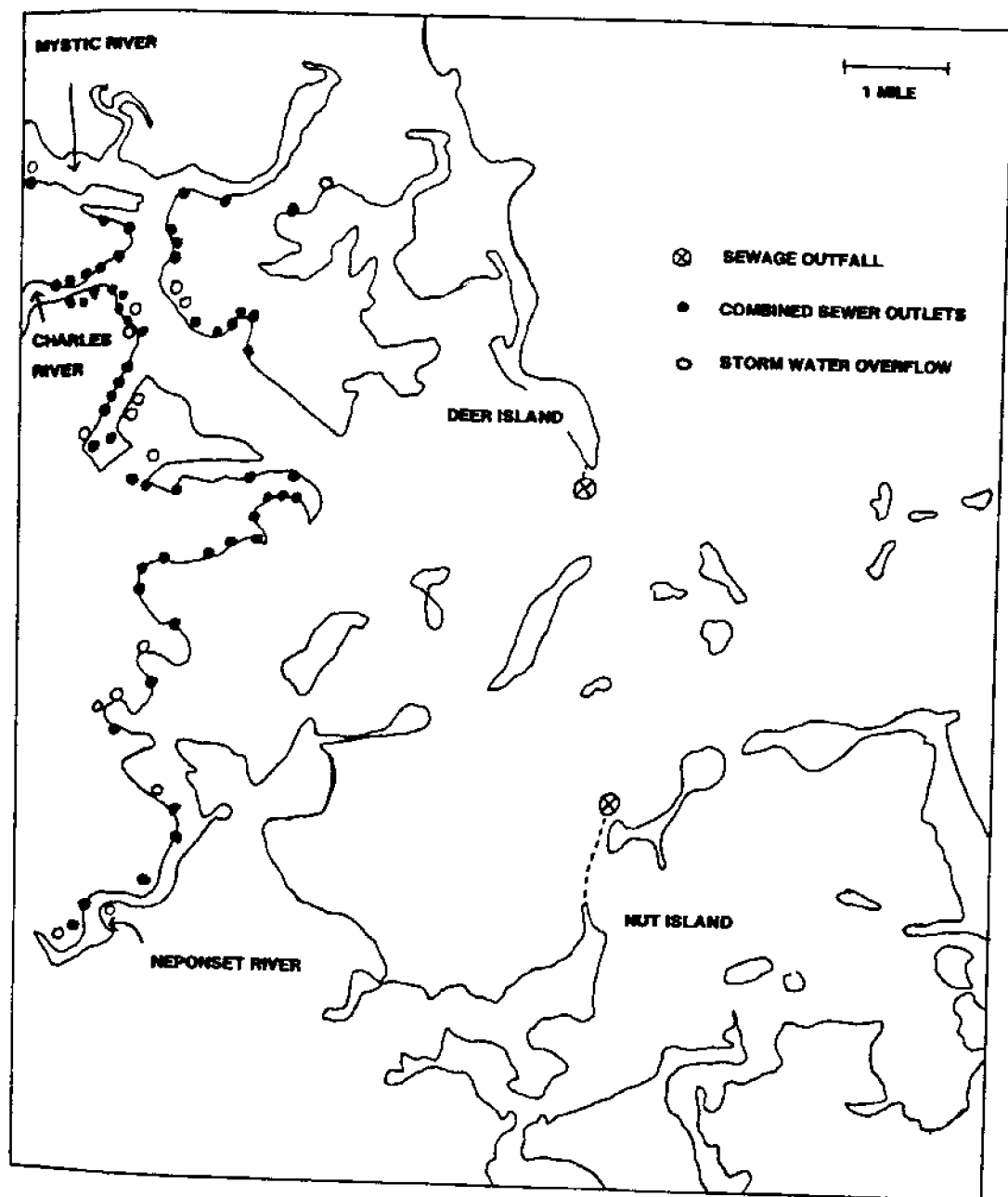
Figure 4.4 Major sources of pollution to Boston Harbor

The VHOC loading of CSOs and direct industrial discharges is difficult to quantify. This is because these smaller sources are both numerous and quite variable. (The effect of CSO loadings is discussed in more detail in Section 4.4.) On the other hand, the wastewater treatment facilities, which account for over 90% of the effluent flow into the system (Kaltofen and Lax, 1985), and whose discharges should contain both the solvents (from industrial inputs) and the haloforms (resulting from chlorination prior to discharge) in high concentrations, can be more readily characterized in terms of VHOC loading by making measurements at only two locations.

In light of this, we chose to model only the VHOCs discharged through the wastewater treatment plants. The validity of this approximation can be tested by making measurements in the harbor and/or using modeling techniques to predict pollutant distributions. If these methods suggest that a particular VHOC has additional sources that are significant (other than the treatment plants), we can conclude that it may be impractical to use that compound as a tracer (at least in Boston Harbor). This, in itself, would be useful information.

Hence, the characterization of the VHOC source function to Boston Harbor centered entirely around measurements at the wastewater treatment plants. Complementary measurements of VHOC concentration in receiving waters were focused in the northern portion of the harbor. Since this region is primarily affected by the Deer Island outfall, effluent measurements were concentrated at the Deer Island treatment plant. Due to the geometry of the harbor and the resulting circulation pattern, as well as the fact that Deer Island discharges approximately two to three times more

effluent than Nut Island, the relative influence of the Nut Island outfall on the northern harbor is small. Hence, its exact characterization was not critical.

4.2 Experimental Methods

Effluent samples were collected at Deer Island from a continuously flowing tap directly connected to the effluent stream. Upon collection, sodium thiosulfate was added to dechlorinate the sample:

$$H^+ + \underset{\substack{\text{oxidizing} \\ \text{chlorine}}}{HOCl} + \underset{\text{thiosulfate}}{2S_2O_3^{2-}} \longrightarrow \underset{\text{chloride}}{Cl^-} + H_2O + S_4O_6^{2-}$$
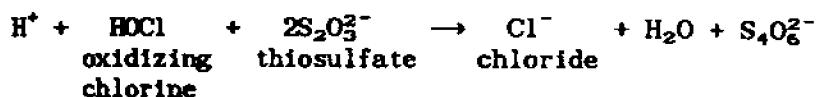
This procedure effectively stops the halogen substitution reactions which lead to the production of THMs. The reason for doing so is discussed in Section 4.3. The samples were stored in 100 mL glass volumetric flasks, which were completely filled and sealed with glass stoppers so that no air remained.

Surface water samples in the harbor were collected by hand, while deep samples were collected with 5 L Nisken bottles (General Oceanics). In an attempt to make sample collection as synoptic as possible, sampling was carried out within the 2 hours surrounding high water slack. (The degree to which our sampling can be considered synoptic is discussed in Chapter 6.) The samples were stored in 100 mL volumetric flasks in the same manner as the effluent samples. Complementary water temperature measurements were also recorded.

Within several hours after collection, the samples were returned to the lab and pipetted down to 100 mL. A solution of bromotrichloromethane in methanol was then injected directly into the water samples as internal standard (5 μL of a 4-part-per-million solution for seawater samples, 5 μL of a 48-part-per- million solution for effluent samples). Samples were then extracted into 1 mL of pentane by shaking for 10 minutes. Extraction efficiencies were 60 to 70% and varied slightly between compounds, but were consistent from sample to sample. The pentane was drawn off into ½-dram vials with Teflon-lined caps. The vials were then stored in a freezer (-20°C) for no more than one week before being analyzed.

Gas chromatographic analyses were subsequently performed on a Carlo Erba HRGC 5160 gas chromatograph. The instrument was equipped with an on-column injector and a nickel-63 electron capture detector. The column used was a fused silica glass capillary, having a length of 50 m, an inner diameter of .32 mm, and methyl phenyl (5%) silicone as stationary phase. The chromatographic parameters were chosen such that all the VHOCs could be separated and measured in the same run in a reasonable amount of time. The gas chromatographic conditions were: injector air cooled; detector temperature 275°C; column temperature program 35° to 165° at 10°/min, 165° to 200° at 35°/min, 2 min at 200°; hydrogen carrier gas rate 30 cm/sec; ECD makeup gas (argon with 5% methane) flow 5 mL/min. The sample was introduced into the instrument by injecting 2 μL of pentane extract directly on column at a rate of 2 μL/sec.

The concentrations of the different halocarbons were determined from standards after peaks were normalized to the internal standard. Standards

were prepared by extracting 100 mL solutions prepared in seawater or distilled water (depending on whether harbor samples or effluent samples were being analyzed) into 1 mL of pentane.

The pentane used to extract the VHOCs was contaminated with several of the solvents to some extent (~1 part per billion in the pentane), and the sample chromatographic peaks were corrected by subtracting this background signal. Unfortunately, the pentane was so contaminated with chloroform relative to observed seawater concentrations, that this compound was precluded from analysis (greater than 10 parts per billion chloroform in the pentane). No other solvent could be found that was sufficiently clean of chloroform.

All samples were taken in duplicate. Replicate injections of the same sample were reproducible to within several percent. Table 4.1 presents the precision (reproducibility) and limits of detection for our analyses. As can be seen, the precision was quite good, ranging from 5 to 10%. The limits of detection were on the order of a few parts per trillion. Even better detection limits could have been achieved (Dyrssen and Fogelquist, 1981), but since the concentrations observed in the harbor were quite high (~100 parts per trillion), no effort was made to do so.

4.3 Results: VHOCs in Sewage Effluent

Measurements were made at Deer Island on seventeen different dates from August 1984 to September 1985. Sampling was concentrated around the spring, summer, and fall months to coincide with and complement the sampling of the harbor waters. Due to the nature of the sampling procedure and

Table 4.1

Precision and Detection Limits for Selected Tracer Compounds

Compound	Precision (%)* Seawater	Effluent	Detection Limit (parts per trillion)
CH_3CCL_3	7.3	4.5	2
$CHCl=CHCl$	6.2	5.9	3
$CHBrCl_2$	7.9	6.5	2
$CHBr_2Cl$	8.8	7.5	2
$CCl_2=CCl_2$	7.6	5.3	1
$CHBr_3$	10.9	9.9	3

*Precision defined as $\frac{1}{n}\left[\sum_{i=1}^{n} \frac{\sigma_i}{\bar{X}_i}\right]$; $n \approx 45$

the volatility of the compounds, sampling could not be done automatically, and was done manually. An effort was made to characterize the source on timescales of hours, days, weeks, and months.

Since we were interested in the mass input rate at the Deer Island source rather than simply the effluent concentration, the variability of both the effluent flow rate and the concentration had to be considered. Figure 4.5 shows the typical variability of the flow rate over a 24-hour period under dry weather conditions (April 10, 1986). This is a classic pattern (Metcalf and Eddy, 1979a), with a minimum occurring in the early morning, and maxima in the mid-morning and early evening. The tide also has some effect on the flow, due to infiltration through leaky tide gates at the CSOs, with higher flows occurring at high tide. Furthermore, there are variations from day to day (e.g., weekend vs. weekday) and month to month due to varying water usage and weather conditions. Over the dates that we sampled, the flow rate ranged from 7.0 m^3/sec to over 15.4 m^3/sec with a mean of 11.3 m^3/sec and standard deviation of 2.5 m^3/sec.

Keeping in mind that we must ultimately use these variable flow rate measurements to characterize the overall variability of the mass input rate at the source, we can proceed to consider measurements of the VHOC concentration in the effluent. In this regard, it is important to consider the location where the effluent is sampled. Halogen substitution reactions between HOCl, HOBr, and organic matter, leading to the production of the trihalomethanes, can occur from the point of chlorination to the point of discharge. Upon discharge the resulting dilution greatly limits the rate of reaction. This is based on empirical kinetic studies (e.g., Kavanaugh
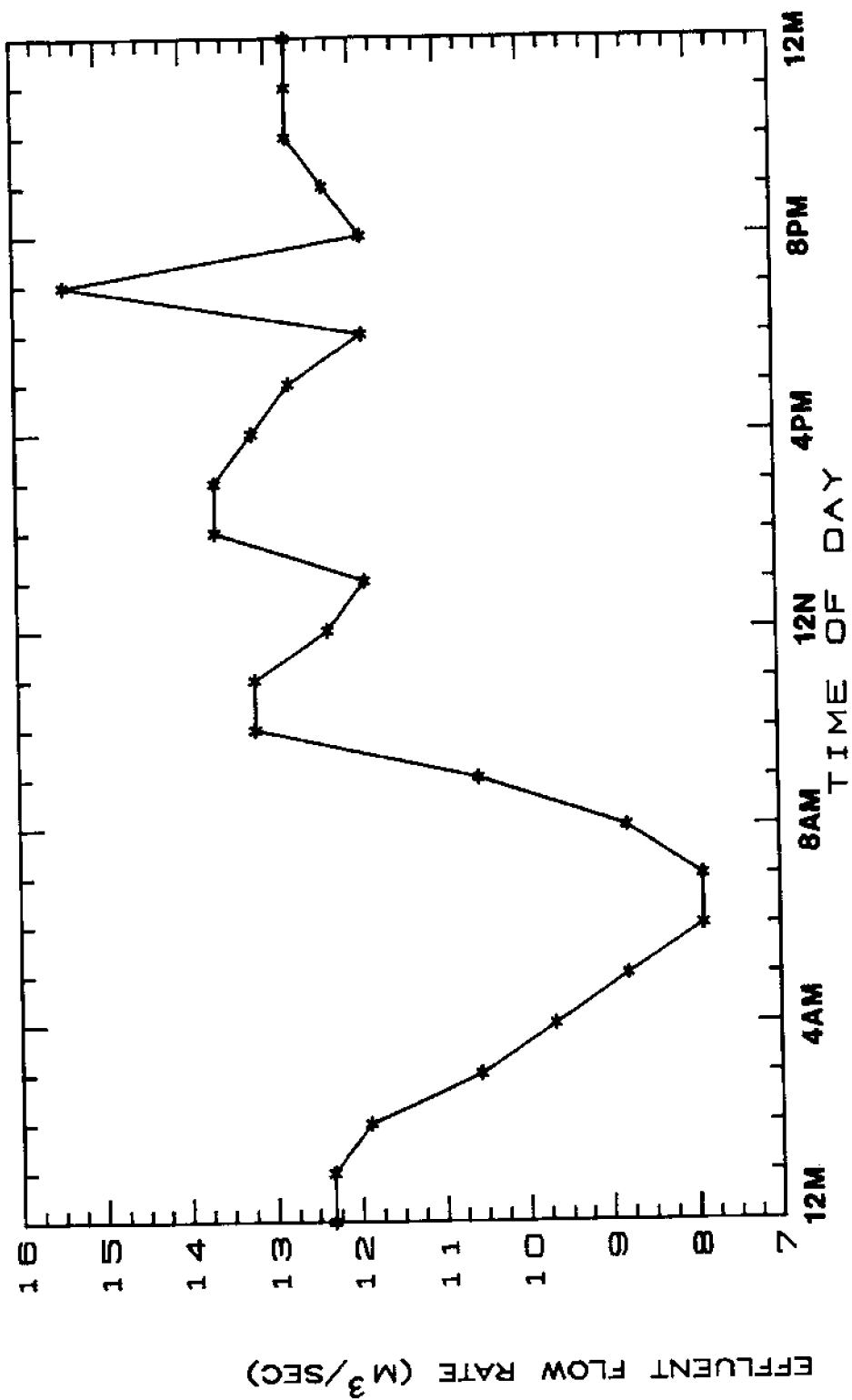
Figure 4.5 Typical daily effluent flow rate variability at Deer Island
(April 10, 1986)

et al., 1978; Gould et al., 1983) which suggest a third-order reaction rate dependence on halogen dosage and a first-order dependence on the organic precursor, where total organic carbon (TOC) is assumed to be indicative of the concentration of precursor. This reaction rate dependence represents an assumed reaction stoichiometry of three moles of halogen consumed per mole of THM formed (Figure 2.1). The corresponding rate expression is:

$$\frac{d[THM]}{dt} = k[HOX]^3[TOC] \tag{4.3.1}$$

where [ ] represents concentrations, k is a rate constant, and X represents Cl and/or Br. In terms of mass rate of change (rather than concentration rate of change),

$$\frac{dM_{THM}}{dt} = k\left[\frac{M_{HOX}}{V}\right]^3\left[\frac{M_{TOC}}{V}\right]V = \frac{kM_{HOX}^3 M_{TOC}}{V^3} \tag{4.3.2}$$

where M_{THM}, M_{HOX}, and M_{TOC} are masses and V is the volume of the reaction system. Hence, diluting the effluent by a factor of 20 (a typical initial dilution, see Chapter 5) effectively slows the reaction by a factor of 8000.

The solvents are not products of these reactions and are unaffected by the duration of the chlorine contact time. It is apparent, however, that to get an accurate representation of the actual trihalomethane concentration in the effluent upon discharge, one should sample the effluent stream as close to the outfall as possible. Dechlorination of the sample upon

collection stops the halogen substitution reactions, mimicking the effect of the subsequent dilution at the time of the discharge.

Due to practical considerations, effluent samples were collected at a point approximately 5 minutes downstream of chlorination and 15 minutes upstream of harbor discharge. Hence, it was necessary to ascertain how much further the trihalomethane reaction proceeded prior to discharge. To accomplish this, samples were collected both at our regular collection point and at a point only 2 minutes upstream of the outfall (Figure 4.6). The trihalomethane concentrations at the former site were approximately 90% of the those at the latter. This suggested that the majority of the THMs were produced within the first 5 minutes after chlorination. Helz et al. (1978), in laboratory experiments in which natural estuarine waters were chlorinated with 5 ppm HOCl, found reaction times on the order of 100 seconds. It is clear that the reaction appears to be relatively fast. Based on our experiment, the THM concentration of the effluent will not increase significantly in the final 2 minutes prior to discharge. Hence we chose to approximate THM effluent concentration at the outfall by simply multiplying sample concentrations by a factor of 1.0/0.9.

Figures 4.7a and 4.7b present typical gas chromatograms of effluent samples. They also serve to illustrate the production of the trihalo-methanes upon chlorination. In Figure 4.7a, the sample was taken from a primary settling tank prior to chlorination (see Figure 4.6). In Figure 4.7b, the sample was taken after chlorination. While the solvents are present in both samples, the three brominated trihalomethanes are present

N

DEER ISLAND

SAMPLE COLLECTION POINT
EMPLOYED IN KINETICS EXPERIMENT

TO OUTFALL

BOSTON HARBOR

MAJOR SAMPLE
COLLECTION POINT

PRIMARY SETTLING TANKS

CHLORINATION

600 FEET
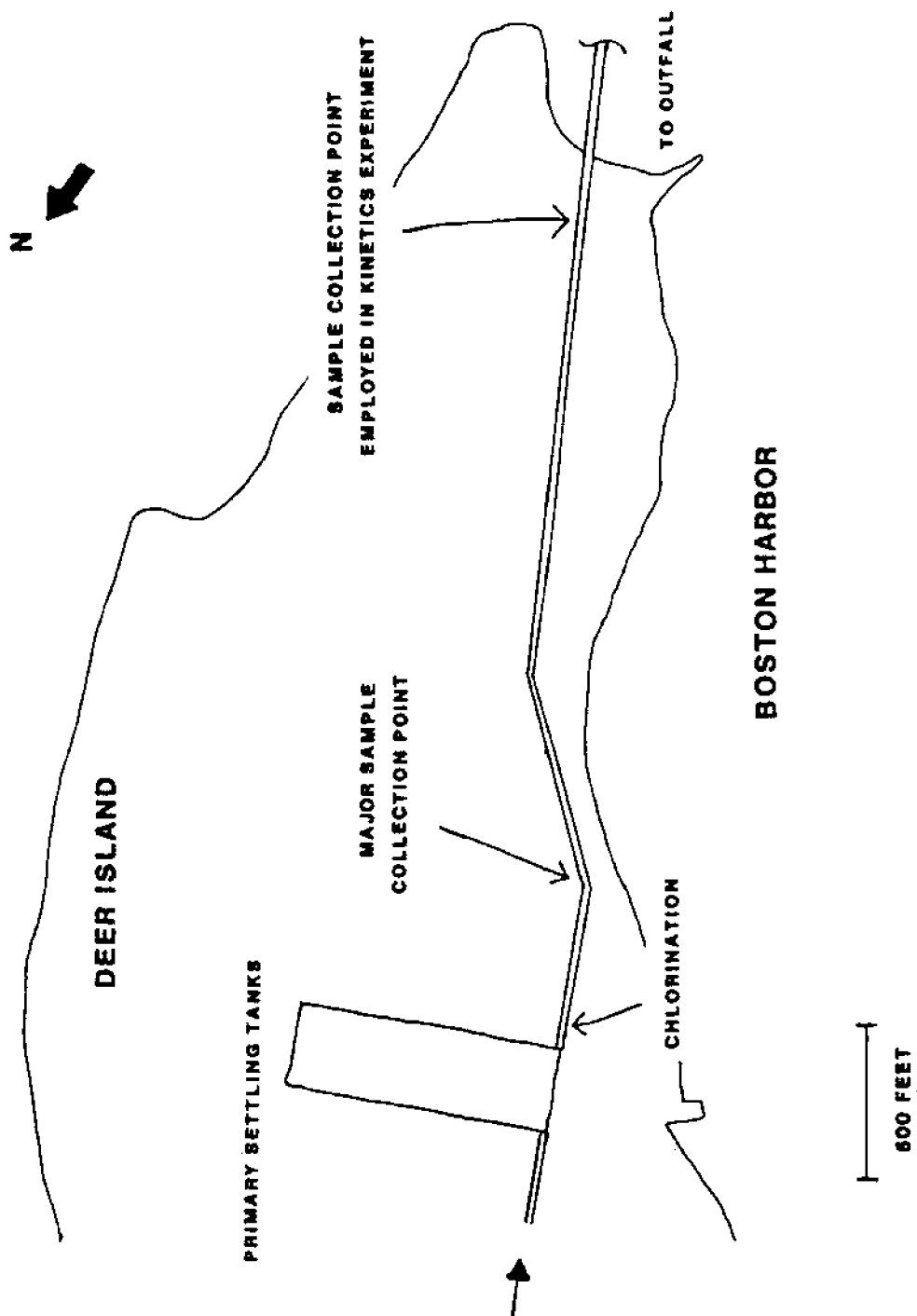
Figure 4.6   Deer Island Schematic

(A) BEFORE CHLORINATION

- A 1,1,1-TRICHLOROETHANE
- B TRICHLOROETHYLENE
- C BROMODICHLOROMETHANE
- D CHLORODIBROMOMETHANE
- E TETRACHLOROETHYLENE

DETECTOR RESPONSE

TIME

(B) AFTER CHLORINATION

- A 1,1,1-TRICHLOROETHANE
- B TRICHLOROETHYLENE
- C BROMODICHLOROMETHANE
- D CHLORODIBROMOMETHANE
- E TETRACHLOROETHYLENE
- F BROMOFORM

DETECTOR RESPONSE

TIME
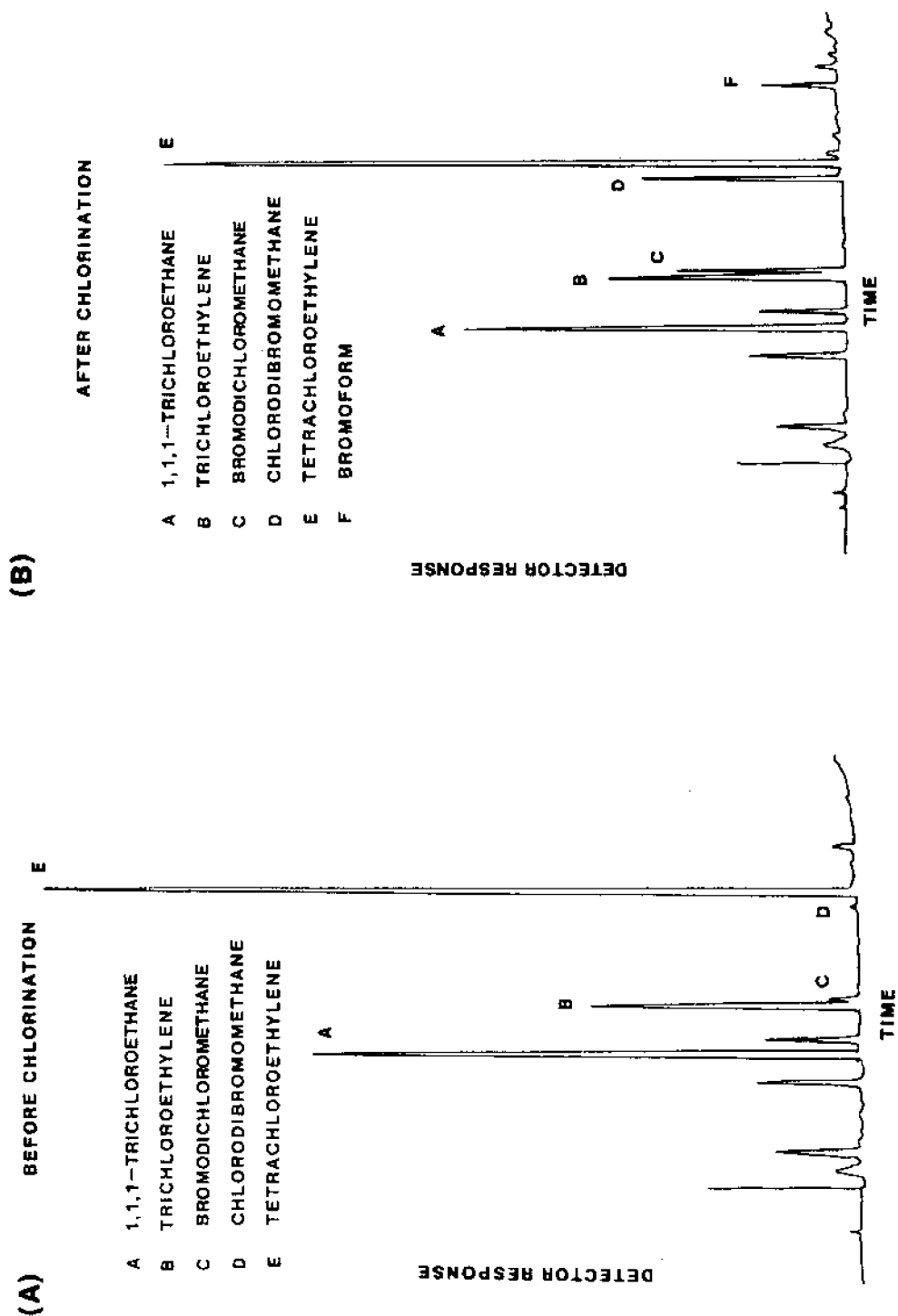
Figure 4.7   Gas Chromatograms of Deer Island Effluent

only at low levels in the unchlorinated sample. The chlorinated sample contains these compounds at significantly higher levels.

The complete set of effluent measurements is tabulated in Appendix II. Table 4.2 summarizes these results. It is evident that the source is widely variable with respect to all of the VHOCs. Furthermore, the fact that the variability in C_0 is the same as that of $C_0 Q_0$ indicates that C_0 and Q_0 are not significantly correlated. The various mass loadings varied on an hourly basis by 10% to 20%, while the variation on a daily basis was substantially greater (~50%) and essentially the same as weekly and monthly fluctuations. This is not surprising in that the major factors affecting the source strength (i.e., effluent flow rate and municipal and industrial loadings) would be expected to vary, for the most part, on the timescale of a day or so (e.g., day/night cycle, weekday/weekend variations, tidal cycle) rather than on an hourly or weekly basis. Seasonal (monthly) variations are apparently no greater than these daily fluctuations. Figures 4.8 and 4.9 illustrate the wide variablity in mass loading that can be observed on a day-to-day basis.

Figure 4.9 also serves to illustrate the fact that the trihalomethanes always tend to covary. This is to be expected since all three compounds are introduced simultaneously into the system as a result of chlorination. Hence, chlorine residual, also plotted in Figure 4.9, is seen to correlate with the THM concentrations. The correlation between the THMs observed in Figure 4.9 is illustrated more clearly in Figure 4.10. The effluent concentration of $CHCl_2Br$ is plotted versus that of $CHClBr_2$. This plot clearly shows the covariance of these compounds over a wide range of concentra-

Table 4.2

Effluent Concentrations and Mass Input Rates
at Deer Island for Selected Tracers*

compound	C_0 concentration† (ppb)	$C_0 Q_0$ mass input† (kg/day)
CH_3CCl_3	9.98 ± 5.01	9.55 ± 5.06
$CHCl=CCl_2$	7.24 ± 1.11	7.52 ± 4.08
$CHCl_2Br$	4.49 ± 2.29	4.11 ± 1.75
$CHClBr_2$	3.34 ± 2.34	2.98 ± 1.80
$CCl_2=CCl_2$	14.50 ± 6.86	14.81 ± 7.94
$CHBr_3$	1.65 ± 1.40	1.39 ± 1.01

*Chloroform is excluded due to solvent contamination. Carbon
tetrachloride was present only at very low levels in the
effluent and at essentially background levels in the harbor,
and is also excluded.

†Mean ± standard deviation; n = 54 with the exception
of bromoform, where n = 40.
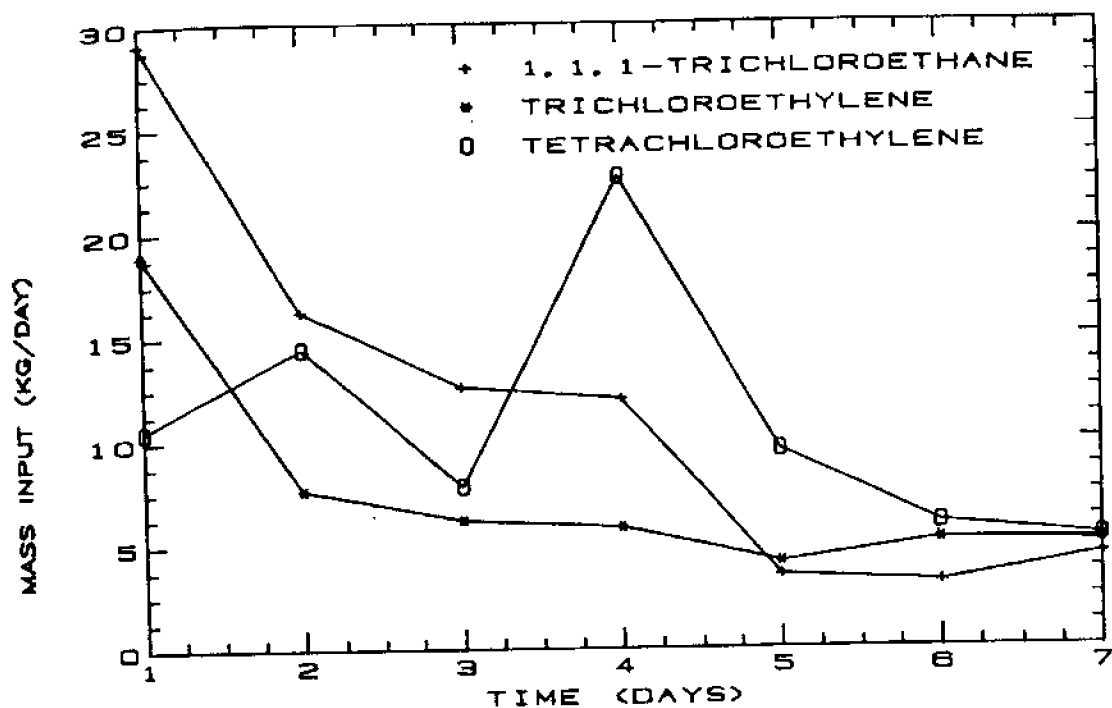
Figure 4.8 Solvent mass loading in Deer Island effluent
(August 28 - September 3, 1985)
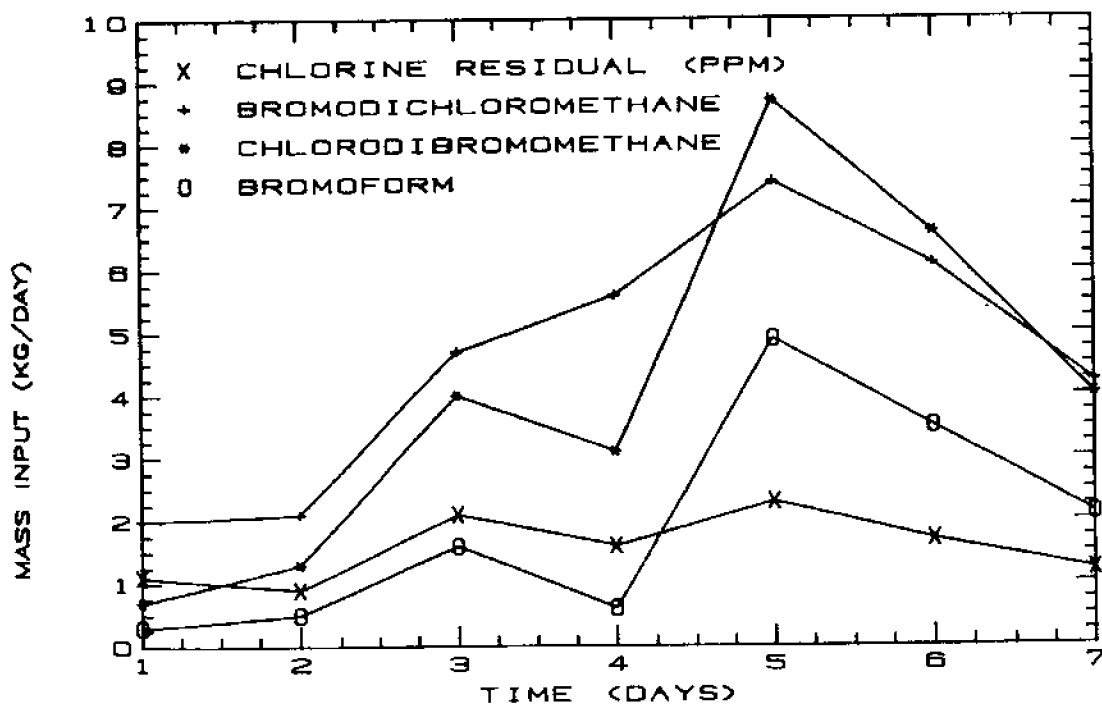
Figure 4.9 Trihalomethane mass loading in Deer Island effluent
(August 28 - September 3, 1985)
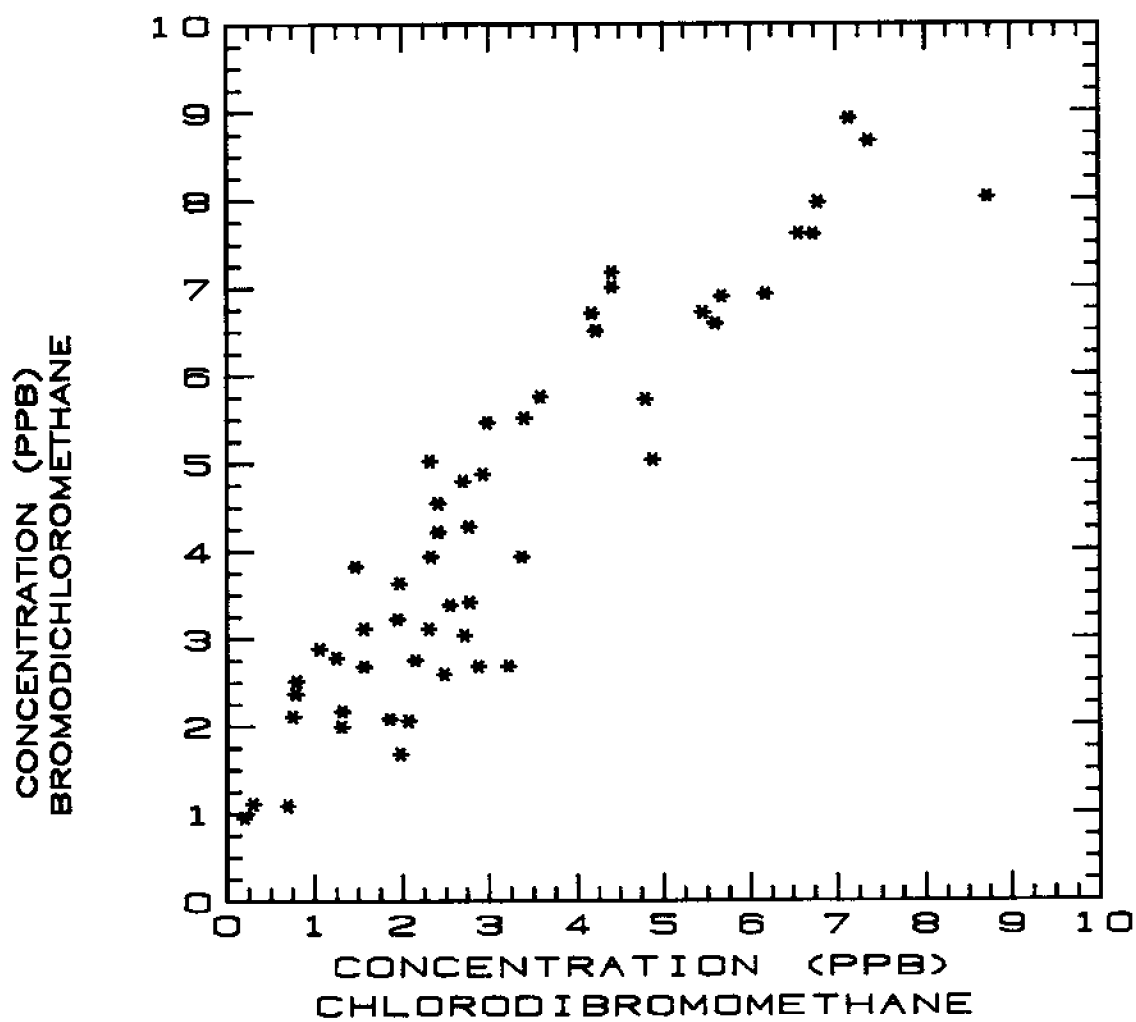
Figure 4.10 Covariance of $CHCl_2Br$ and $CHClBr_2$ in Deer Island effluent

tions. As pointed out by Helz (1980), the chlorine-to-bromine ratio in the trihalomethane products depends on the salinity (more specifically, the bromide ion concentration). Low salinities favor the more chlorinated THMs. As can be seen in Table 4.2 and Figure 4.9, the typical salinity of the effluent generally tends to slightly favor the more chlorinated THMs. (This trend may also be due, to some extent, to chlorinated drinking water inputs.)

It is evident from these measurements that the mass loadings of VHOCs in the Deer Island effluent vary by up to 50% on a daily basis. This makes source characterization more difficult. It may be the case, however, that dispersion processes within the harbor damp out some of this variation, allowing these loadings to be treated approximately as constants for modeling purposes. The magnitude of the error incurred by making this assumption is investigated in Section 5.4.

4.4 Results: VHOCs in Boston Harbor

Seawater samples were collected in Boston Harbor on three separate occasions (October 30, 1984; April 25, 1985; and July 2, 1985). Sampling was focused in the northwest portion of the harbor detailed in Figure 4.11. Figures 4.12 through 4.29 present the results of the VHOC measurements in the harbor. For each date, measurements of 3 solvents (CH_3CCl_3, $CHCl=CCl_2$, and $CCl_2=CCl_2$) and 3 haloforms ($CHCl_2Br$, $CHClBr_2$, and $CHBr_3$) are shown. Results are presented as means and standard deviations of duplicate surface and deep-water samples.

Figure 4.11 Sampling area

Figure 4.12 Tracer Concentrations in Boston Harbor (parts-per-trillion) at High Water Slack (surface and deep water measurements; mean of duplicates)

October 30, 1984

146 ± 4
143

192 ± 14
196 ± 13

215 ± 8
168 ± 16

141 ± 4
147 ± 6

421 ± 32
203 ± 5

149
160 ± 10

128 ± 9
137 ± 1

131 ± 4
134 ± 2

129 ± 1
134 ± 1

1 km

TETRACHLOROETHYLENE

Figure 4.13 Tracer Concentrations in Boston Harbor (parts-per-trillion) at High Water
Slack (surface and deep water measurements; mean of duplicates)

October 30, 1984

157 ± 7
288

130 ± 5
187 ± 10

167 ± 5
155 ± 18

94 ± 0
171 ± 6

450 ± 58
213 ± 19

96 ± 3
147 ± 7

153 ± 9
225 ± 18

77 ± 5
116 ± 5

131 ± 0
211 ± 10

1 km

TRICHLOROETHYLENE

Figure 4.14 Tracer Concentrations in Boston Harbor (parts-per-trillion) at High Water Slack (surface and deep water measurements; mean of duplicates)

October 30, 1984

34 ± 1
37 ± 2
*

38 ± 0
27 ± 2
*

78 ± 10
34 ± 1
*

29 ± 3
28 ± 3
*

26 ± 1
32 ± 7
*

27 ± 6
25 ± 1
*

29 ± 1
28 ± 2
*

330 ± 18
30 ± 0
*

418
55
*

1 km

BROMODICHLOROMETHANE

Figure 4.15 Tracer Concentrations in Boston Harbor (parts-per-trillion) at High Water Slack (surface and deep water measurements; mean of duplicates)

Figure 4.16 Tracer Concentrations in Boston Harbor (parts-per-trillion) at High Water Slack (surface and deep water measurements; mean of duplicates)

CHLORODIBROMOMETHANE

October 30, 1984

94 ± 2
22

19 ± 1
19 ± 1

20 ± 0
13 ± 1

18 ± 1
18 ± 1

31 ± 1
19 ± 1

14 ± 2
13 ± 0

78 ± 3
19 ± 1

20 ± 9
15 ± 1

17 ± 0
17 ± 0

1 km

Figure 4.17 Tracer Concentrations in Boston Harbor (parts-per-trillion) at High Water Slack (surface and deep water measurements; mean of duplicates)

July 2, 1985

751 ± 9
380 ± 18

328
286 ± 14

367 ± 18

370 ± 4
367 ± 0

403 ± 13
364 ± 5

289
309 ± 37

289 ± 0
303 ± 9

341 ± 0
316 ± 9

1 km

1,1,1—TRICHLOROETHANE
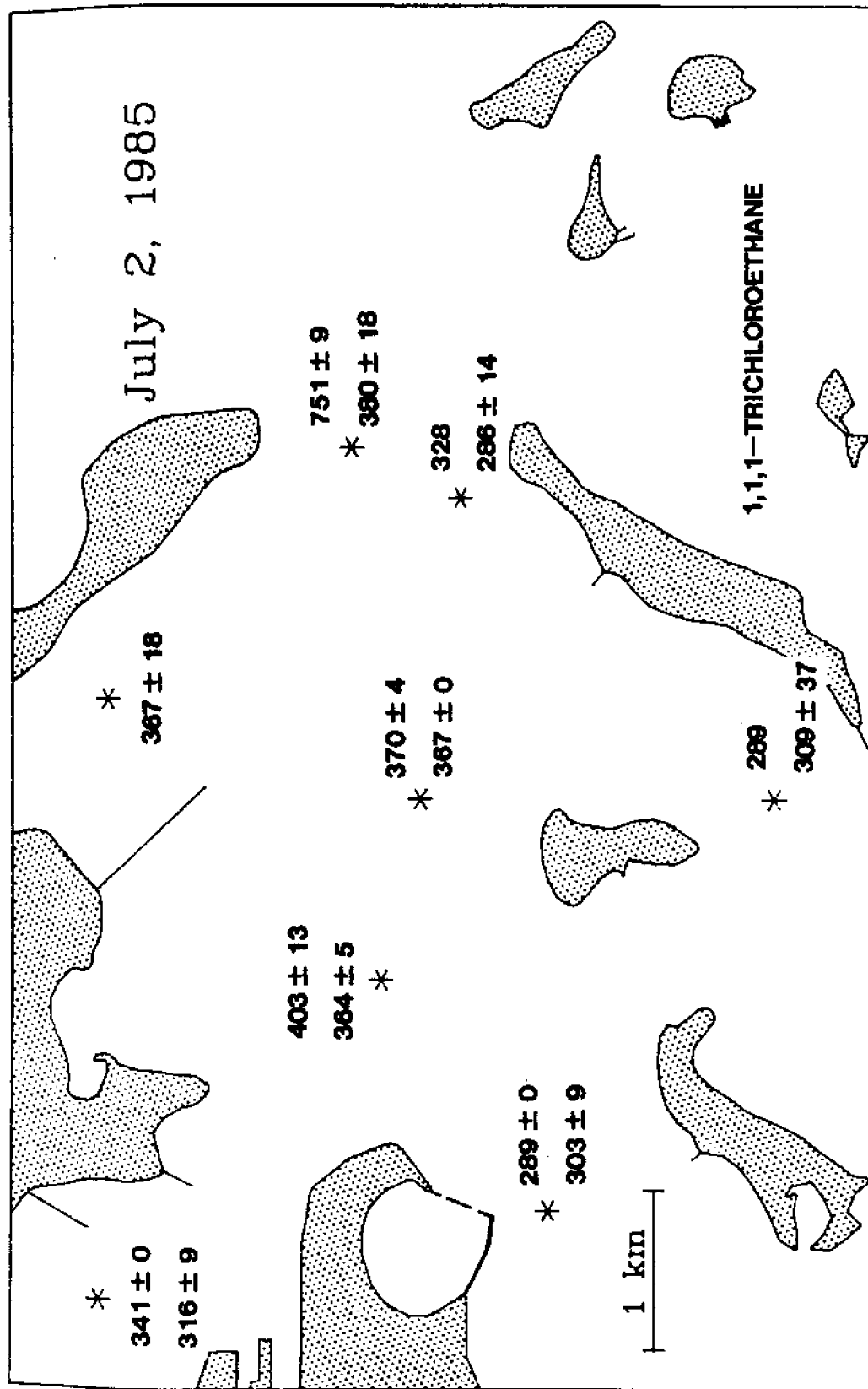
Figure 4.18   Tracer Concentrations in Boston Harbor (parts-per-trillion) at High Water Slack (surface and deep water measurements; mean of duplicates)
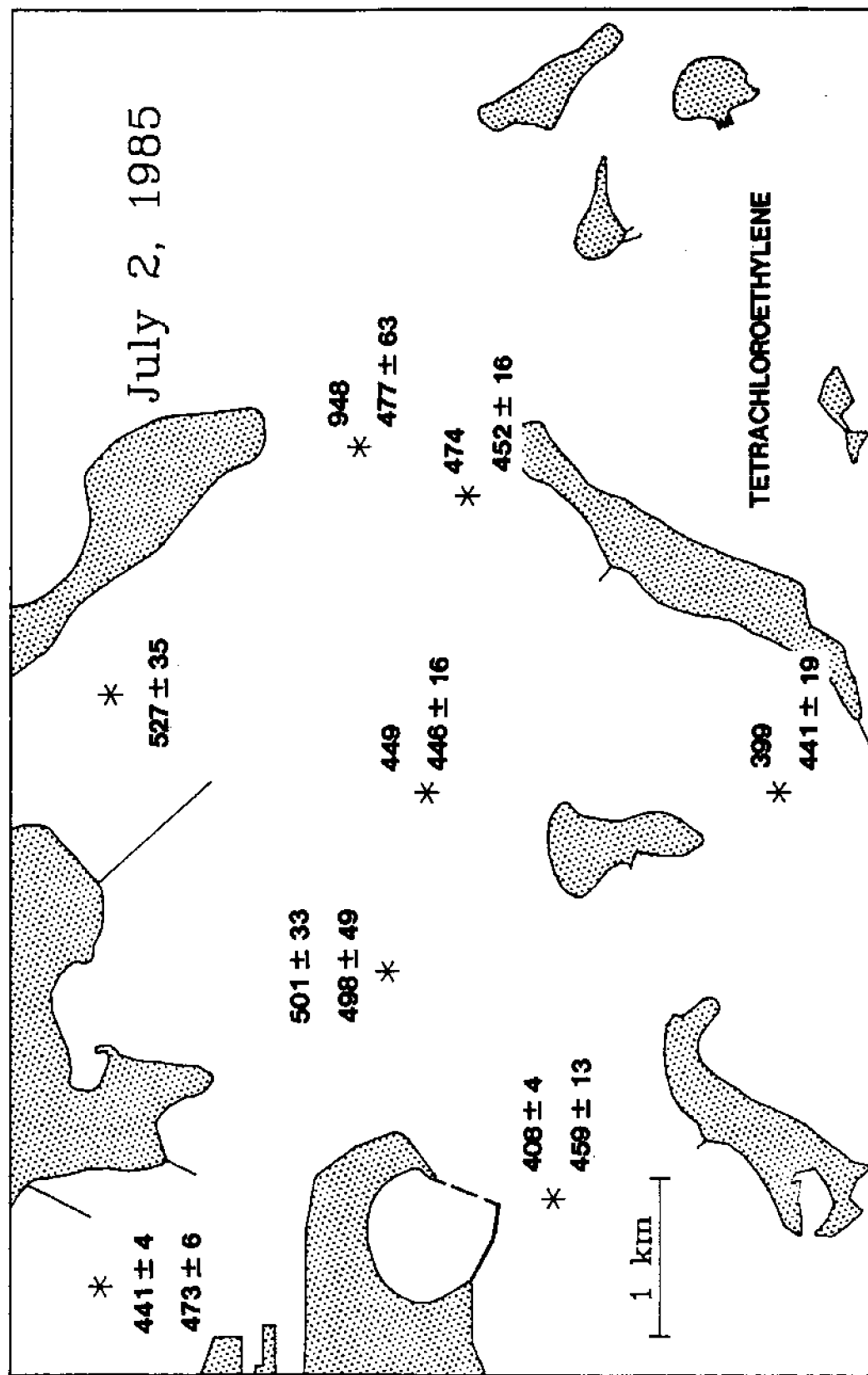
Figure 4.19 Tracer Concentrations in Boston Harbor (parts-per-trillion) at High Water Slack (surface and deep water measurements; mean of duplicates)

July 2, 1985

759 ± 7
284 ± 6

239
239 ± 0

272 ± 6

276 ± 0
272 ± 6

267 ± 0
272 ± 6

220
239 ± 0

234 ± 7
272 ± 6

1 km

285 ± 0
281 ± 6

TRICHLOROETHYLENE
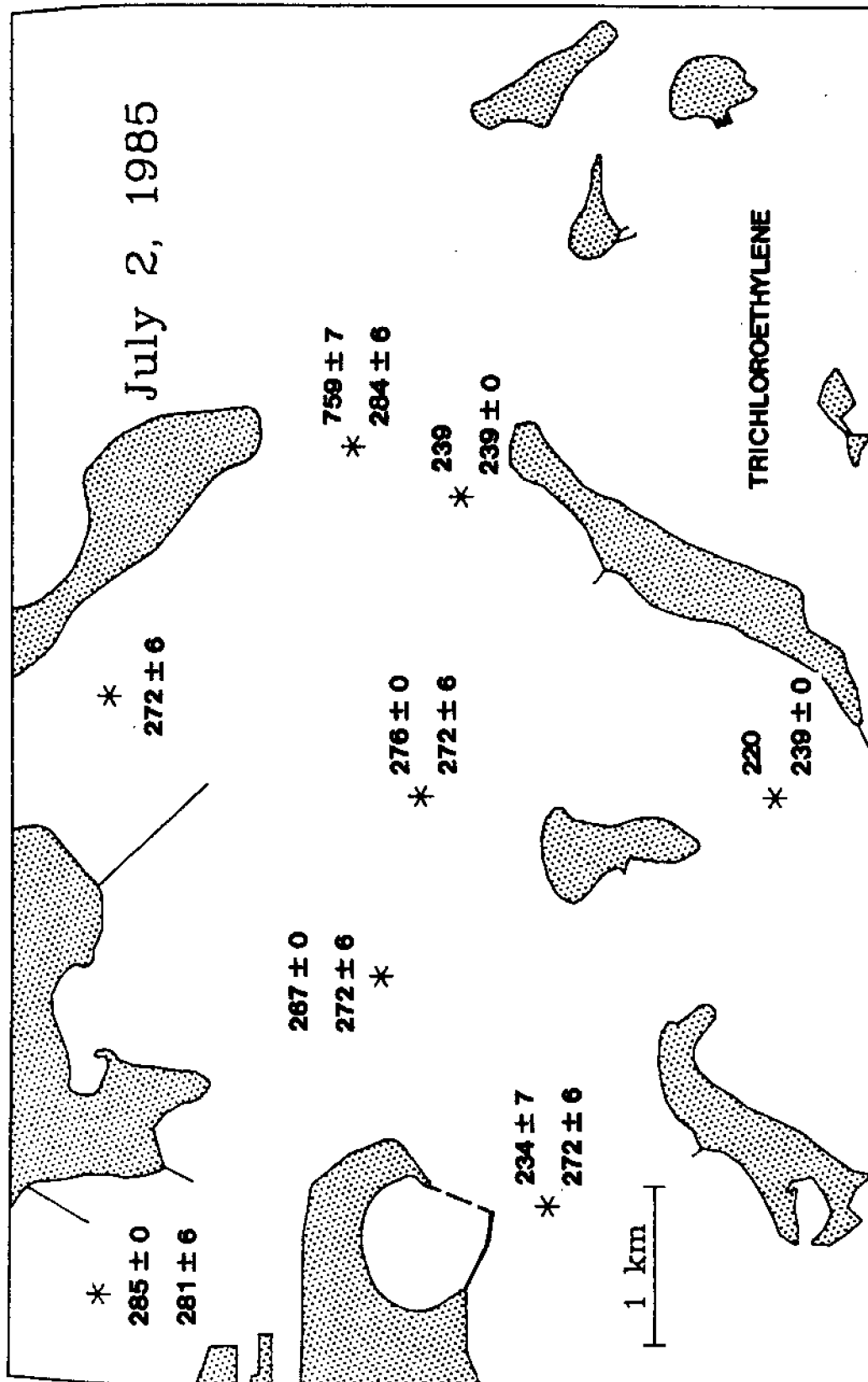
Figure 4.20 Tracer Concentrations in Boston Harbor (parts-per-trillion) at High Water Slack (surface and deep water measurements; mean of duplicates)

July 2, 1985

315 ± 16
85 ± 0

46

40 ± 3

59 ± 0

96 ± 3
92 ± 4

42

46 ± 0

85 ± 0
62 ± 4

44 ± 3
49 ± 4

40 ± 3
49 ± 4

1 km

BROMODICHLOROMETHANE
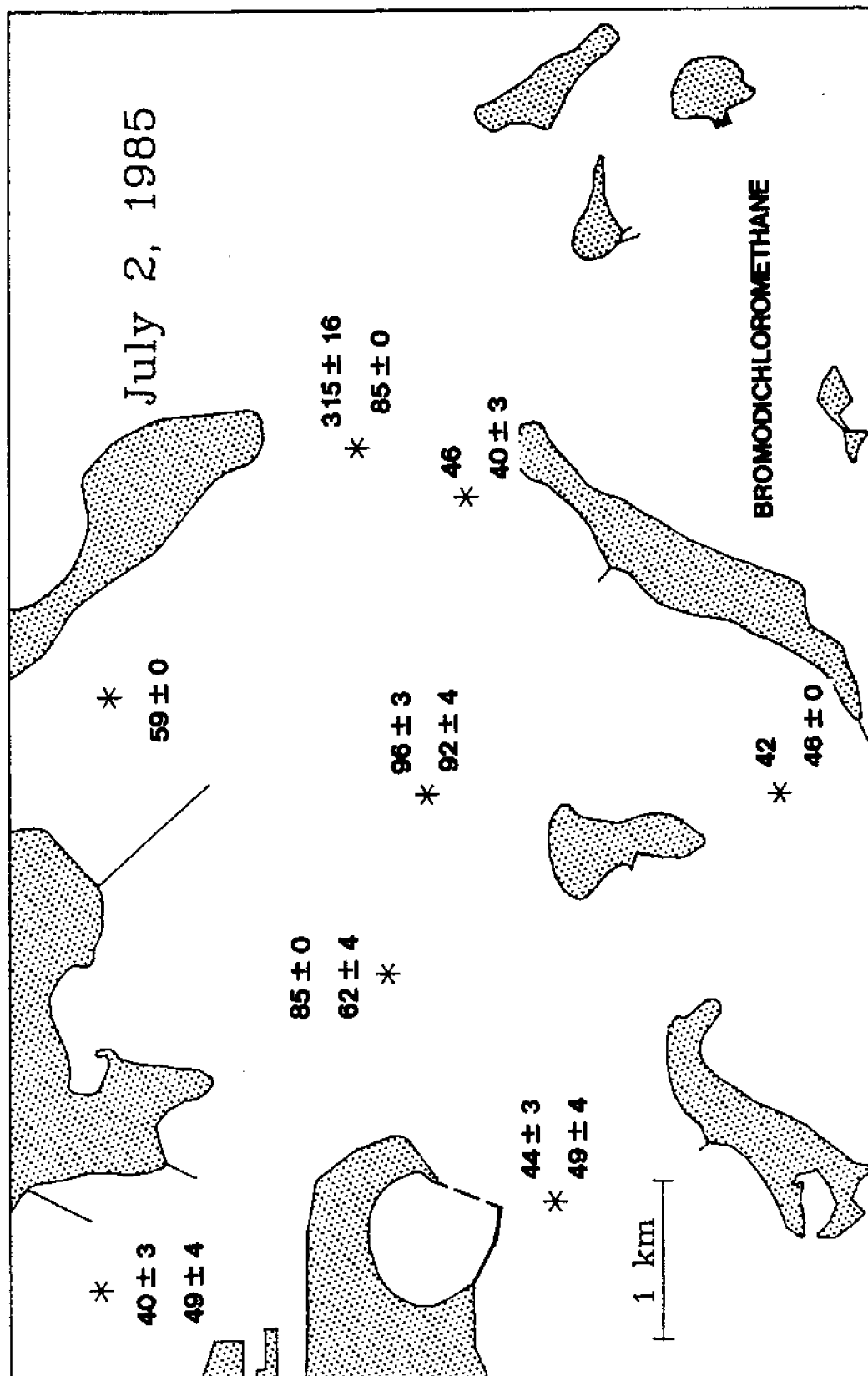
Figure 4.21 Tracer Concentrations in Boston Harbor (parts-per-trillion) at High Water
Slack (surface and deep water measurements; mean of duplicates)
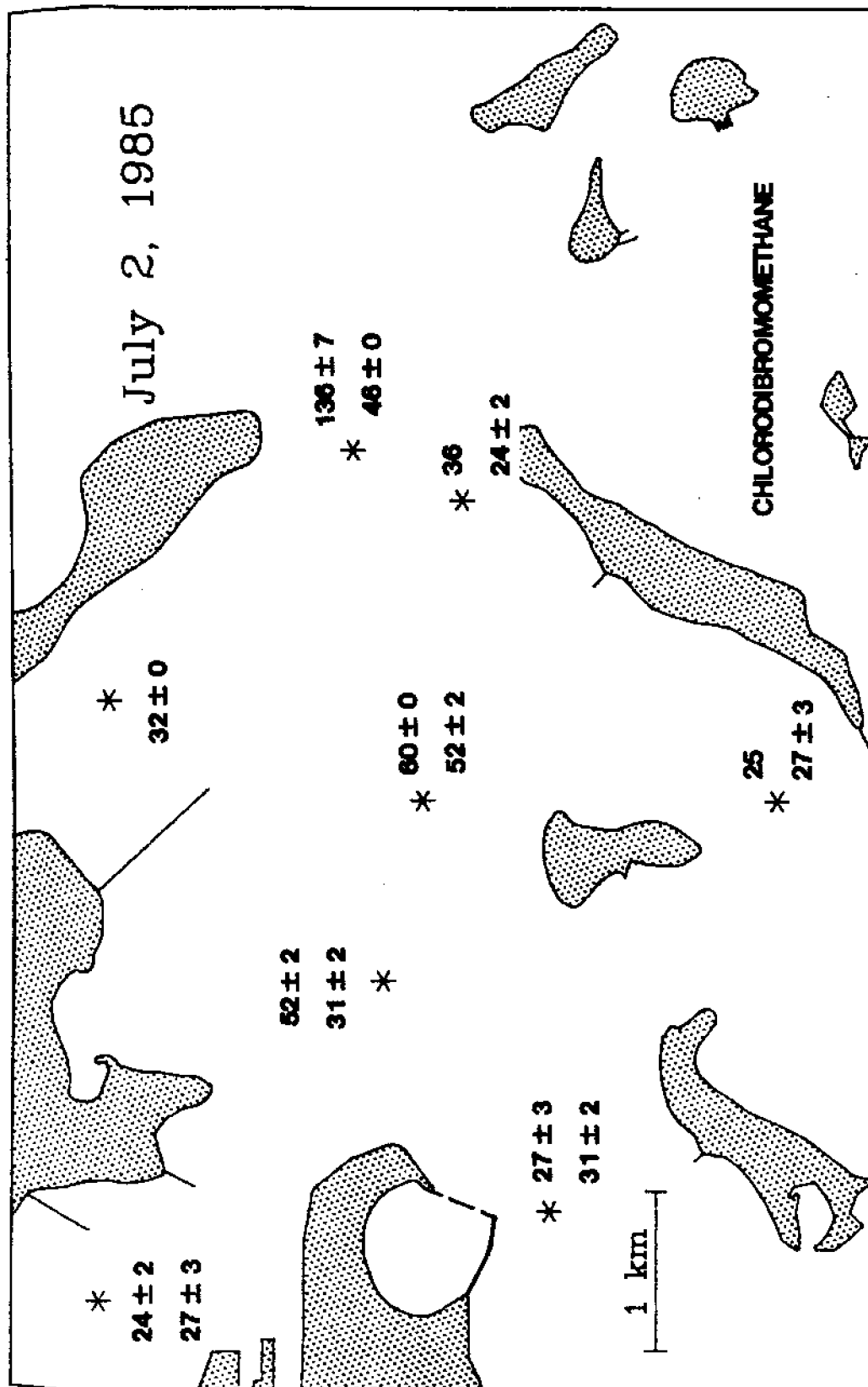
Figure 4.22 Tracer Concentrations in Boston Harbor (parts-per-trillion) at High Water Slack (surface and deep water measurements; mean of duplicates)
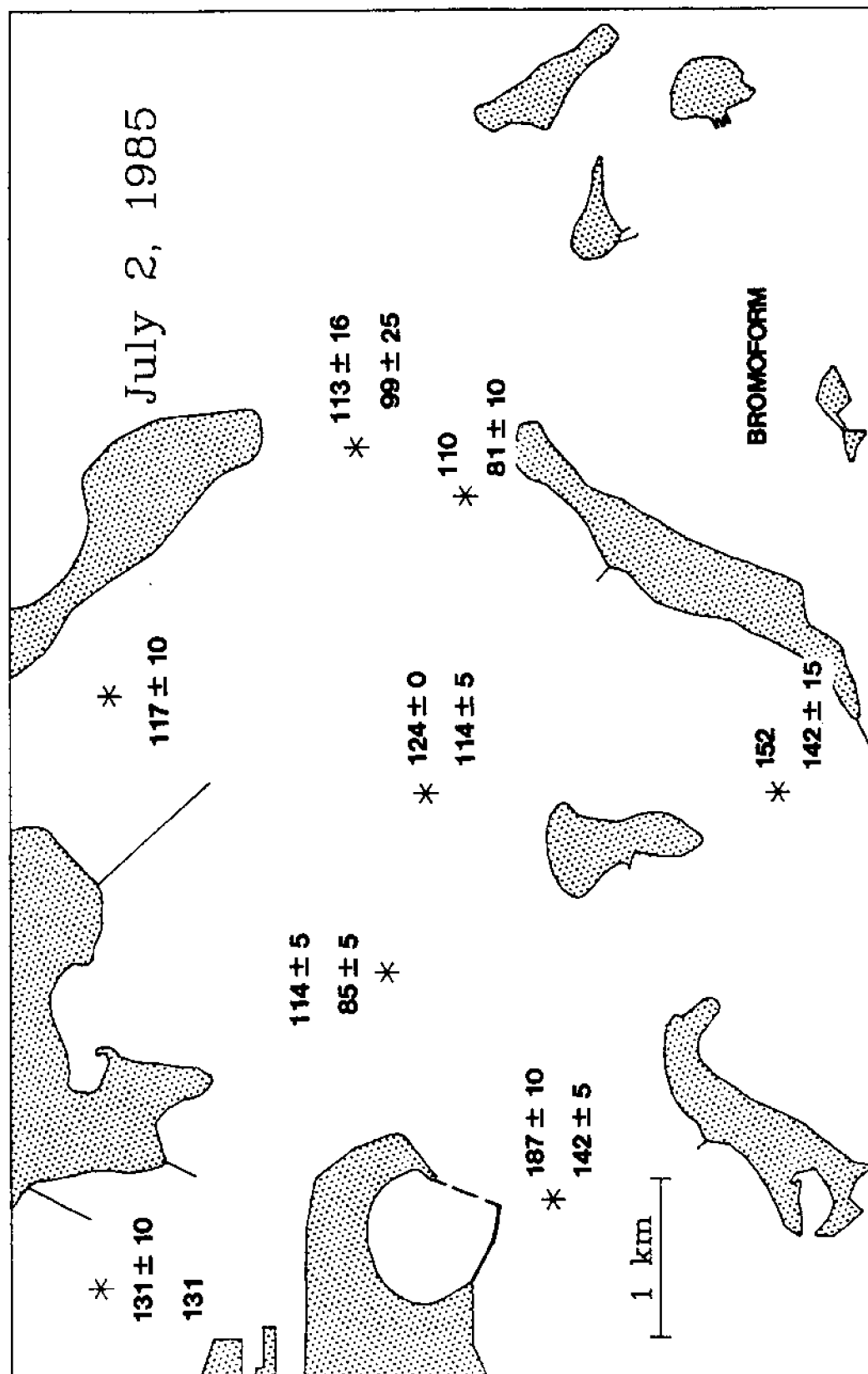
Figure 4.23 Tracer Concentrations in Boston Harbor (parts-per-trillion) at High Water Slack (surface and deep water measurements; mean of duplicates)

April 25, 1985

369 ± 22
203 ± 0

2472 ± 112
1210 ± 56

431 ± 110
365 ± 59

394 ± 126
462 ± 94

465
447 ± 28

285 ± 54
276 ± 4

288 ± 26
288 ± 84

304 ± 42
347 ± 68

1,1,1—TRICHLOROETHANE

1 km
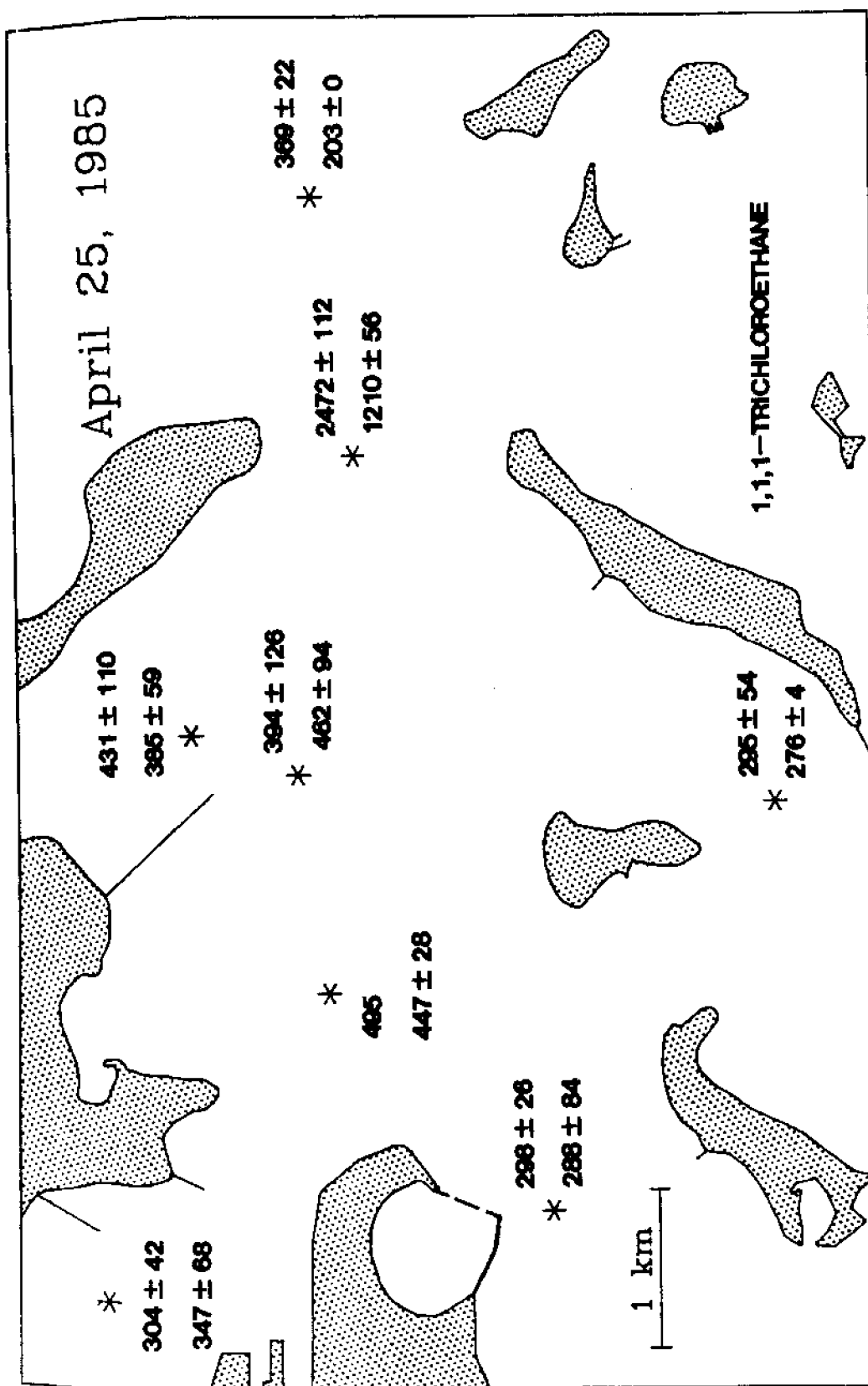
Figure 4.24   Tracer Concentrations in Boston Harbor (parts-per-trillion) at High Water
Slack (surface and deep water measurements; mean of duplicates)
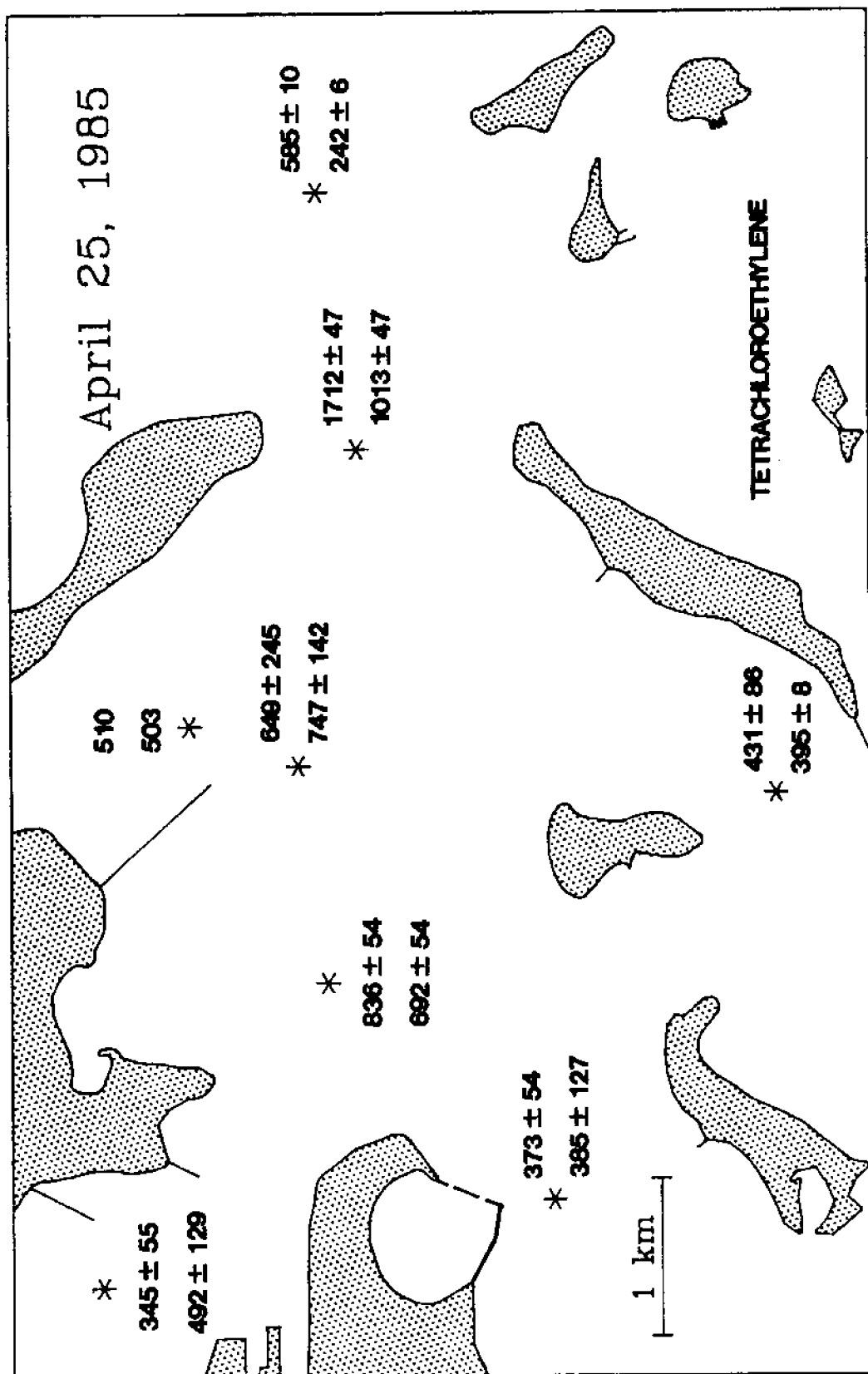
Figure 4.25   Tracer Concentrations in Boston Harbor (parts-per-trillion) at High Water Slack (surface and deep water measurements; mean of duplicates)
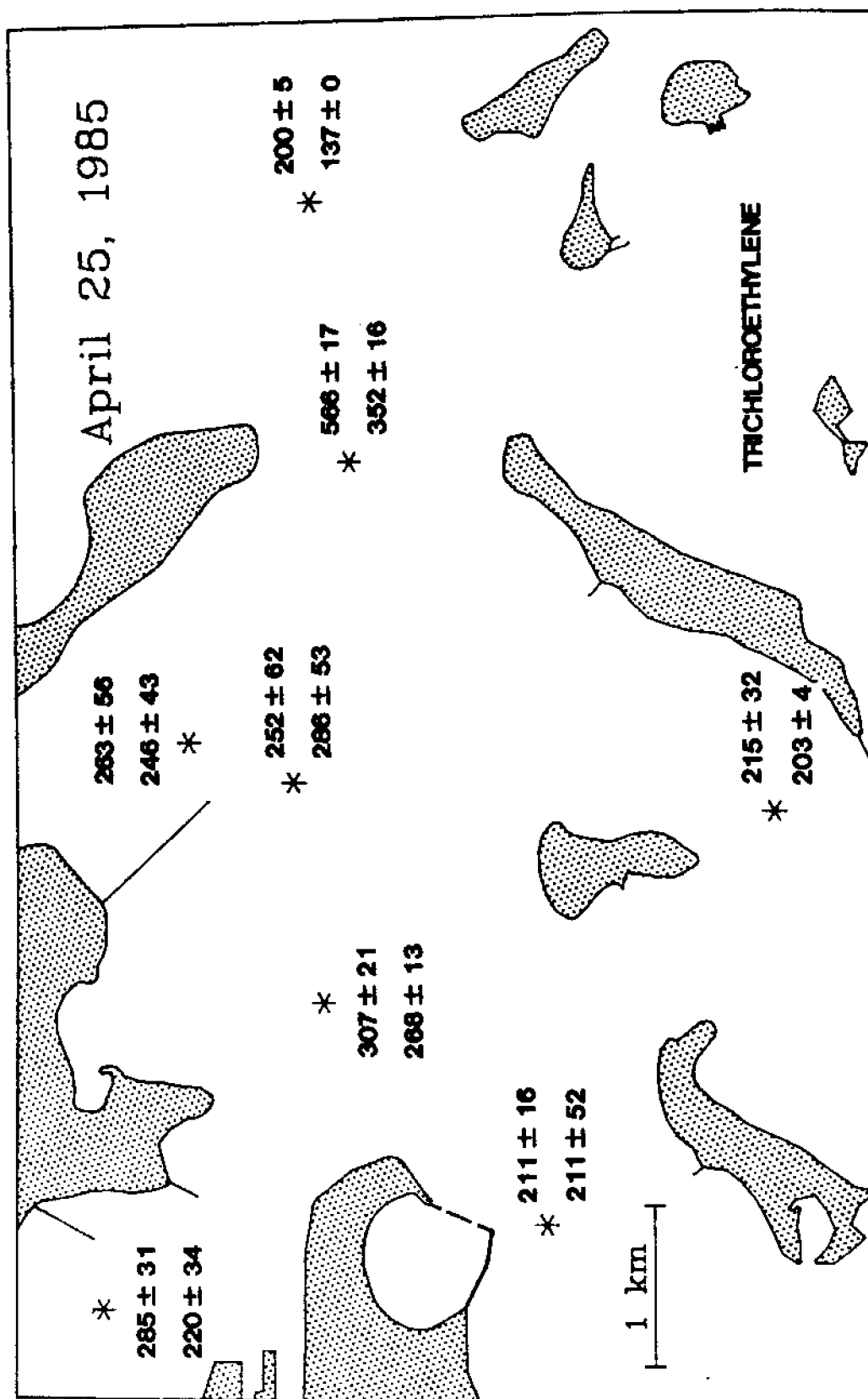
Figure 4.26   Tracer Concentrations in Boston Harbor (parts-per-trillion) at High Water Slack (surface and deep water measurements; mean of duplicates)

April 25, 1985

36 ± 0
21 ± 0

83 ± 1
58 ± 1

BROMODICHLOROMETHANE

47 ± 12
38 ± 5

49 ± 4
56 ± 16

37 ± 6
36 ± 1

58 ± 4
54 ± 1

34 ± 1
34 ± 8

34 ± 4
38 ± 7

1 km
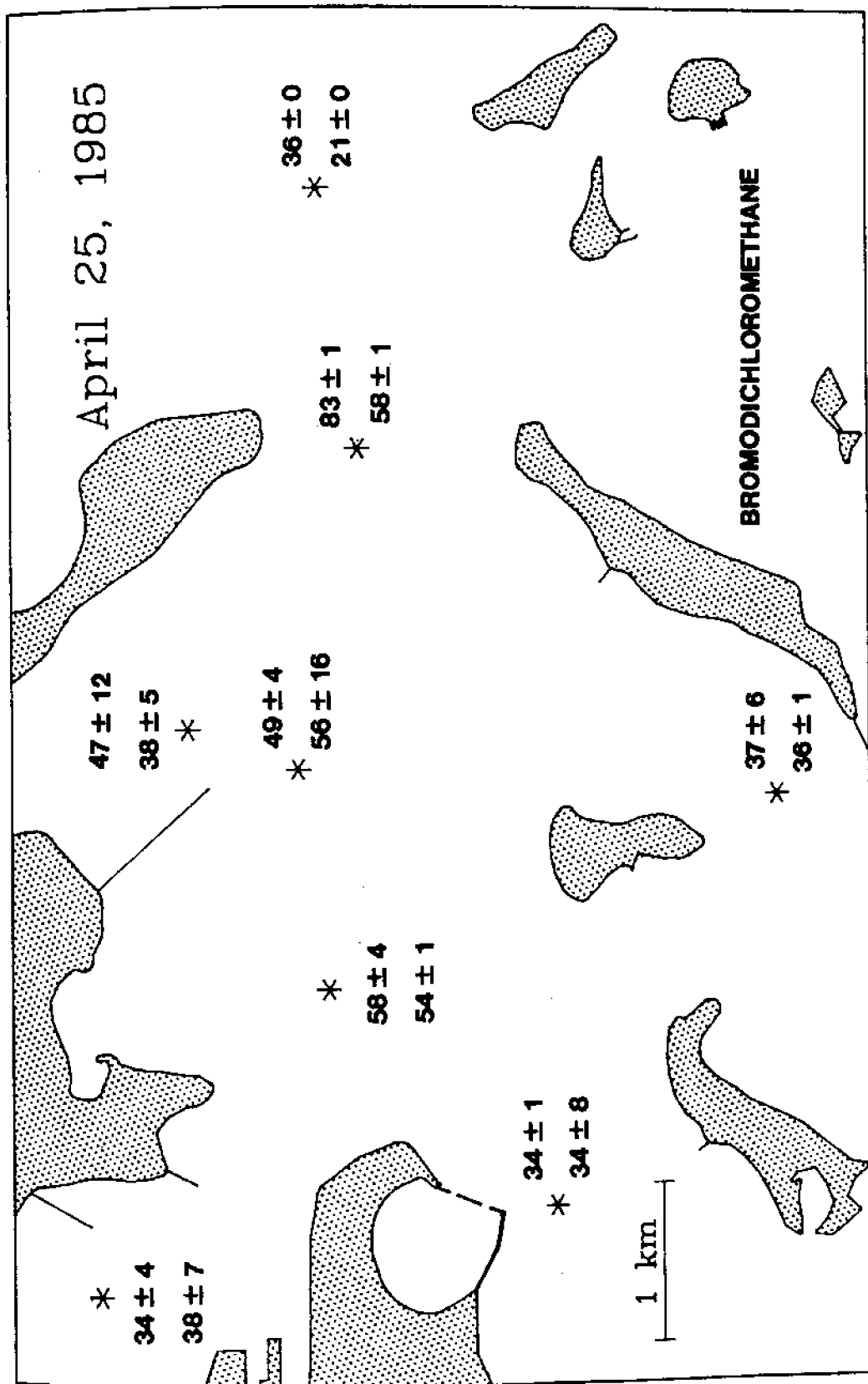
Figure 4.27 Tracer Concentrations in Boston Harbor (parts-per-trillion) at High Water
Slack (surface and deep water measurements; mean of duplicates)
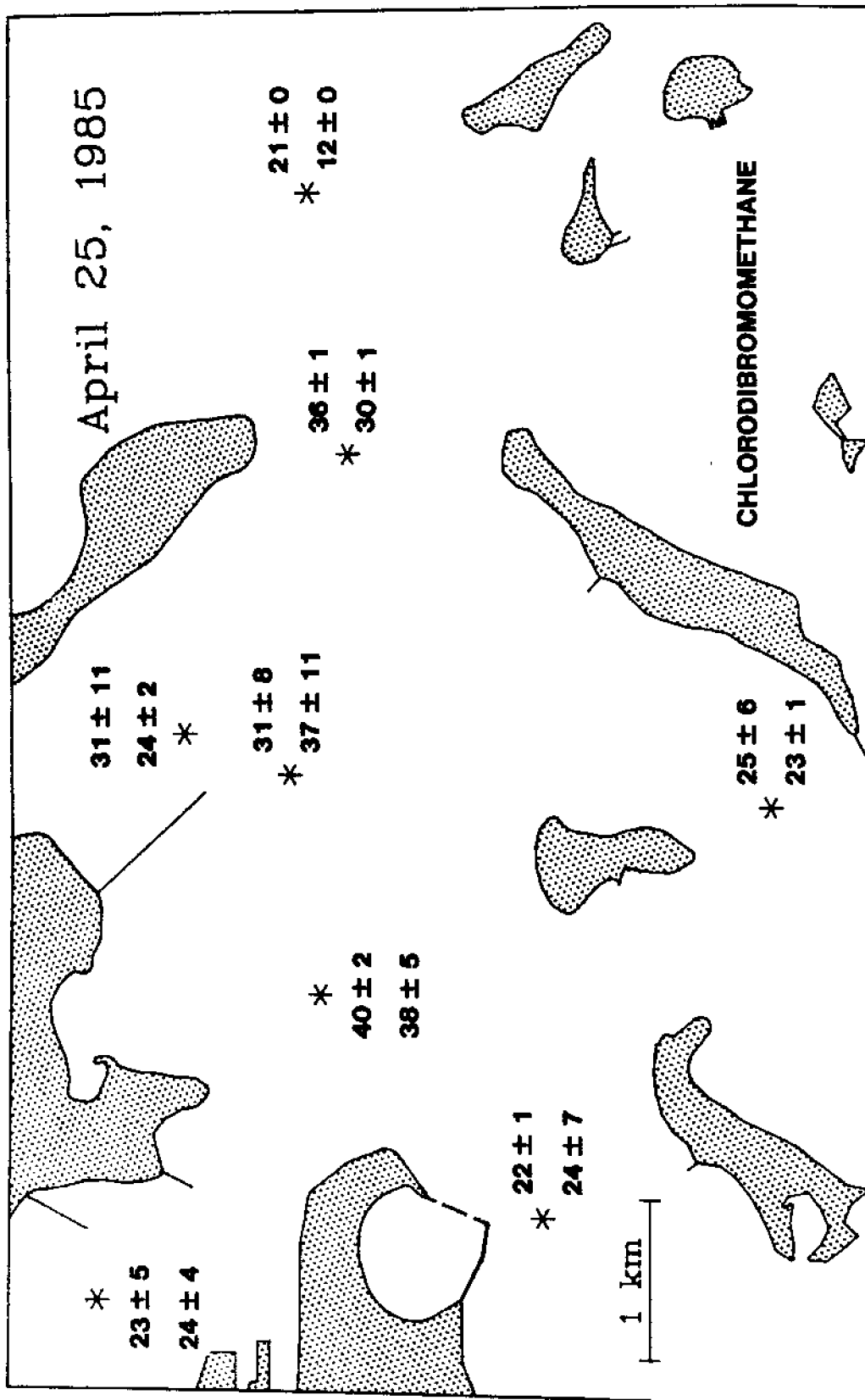
Figure 4.28 Tracer Concentrations in Boston Harbor (parts-per-trillion) at High Water Slack (surface and deep water measurements; mean of duplicates)
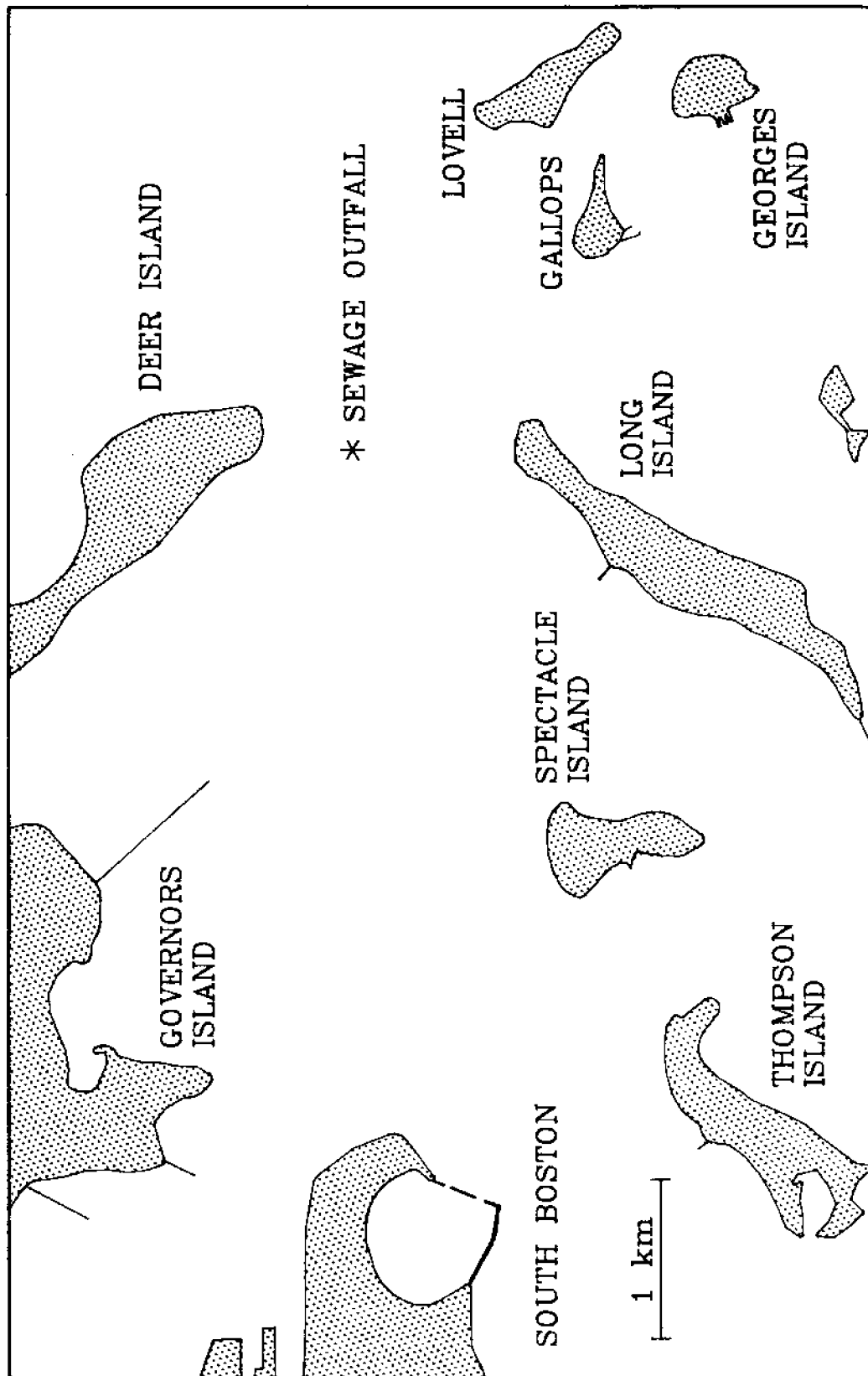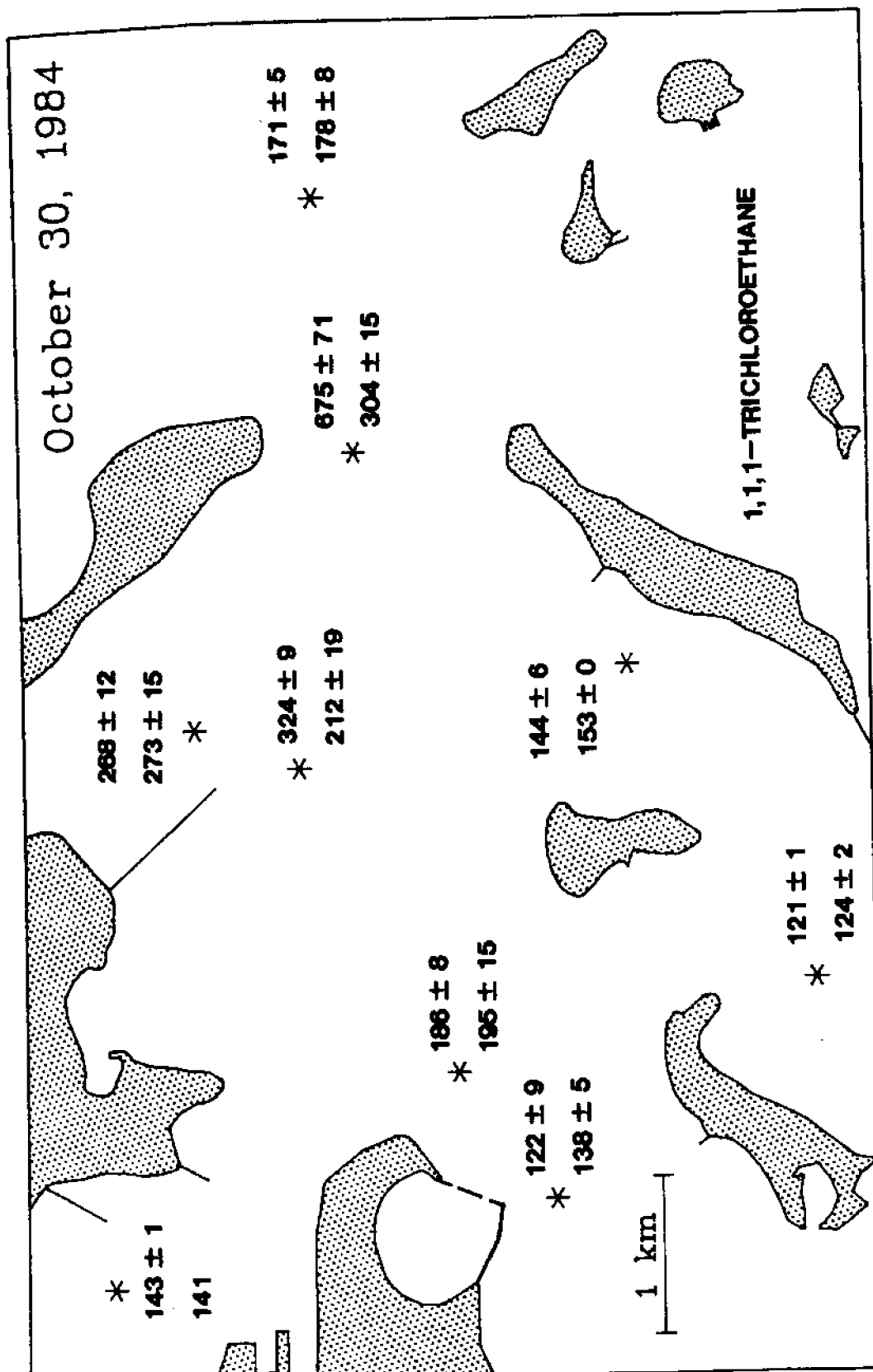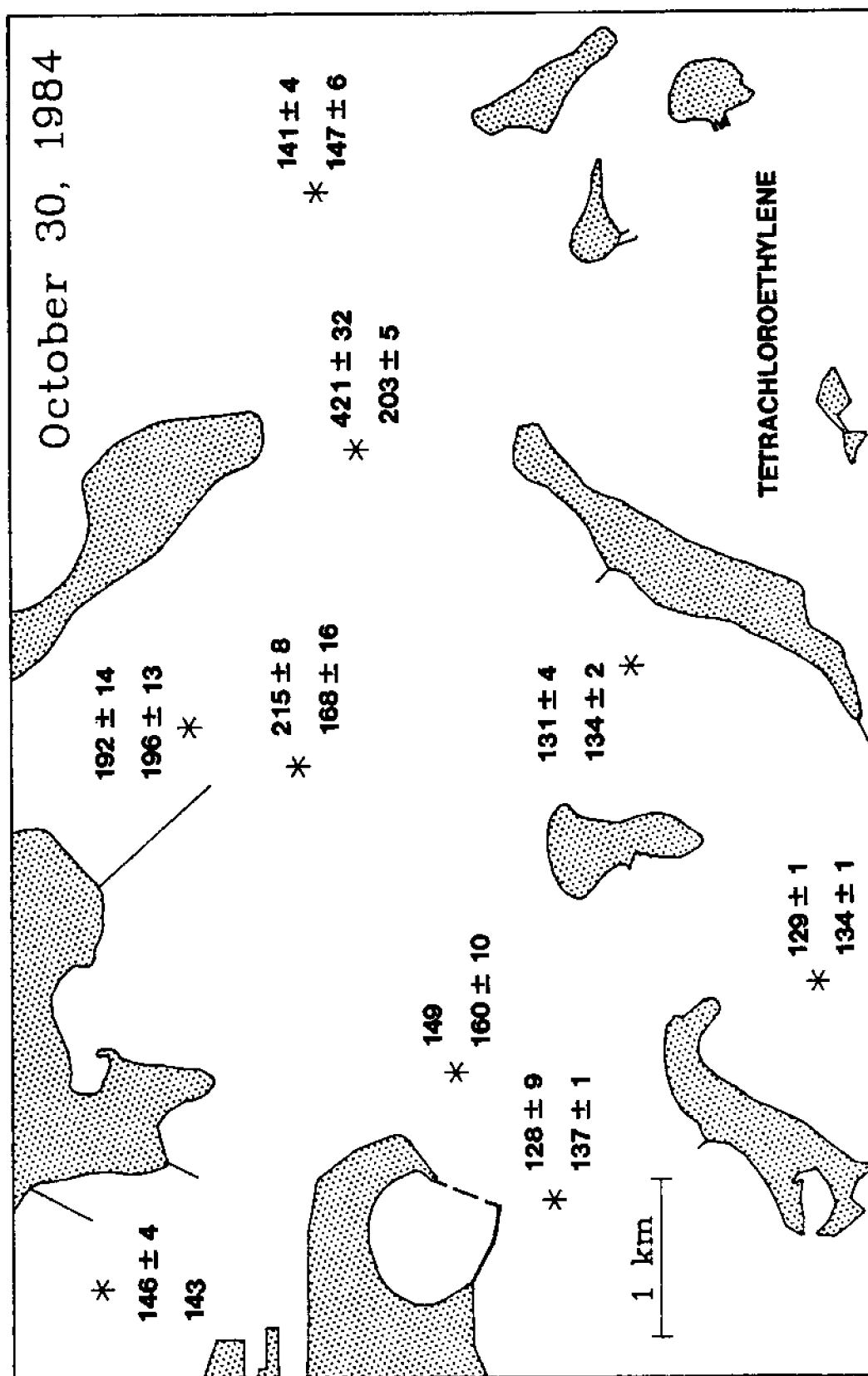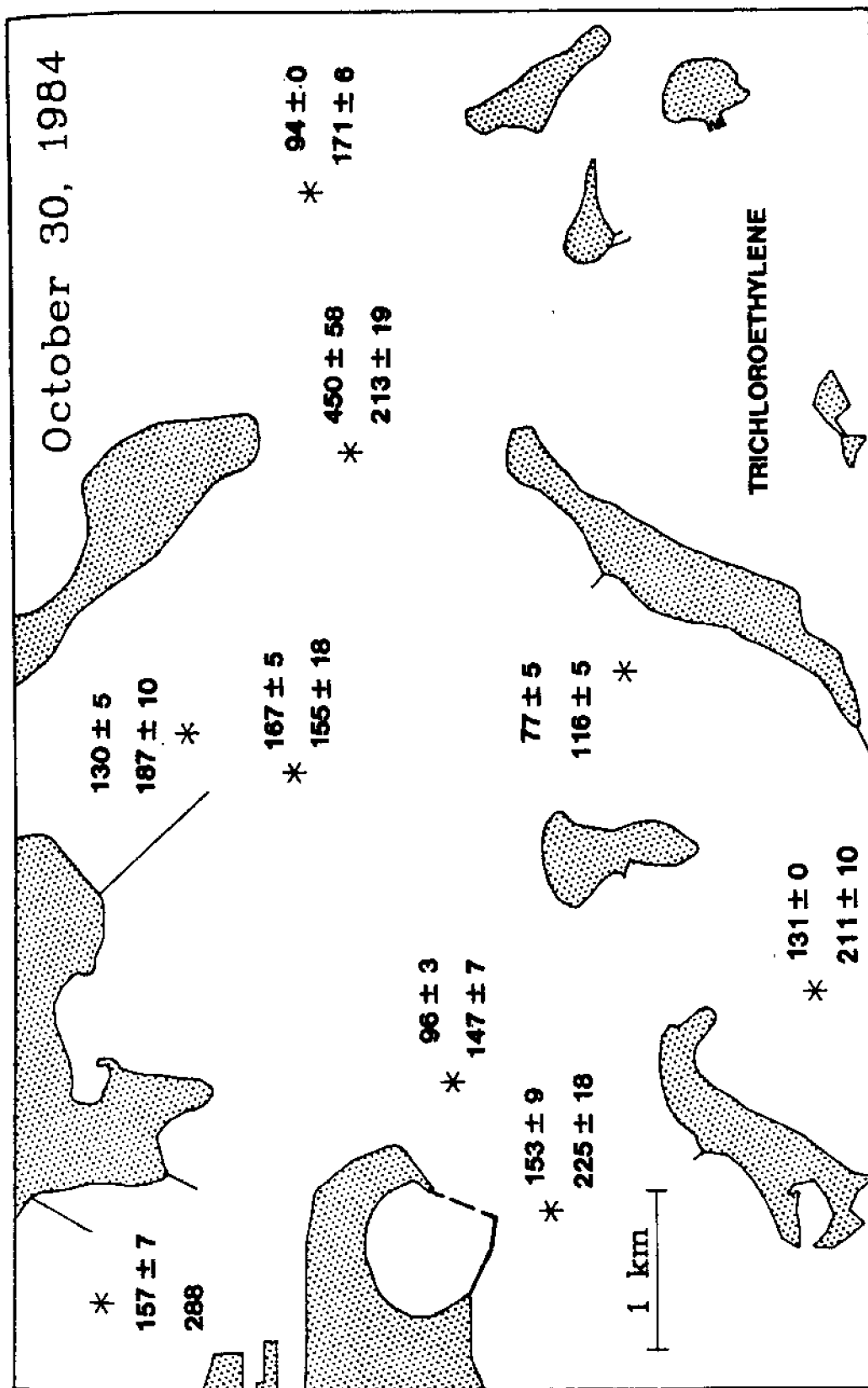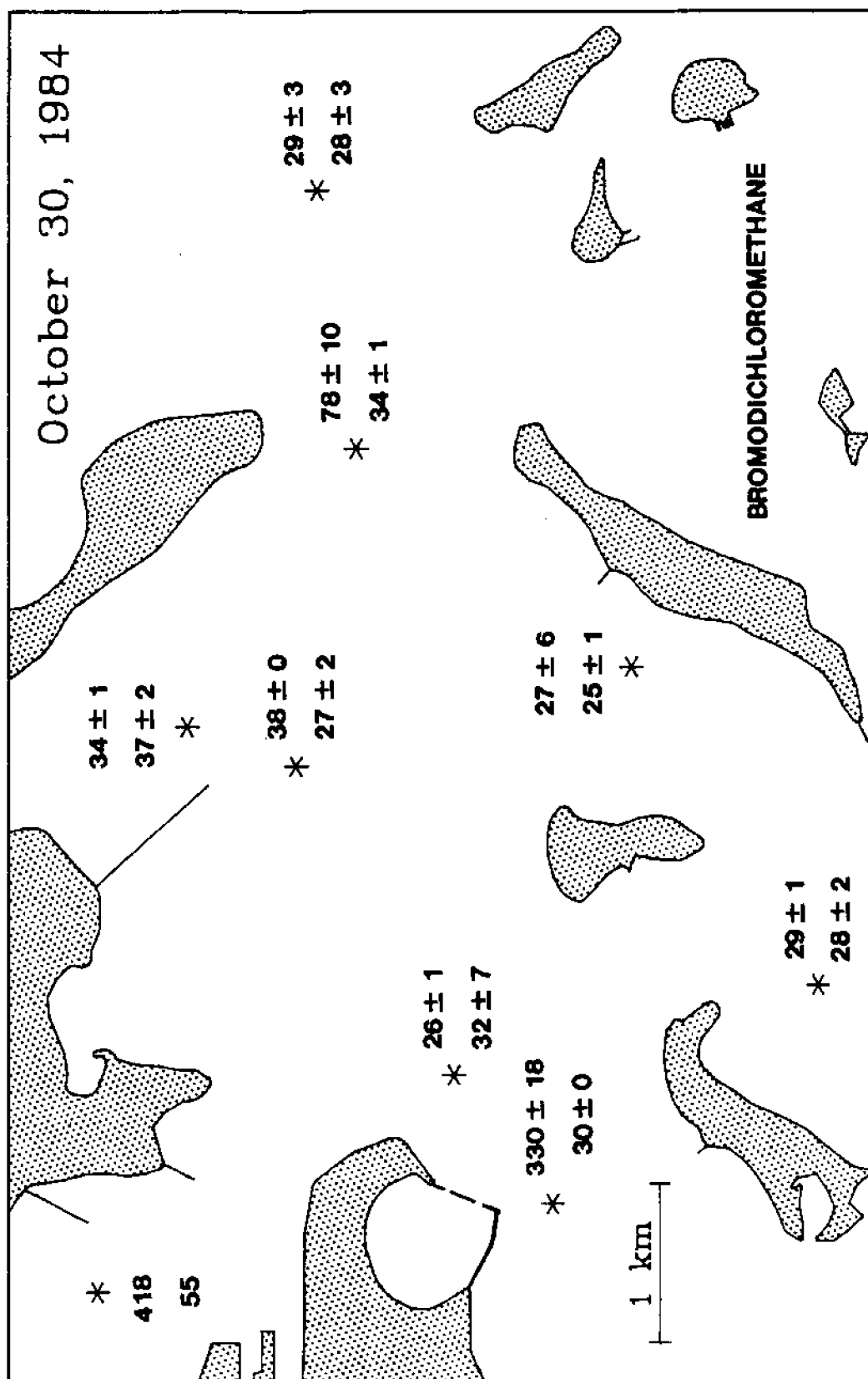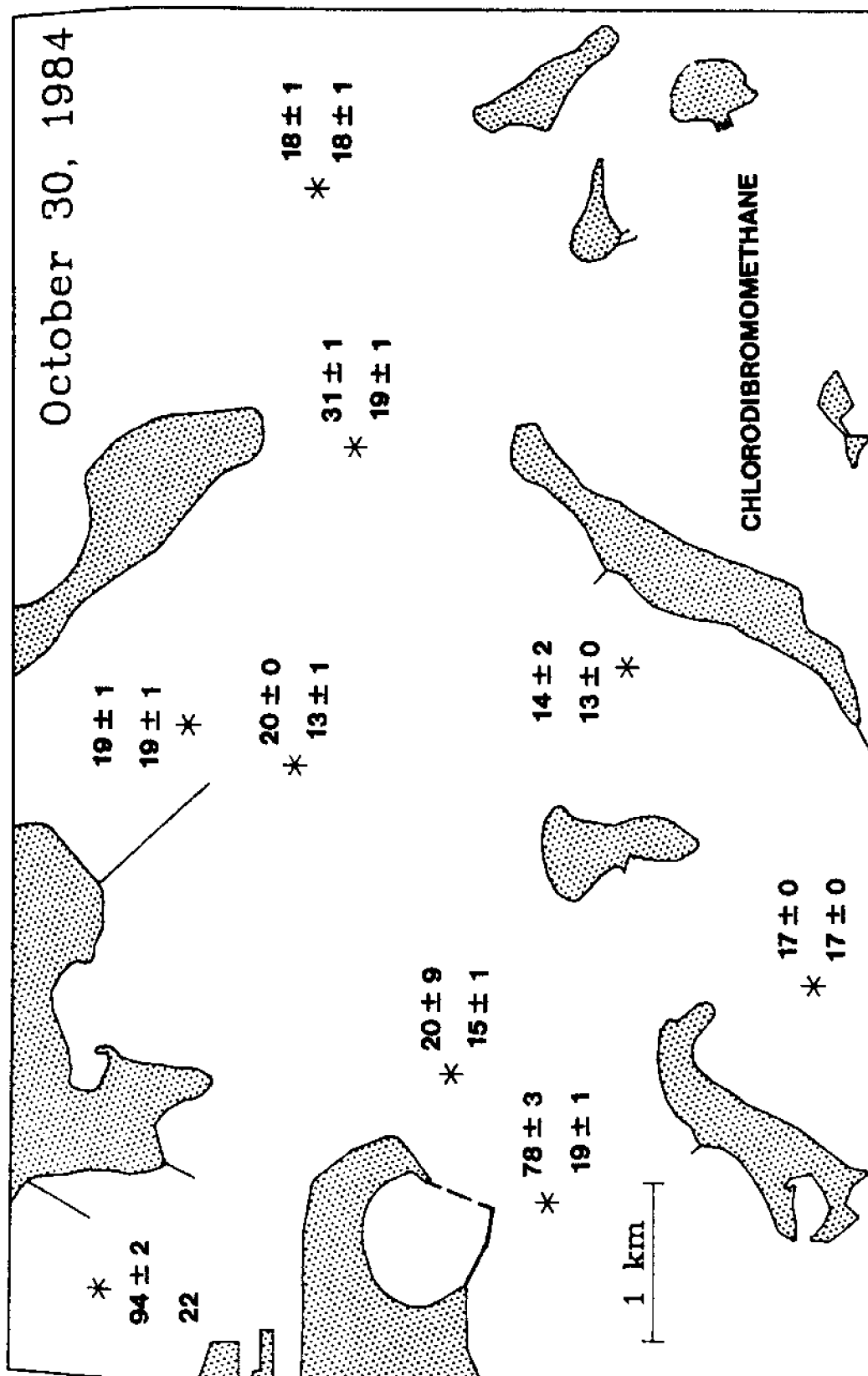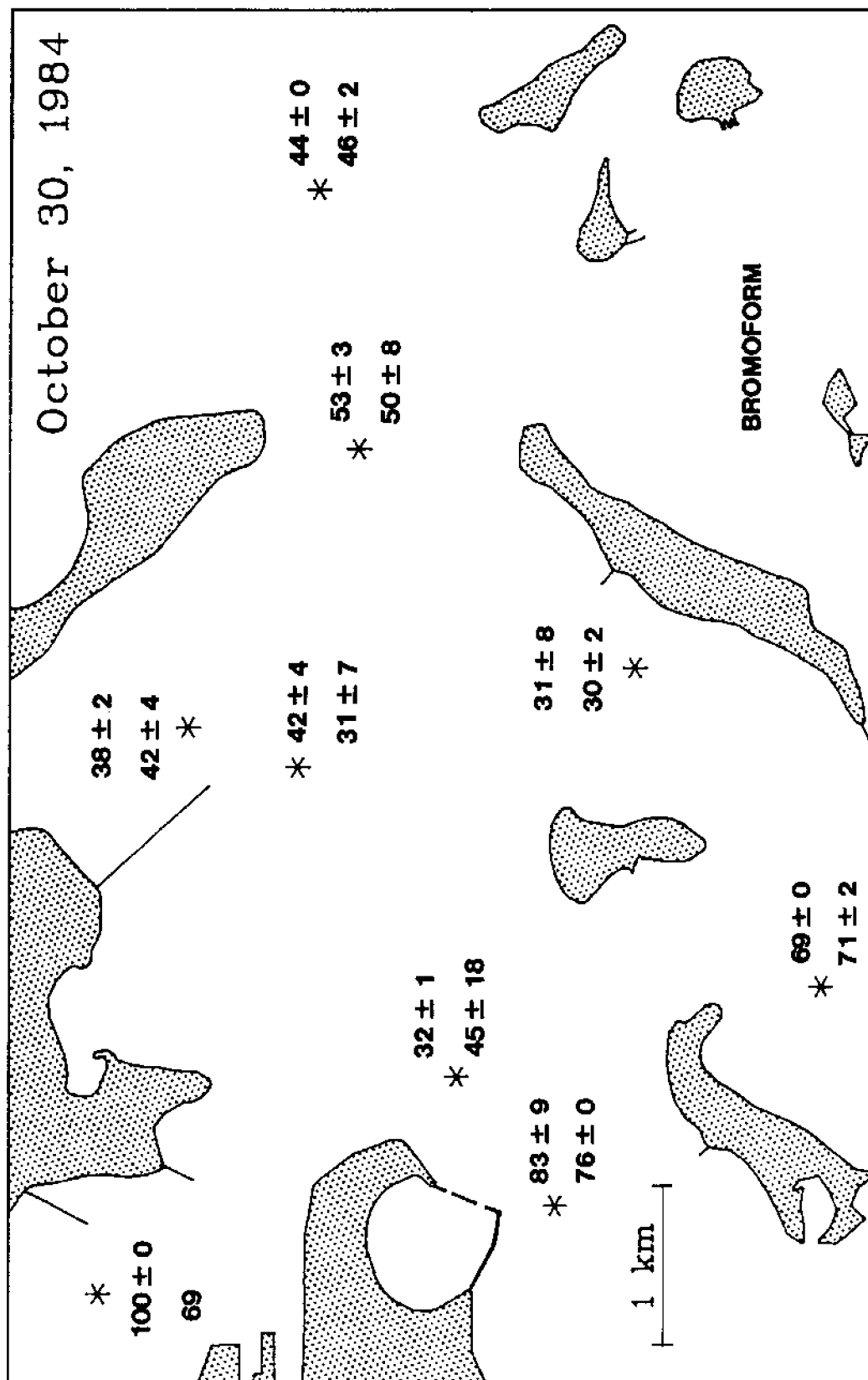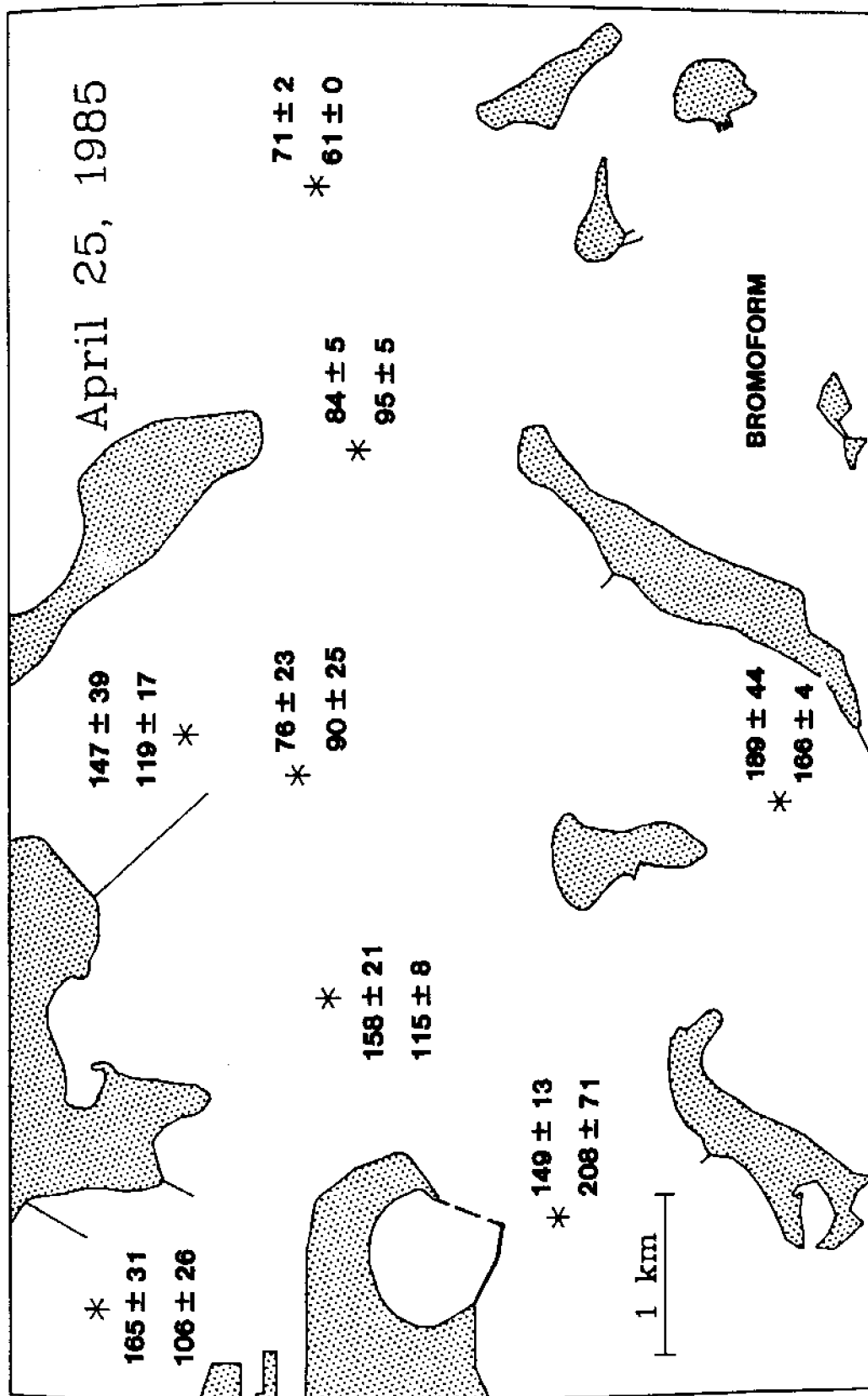
Figure 4.29 Tracer Concentrations in Boston Harbor (parts-per-trillion) at High Water Slack (surface and deep water measurements; mean of duplicates)

Based on these results, a number of important points can be made and several interesting conclusions can be drawn:

1) The average dilution of the VHOCs (and hence sewage effluent) in the immediate vicinity of the outfall ranges from 15 to 40×. (Note that this calculation is based on the concentration in the sewage effluent measured several hours prior to sampling, which, due to the source variability, would account for most of the variation from compound to compound on a given date.) These values are consistent with predictions obtained using near field jet models (e.g., Metcalf and Eddy, 1979b) and prior tracer measurements (Metcalf and Eddy, 1984).

2) In October, haloform concentrations in nearshore surface waters are drastically elevated relative to deeper waters and waters further out into the harbor. The solvents, on the other hand, do not follow this pattern. This is a result of the chlorination of combined stormwater and sewer overflows. The Charles River Estuary Facility, a major CSO located in the Inner Harbor, is presently one of only two CSOs in the harbor that chlorinates its discharges (which result from storms and Deer Island breakdowns). The facility discharged 2×10^4 m^3 of chlorinated effluent on October 29, the day before we sampled. The other two sampling dates, which were dry periods during which no chlorinated CSO releases were made, show no such effect. Although it is interesting that this suite of compounds allows one to distinguish between treatment plant and CSO inputs (and this in itself could be useful), it is clear that in order to avoid complicating the source

function of the THM tracers, one should sample during dry periods when CSO inputs are minimal. (These inputs would probably take several days to a week to become negligible.)

3) With the exception of the THMs in October, for most locations away from the buoyant plume, the surface and deep water concentrations are similar (within ~15%), implying that the water column is relatively well mixed. This is also supported by temperature data. This is the case even in July, when we expect the water column to be the most stratified (with respect to the other dates). This supports the validity of our two-dimensional modeling approach.

4) On all three dates, bromoform concentrations actually increase away from the outfall at Deer Island, suggesting the presence of another source on the western edge of the harbor. This is discussed in more detail in Chapter 6.

5) Throughout the sampling domain, the VHOC concentrations are, at most, only a few times lower than the concentration in the immediate vicinity of the outfall. This suggests that although tidal velocities are large, the harbor flushing efficiency is rather low and water essentially moves in and out without significantly exchanging with "clean" bay water.

6) Although the general concentration distributions are similar, there does appear to be some variability from compound to compound and date to date. This could be due to variations in physical mixing and volatilization rates from date to date (due to environmental conditions) and variations in volatilizaiton rates from compound to compound (due to

their physiochemical parameters). It is difficult to say much more, however, without ancillary information regarding the physical mixing processes.

Although these rather qualitative conclusions are interesting and quite useful in and of themselves, more quantitative information can be obtained by using the VHOC measurements in conjunction with modeling efforts. This is discussed in Chapters 5 and 6.

Chapter 5

Application of Numerical Models to Boston Harbor

The mathematical models used to simulate pollutant transport in Boston

Harbor were presented in Chapter 3. In this chapter, the specific applica-

tion of these models to Boston Harbor is described. After first briefly

discussing previous modeling efforts, the computational domain is defined

and the various input parameters for TEA and ELA are described. In addi-

tion, the results of the model simulations are presented, and based on

these results, some qualitative conclusions regarding pollutant transport

in the harbor are drawn.

5.1 Previous Modeling Efforts

Due to the great complexity of the Boston Harbor system, it has been

recognized for some time that a thorough analysis of water quality problems

in the harbor would require the use of mathematical models. An initial

modeling effort was carried out by Hydroscience, Inc., (1971) to model the

effects of both Deer Island discharges and the combined sewer overflows.

This simple modeling effort represented harbor hydrodynamics as a combina-

tion of freshwater advection and tidally-averaged dispersion. A more real-

istic approach followed (Hydroscience, Inc., 1973) which utilized a formal

hydrodynamic model in conjunction with the advection-diffusion model em-

ployed previously. Calibration was based on circulation information ob-

tained by the National Ocean Survey in 1971. Nevertheless, these analyses

were restricted by computational expense.

In the early 1970s researchers at MIT developed a set of finite element computer models (CAFE and DISPER) and began to apply them to Massachusetts Bay (Connor and Wang, 1973; Leimkuhler, 1974; Wang and Connor, 1975; Christodoulou et al., 1976). These efforts were primarily concerned with the NOMES (New England Offshore Mining Environmental Study) project, and as such, made no effort to specifically model Boston Harbor. Pagenkopf et al. (1976) applied the models with high resolution in Duxbury Bay and Plymouth Harbor as part of an environmental impact assessment of the Pilgrim Nuclear Power Station at Rocky Point.

Metcalf and Eddy (1979b) conducted a comprehensive modeling study using CAFE and DISPER as part of the 301(h) Waiver Application filed by the Metropolitan District Commission with the EPA. Since their objective was to predict the effect of a proposed outfall located seven miles offshore of Deer Island, calibration focused on hydrodynamic observations near this site. Metcalf and Eddy (1982) later concentrated their modeling efforts on the harbor area itself. However, the computational grid was fairly coarse and the analysis did not include additional field surveys to address the specific needs associated with calibration of the new grid, having been intended only as a coarse screening of a number of widely varying discharge alternatives.

A more refined harbor modeling study was carried out by EG&G (1984a), again using CAFE and DISPER. An attempt was made to better resolve the complex geometry of the harbor. Modeled circulation results were compared to NOAA Tidal Current Charts and measured drogue tracks. While agreement

was not exact, the main features of the circulation pattern were repro-
duced. No attempt was made to validate the transport model.

Unfortunately, these studies have suffered from two major drawbacks:
1) the use of CAFE and DISPER precluded the use of a finely resolved grid
within the harbor and the possibility of long simulations due to the re-
quirement of small timesteps dictated by stability constraints associated
with the numerical solution technique used in CAFE (e.g., CAFE is typically
run for only one tidal cycle); and 2) although some attempts were made to
verify the accuracy of the circulation model, little or no attempt was made
to validate the transport model. In as much as the ultimate goal of model-
ing efforts such as these is to predict contaminant concentrations, it
seems essential that complementary tracer experiments be obtained in order
to accurately calibrate (and validate) the transport model.

The present work makes an effort to address both of these limitations.
The use of TEA and ELA allows one to better resolve the complex geometry of
the harbor and run long simulations without incurring large computational
expense. Furthermore, emphasis is placed on calibrating the transport
model against chemical tracer experiments, rather than only comparing
results of the circulation model to hydrodynamic measurements.

5.2 The Finite Element Grid

Before the domain could be discretized into finite elements, it was
necessary to establish the location of the outer ocean boundary. As point-
ed out by Wang and Connor (1975), there are a number of considerations that
must be kept in mind when deciding where to create this artificial boun-

dary. First, the location should be chosen where data are available for use as boundary conditions. Second, in as much as we expect any such data to be only approximate, boundaries should be chosen as far away from the area of interest as possible. Finally, since the effect of wind on the boundary condition may be significant, the boundary should be established in deep water if possible.

In light of these considerations, we chose to model the entire Massachusetts Bay with a relatively coarse grid while applying high resolution to the harbor itself. Figure 5.1 illustrates the finite element grid. The majority of this grid has land boundaries. The open-ocean boundary extends linearly from Cape Ann to Cape Cod. This boundary has been studied to some extent (Pagenkopf et al., 1976) and Tide Table information is available at the edges.

A detail of Boston Harbor is shown in Figure 5.2, illustrating the level of grid resolution. As can be seen, the characteristic length scale of an element varies from 10 km in the outer bay to several hundred meters in highly resolved portions of the harbor. High resolution is applied in areas of high concentration gradient (e.g., near outfalls) and between islands. The resolution within the harbor is greater than in any previous modeling efforts (e.g., EG&G, 1984b).

The grid consists of 888 elements having 552 corner nodes. The circulation model is applied to this entire grid. The domain of the transport model, on the other hand, consists only of the elements shown in Figure 5.2. This detailed grid of Boston Harbor contains 694 of the original 888 elements. Since ELA utilizes quadratic rather than linear basis functions,
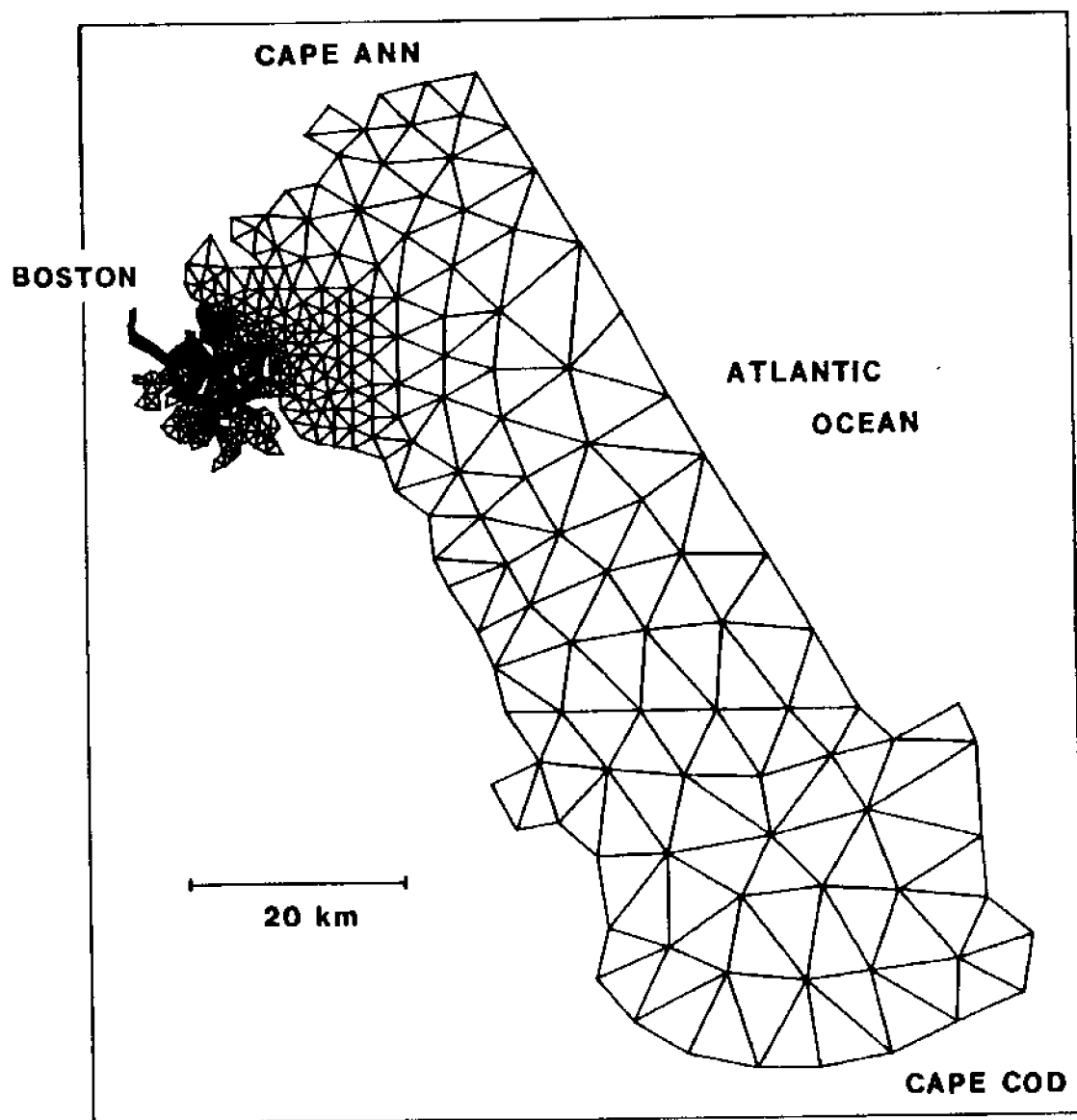
Figure 5.1   Finite element grid of Massachusetts Bay
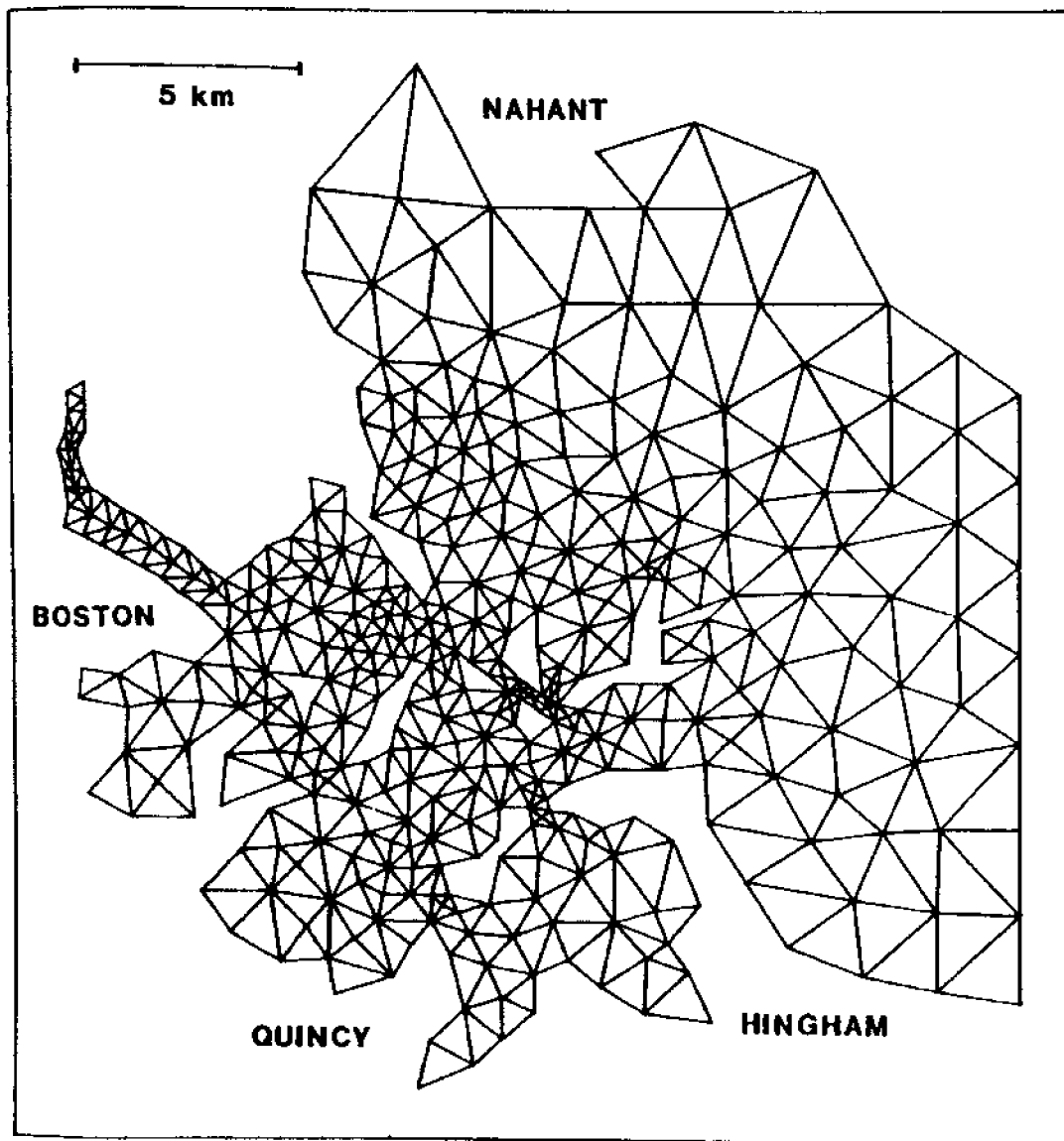
Figure 5.2 Finite element grid - detail of Boston Harbor

there are six nodes associated with each element (three corner nodes and three nodes bisecting the sides). This quadratic grid has a total of 1575 nodes.

5.3 Application of TEA to Massachusetts Bay

A representative record of current velocity in Boston Harbor is shown in Figure 5.3. EG&G (1984a) harmonically analyzed a number of current meter records (of which Figure 5.3 is a representative sample) to extract the periodic constituents attributable to the tides. They concluded that although the magnitude of the non-tidal or residual signal varies from location to location, its influence on the overall variance in current velocity is minor. That is, the tides account for a large proportion of the total variance of the record. Moreover, it is apparent from Figure 5.3 that the semidiurnal (M_2) tide dominates the observed pattern. A spring/ neap cycle (with a period of around 2 weeks) is also discernible. The harmonic analyses indicate the the M_2 constituent accounts for 60 to 70% of the observed variation in tidal velocity (Table 5.1).

Although tidal velocities are an order of magnitude greater than non-tidal (residual) velocities, it is the net or residual circulation, rather than the mean tidal circulation, that governs the eventual fate of pollu-tants and the flushing efficiency of a coastal embayment (Cheng and Casul-li, 1982). Processes contributing to the residual circulation include local bathymetry, low frequency forcings due to wind or large scale cur-rents, and nonlinearities and interaction between several forcing frequen-cies. If these processes were unimportant, the tide would only serve to
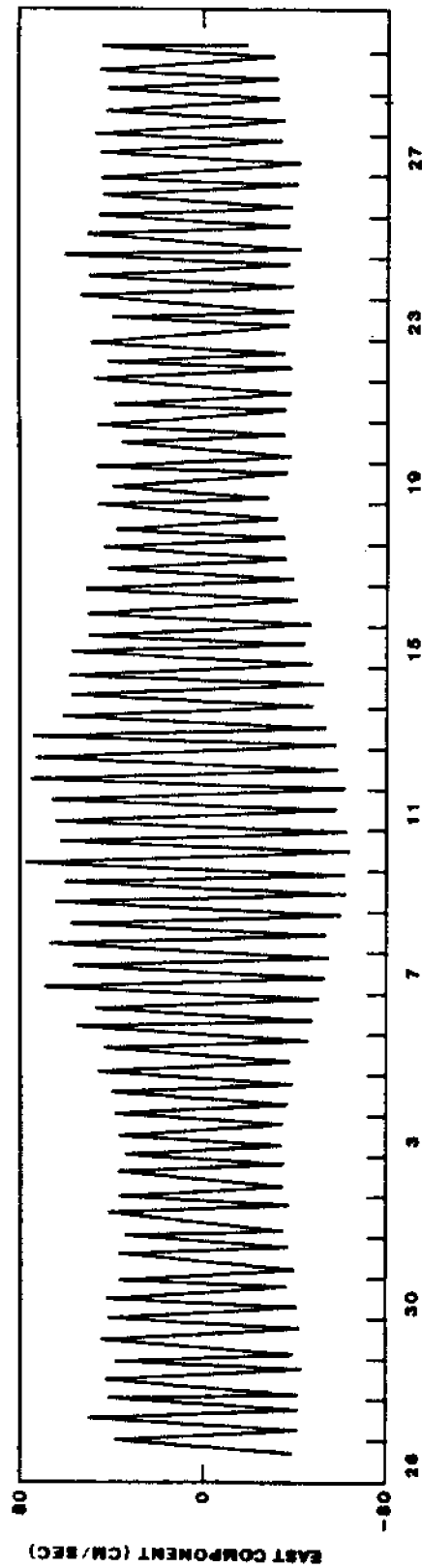
Figure 5.3 East Component of Current Meter Record Approximately 3 km East of Deer Island Light (EG&G, 1984b)

Table 5.1

Results of Harmonic Analysis of Current Meter Records
at a Site Approximately 1 Mile East
of Deer Island Light

Date	Depth†	Major axis amplitude (cm/sec)		
		Total*	M_2	$\%M_2$
6/17/83--7/20/83	15 ft	74.69	49.89	67
7/26/83--8/30/83	15 ft	79.42	47.90	60
8/ 3/83--10/6/83	15 ft	77.40	45.72	60
6/17/83--7/18/83	45 ft	43.66	25.50	58

† relative to mean low water

* sum of Q_1, O_1, M_1, K_1, J_1, MU_2, N_2, M_2, L_2, and S_2 tidal
constituents

(from EG&G, 1984b)

move water parcels back and forth producing no net movement. Although it
is difficult to quantify the effects of complex bathymetry and nonlinear
interactions, previous studies (Pagenkopf et al., 1976; Metcalf and Eddy,
1984) have noted the importance of low frequency forcings on the net circu-
lation patterns.

Residual circulation is best illustrated by simulating particle tra-
jectories in which a parcel of water is tracked through several tidal
cycles. To do so, linear TEA was run using only the M_2 tide as a forcing
function (detailed input parameters will be presented below). Figure 5.4
traces the path of two water parcels over four tidal cycles. Parcel A was
released at high tide while parcel B was released at low tide. Note that
parcel A essentially returns to its original position after four cycles
while parcel B exhibits a net northerly drift. This may be due to the
complex bathymetry within the harbor, which could generate some residual
circulation (errors in TEA could also be partially responsible for this
effect). The bathymetry of the outer harbor is much more regular, and in
the absence of any other forcing functions, very little net circulation is
produced.

This point is again illustrated in Figure 5.5. Again two particle
trajectories are shown, one starting at high tide (A), the other at low
tide (B). In this case, the particles originate from a point well outside
of the inner harbor. Due to the regular bathymetry of this region, little
net circulation is exhibited.

For the simulation in Figure 5.6, a steady southerly current was
superimposed on the M_2 tide. The current was generated by imposing a line-

Figure 5.4   Particle Trajectories Over Four Tidal Cycles (M_2 forcing only)

A RELEASED AT HIGH TIDE

B RELEASED AT LOW TIDE

NAHANT

DEER ISLAND
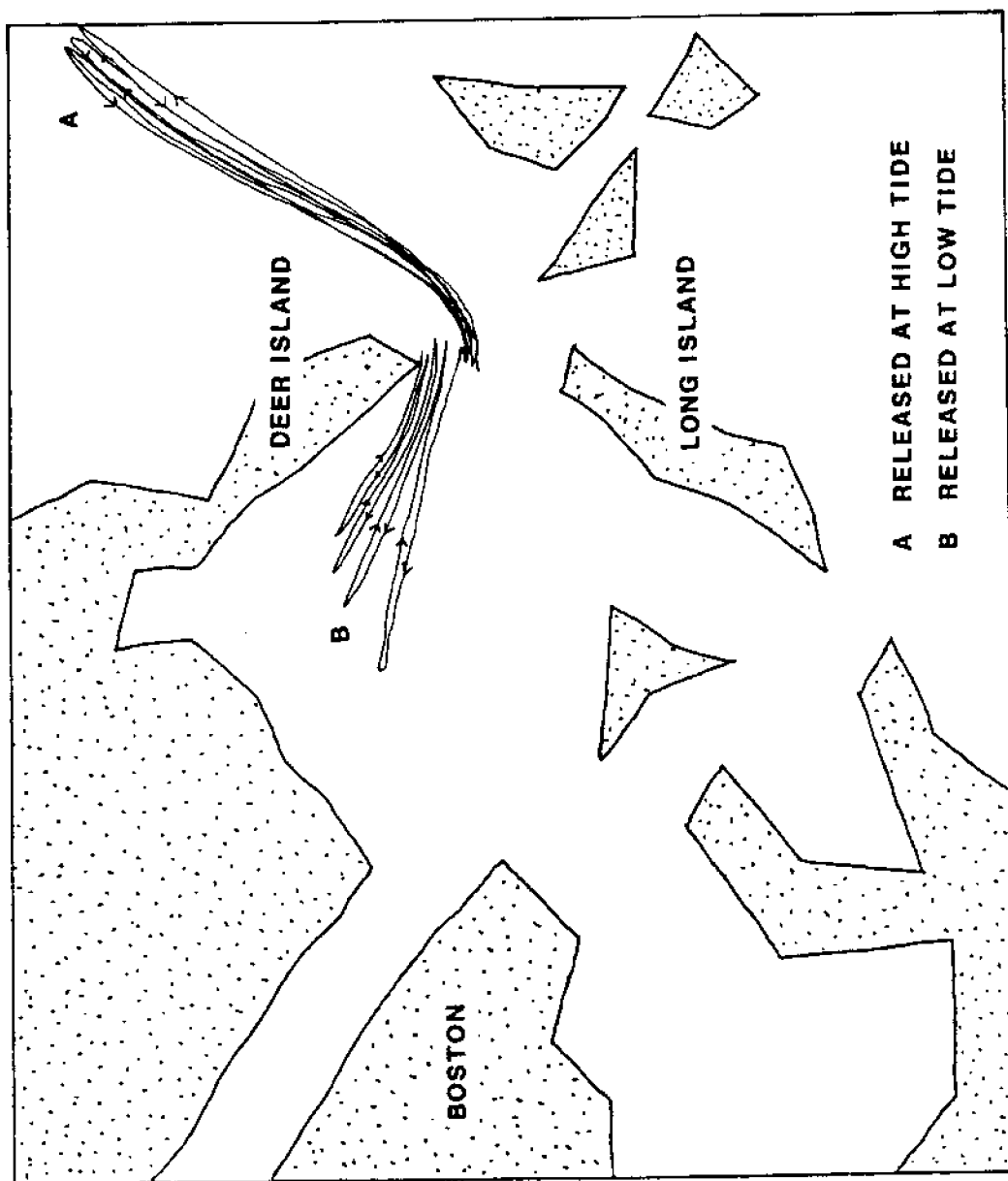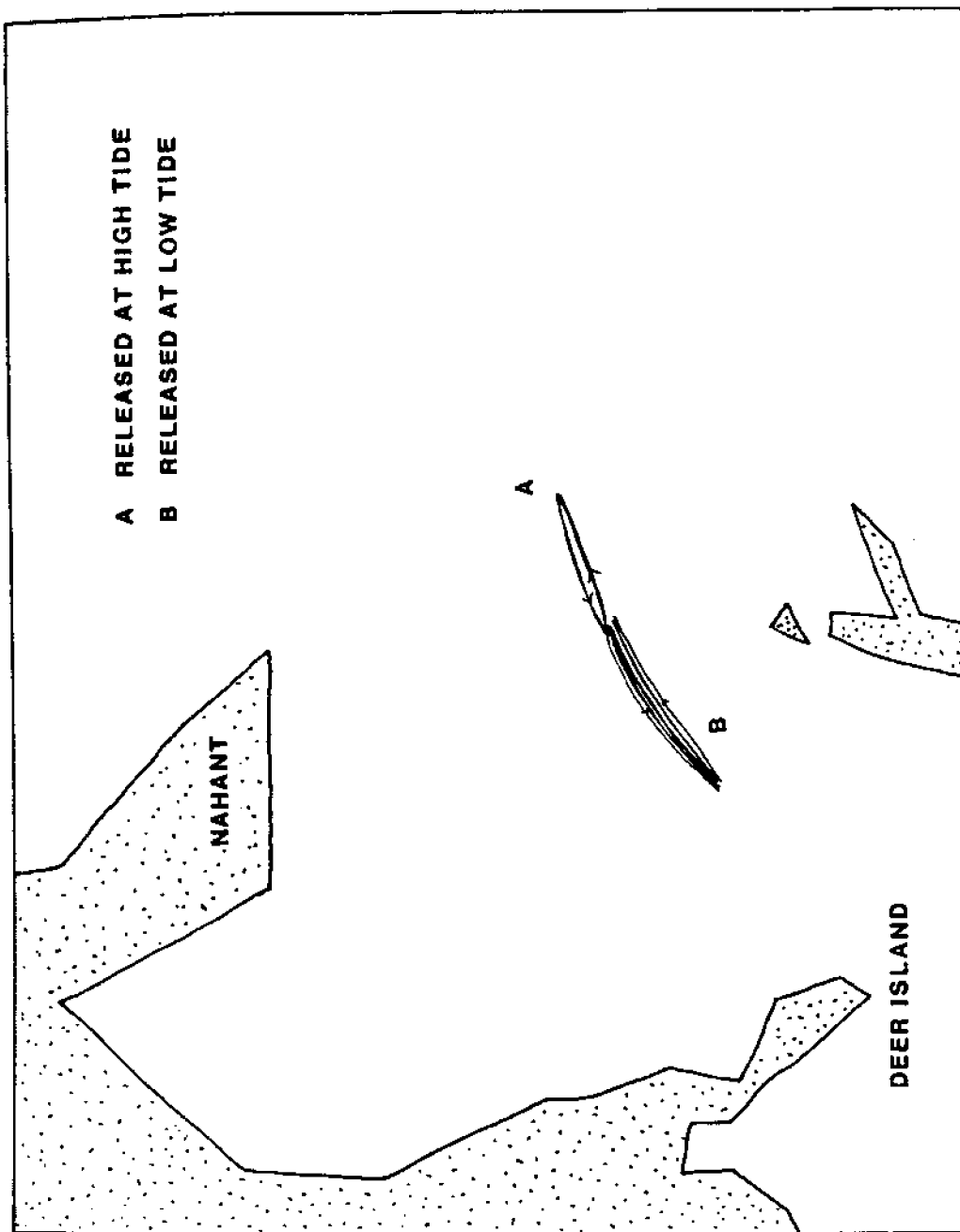
Figure 5.5   Particle Trajectories Over Four Tidal Cycles (M_2 forcing only)

A RELEASED AT HIGH TIDE

B RELEASED AT LOW TIDE

NAHANT

DEER ISLAND
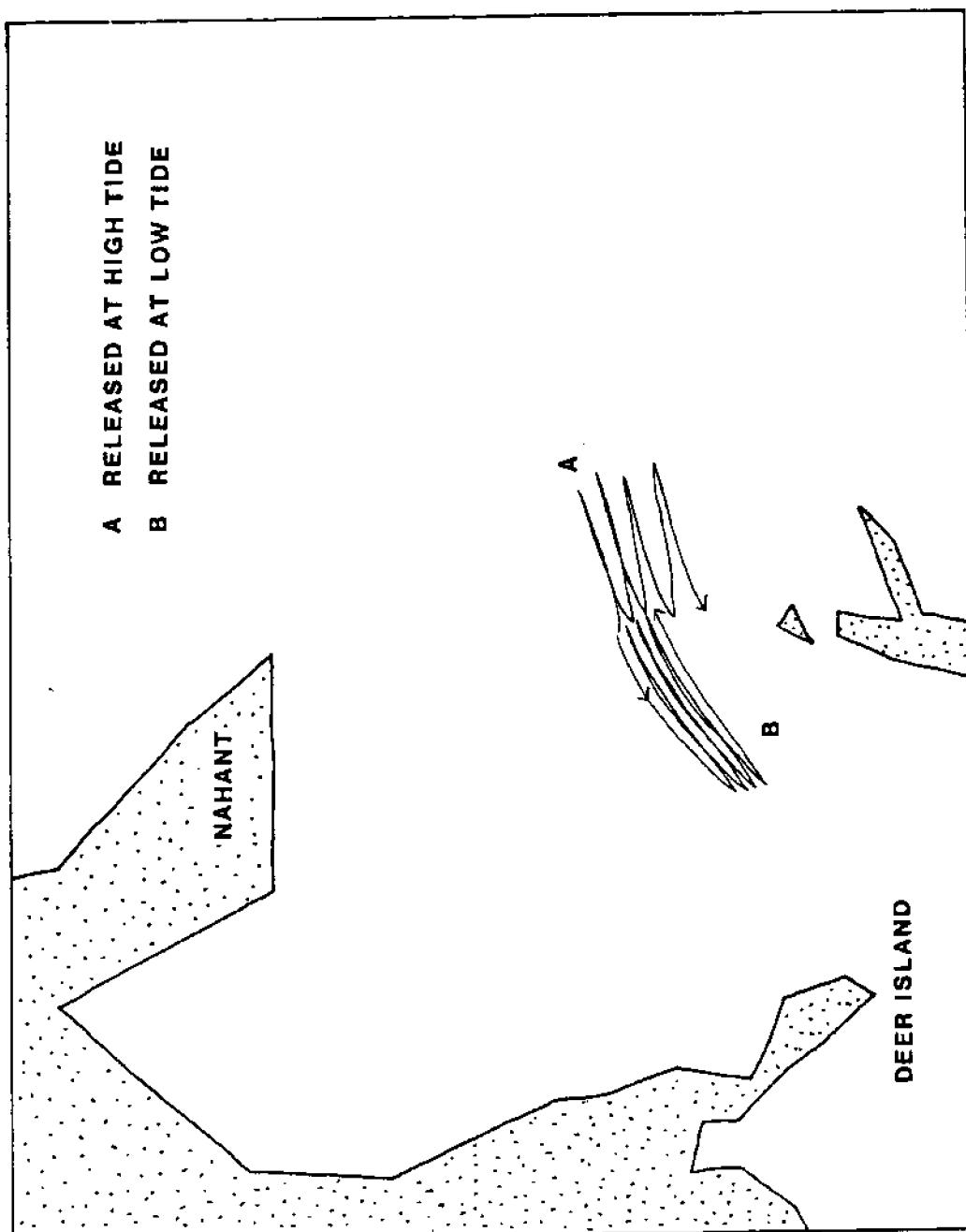
Figure 5.6 Particle Trajectories Over Four Tidal Cycles (M_2 forcing with steady southerly current superimposed)

ar elevation gradient (relative to mean water level) along the ocean boundary ranging from 0.00 m at Cape Cod to 0.04 m at Cape Ann (Wang and Connor, 1975) and forcing the system at zero frequency. This results in a net southerly drift, as expected, and to the extent that this is a representative elevation gradient, serves to illustrate the magnitude of the effect steady forcings can have on net circulations. Although these forcings have little effect on the instantaneous velocities, their influence on the net circulation can be significant. (Particle trajectories are not sensitive to wind since TEA produces depth-averaged circulation patterns, which are insensitive to wind effects. However, wind is important in creating vertical shear, which, in turn, is modeled as dispersion.)

Unfortunately, field data suggest that both observed net drift and low frequency forcings which could cause the drift tend to be seasonally variable and unpredictable in Boston Harbor and Massachusetts Bay. The variability in wind is illustrated in Figure 5.7. With respect to steady currents, Metcalf and Eddy (1984) noted that although there appears to be a bias for a long-term southerly current, in the short term (depending on weather conditions and seasonal changes) net drift in any direction is possible.

As has been pointed out in Chapter 3, we chose to use the linear version of TEA in this work. As has been illustrated above, nonlinear interactions undoubtably play an important role in producing the residual circulation in Boston Harbor and such effects cannot be adequately modeled by linear TEA. However, it was felt that linear TEA could accurately represent the major features of the circulation pattern, and that a de-
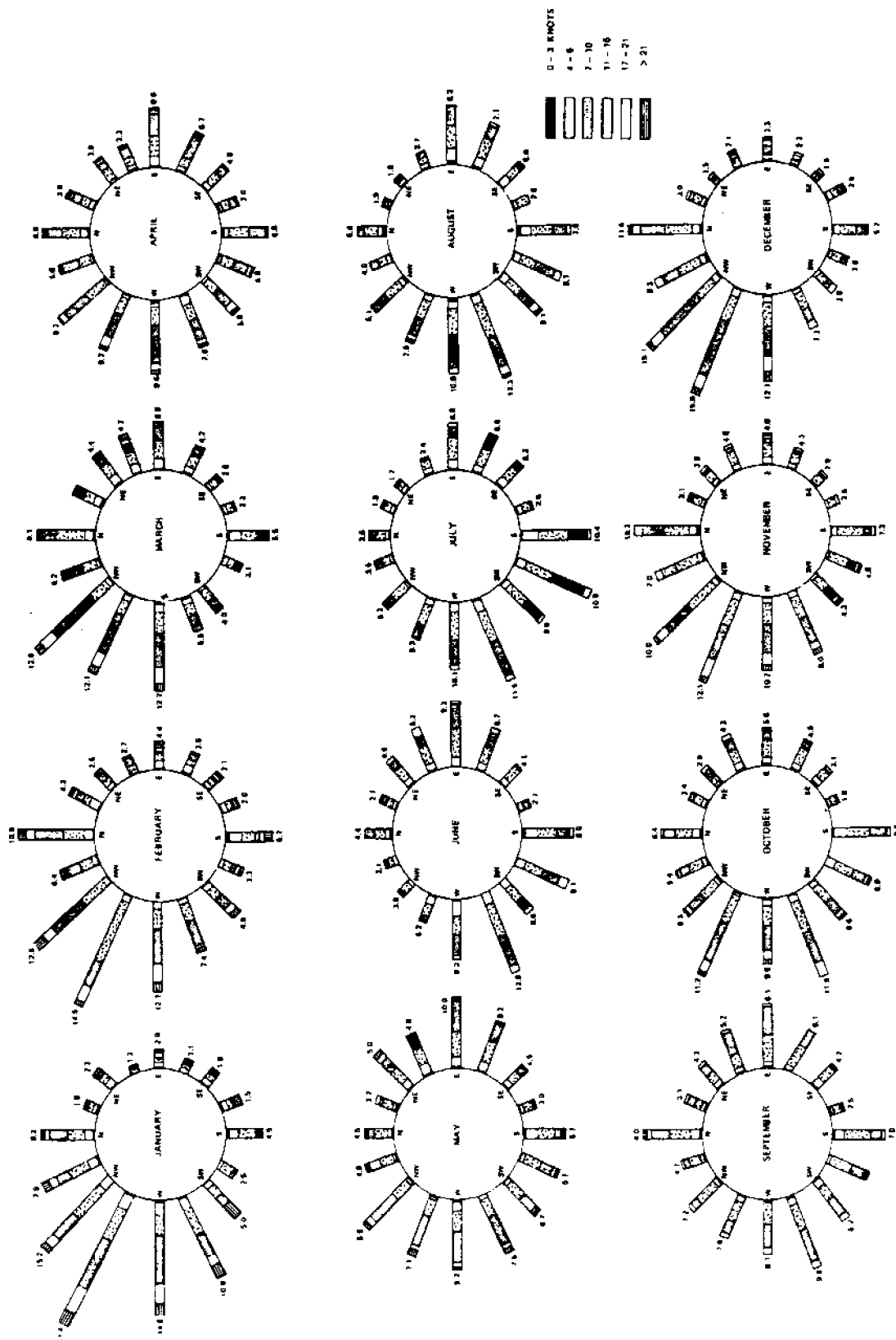
Figure 5.7 Wind Roses from Historical Data (Metcalf & Eddy, Inc., 1979b)

tailed attempt to model and validate the residual circulation was beyond the scope of the present work.

Such a decision was ultimately based on the following factors: 1) the field data necessary to validate and calibrate the residual circulation modeled by nonlinear TEA do not presently exist; 2) residual circulation appears to be quite sensitive to low frequency forcings, which are variable, unpredictable, and difficult to model, and it is likely that nonlinear tidal dynamics are no more important in driving the residual circulation than these highly variable low frequency forcings; 3) the use of nonlinear TEA would have increased computational expense by several orders of magnitude. Not only is linear TEA considerably less expensive than nonlinear TEA, but, more importantly, it facilitates the incorporation of efficiency procedures within the transport model ELA which account for tremendous savings in calculations involving periodic circulation (Section 5.4).

Furthermore, given: 1) the variabilty in the low frequency forcings as indicated above; 2) the absence of historical data to calibrate the resulting residual circulation; 3) the fact that our chemical data were collected within the harbor (as opposed to in the outer bay which would be more sensitive to low frequency forcing); and 4) the predominance of the M_2 consitituent in current records, we chose to simulate circulation using the semidiurnal (M_2) constituent as the only forcing function. In making this approximation, we were, in effect, choosing to model only the major features of the advective velocity field with TEA. The additional mixing, not explicitly accounted for by the circulation model, is then represented

through the use of an elevated, seasonally dependent dispersion coefficient within the transport model.

Having made this decision, it was then only necessary to decide upon appropriate boundary conditions. Due to a lack of data along the open ocean boundary, several simplifying assumptions were made. The tidal amplitude was prescribed as varying linearly from 1.31 m at Cape Ann (Gloucester) to 1.37 m at Cape Cod (Race Point). Furthermore, it was assumed that the tide was in phase all along the ocean boundary. These choices were based on records of mean tide level and high water phase shifts at Gloucester and Race Point (NOAA, 1984). The system was then forced at a frequency ω, where

$$\omega = 2\pi/T \qquad\qquad (5.3.1)$$

and T = 12.4 hrs. The linearized bottom friction factor was taken as 0.00488 m/s (Westerink, 1984b).

In light of the fact that calibration of a dispersion coefficient within the transport model would, to some extent, account for inadequacies in the simulation of the advective velocity field, and that hydrodynamic field data in the harbor are sparse (some Eulerian data, no good Lagrangian data), no attempt was made to specifically fit modeled circulation results to field measurements. Nevertheless, in order to assure ourselves that we were representing the major features of the circulation pattern, qualitative comparisons were made against measured currents reported in Tidal Current Charts (NOAA, 1974) and records of mean tide level at a number of

-126-

stations (NOAA, 1984). Figures 5.8 through 5.11 show simulated current velocities in Boston Harbor at four different times within the semidiurnal cycle. (Note that at some points along the shoreline, TEA allows some leakage onto land. This is because TEA treats flux boundary conditions as natural rather than essential and hence allows some error.) Figure 5.12 though 5.15 illustrate the corresponding velocities from Tidal Current Charts. (These velocities represent the current at the time of spring tides, and should therefore be somewhat larger than our simulated velocities which are based on mean tidal amplitudes. They can be scaled down accordingly by multiplying by a factor of about 0.7.) As can be seen, the simulated velocities compare favorably. Table 5.2 contains recorded mean tide levels at a number of stations from Cape Ann to Cape Cod. These stations are supermimposed on simulated tidal amplitudes in Figure 5.16. Again, the comparison is qualitatively good. (Tidal phases could have been treated analogously. However, the corresponding M_2 phase observations were not readily obtainable.)

Hence, it appears that linear TEA does accurately represent the major features of the mean circulation pattern. Of course, use of only the M_2 tide results in some inaccuracies, including overprediction of tidal excursions (and velocities) during neap tide and underprediction during spring tide. However, given the scope of the present study, it appears that our results provide a reliable basis for the application of the transport model, ELA, to Boston Harbor. Nevertheless, the importance of the residual circulation cannot be overemphasized and future studies (employing nonlinear TEA and low frequency forcings) should focus on this.

1 KNOT
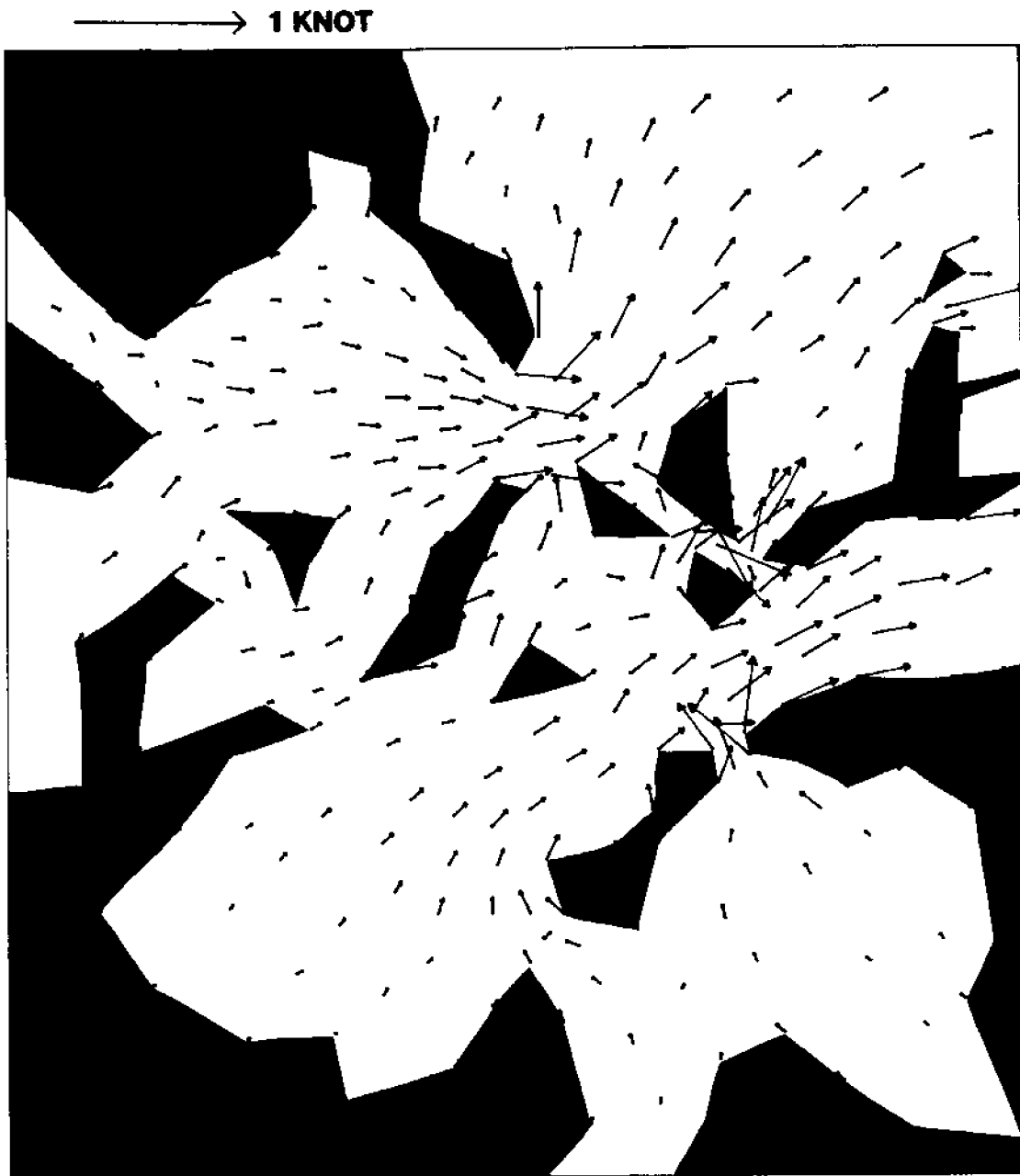
Figure 5.8 Simulated Current Velocities in Boston Harbor
1 Hour After High Tide

1 KNOT
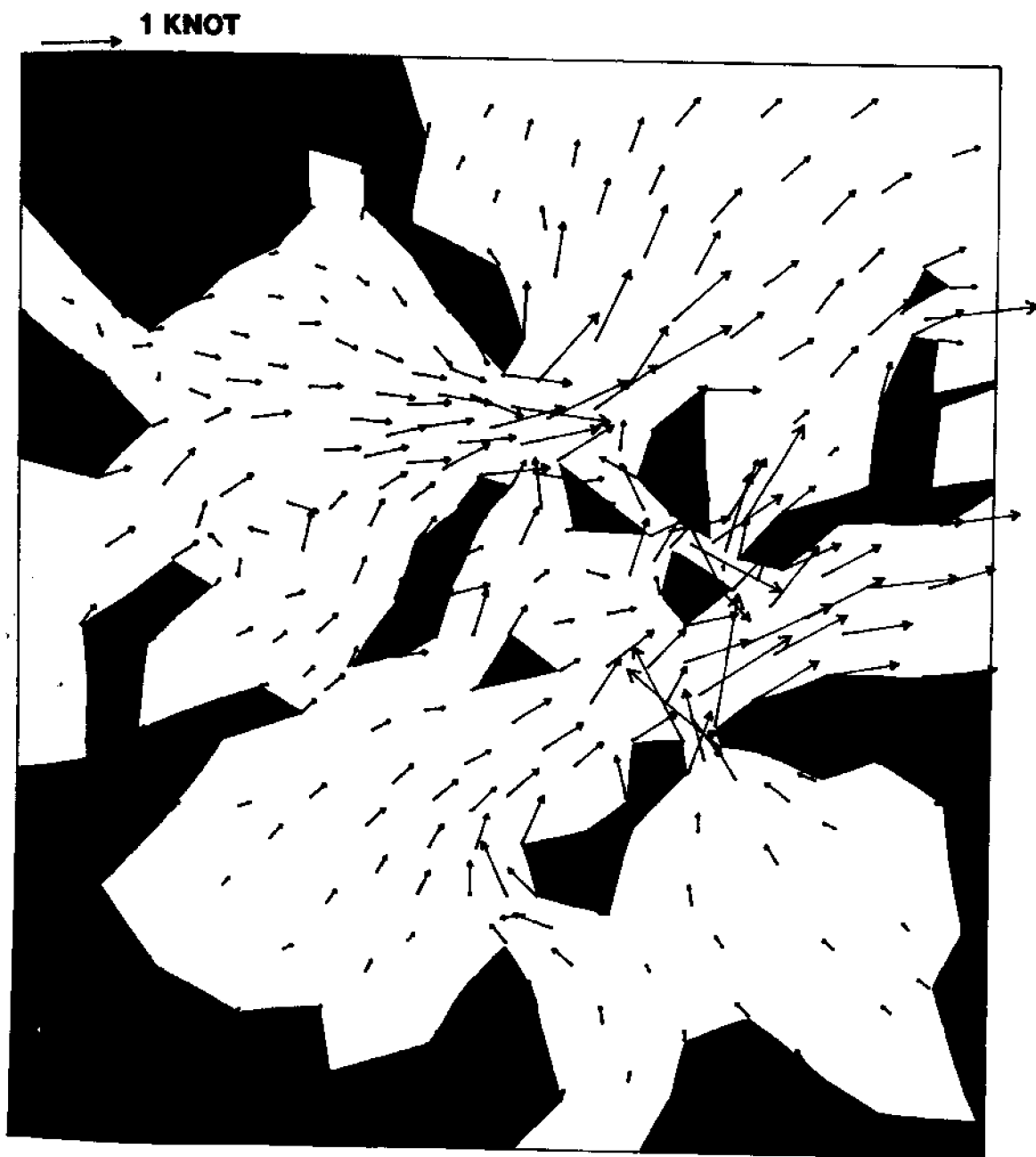
Figure 5.9   Simulated Current Velocities in Boston Harbor
4 Hours After High Tide

1 KNOT
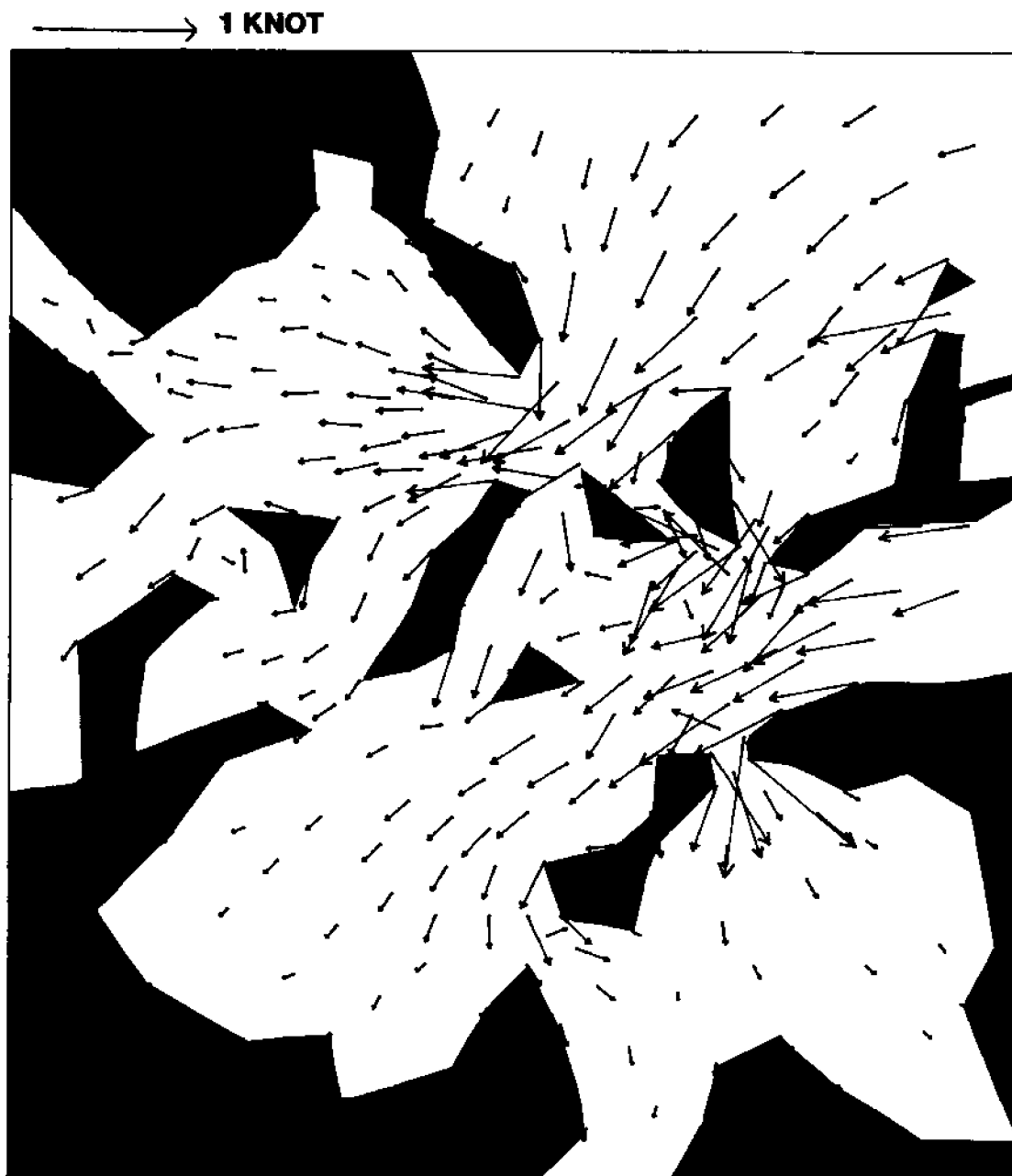
Figure 5.10 Simulated Current Velocities in Boston Harbor
1½ Hours After Low Tide

1 KNOT
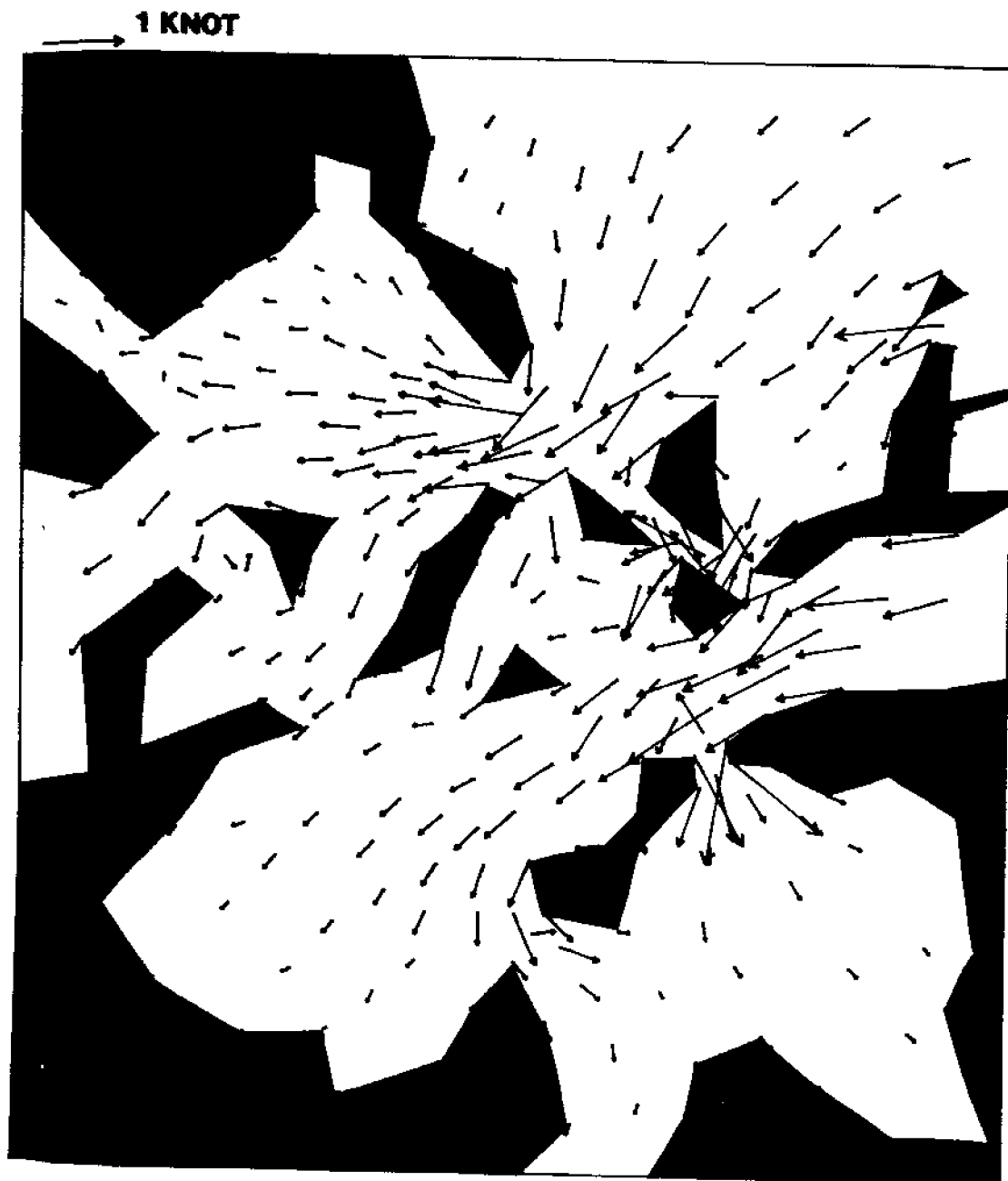
Figure 5.11 Simulated Current Velocities in Boston Harbor 4½ Hours After Low Tide
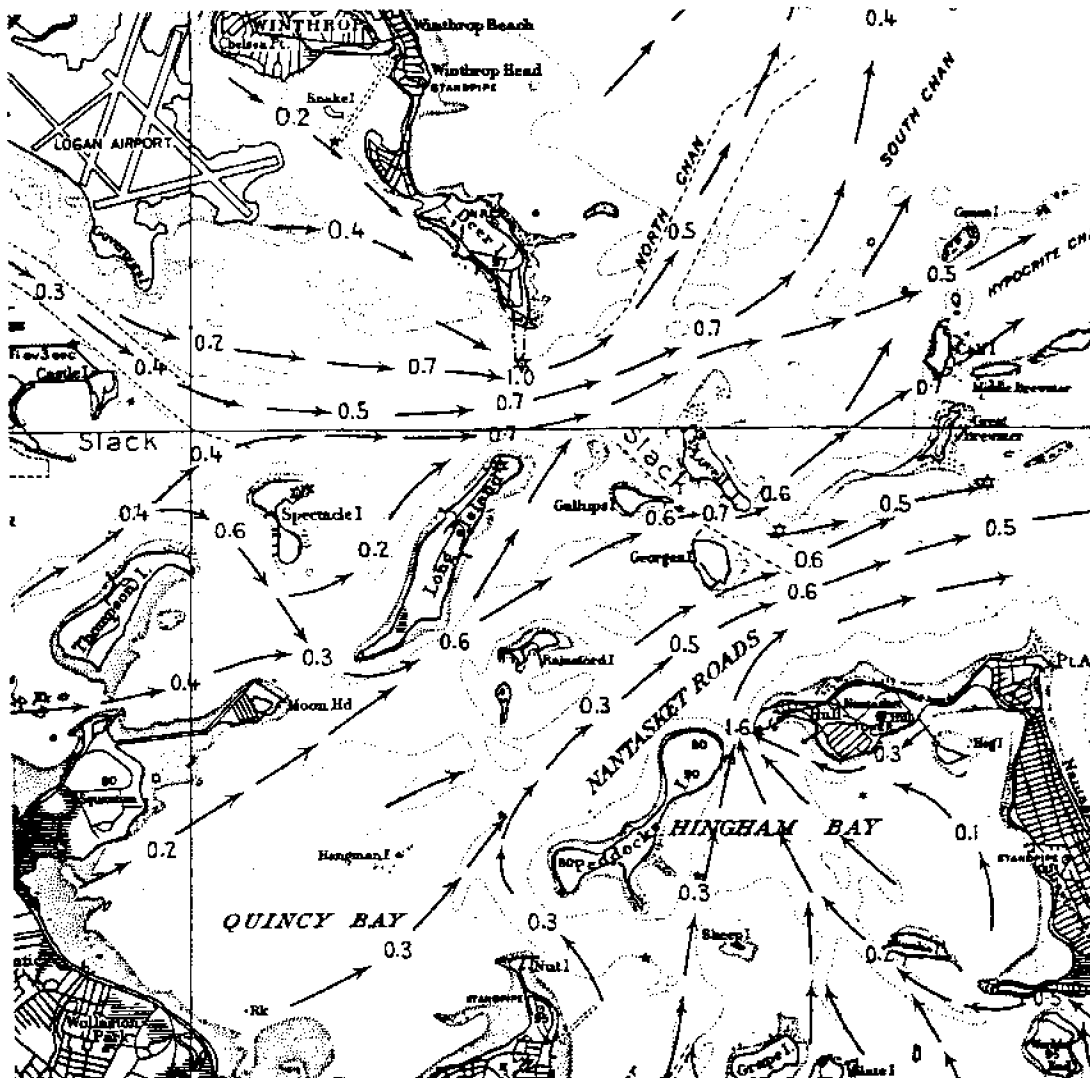
Figure 5.12 Current Velocities in Boston Harbor 1 Hour After
High Tide (from NOAA Tidal Current Charts)
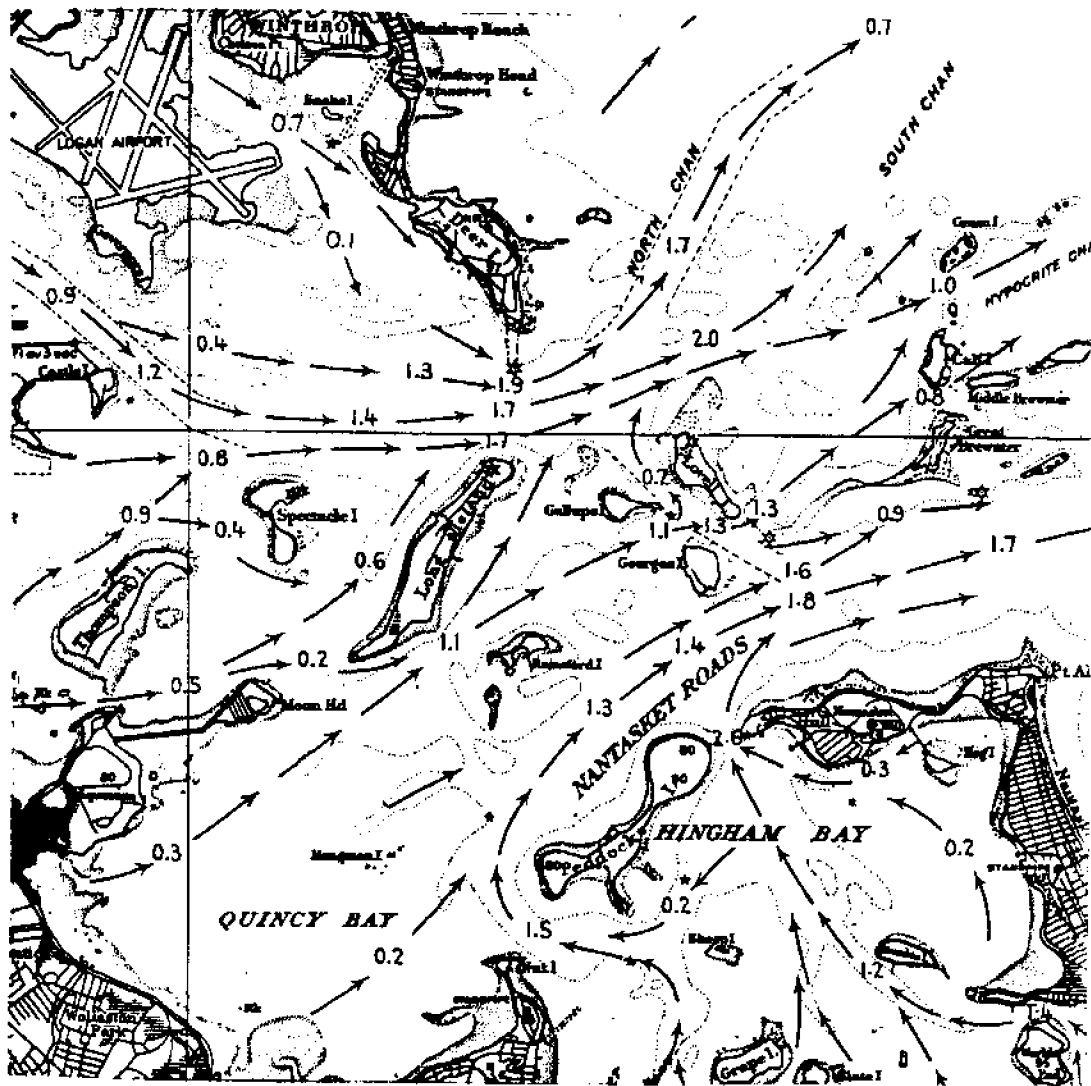
Figure 5.13 Current Velocities in Boston Harbor 4 Hours After High Tide (from NOAA Tidal Current Charts)
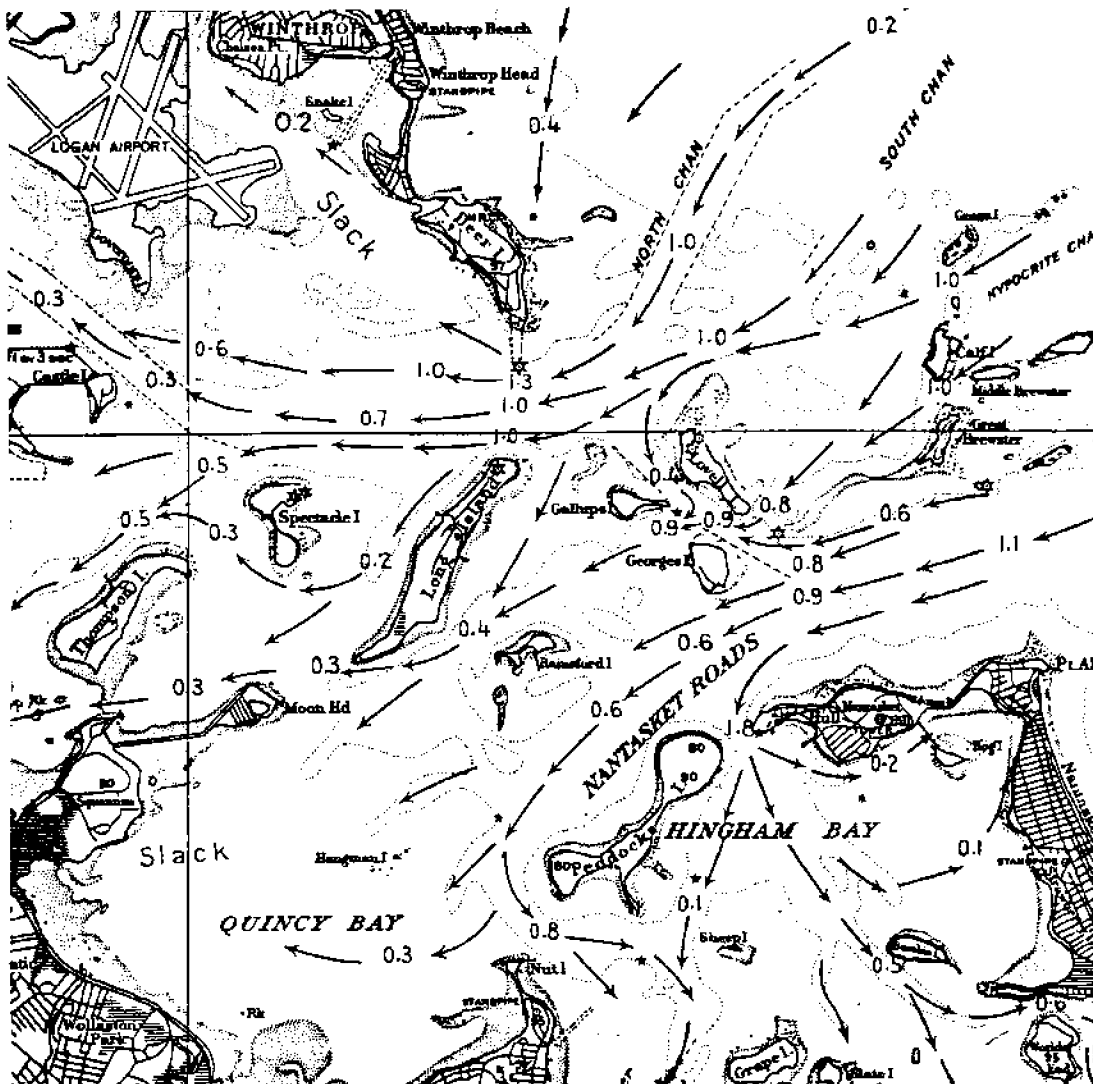
Figure 5.14 Current Velocities in Boston Harbor 1½ Hours After Low Tide (from NOAA Tidal Current Charts)
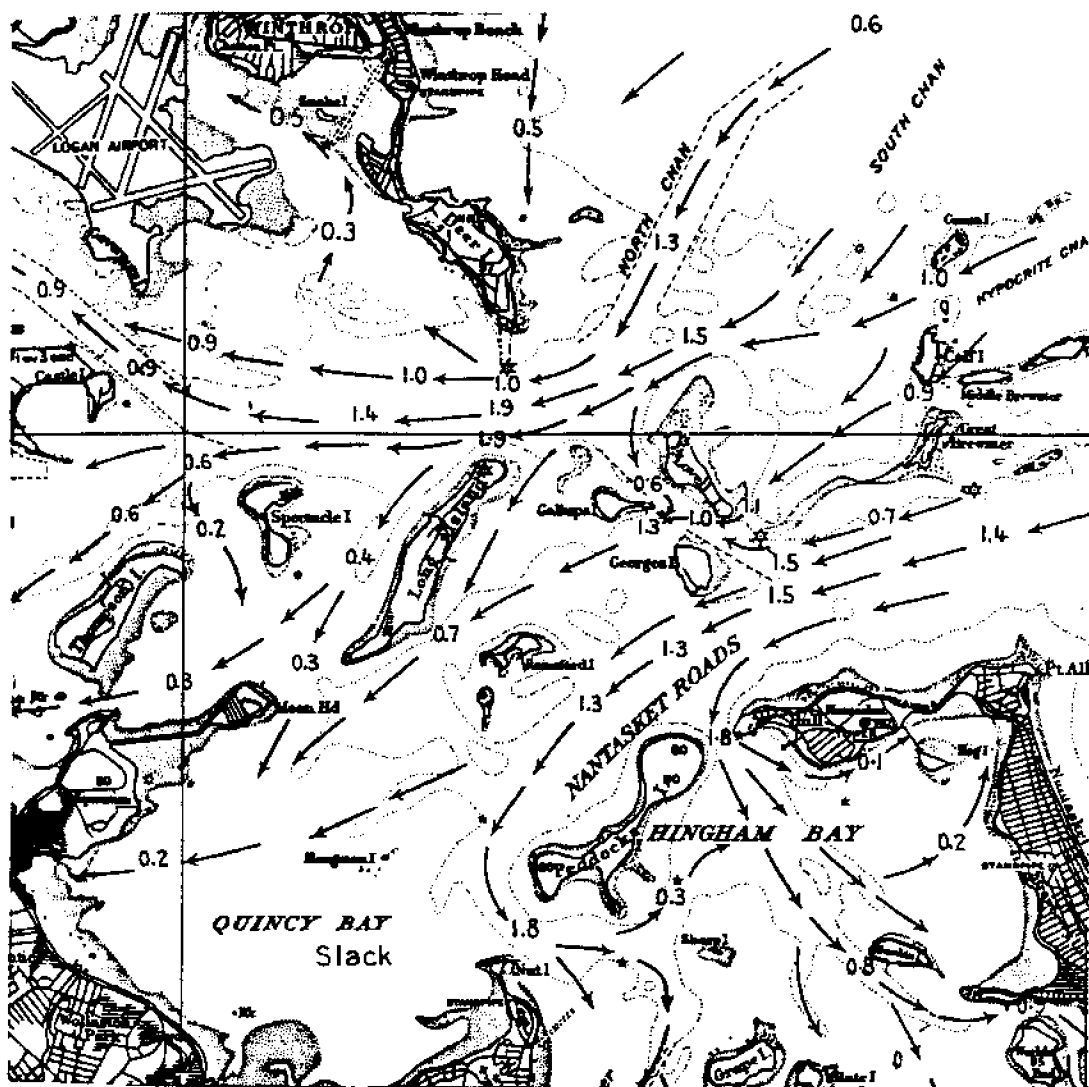
Figure 5.15 Current Velocities in Boston Harbor 4½ Hours After
Low Tide (from NOAA Tidal Current Charts)

Table 5.2

Mean Tide Level from Gloucester to Race Point

Station	Mean tide level (m)
Glousecter	1.31*
Salem	1.34
Boston Light	1.37
Hull	1.43
Cohasset Harbor	1.34
Scituate	1.34
Plymouth	1.43
Race Point	1.37*

* boundary condition

(from NOAA, 1984)
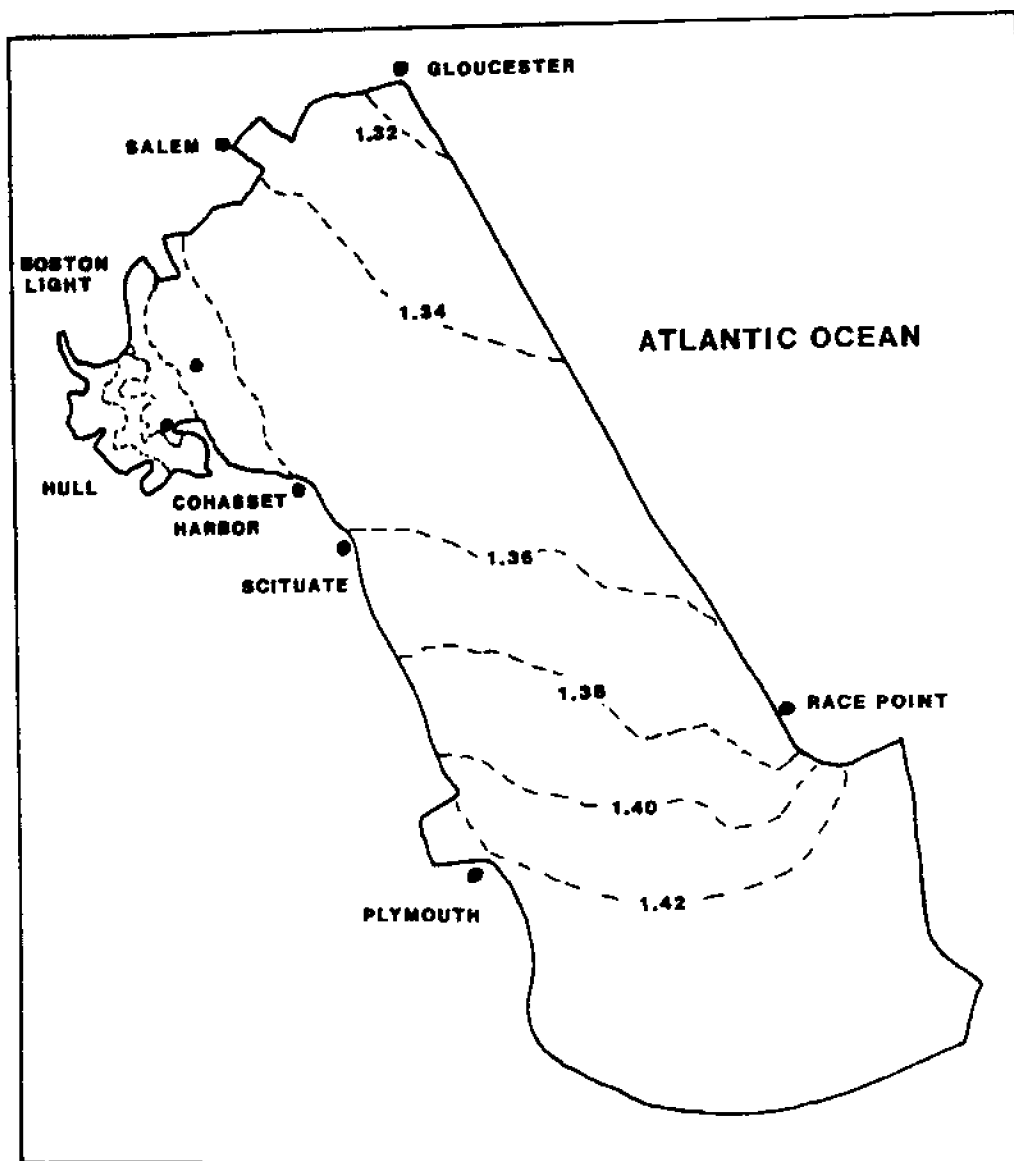
Figure 5.16 Simulated Tidal Amplitudes in Massachusetts Bay

5.4 Application of ELA to Boston Harbor

Use of linear TEA with only M_2 forcing facilitates the incorporation of some efficiency procedures within the Lagrangian tracking algorithm of ELA. As was outlined in Chapter 3, ELA decouples the advection-diffusion equation into a pure advection component and a pure diffusion component. Computationally, the advection step, in which water parcels are tracked backward in time along their characteristic lines from every node every timestep, can account for the majority of the cost (~75% for a typical Boston Harbor calculation). By assuming only M_2 forcing with linear TEA, these particle trackings only have to be carried out for one tidal cycle. Since each subsequent cycle is identical to the first, the feet of the characteristic lines need only be computed at every timestep within the first cycle and then saved. By choosing the timestep as some fraction of the tidal cycle, the saved feet of the characteristic lines can then be used in subsequent cycles. This results in substantial computational savings (Section 5.5).

As outlined in Table 3.2, in addition to information regarding the velocity field (output from TEA), ELA requires as input boundary conditions, source strength and location, dispersion coefficients, and decay rates (piston velocities). If the boundary is defined far enough from the source, the boundary condition can simply be set at zero concentration. Since the volatilization rates of our tracers are fairly high (an anticipated half-life on the order of days to weeks), a zero concentration boundary condition seemed reasonable. Hence, this condition was applied all along the open ocean boundary of the domain defined in Figure 5.2.

Based on considerations discussed in Chapters 2 and 4, the two wastewater treatment plants discharging effluent into Boston Harbor were assumed to be the only major sources contributing VHOCs to the system. These two treatment plants are located on Deer and Nut Islands. The location of the major outfalls has been illustrated in Figure 4.4. These outfalls are also illustrated in the computational domain in Figure 5.17.

Source information must be specificed by the effluent flow rate, Q_0, the pollutant concentration in the effluent, C_0, and the initial dilution. As pointed out in Chapter 4, C_0, Q_0, and the product C_0Q_0 all tend to be temporally variable. We chose to input C_0Q_0 as a constant but use it as one of the independent variables for fitting model predictions to measured data. This was accomplished by holding Q_0 constant for all simulations and allowing C_0 to act as a model variable, varying from run to run. Simulated concentations everywhere in the computational domain are directly proportional to C_0Q_0. In as much as Q_0, C_0, and C_0Q_0 are not constants, treating them as such in the model incurs some error. This will be discussed in some detail below.

Initial dilutions are dependent on the characteristics of the outfall diffusers. In addition, they are functions of the current velocity at the outfall location. Based on observations at the two outfalls (Metcalf and Eddy, 1979b), the following relationships were used:

$$S_D = 50.5U + 6.5 \qquad\qquad (5.4.1)$$

$$S_N = 31.7U + 5.5 \qquad\qquad (5.4.2)$$
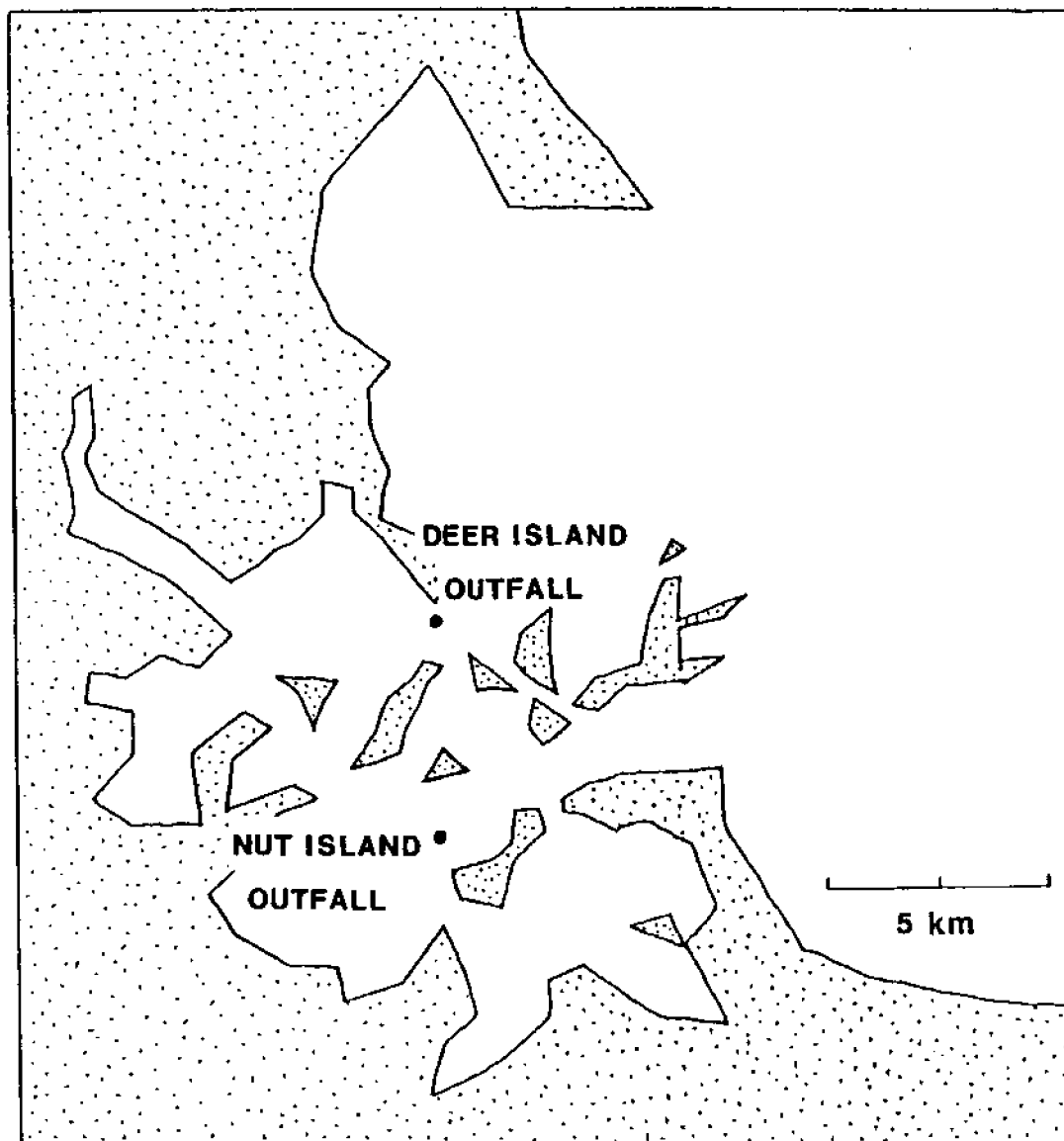
Figure 5.17   Location of Modeled Sewage Outfalls on Computational Grid

where

S_D is the initial dilution at Deer Island

S_N is the initial dilution at Nut Island

U   is the current speed (m/sec)

The dispersion coefficients, D_{xx}, D_{yy}, D_{xy}, and D_{yx} in equation
(3.3.1) represent the physical mechanisms causing horizontal spreading of a
contaminant within the water column. These mechanisms include: 1) turbu-
lent diffusion, the mixing due to small scale turbulent velocity fluctua-
tions; 2) vertical shear, velocity nonuniformities over the thickness of
the water column which effectively create a horizontal spreading in the two-
dimensional concentration field (in a three-dimensional model, this shear
effect would be incorporated into the advective terms in the governing
equation); and 3) sub-grid scale dispersion, resulting from the spatial
discretization of the domain, since eddies can only be resolved by the
advective terms if they are larger than the length scale of the elements of
the numerical grid. Additionally, any inaccuracies in representing the
advective velocity field (due to use of linear TEA, no low frequency forc-
ings, and only the M_2 tidal constitutent) are implictly included in the
dispersion coefficients when calibrating the model.

Due to the highly periodic nature of the tidal phenomenon, the disper-
sion coefficient should be time dependent. However, use of a temporally
constant dispersion coefficient facilitates matrix manipulation within the
numerical model (the diffusion matrix only needs to be inverted once) and
is justified by the large ratio of total simulation time to tidal period
(~30 to 60). Also, the dispersion coefficient should be spatially variable

and anisotropic, but this variability is difficult to quantify. Hence, considering these factors, we chose to model the dispersion coefficient as homogeneous, isotropic, and temporally constant ($D_{xx} = D_{yy} = D_{xy} = D_{yx} = D$).

Because D must account for additional mixing not explicitly represented by TEA, calibrated values were expected to be large. To some extent, these artifically high dispersion coefficients reflect the magnitude of the residual circulation and thus the efficiency of flushing. In fact, in Chapter 6 the calibrated dispersion coefficients will be used to estimate a harbor flushing rate. Note that the maximum physical value of D possible is approximately L^2/T where L is the tidal excursion (~3-4 km) and T is the tidal period (12.4 hrs). Hence, $D_{max} \approx 200-350$ m^2/sec. Values of D ranging from 30 m^2/sec to 150 m^2/sec were used for our simulations.

The piston velocity, k, was used as a third independent variable (along with C_0 and D) to fit model predictions to observations. Values of k ranging from 1 cm/hr to 11 cm/hr (reflecting the anticipated range of values) were used. Piston velocities and volatilization have been discussed in detail in Chapter 2. Like dispersion coefficients, piston velocities are temporally and spatially dependent. These variations, however, are difficult to quantify and model. Hence, our piston velocities represent effective mean values over the length of the simulation and the region examined. This will be discussed again in Chapter 6.

The timestep used for our simulations was T/4 (where T = 12.4 hrs) or roughly 3.1 hrs (Baptista, 1985). Simulations were run until concentration distributions reached a pseudo-steady state. That is, the simulations were

started with an empty harbor (the inital condition being C = 0 everywhere) and it took a finite amount of time for losses (decay and flushing) to balance the continuous input. This is illustrated in Figure 5.18 where total mass in the system is plotted versus time. (It is suspected that the small periodic fluctuations in total mass are primarily due to inaccuracies in TEA.) Simulations were run until the curve had leveled off to approximately 95% of the asymptotic level. Depending on the value of k used, this could take anywhere from several days to a month of simulated time.

Figures 5.19 through 5.26 present results of model simulations with different values of D and k in the form of contour maps of predicted concentration. (For all simulations presented, the mass loading was 10.7 kg/day at Deer Island and 2.7 kg/day at Nut Island.) Based on these results, several generalizations regarding both model behavior and harbor mixing can be made:

a) Not unexpectedly, the model appears to be quite sensitive to both D and k.

b) Substantial spatial variation in concentration occurs near the source. In particular, a "hot spot" is simulated at a distance of one tidal excursion from the source at high and low tides. This is due to the variation of dilution with current speed and tends to be reinforced with successive tidal cycles. Such an effect is resolvable due to our puff algorithm (described in Appendix I). Any variation in source concentration (if represented as model input) would result in similar near field variability.

-143-
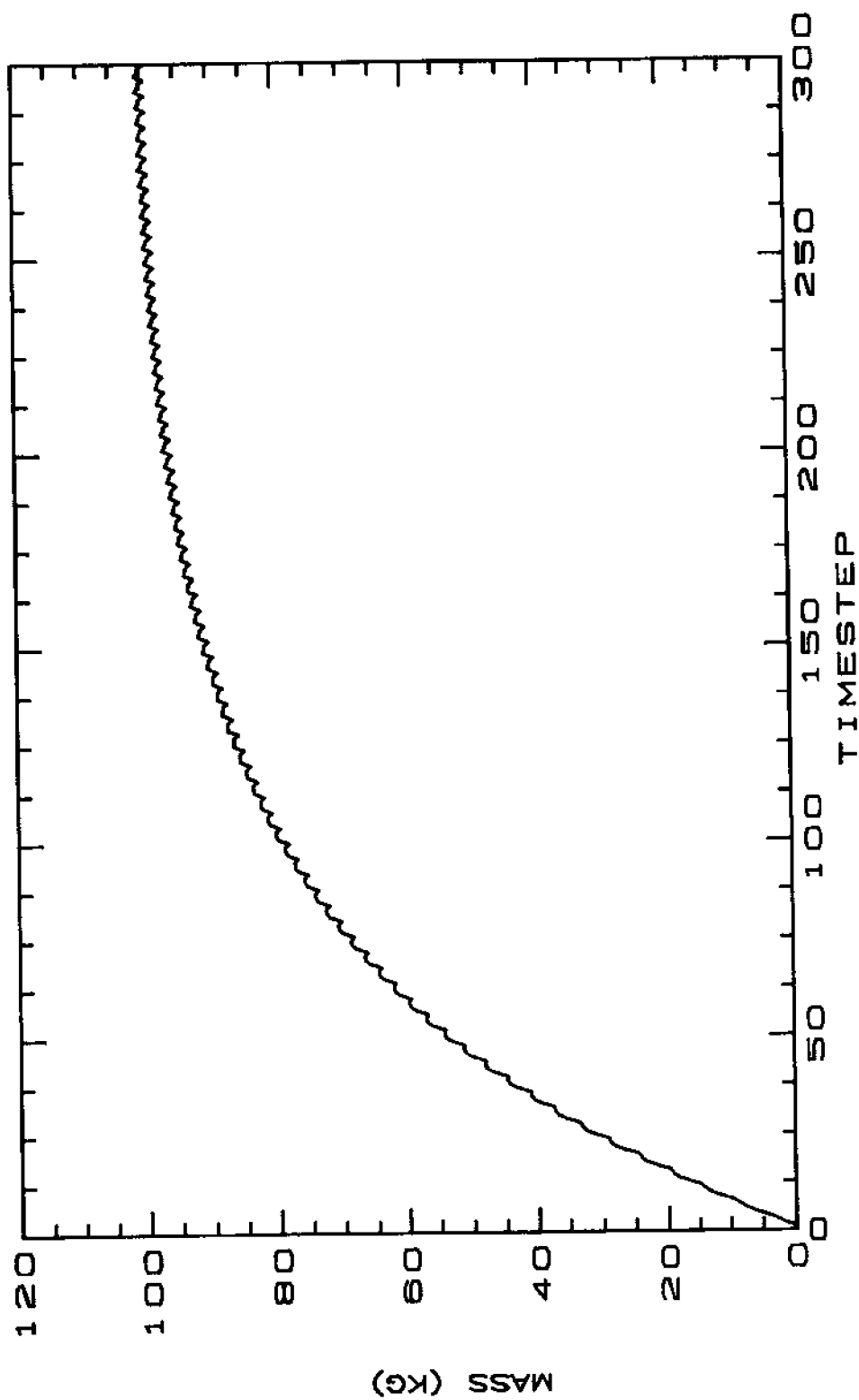
Figure 5.18 Total Mass in System versus Timestep (timestep = 3.1 hrs; D = 60 m²/sec; k = 1 cm/hr; $C_0 Q_0$ = 13.4 kg/day)

Figure 5.19 Simulated Concentrations (parts-per-trillion) in Boston Harbor at High Water Slack ($D = 60$ m^2/sec; $k = 1$ cm/hr)
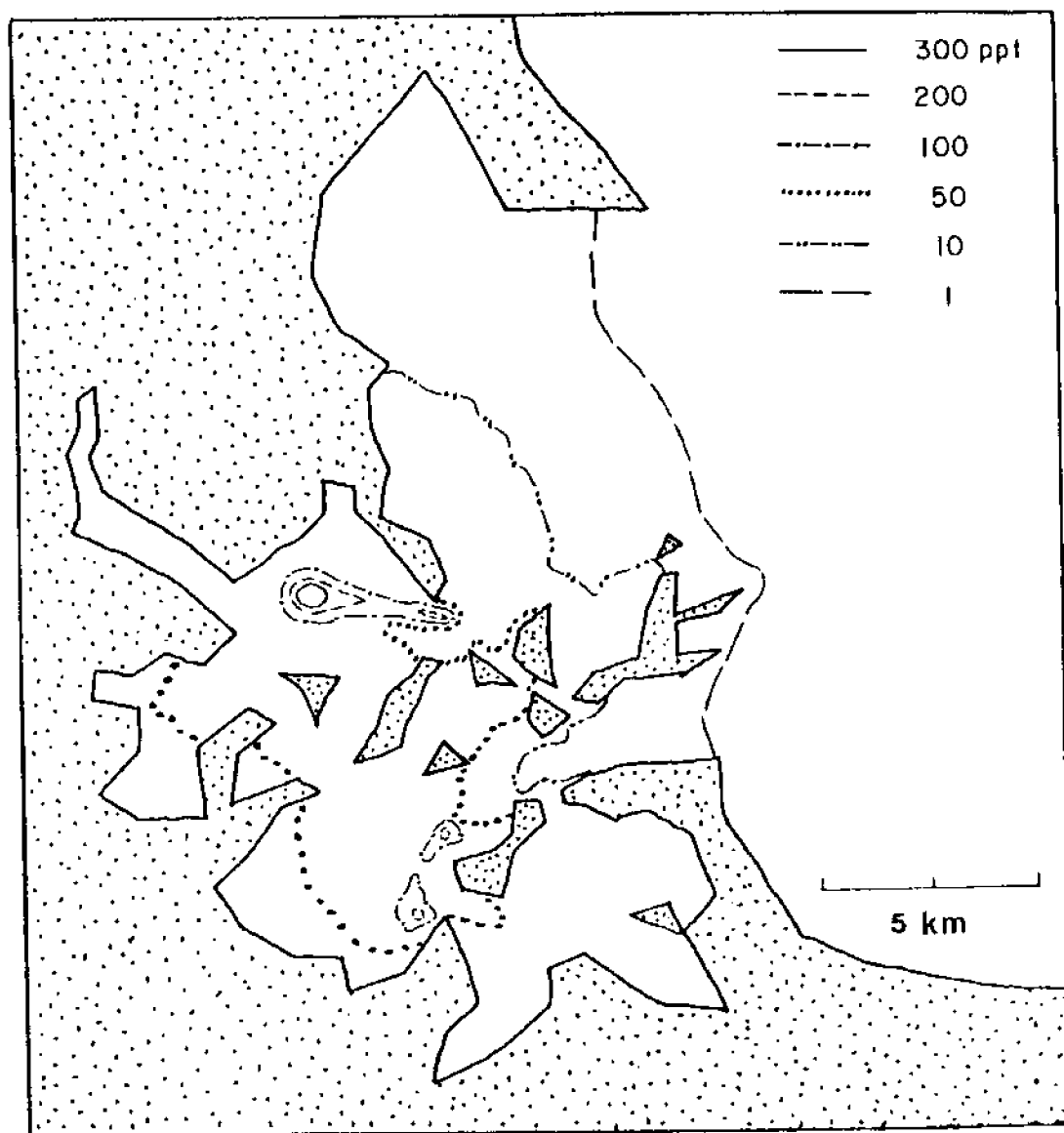
Figure 5.20 Simulated Concentrations (parts-per-trillion) in Boston Harbor
at High Water Slack (D = 60 m^2/sec; k = 4 cm/hr)
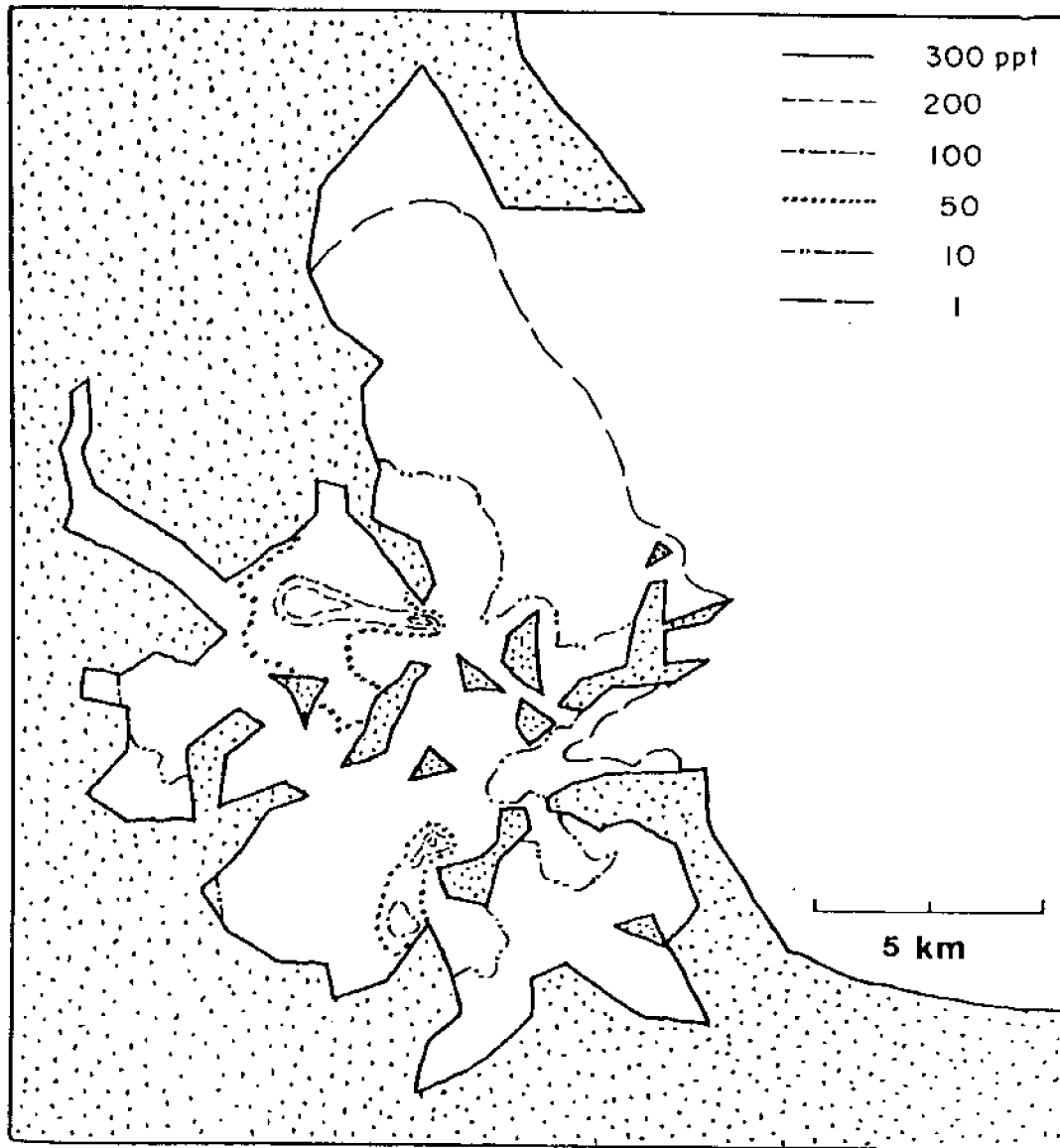
Figure 5.21 Simulated Concentrations (parts-per-trillion) in Boston Harbor at High Water Slack (D = 60 m^2/sec; k = 7 cm/hr)
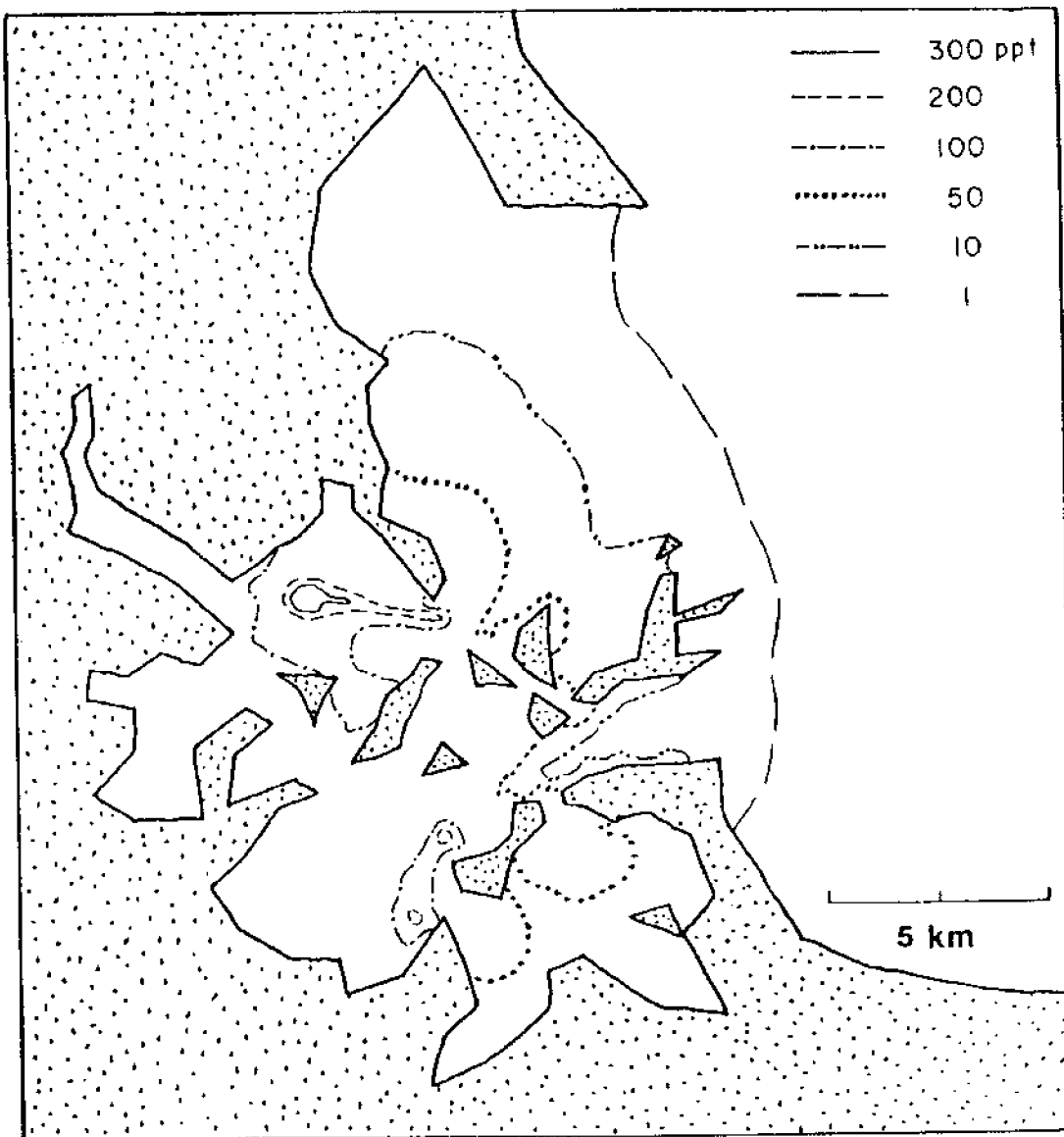
Figure 5.22   Simulated Concentrations (parts-per-trillion) in Boston Harbor
at High Water Slack ($D = 30$ m^2/sec; $k = 4$ cm/hr)
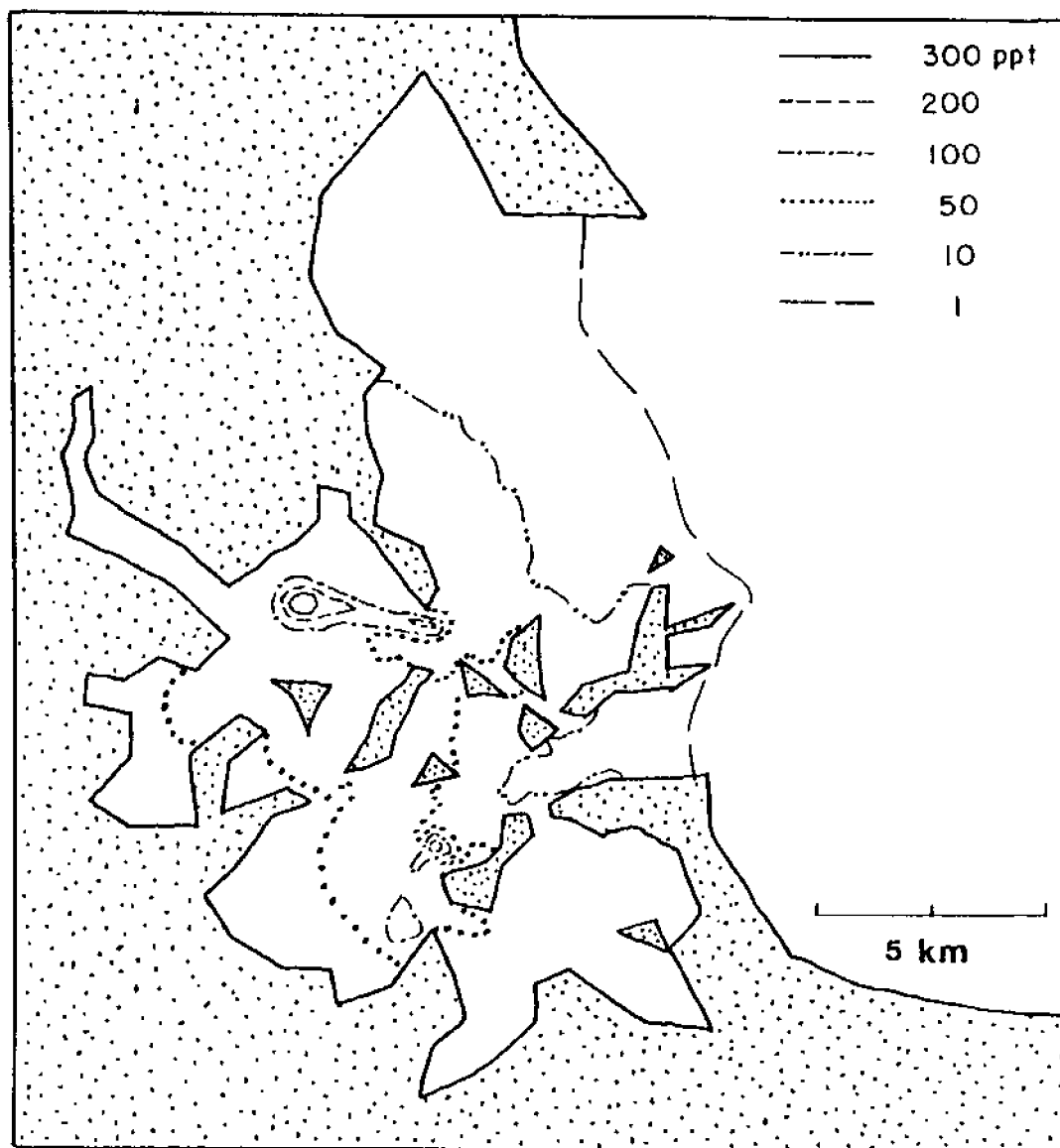
Figure 5.23 Simulated Concentrations (parts-per-trillion) in Boston Harbor at High Water Slack ($D = 70$ m^2/sec; $k = 4$ cm/hr)
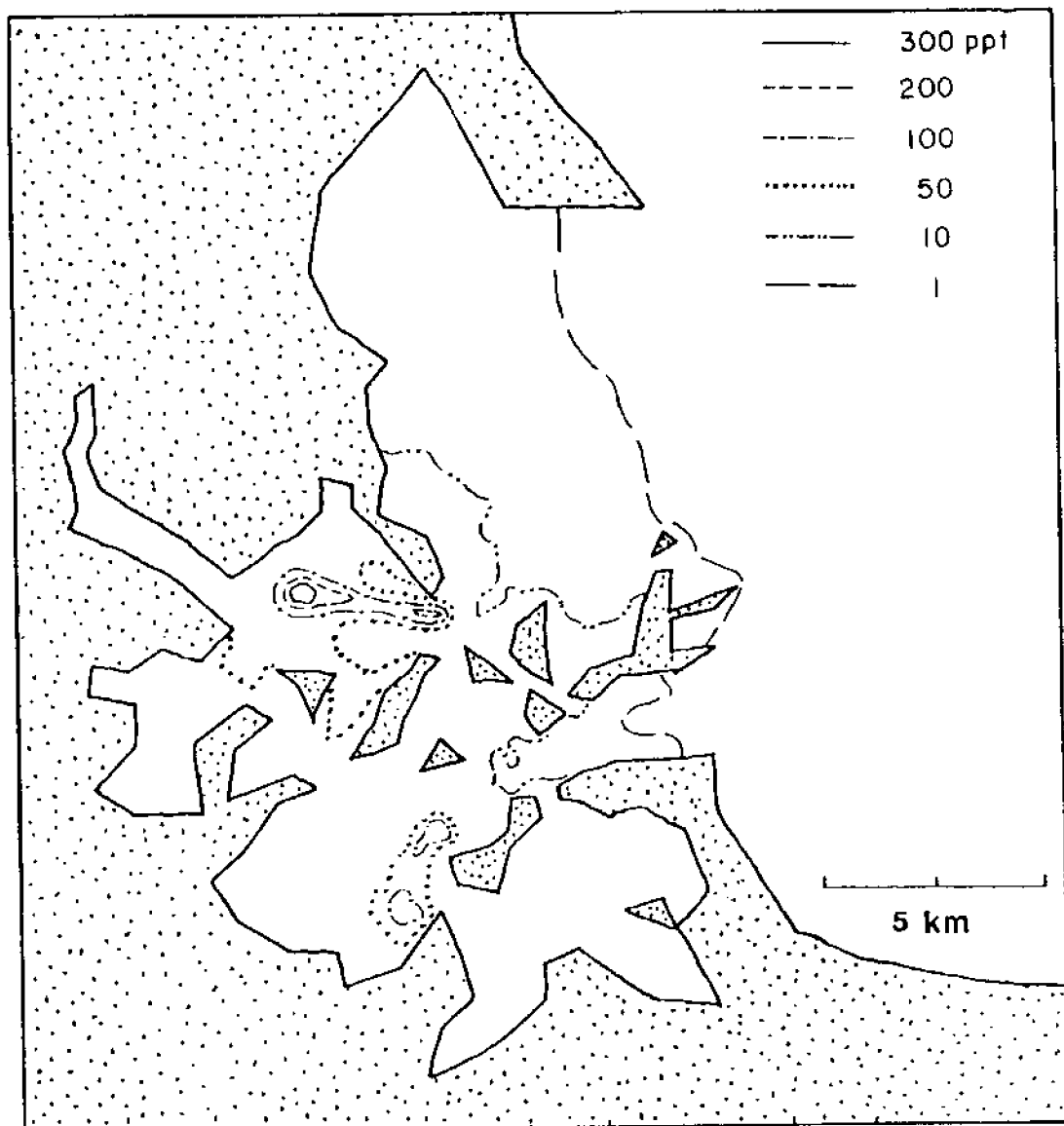
Figure 5.24   Simulated Concentrations (parts-per-trillion) in Boston Harbor
at High Water Slack (D = 110 m^2/sec; k = 4 cm/hr)
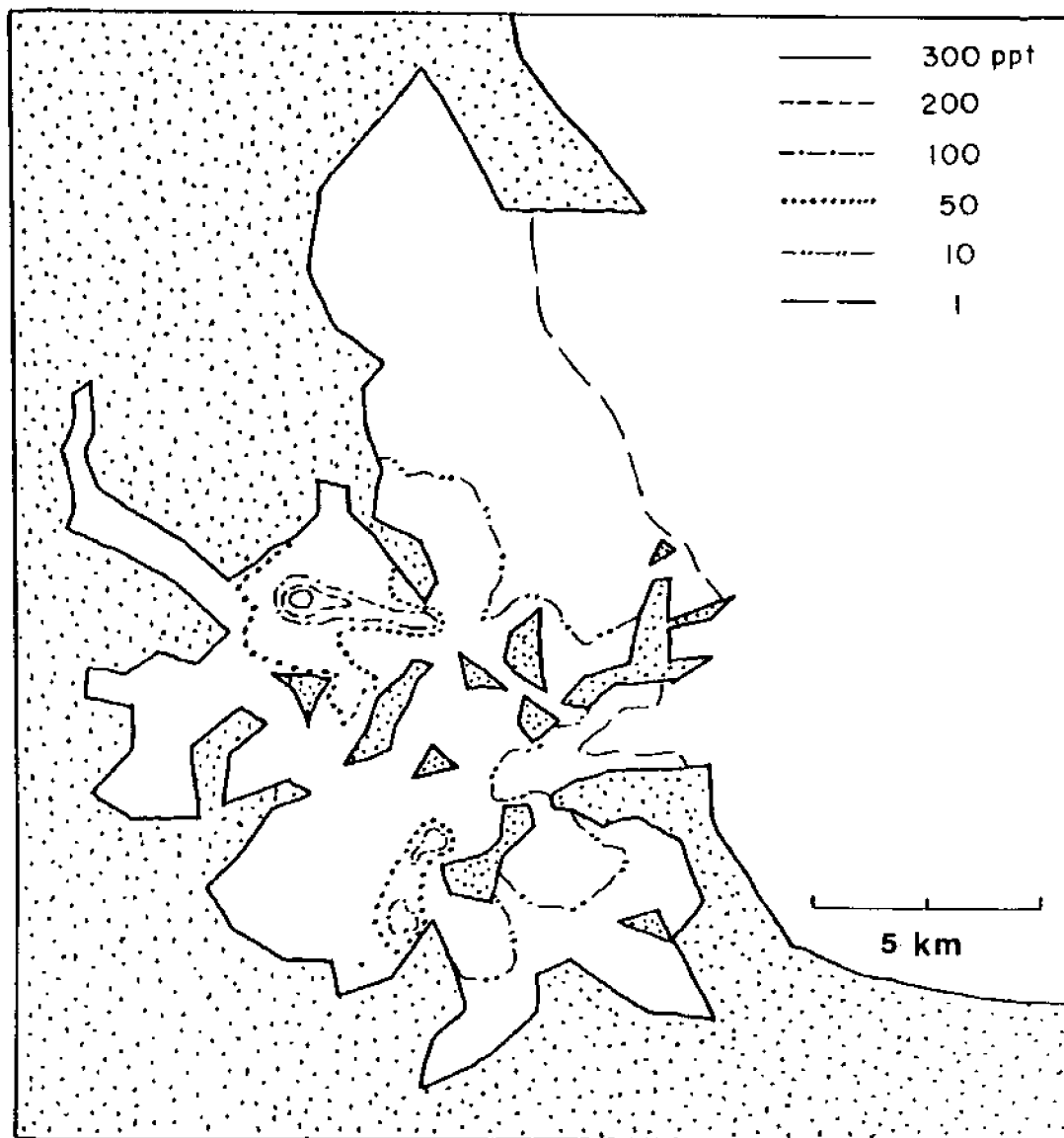
Figure 5.25 Simulated Concentrations (parts-per-trillion) in Boston Harbor at High Water Slack ($D = 75$ m^2/sec; $k = 6$ cm/hr)
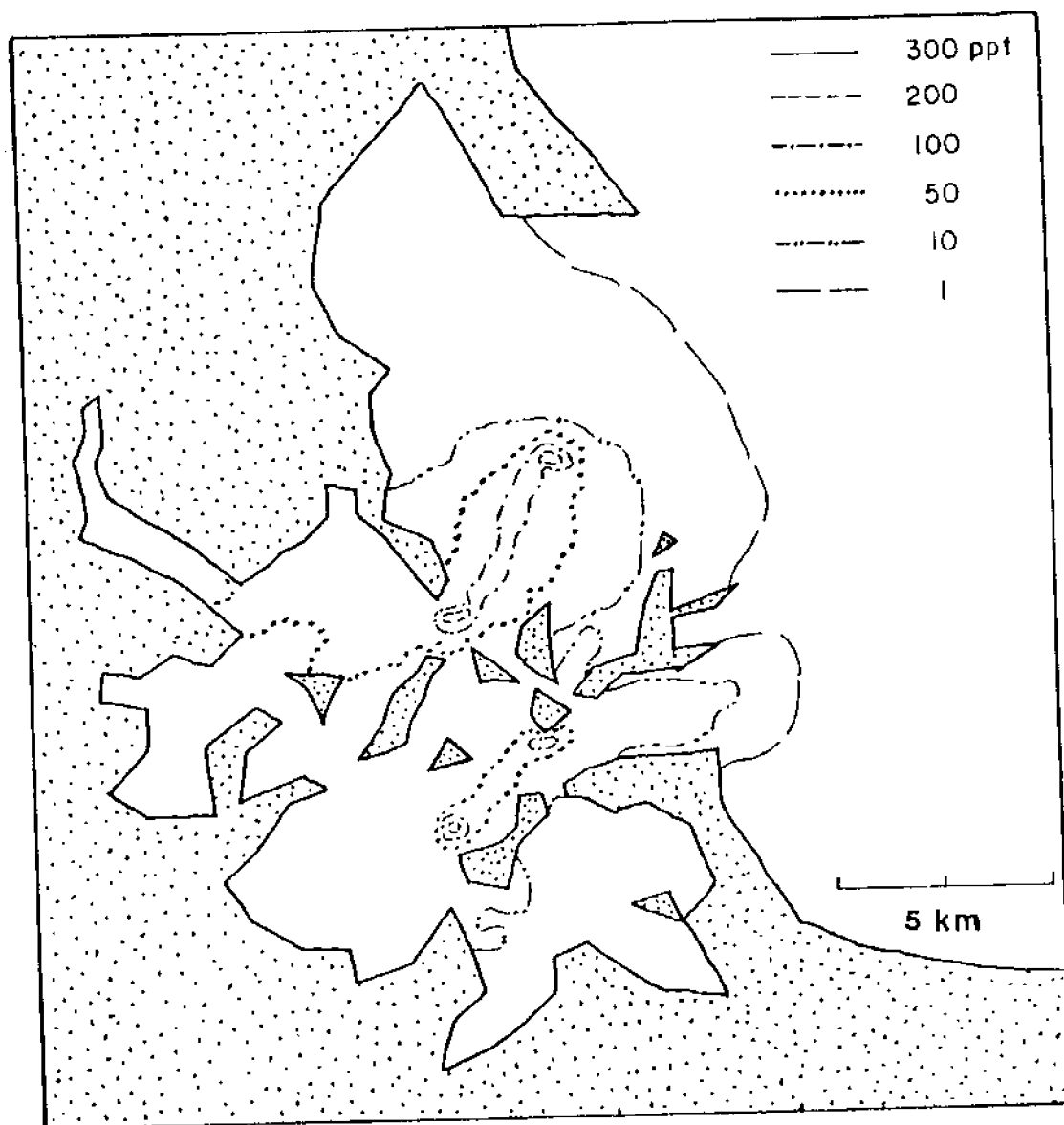
Figure 5.26   Simulated Concentrations (parts-per-trillion) in Boston Harbor
at Low Water Slack (D = 75 m^2/sec; k = 6 cm/hr)

c) Even though sewage discharges are located where tidal velocities are highest, simulated flushing is inefficient (regardless of the value of D) and one sees substantial contaminant concentrations in some portions of the harbor far from the outfalls.

d) Contaminants may be carried well into Massachusetts Bay before they are diluted by more than a factor of 100.

As a final point before proceeding to discuss the actual model calibration in the next chapter, we return to the question of treating C_oQ_o as a constant. In order to get some indication of the magnitude of the error incurred by inputting C_oQ_o as constant rather than time-variable, the following test problem was constructed. The model was run with given values of k and D and C_oQ_o was input as constant and equal to the value A. The simulation was then rerun with the same values of k and D, but with C_oQ_o defined as time varying such that:

$$C_oQ_o = A + (A/2) \cos\frac{2\pi}{T}t$$

(5.4.3)

where T = 12.4 hrs and t = 0 corresponds to high tide. The variability implied in (5.4.3) is similar to that described in Chapter 4 (~50%), and was visualized as a worst-case scenario in terms of comparison with tests using a constant value of A in that the tide would reinforce any effect. (In addition, we might expect an actual variation of this frequency due to the leaky tide gates mentioned previously.)

The resulting concentration contours for the two cases are presented in Figure 5.27 and 5.28. As can be seen, the results are quite similar. A closer inspection reveals that the run with time-variable C_0Q_0 results in slightly higher average concentrations. This is a consequence of the fact that the first-order decay rate is depth dependent, being the quotient of a constant piston velocity and variable depth. Therefore, due to tidal dynamics, the total mass in the system is a function of how and where the mass is input.

A quantitative comparison can be made by observing the time-varying concentration at a number of nodes for both simulations. The ratio of concentration predicted with variable Q_0C_0 to concentration predicted with constant Q_0C_0 at these nodes can then be plotted versus time. Figures 5.29 and 5.30 represent typical results. Figure 5.29 shows the results for a node within the harbor in the path of the plume. Figure 5.30 represents results for a node well outside the harbor mouth ($\sim$5 km northeast of the Deer Island outfall). At these (and other nodes not presented here) the concentration difference was no more than 20 to 30% between simulations (oftentimes, much less). This is about half of the variabiity introduced at the source (50%). Hence, the model does significantly damp the spatial and temporal variability due to time-varying discharge concentrations. Thus, given the other approximations of the model and the fact that this represents a worst-case scenario, it was concluded that treating the input as constant was acceptable.
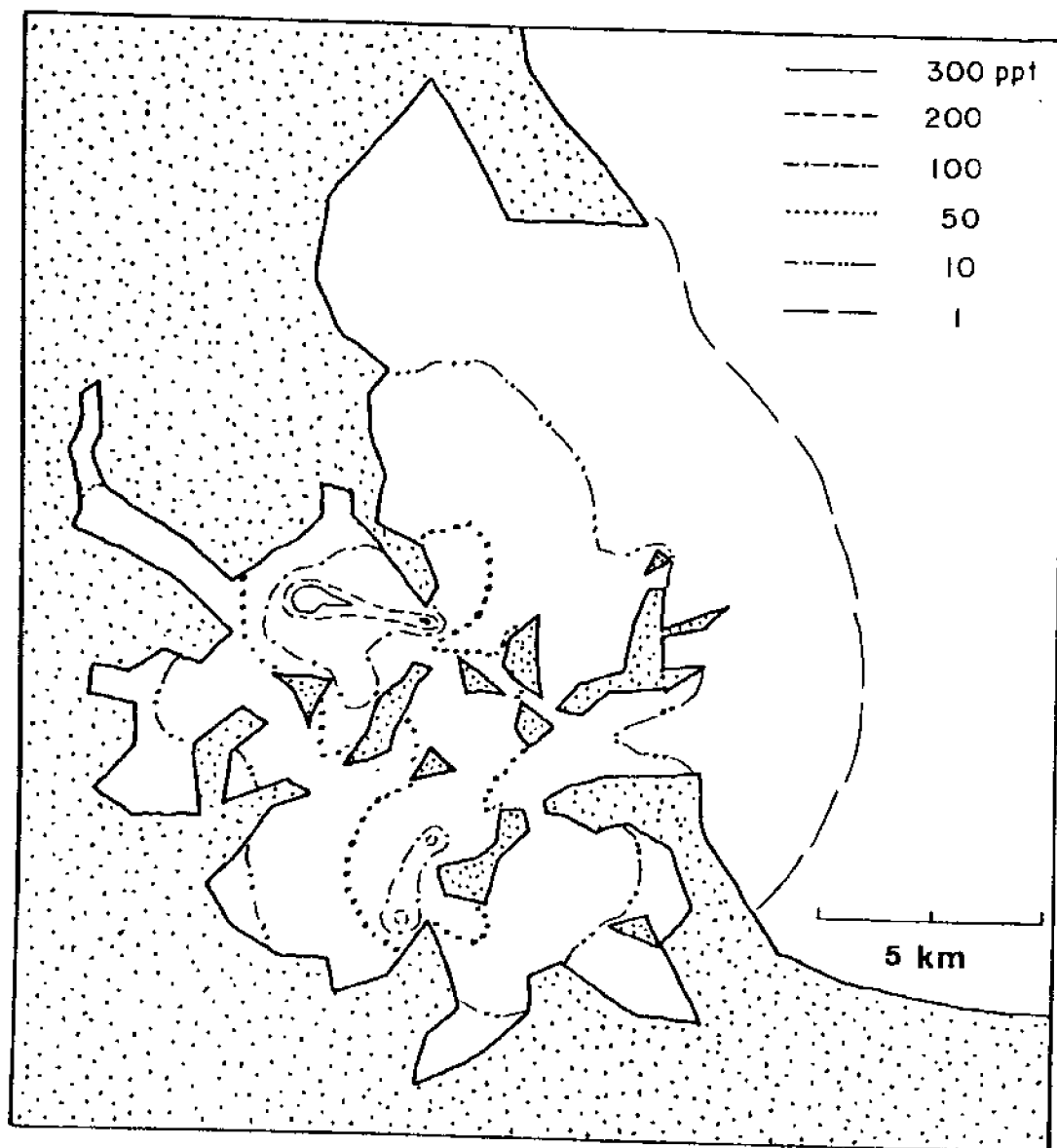
Figure 5.27 Simulated Concentrations (parts-per-trillion) in Boston Harbor at High Water Slack ($D = 10 \ m^2/sec$; $k = 10 \ cm/hr$; constant source strength)
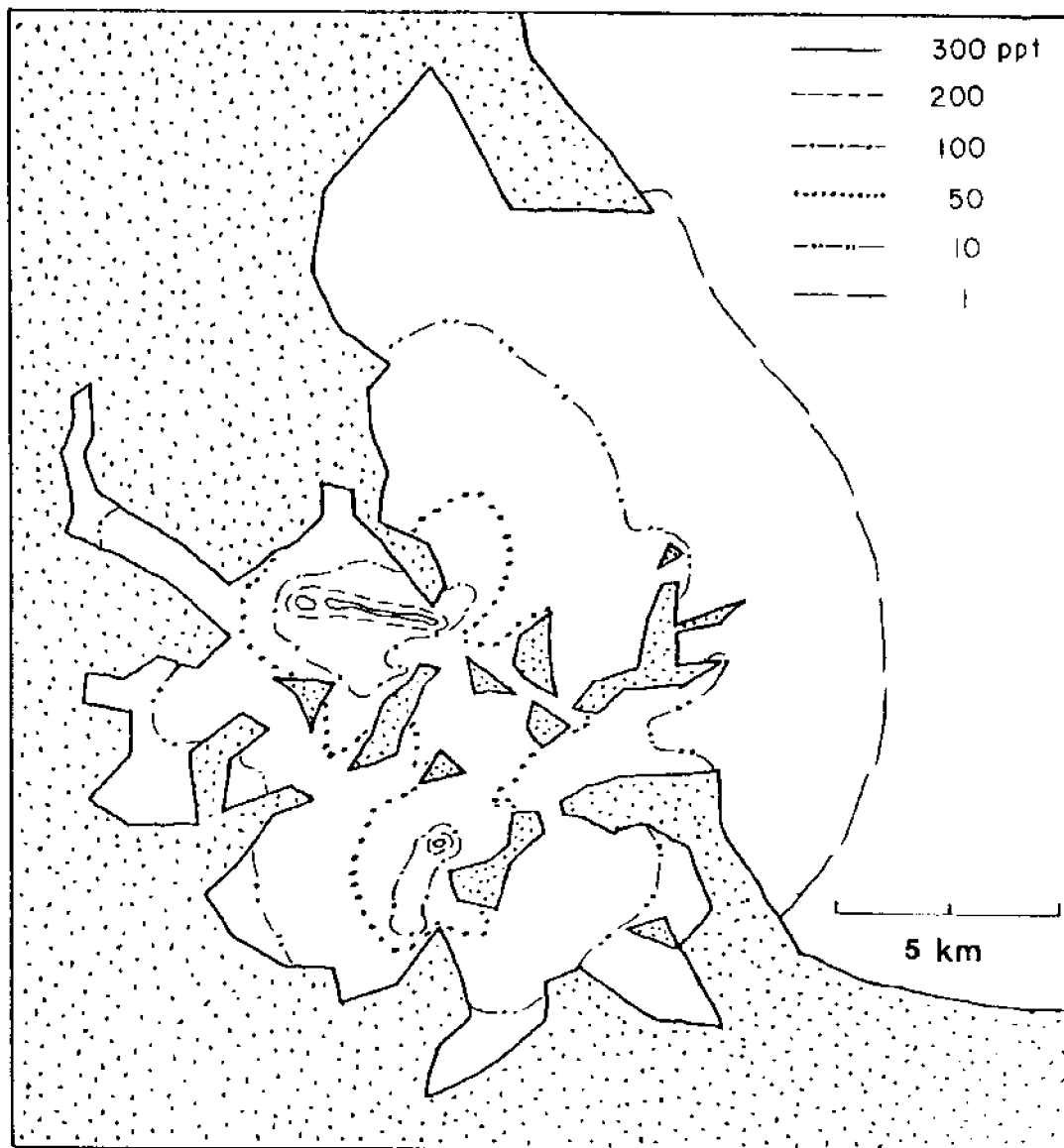
Figure 5.28 Simulated Concentrations (parts-per-trillion) in Boston Harbor at High Water Slack (D = 10 m^2/sec; k = 10 cm/hr; variable source strength)
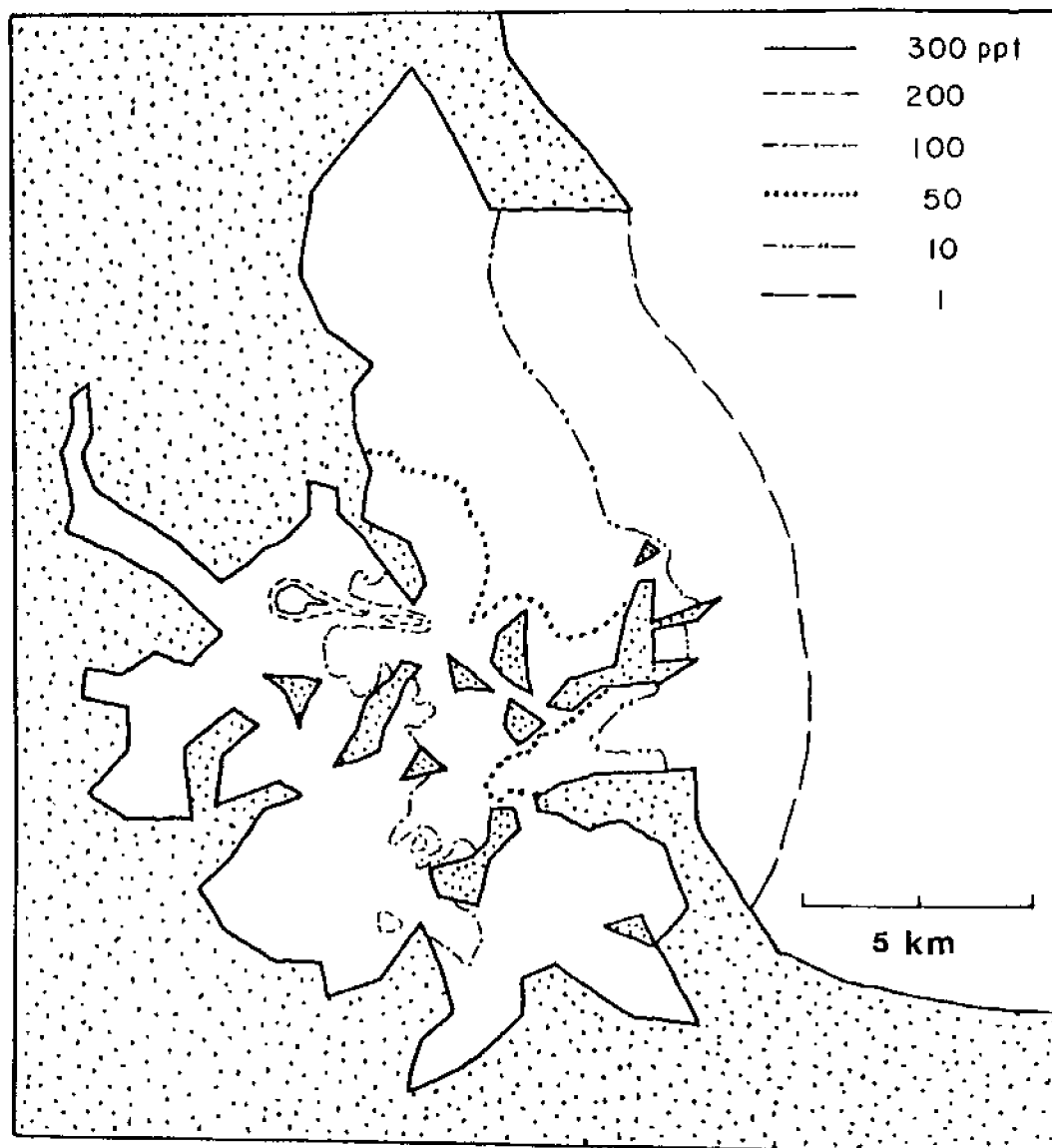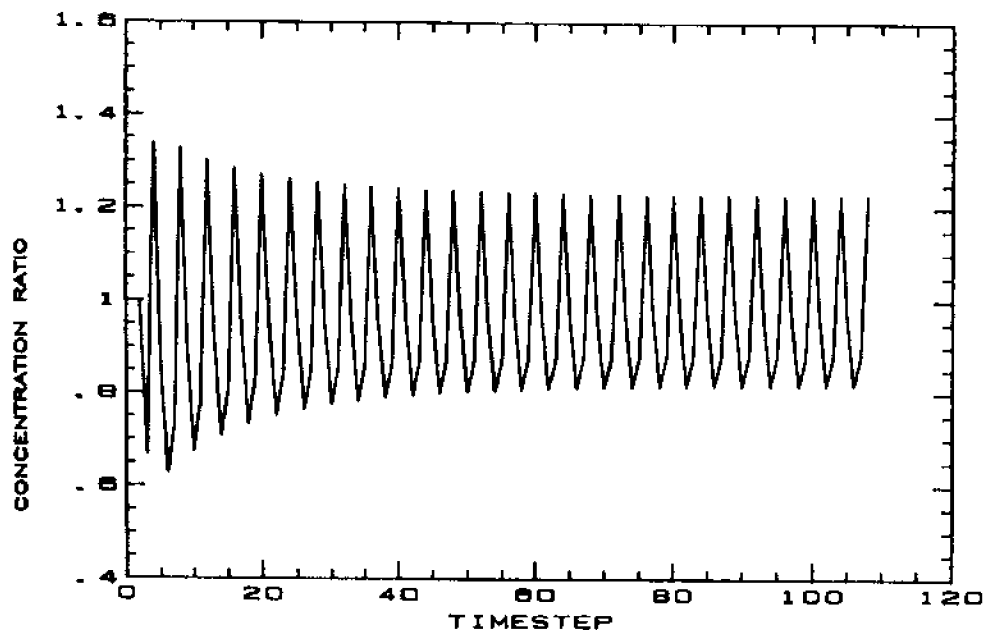
Figure 5.29 Ratio of Simulated Concentration with Variable C_0Q_0 to Simulated Concentration with Constant C_0Q_0 as a Function of Time for a Node in the Path of the Deer Island Plume Within the Harbor
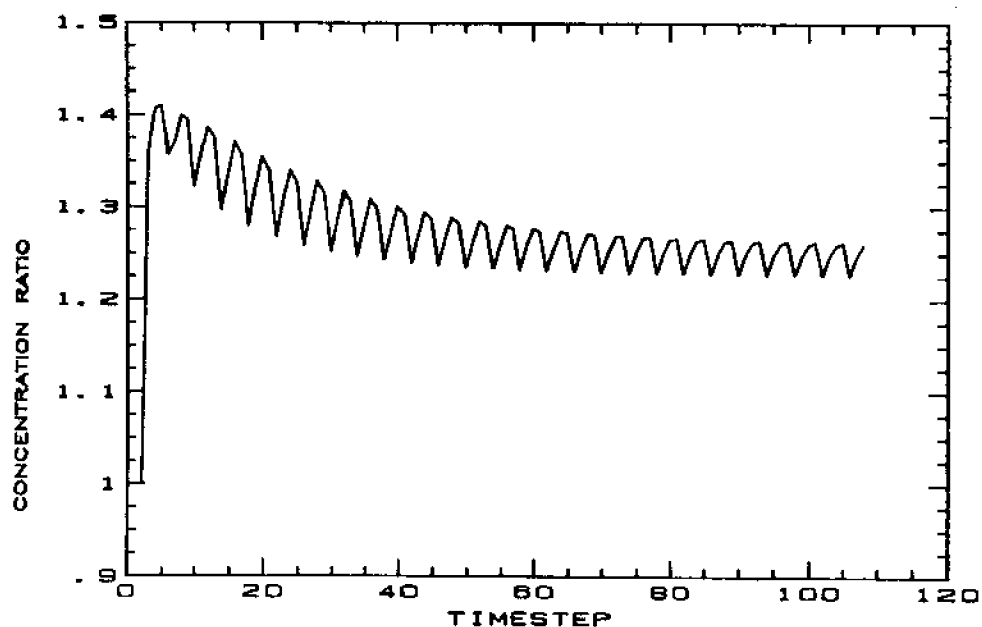
Figure 5.30 Ratio of Simulated Concentration with Variable C_0Q_0 to Simulated Concentration with Constant C_0Q_0 as a Function of Time for a Node Approximately 5 km Northeast of the Deer Island Outfall

5.5 Computational Expense

Table 5.3 summarizes the computational expense incurred by TEA and ELA for simulations of one tidal cycle (12.4 hrs) and 60 tidal cycles. It also serves to illustrate the effect of the computational efficiency procedures previously discussed. Computer simulations were made on a Digital VAX 780 and a Digital Microvax II. Computational times for the two machines were quite similar.

While Table 5.3 is largely self-explanatory, two points are worth reiterating. First, nonlinear TEA is always more expensive than linear TEA. The magnitude of this difference depends on the number of harmonics and number of iterations used in nonlinear TEA. In general,

$$C_{TNL} \approx C_{TL} \times N_H \times N_I \tag{5.5.1}$$

where C_{TNL} is the cost of nonlinear TEA, C_{TL} is the cost of linear TEA using 1 forcing frequency, N_H is the number of harmonics, and N_I is the number of iterations. The cost of linear TEA is directly proportional to the number of forcing frequencies.

Secondly, it is clear that using the efficiency procedures within the tracking algorithm in ELA results in large computational savings for long simulations. This is because only the dispersion and decay steps must be repeated every timestep, while the advection calculations need only be carried out for one cycle. For example, using a 12.4/6 ≈ 2.1-hour time-step, the cost of 60 tidal cycles is only 4 times greater than the cost of one. For a 12.4-hour timestep, the cost of 60 cycles is less than twice

Table 5.3

Approximate Computational Expense of TEA/ELA

Circulation	CPU minutes*
I. linear TEA[a]	20
II. nonlinear TEA[b]	2000

Transport	1 tidal cycle	60 tidal cycles	
		(using I)	(using II)‡
Backtracking of characteristics	66	66	3960
Matrix inversion	10	10†	10†
Back substitution, interpolation, decay			
$\Delta t \approx 2.1$ hrs	4	240	240
$\Delta t \approx 12.4$ hrs	2/3	40	40
Total			
$\Delta t \approx 2.1$ hrs	80	316	4210
$\Delta t \approx 12.4$ hrs	76 2/3	116	4010

a 1 frequency
b estimated time based on 10 frequencies and 10 iterations
* DEC VAX 780 computer
† one time calculation only if coefficients (D) are temporally constant
‡ nonperiodic circulation

the cost of one cycle. Such savings make it economically feasible to run a
large number of simulations.

Chapter 6

Model Calibration

In Chapters 4 and 5 chemical measurements and model simulations were used separately to draw some qualitative conclusions regarding pollutant transport in Boston Harbor. In this chapter, the same chemical measurements are used in conjuction with modeling efforts to elucidate some more quantitative information.

Such an exercise has a dual purpose. First, by comparing model predictions to observations, one can begin to evaluate the predictive capabilities of the model. Oftentimes, this process can be used to identify specific model weaknesses which can subsequently be improved upon. In effect, it allows one to evaluate whether the pertinent physical and chemical processes are being included in, and adequately represented by, the model.

Second, by adjusting model parameters to calibrate simulated concentrations to observed concentrations, one can obtain information regarding the processes represented by these parameters. This is the classic "inverse problem" of using experimental data on a dependent variable (e.g., concentration) to obtain values for the independent variables (e.g., dispersion coefficients and volatilization rates).

Model calibration and parameter estimation can become quite involved. Our limited data, however, did not warrant the use of a highly complex technique. The relatively simple calibration procedure that was used is

described in the following section. Calibration results are then presented and discussed, and based on these results, a number of conclusions are drawn.

6.1 Calibration Procedure

As has been pointed out in Chapter 5, ELA was calibrated using the dispersion coefficient D, the piston velocity k, and the source strength C_0Q_0 (more precisely, C_0, since as mentioned in Chapter 5, Q_0 was held constant and C_0 was the actual parameter being varied) as the independent variables. Calibrations were based on comparisons between measurements and simulated concentrations at the corresponding nodes. The measured concentration at each site was taken as the average of the surface and deep water values. Measurements were compared to simulated concentrations at high water slack. Since the measurements were not completely synoptic with high tide, the model was used to track the positions of the sampled water parcels backward or forward in time to high water slack. It was found that due to the small tidal velocites before and after high water slack, the temporal error incurred by not sampling synoptically was no greater than the spatial uncertainty of the sampling location (approx. 100 m).

Measurements made in areas of high concentration gradient (i.e., directly in the contaminant plume) were not used. Six sampling sites within the harbor were used for calibrating the model to all six compounds on all three dates, with the exception of October. Only three sites were used for the trihalomethanes in October due to interference from CSO inputs

(Section 4.4). The sampling sites were associated with nodes on the computational grid whose locations are shown in Figures 6.1 through 6.3.

A total of 22 model simulations were run using different combinations of D and k. The value of C_0 was not varied since the concentration everywhere in the harbor is simply directly proportional to C_0. The different combinations of D and k that were used are presented in Figure 6.4.

The first step in the calibration procedure was to choose an analytical interpolation function that could be used to approximate simulated concentrations at the calibration nodes for all values of the input parameters D, k, and C_0. This was necessary because we wished to compare observed concentrations to simulated concentrations resulting from any combination of the model parameters D, k, and C_0, not just the 22 combinations of these parameters that we specifically simulated. After experimenting with several functions, the following approximation function was chosen:

$$C_i = C_0 \left[a_{11}x + a_{12}y + a_{13}xy + a_{14}x^2 + a_{15}y^2 + a_{16}x^2y + a_{17}xy^2 + a_{18}x^2y^2 + a_{19} \right] \qquad (6.1.1)$$

where

$$x = 1/D \qquad (6.1.2)$$

and

$$y = 1/k \qquad (6.1.3)$$
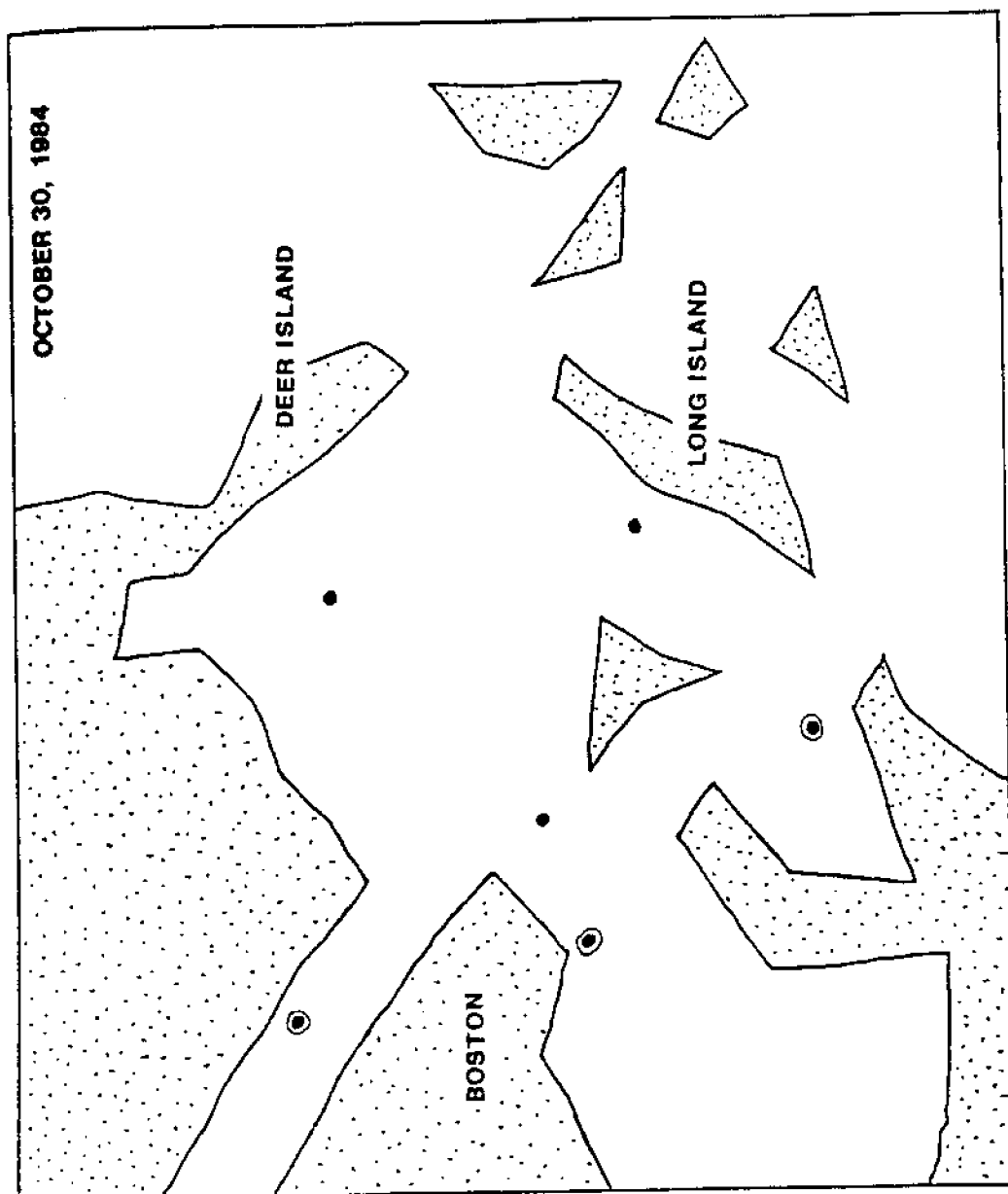
Figure 6.1 Location of Calibration Nodes for October 30, 1984 Sampling Date
(circled nodes were not used for trihalomethane calibrations)

APRIL 25, 1985

DEER ISLAND

LONG ISLAND

BOSTON
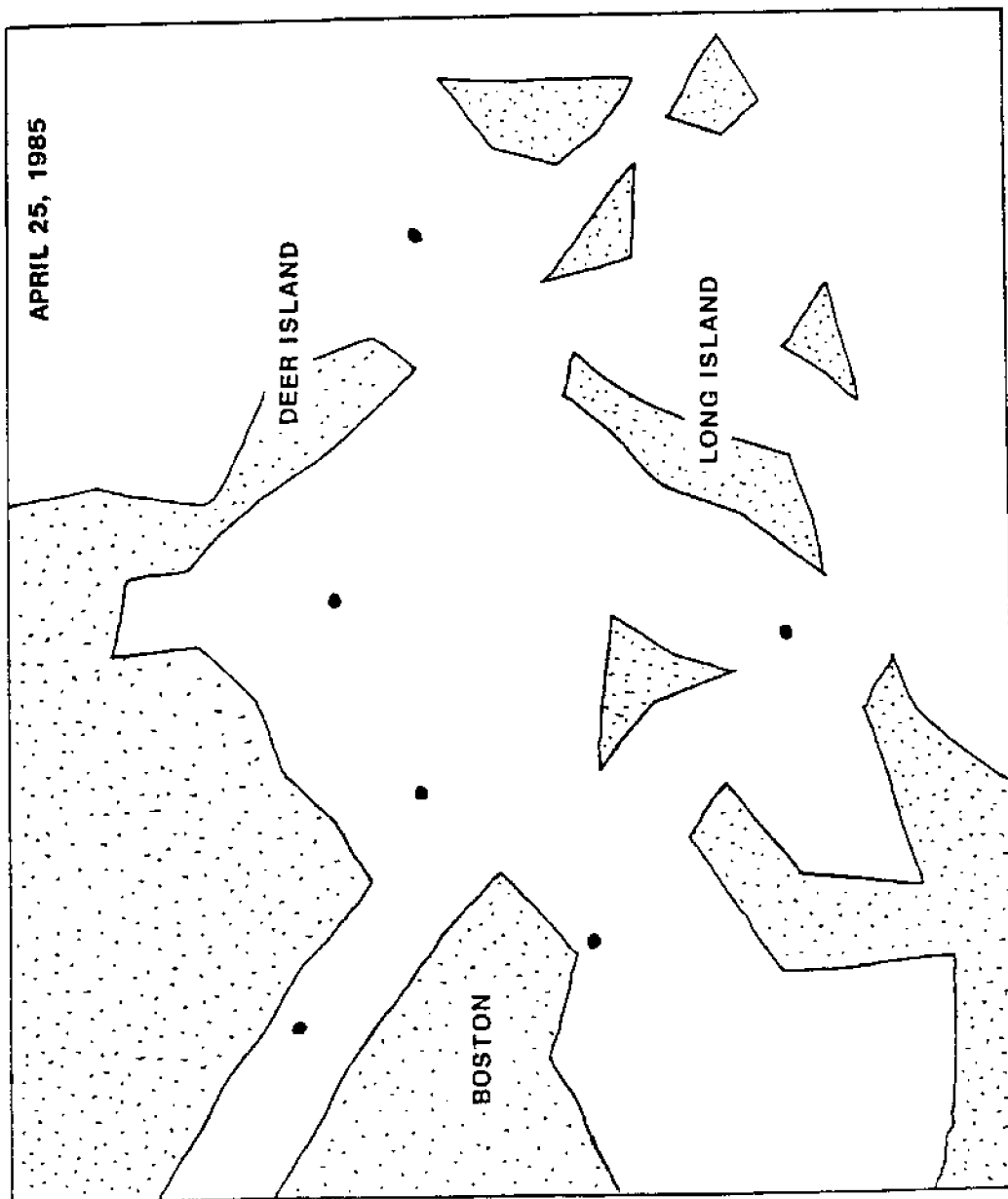
Figure 6.2 Location of Calibration Nodes for April 25, 1985 Sampling Date

JULY 2, 1985

DEER ISLAND

LONG ISLAND

BOSTON
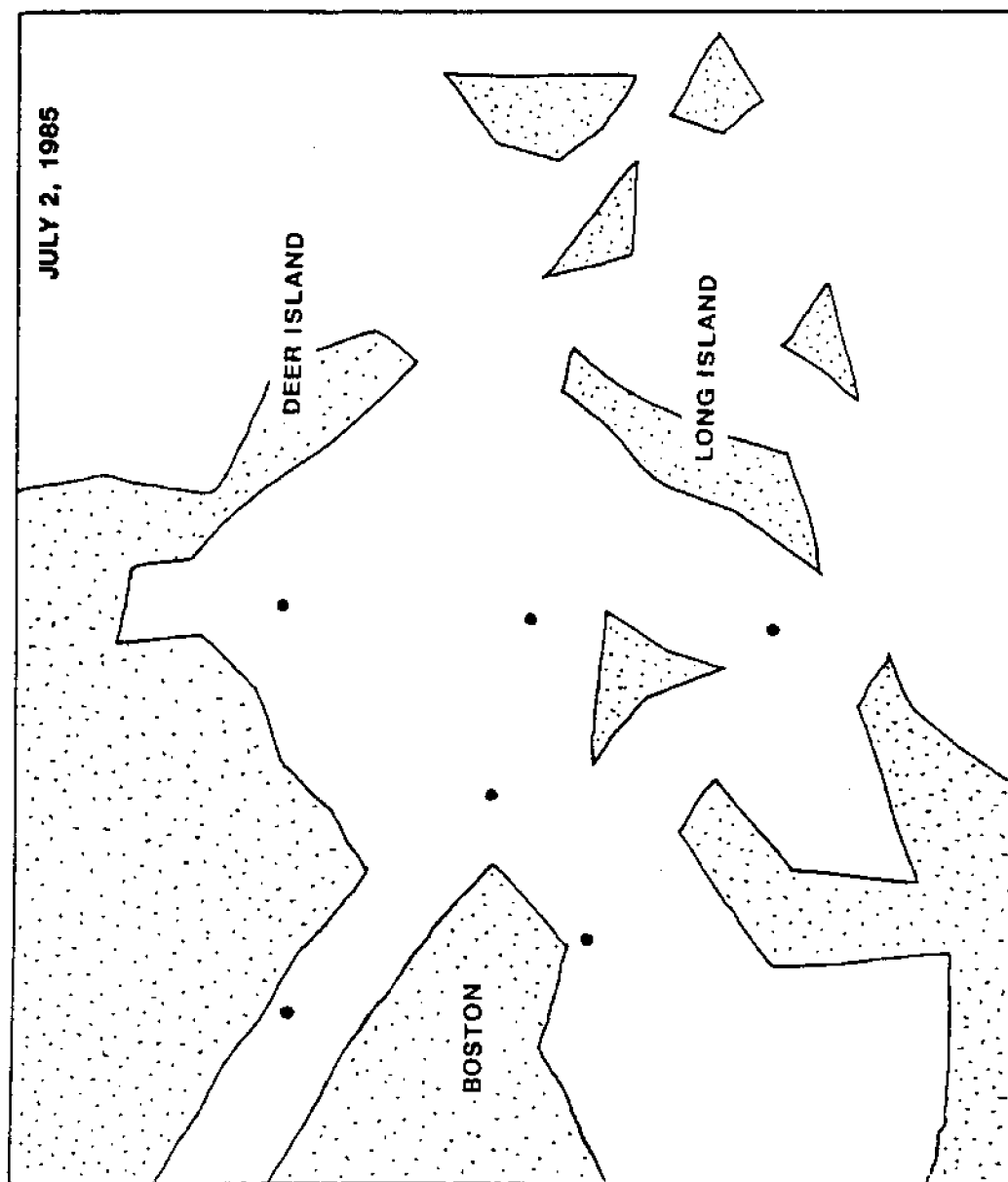
Figure 6.3 Location of Calibration Nodes for July 2, 1985 Sampling Date
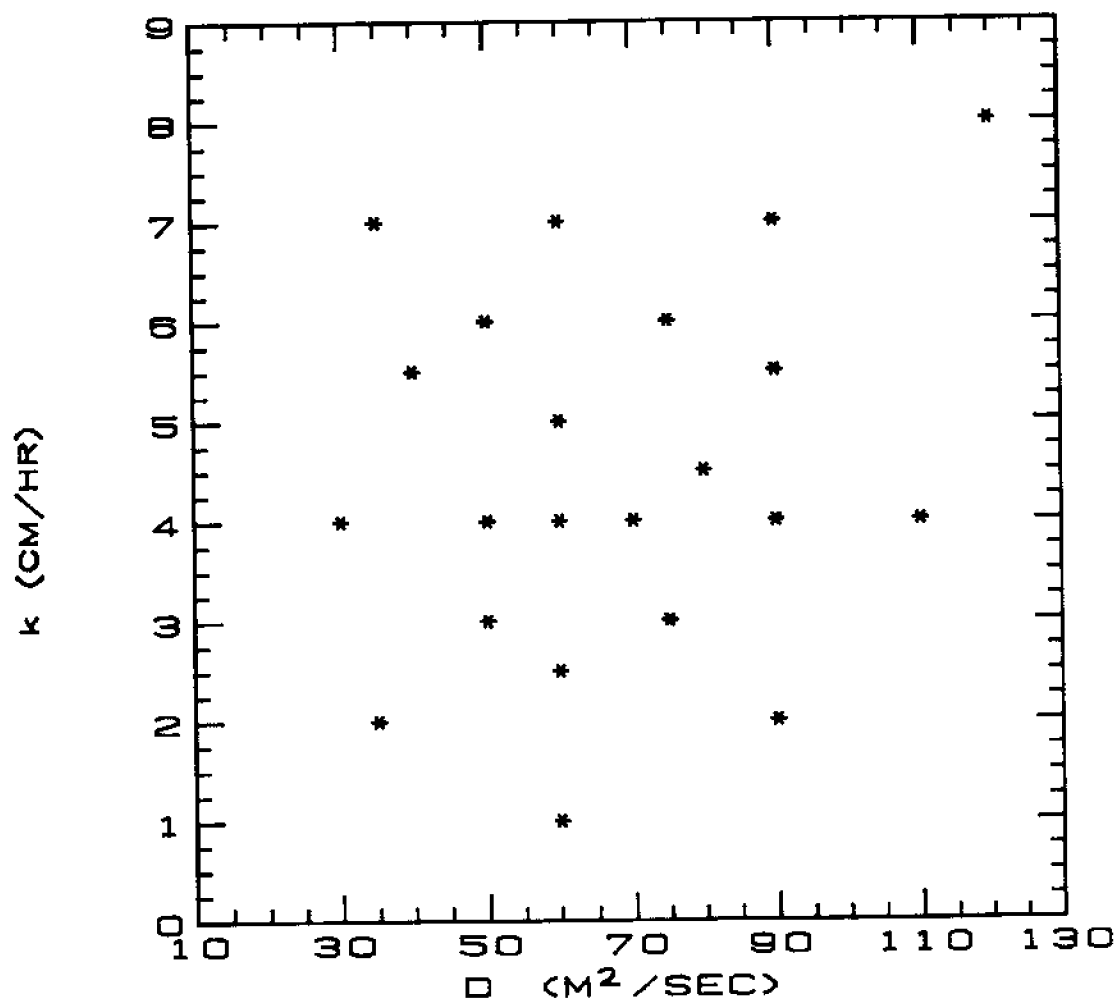
Figure 6.4 Combinations of D and k Used in Model Simulations

C_i is the simulated concentration at node i and a_{11} through a_{19} are fitting parameters. For each node corresponding to a measurement site, equation (6.1.1) was fit to the data (i.e., the 22 model runs, consisting of values of D, k, C_0, and a corresponding C_i for each run) using a multivariate linear regression. This procedure produced values of a_{11} through a_{19} at each calibration node. A resulting approximation function for C_i/C_0 at a typical calibration node is plotted as a function of D and k in the form of a contour map in Figure 6.5. The 22 data points used to generate the function are superimposed on the plot. As can be seen, the function is smooth and well-behaved. At each calibration node, greater than 99% of the variation (represented by the 22 model runs) could be explained by the function. Hence, these functions proved to be excellent interpolators.

The chosen functions (reciprocal biquadratic dependence on D and k) result in concentrations that decrease smoothly at high values of D and k and increase rapidly at low values of D and k. As a result, they act as good extrapolators at high values of D and k but poor extrapolators at low values of D and k.

Having described the simulated concentration at any node as a continuous function of the input parameters (D, k, and C_0), the error between the simulated concentration and the measured concentration at a given node was defined as:

$$E_{ij} = \frac{C_{ij}^m - C_i}{C_{ij}^m} \qquad (6.1.4)$$
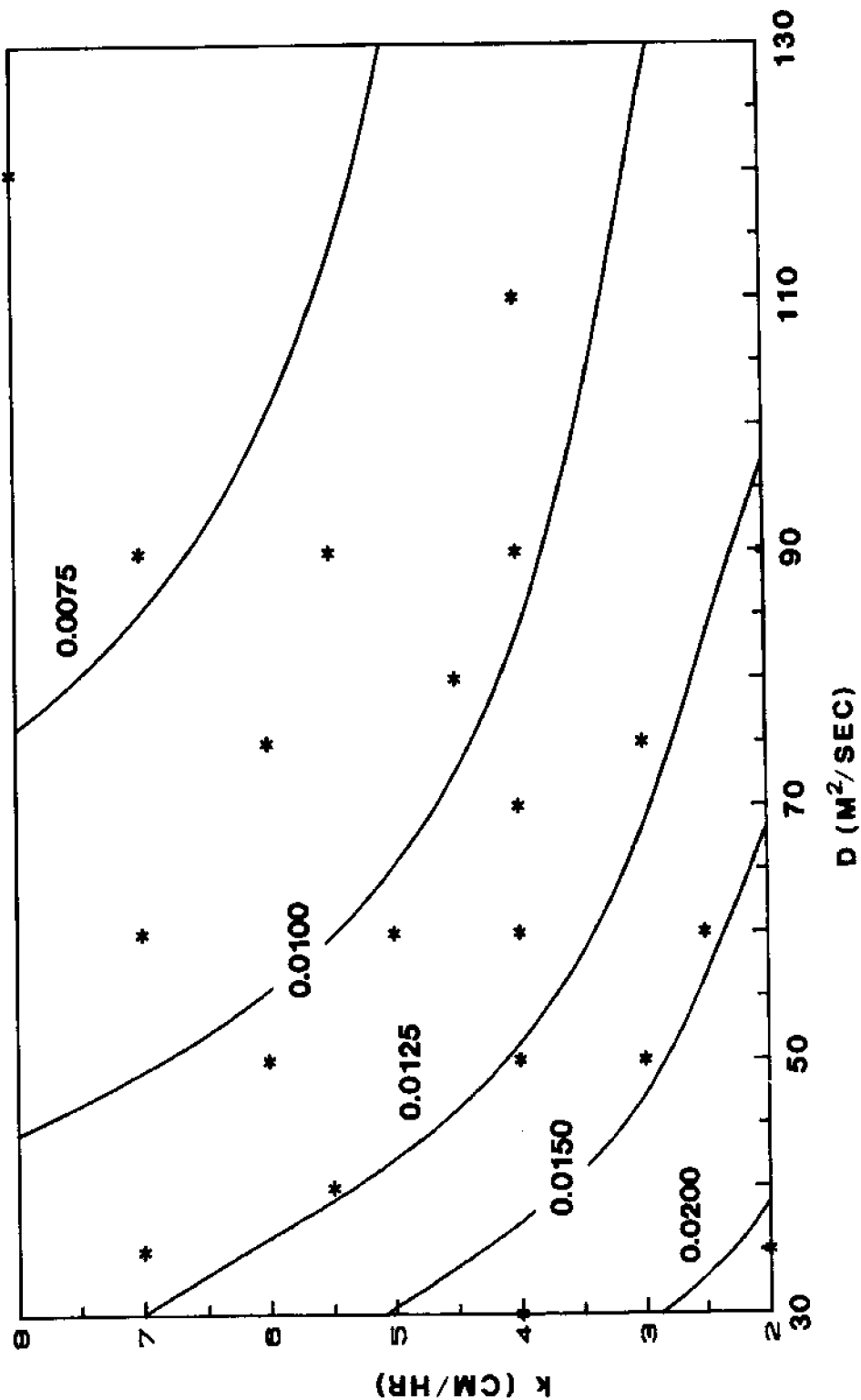
Figure 6.5 Approximated Values of C_1/C_0 at a Typical Calibration Node Plotted as a Function of D and k

where E_{ij} is the relative fitting error at node i for compound j, C_{ij}^m is the measured concentration of compound j at node i, and C_i is the simulated concentration at node i (a function of D, K, and C_o).

Based on this, the root mean square relative error for a given calibration becomes:

$$E_j^R = \left[\frac{1}{n} \sum_{i=1}^{n} E_{ij}^2 \right]^{\frac{1}{2}} \qquad (6.1.5)$$

where E_j^R is the total relative fitting error for compound j on any given date, n is the number of calibration nodes, and E_{ij} is as specified above. By minimizing E_j^R with respect to D, k, and C_0, best-fit values of these three parameters were obtained for each compound on each date.

6.2 Calibration Results

The relative fitting error, E_j^R, is a function of the three independent variables D, k, and C_0. Figures 6.6 through 6.9 present some representative calibration results in which contours of error, E_j^T, are plotted as a function of two of the parameters, while the remaining parameter is held constant. As can be seen, the error contours tend to form long shallow valleys. This result indicates that the three parameters are not entirely independent in their influence on concentration and therefore cannot be completely separated from one another.

BROMODICHLOROMETHANE $D = 75\ M^2/SEC$

CONTOURS

1	.15
2	.2
3	.25
4	.3

k (CM/HR)

C_o (PPB)

APRIL 25, 1985
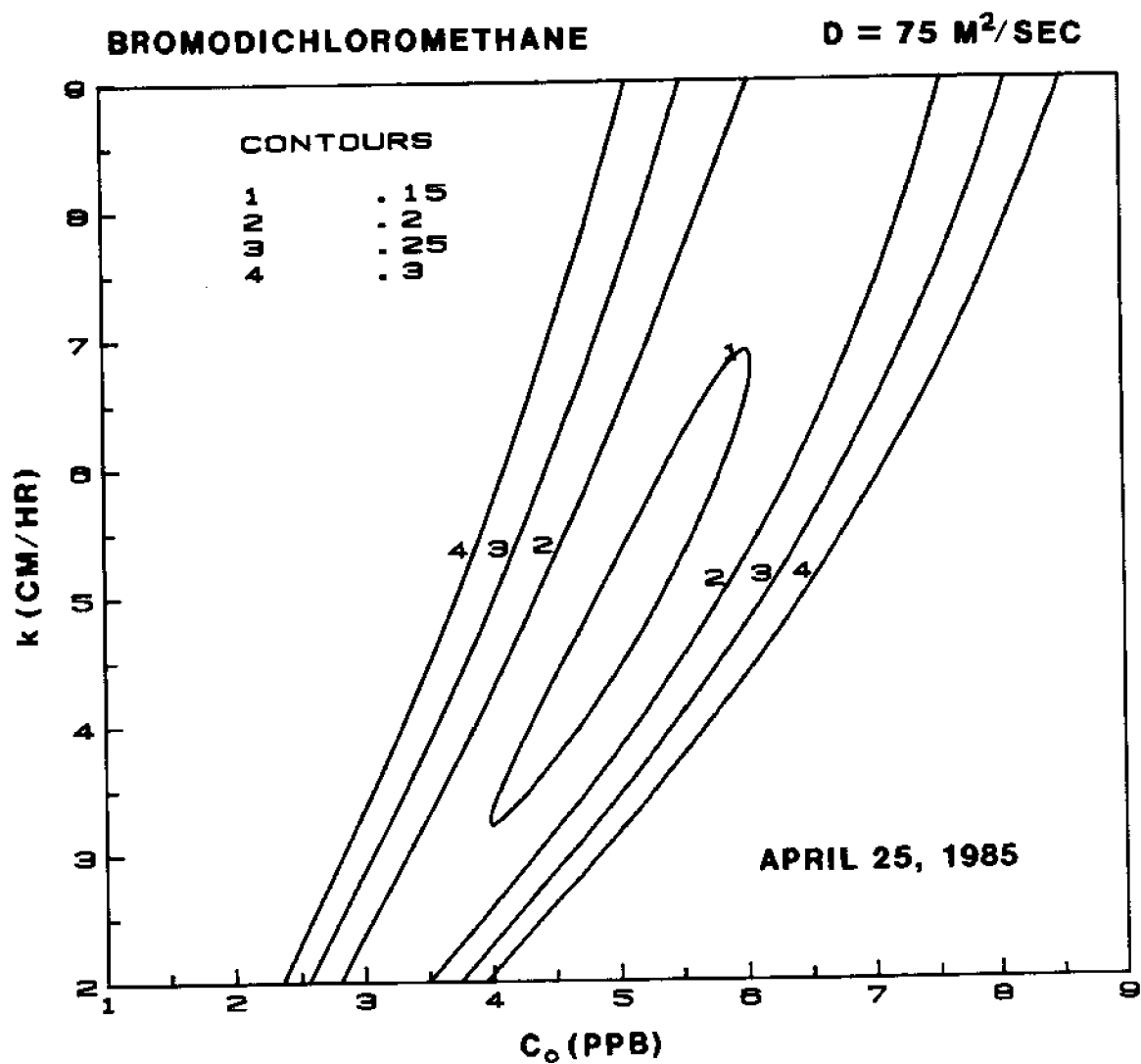
Figure 6.6   Contours of Relative Error Plotted as a Function of k and C_0 at a Fixed Value of D
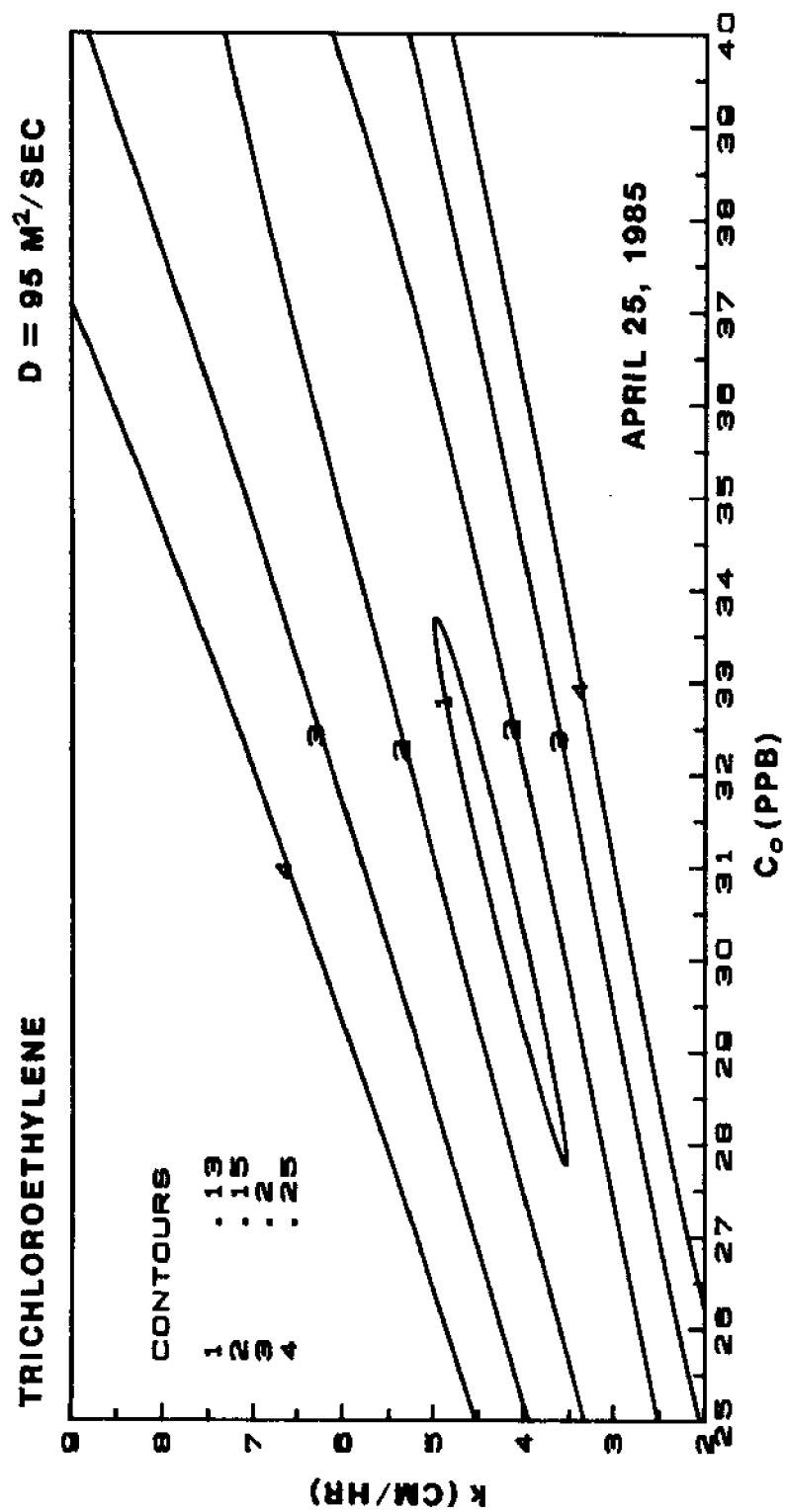
Figure 6.7 Contours of Relative Error Plotted as a Function of k and C_0 at a Fixed Value of D
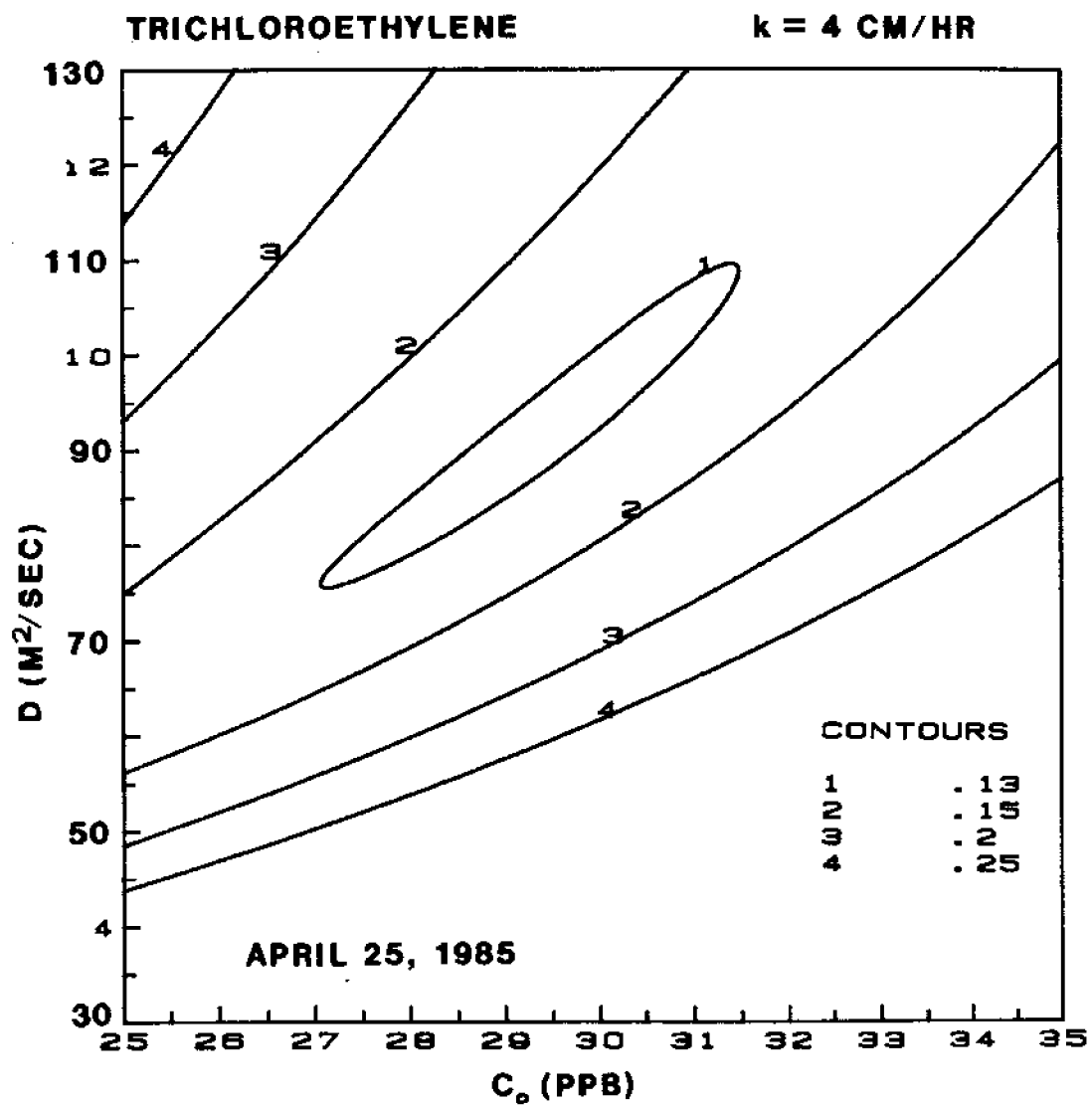
Figure 6.8 Contours of Relative Error Plotted as a Function of D and C_0 at a Fixed Value of k
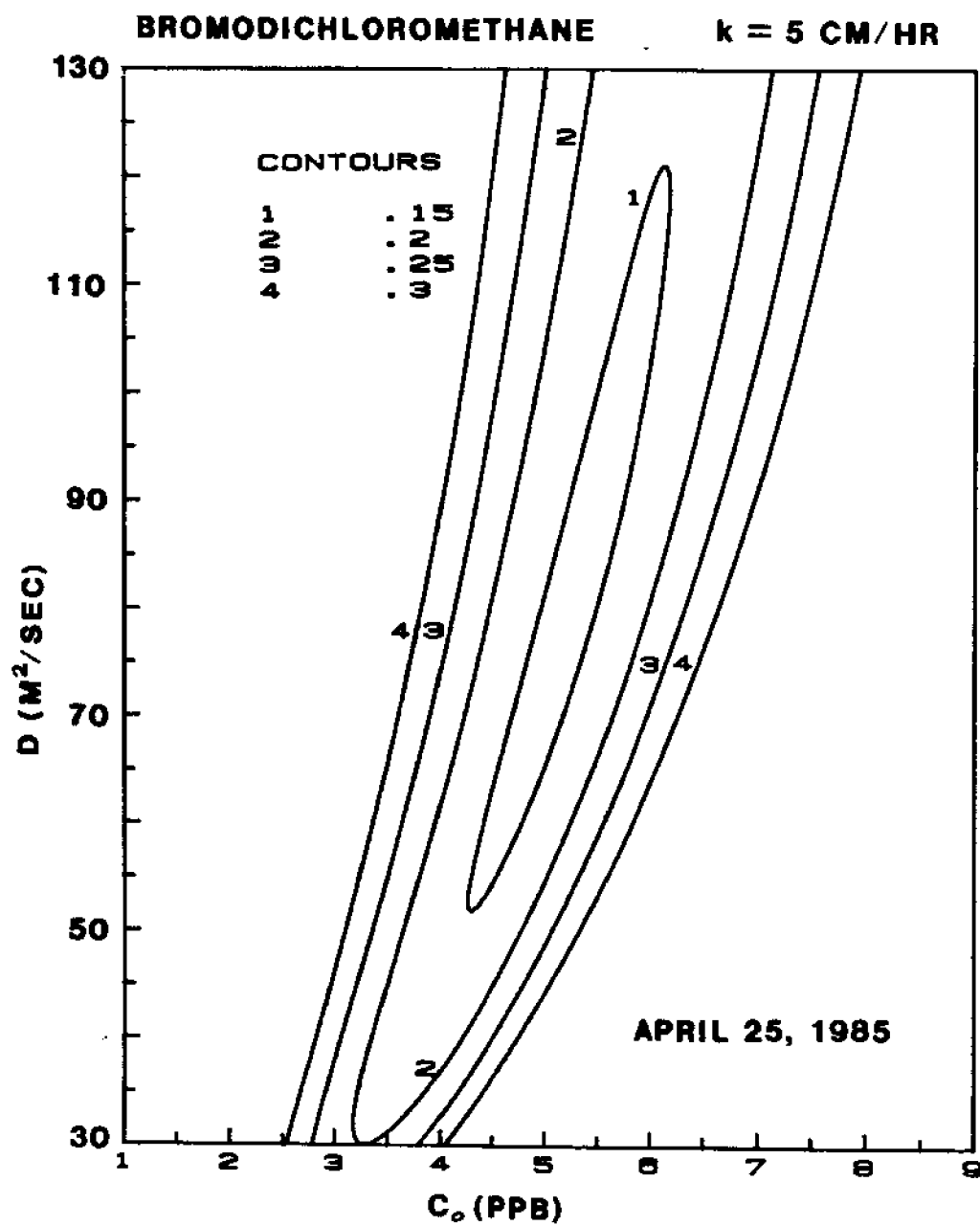
Figure 6.9 Contours of Relative Error Plotted as a Function of D and C_0 at a Fixed Value of k

This behavior results not from poor model performance or parameter choice, but rather from a lack of sufficient calibration data. Consider specifically Figures 6.6 and 6.7, in which error contours are plotted as a function of k and C_0 at a constant value of D. The long shallow valleys are particularly evident in these plots, indicating that k cannot be adequately separated from C_0. Although both of these parameters influence the total mass in the system (mass increases as C_0 increases and k decreases), the value of C_0 affects the concentration in the harbor everywhere equally, while the effect of k on the concentration distribution has a spatial dependence. Our sampling coverage, however, is unable to adequately discern this difference.

To illustrate why this is the case, consider the following one-dimensional transport equation as an analogy to our more complicated multi-dimensional problem:

$$\frac{\partial c}{\partial t} = D\frac{\partial^2 C}{\partial x^2} - \frac{k}{h}C \tag{6.2.1}$$

The steady-state solution to this equation for a continuous plane source located at $x = 0$ is (Harleman, 1980):

$$C = \frac{C_0 Q''h^{\frac{1}{2}}}{2(kD)^{\frac{1}{2}}} \exp\left[\pm x(k/hD)^{\frac{1}{2}}\right] \tag{6.2.2}$$

where the minus sign applies for positive values of x and the plus sign for negative values of x. Q'' is a source flow rate (volume/time·area), h is a mean depth, D is the dispersion coefficient, k is a piston velocity, C_0 is

the source concentration, C is concentration, and x is distance. The solution is illustrated graphically using two separate sets of parameters in Figure 6.10.

Both curves have identical values of D, Q", and h. However, in curve B, C_0 is 25% lower and k is 40% lower than in curve A. (This example is intended to illustrate qualitative behavior and hence the actual values and units of X, D, Q", h, C_0, and k are unimportant.) As can be clearly seen, it is difficult to discern a difference between the two curves near the source. Only by examining the curves far from the source ($|x| > 1$) can they be distinguished.

This simple example is similar to the situation encountered in our calibrations. The calibration points that were used were located in a relatively small region within several kilometers of the source (see Figures 6.1 through 6.3). The insensitivity and interdependence of the calibrated parameters suggest that this is analogous to having all of the calibration points located between $x = -1$ and $x = 1$ in Figure 6.10. Hence we are unable to adequately separate the effects the various parameters have on the concentration distribution. As a result, the calibration results must be interpreted with caution. In particular, the inverse problem, in which observations of concentration are used to infer information regarding the value of k and D, can only be solved by constraining one or more of the parameters. Clearly, accurate and effective use of this method for investigating volatilization and mixing will require synoptic observations both near the source and in the extended far field.
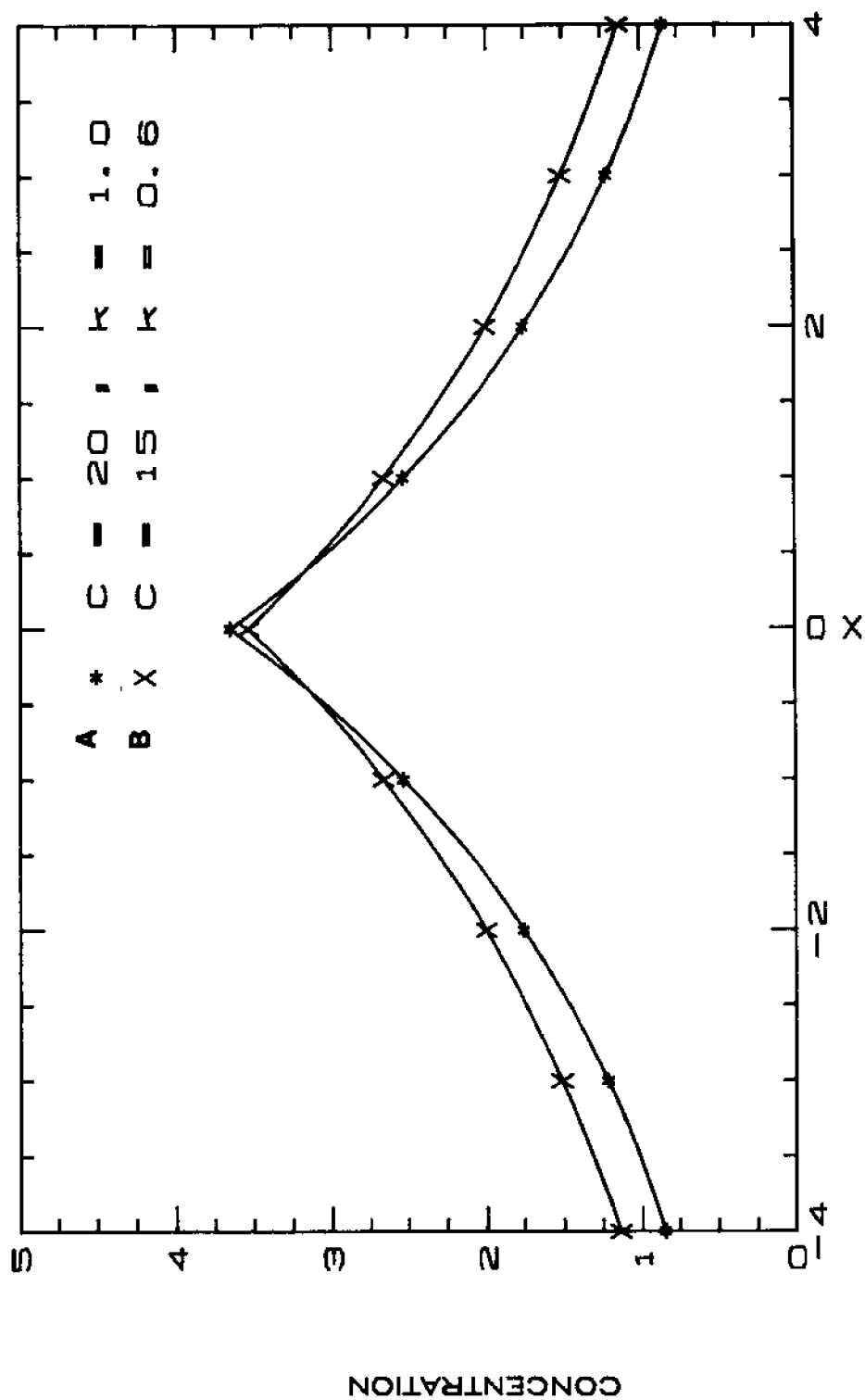
Figure 6.10 Steady State Solution to Equation (6.2.1) for a Continuous Plane
Source at X = 0 (D = 7.5; Q" = 1; h = 1)

Table 6.1 tabulates the results of the calibrations. For each compound on each date, the values of D, k, and C_0Q_0 that resulted in the best fit are given along with the corresponding minimum error. In the following section, these calibration results are used to draw some general conclusions regarding the tracer experiments and model performance. The more difficult inverse problem (in which information regarding D and k is inferred) is addressed in Section 6.4.

6.3 General Discussion of Calibration Results

Calibration data limitations discussed above seriously restrict solution of the inverse problem. On the other hand, the results of Table 6.1 can still be used quite effectively to: 1) elucidate information regarding the behavior of the tracers in the Boston Harbor system; and 2) reach some preliminary conclusions regarding model performance. This is done by considering the values of the best-fit parameters and evaluating the magnitude of the fitting error. The former consists of examining the best-fit parameters to determine whether or not they represent physically realistic values. Since we have actual measurements of C_0Q_0, and have some knowledge of the factors governing k (Chapter 2), these two parameters can be readily evaluated in this manner. This is more difficult to do in the case of D, however, since this parameter is used not only to represent dispersion processes, but also to correct for inaccuracies in our representation of the mean velocity field (e.g., due to low-frequency forcing or nonlinear dynamics). We do know, however, that on any given date the value of D must be the same for each tracer since the physical mixing processes act equally

Table 6.1

Calibration Results: Best Fit Values of D, k, and C_oQ_o

Date	Compound	D (m^2/sec)	k (cm/hr)	C_oQ_o[a] (kg/day)	E[†] $(\%)$	n[‡]
10-30-84	CH_3CCl_3	50	4.5	26.1	12.3	6
"	$CCl_2=CCl_2$	45	2.3	15.5	4.4	6
"	$CHCl=CCl_2$	60	<1*	12.5	25.4	6
"	$CHCl_2Br$	45	2.7	3.2	2.9	3
"	$CHClBr_2$	50	1.1	1.4	2.6	3
"	$CHBr_3$	45	1.3	3.0	0.6	3
4-25-85	CH_3CCl_3	80	6.5	83.8	16.6	6
"	$CCl_2=CCl_2$	70	6.1	103.4	20.4	6
"	$CHCl=CCl_2$	95	4.3	48.8	12.9	6
"	$CHCl_2Br$	75	4.8	7.9	14.1	6
"	$CHClBr_2$	85	4.4	5.2	13.5	6
"	$CHBr_3$	>150*	<1*	38.0	14.0	6
7-2-85	CH_3CCl_3	>150*	5.9	95.5	4.9	6
"	$CCl_2=CCl_2$	>150*	3.4	95.2	3.6	6
"	$CHCl=CCl_2$	>150*	3.0	51.1	6.5	6
"	$CHCl_2Br$	100	10.4	18.2	19.2	6
"	$CHClBr_2$	105	9.0	10.0	21.2	6
"	$CHBr_3$	>150*	<1*	21.9	19.9	6

a input at Deer Island based on a modeled Q_o of 18.4 m^3/sec
† root mean square relative error
‡ number of calibration points
* outside range of calibration values (k = 1-11 cm/hr, D = 30-150 m^2/sec)

on all dissolved substances. Hence, we can draw conclusions based on the relative value of the calibrated dispersion coefficients from compound to compound.

6.3.1 Behavior of Tracer Compounds

The results of model calibrations will first be used to evaluate the behavior of the tracer compounds. It is easiest to begin by examining the various calibrated values of C_oQ_o, since this is the parameter about which the most information is known (Table 4.2 and Appendix II). A comparison of calibrated values of C_oQ_o to measured values of C_oQ_o separates the tracers into two groups: 1) the solvents and bromoform, whose calibrated values are up to 10 times greater than observed values; and 2) bromodichloromethane and chlorodibromomethane, whose calibrated values are within or slightly above observed ranges. It is also apparent that in July the values of D for the solvents and bromoform are at least 1½ times higher and the values of k are at least two to three times lower than the corresponding values for $CHCl_2Br$ and $CHClBr_2$. The bromoform calibration in April follows the same pattern.

These results suggest that there may be other sources of both solvents and bromoform in the harbor that have not been accounted for, and that the calibration procedure is attempting to account for these sources by adjusting the values of D, k, and C_oQ_o. The extra mass could be accounted for by increasing C_oQ_o and/or decreasing k and could then be mixed in the direction of the unmodeled sources by elevating the dispersion coefficient.

It has been noted in the previous section that C_0Q_0 and k cannot be adequately separated. Conceivably, this could account for the elevated values of C_0Q_0 since one could constrain the value of C_0Q_0 to remain in the observed range without drastically increasing the fitting error by simultaneously decreasing the values of k (i.e., moving along the valley in Figure 6.6 or 6.7). However, there is no known volatilization mechanism that would result in lower values of k for the solvents than for the haloforms (Chapter 2). Since constraining the value of C_0 would result in an even lower ratio of k(solvent) to k(haloform), this does not seem feasible. Along similar lines, while all volatilization theories predict values of k for bromoform to be less than or equal to those for the other two haloforms, no theory results in values that are as much as five to ten times lower (as is the case in April and July).

These conclusions are supported by available data which, while qualitative, suggest that a number of additional sources may indeed be present. Kaltofen and Lax (1985) summarize the available information on the known discharges into Boston Harbor. Other than the treatment plants, additional potential sources of the solvents include: 1) numerous industrial outfalls located on the various tributaries (i.e., the Mystic, Chelsea, Charles, and Neponset Rivers) and in the Inner Harbor whose discharges (quantified in Section 4.1) contain chlorinated solvents (e.g., Monsanto, Exxon); 2) numerous shoreline landfills (e.g., Spectacle Island, sites in Chelsea) which may contribute solvents to the harbor via groundwater leaching; and 3) unpermitted outfalls around the perimeter of the harbor that discharge degreasing and cleaning agents. Although these sources are small and diffi-

-181-

cult to quantify, they are quite numerous and the solvents may be highly concentrated in their discharges. Hence, it is not inconceivable that as a whole they are comparable in magnitude to the treatment plants as sources of chlorinated solvents.

As pointed out in Chapter 2, the only significant sources of bromoform to natural waters are chlorinated discharges. In addition to the chlorinated treatment plant discharges, two power plants discharge cooling water to Boston Harbor that is periodically chlorinated. The Boston Edison L St. Generating Station in South Boston discharges up to 11 m^3/sec of cooling water to the Reserve Channel. The Boston Edison Mystic Station discharges up to 40 m^3/sec of cooling water to the Mystic River. Although power plants only chlorinate periodically (e.g., once or twice a day for one hour), this would still amount to several m^3/sec of chlorinated effluent. Since this effluent typically contains bromoform at part-per-billion concentrations (Battelle, 1982), it is clear that the input of bromoform from the power plants could be comparable to the input from the treatment facilities. Note that the power plants do not introduce any significant amounts of the other two haloforms ($CHCl_2Br$ and $CHClBr_2$), since chlorination of water having any appreciable salinity ($>$ 8 parts per thousand) results almost exclusively in the production of bromoform (Helz, 1978).

Summarizing, it appears that only $CHCl_2Br$ and $CHClBr_2$ can be used effectively as tracers in Boston Harbor. The three solvents simply have too many uncharacterizable sources. Given the widespread use and disposal of the chlorinated solvents (Chapter 2), it is likely that this is the case in other coastal regions as well. On the other hand, although this study

made no attempt to do so, it should be relatively easy to characterize cooling water discharges with respect to bromoform, and since these sources are small in number, and easy to identify, bromoform may still prove to be an effective tracer.

6.3.2 Model Performance

The complete evaluation of a complex numerical model requires a large amount of data. Few, if any, complex circulation and transport models are adequately validated. Nevertheless, limited data can often be used to draw some general conclusions regarding the behavior of a model. In our case, several general statements regarding model performance can be made.

The model simulations appear to agree well with observations. The relative fitting errors in Table 6.1 range from 1% to 20%, and considering the uncertainties involved (e.g., measurement errors, modeling assumptions discussed in Chapter 5), this is a reasonable agreement. More importantly, for the case of the two haloforms (whose results are not biased by the presence of unmodeled sources), the best-fit parameters are physically realistic. The values of C_0 are within (or slightly above) the observed ranges. In addition, they have the correct relative magnitude (the concentration of $CHCl_2Br$ being somewhat greater than that of $CHClBr_2$). The values of k are also in expected ranges based on empirical equations (e.g., Wolff and van der Heijde, 1982) and previous studies (e.g., Emerson, 1975; Peng et al., 1979). This will be discussed in more detail in 6.4.1. Although the value of D is several times higher than one might expect for pure dispersion, this is to be expected since this parameter was used not

-183-

only to represent dispersive processes, but also to account for advective processes not adequately modeled by TEA. The calibrated values of D are still less than the D_{max} defined in Chapter 5.

The fact that the model calibrations were able to indicate the presence of other sources is another positive reflection on model behavior. In fact, this is the kind of problem that an effective harbor management tool would be called on to solve.

More complete validation of TEA and ELA will require large-scale hydrodynamic and chemical measurements throughout the region. The results of this study indicate that the models seem to adequately represent the major processes involved and further validation efforts are therefore justified.

6.4 Solution of the Inverse Problem (Parameter Estimation)

Hydrodynamic circulation and transport models such as TEA and ELA can be used for two purposes. First, after having been validated by hydrodynamic and chemical observations, they can be used to predict circulation patterns and concentration distributions. Second, they can be used to solve the inverse problem in which the models are calibrated using experimental data in order to infer information regarding processes represented by model parameters.

The following two subsections address the inverse problem. In 6.4.1, model calibrations are used to infer information regarding volatilization by examining best-fit values of k. In 6.4.2, best-fit values of D are used

to infer a harbor flushing time. Given the results of 6.3.1, only $CHCl_2Br$ and $CHClBr_2$ are used to draw these inferences. Although the analyses are somewhat restricted due to a lack of calibration data, they are still highly informative.

6.4.1 Volatilization in Boston Harbor

As pointed out by Broecker and Peng (1984), existing methods for studying volatilization processes in natural waters are difficult or impossible to apply to coastal regions and are typically used only in simple lake, stream, or open-ocean systems (e.g., Peng et al., 1974; Emerson, 1975; Duran and Hemond, 1984). Hence, one of the objectives of this work was to investigate the use of multiple nonconservative tracers in conjunction with modeling efforts as a tool for studying volatilization processes in natural waters. Such a method, if proved to be feasible in Boston Harbor, could then be applied to other regions where traditional methods are not applicable. The general procedure has been discussed in some detail in the preceding chapters. Results are presented and discussed below.

Figures 6.11 and 6.12 and Table 6.2 summarize the environmental conditions in the harbor for the two weeks prior to each sampling date. Figure 6.11 presents observed wind speeds and Figure 6.12 presents observed wave height at Boston Harbor Light Station (Figure 4.2). As was illustrated in Figure 2.3, the piston velocity is extremely sensitive to environmental conditions, primarily windspeed and wave climate. These figures indicate that these parameters were highly variable in the two weeks prior to sam-
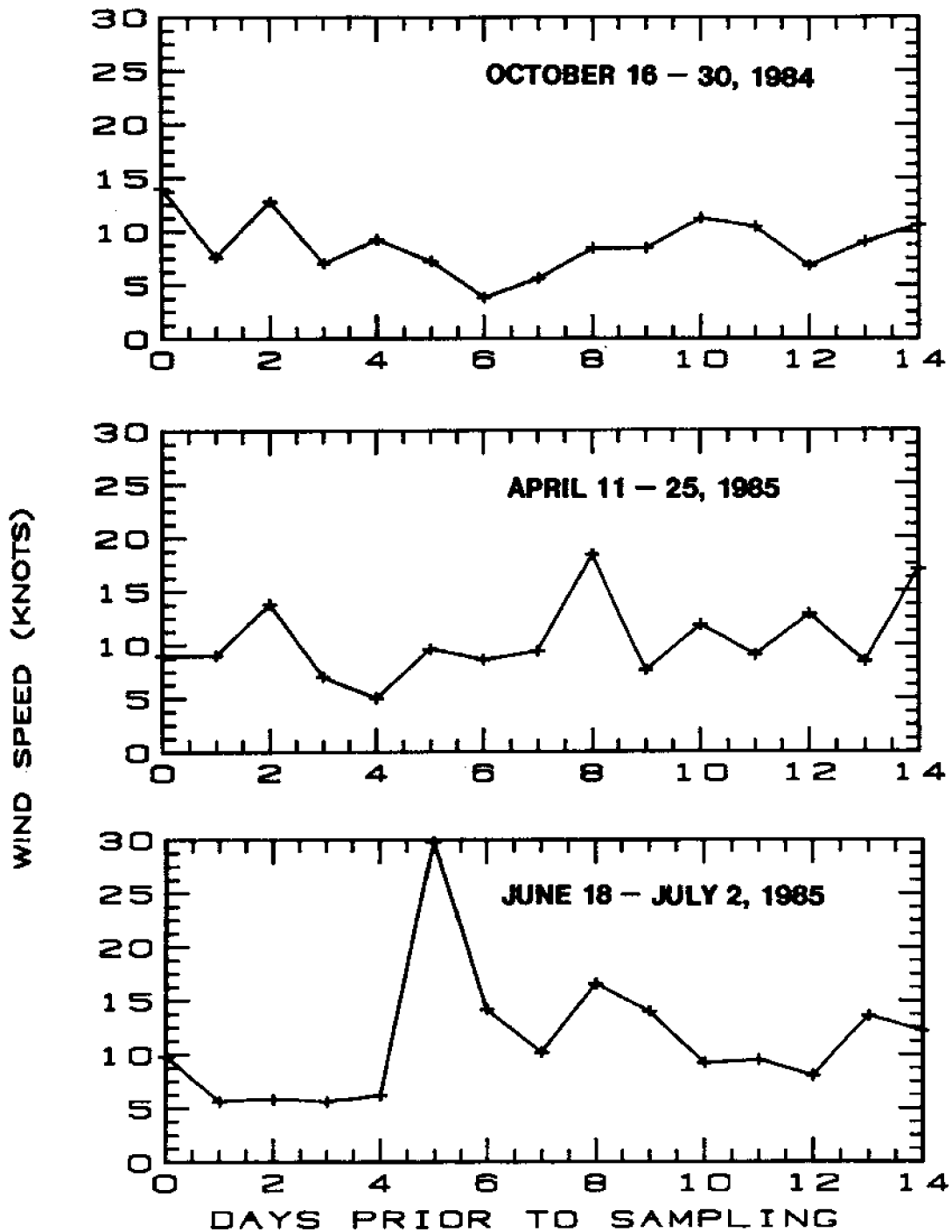
Figure 6.11 Observed Wind Speeds Two Weeks Prior to Each Sampling Date at Boston Harbor Light Station
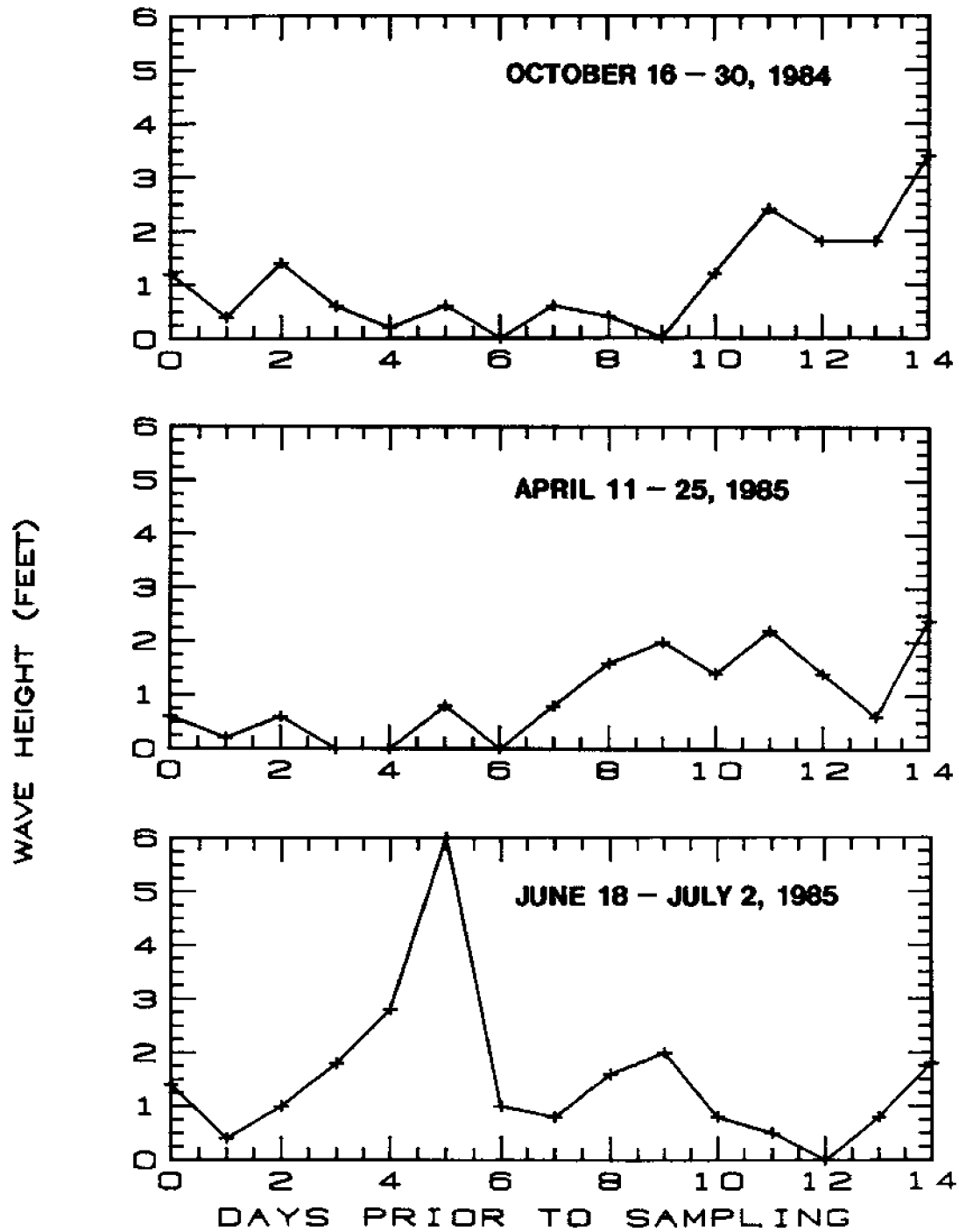
Figure 6.12 Observed Wave Height Two Weeks Prior to Each Sampling Date at Boston Harbor Light Station

Table 6.2

Effective Mean Wave Heights and Wind Speeds[*]
at Boston Harbor Light Station
Two Weeks Prior to Each Sampling Date

	Wave height (ft)	Wind speed (knots)
October 16–30, 1984	0.9	9.0
April 11–25, 1985	0.8	10.0
June 18–July 2, 1985	1.6	10.9

---

[*] Based on an exponential filter:

$$\langle W(t) \rangle_{\substack{\text{effective}\\ \text{mean}}} = A\left[1 - e^{-k\Delta t}\right] \sum_{i=0}^{\infty} W(t-i\Delta t)e^{-ki\Delta t}$$

where A is a normalization factor such that

$$A\left[1 - e^{-k\Delta t}\right] \sum_{i=0}^{\infty} e^{-ki\Delta t} = 1$$

and k is chosen to represent an average first-order decay rate (due to volatilization and flushing). For these calculations, k was chosen as 1/14 day^{-1} based on estimated decay rates (see results of this section and Section 6.4.2)

pling, especially in July. Furthermore, one would expect different portions of the harbor to be subjected to different wind and wave conditions. Hence, the calibrated values of k represent an effective mean of a temporally and spatially varying piston velocity.

As pointed out in Section 6.2, in the absence of adequate calibration data, it is impossible to separate k from C_0Q_0. Hence, in order to evaluate the magnitude of the piston velocity, it is necessary to constrain the value of C_0Q_0. If we had an accurate estimate of the mean value of C_0Q_0 for several weeks prior to sampling, this would present no problem. However, observations of the source strength were only made for several hours prior to sampling the harbor, and due to the variability of the source, these observations do not necessarily reflect the mean input. As a result, it is not possible to obtain a precise estimate for k.

Table 6.3 presents calibration results for $CHCl_2Br$ and $CHClBr_2$. These results were generated by forcing C_0Q_0 to a given value and then minimizing the error with respect to D and k. Values of C_0Q_0 were chosen to represent the ranges ($\pm$ one standard deviation from the mean) observed in Deer Island sewage effluent (Table 4.2 and Appendix II). Figure 6.13 presents these results graphically for $CHClBr_2$ on the April sampling date. Each curve represents a different value of C_0Q_0 and describes (as a function of k) the minimum error for varying values of D. Similar results (not shown) were produced for both compounds on all three dates.

Based on these results, it is difficult to distinguish different piston velocities from date to date or compound to compound. Nevertheless, it can be stated that the piston velocity for these compounds on all three

Table 6.3

Calibrated Piston Velocities for $CHCl_2Br$ and $CHClBr_2$

Date	$CHCl_2BR$ $C_0Q_0^{a,b}$ (kg/day)	k (cm/hr)	E^d (%)	$CHClBr_2$ $C_0Q_0^{a,c}$ (kg/day)	k (cm/hr)	E^d (%)
10-30-84	2.36	1.4	5.5	1.18	1.3	11.6
"	3.24	2.8	2.9	2.08	2.5	6.5
"	4.11	3.7	3.5	2.98	4.3	9.6
"	4.99	4.4	4.5	3.88	6.1	11.1
"	5.86	5.4	5.4	4.78	7.5	12.2
4-25-85	2.36	<1*	--	1.18	<1*	--
"	3.24	1.9	15.5	2.08	1.6	15.3
"	4.11	2.5	14.7	2.98	2.8	14.0
"	4.99	3.2	14.6	3.88	3.5	13.7
"	5.86	3.6	14.4	4.78	4.0	13.5
7-2-85	2.36	<1*	--	1.18	<1*	--
"	3.24	1.1	32.9	2.08	1.1	28.6
"	4.11	1.9	23.5	2.98	2.6	23.0
"	4.99	2.8	21.9	3.88	3.7	22.6
"	5.86	3.3	21.5	4.78	4.4	22.1

* outside range of calibration values
a based on modeled Q_0 of 18.4 m^3/sec at Deer Island
b C_0Q_0 = 4.11 ± 1.75; n = 54 (Table 4.2)
c C_0Q_0 = 2.98 ± 1.80; n = 54 (Table 4.2)
d root mean square relative error

CHLORODIBROMOMETHANE
APRIL 25, 1985
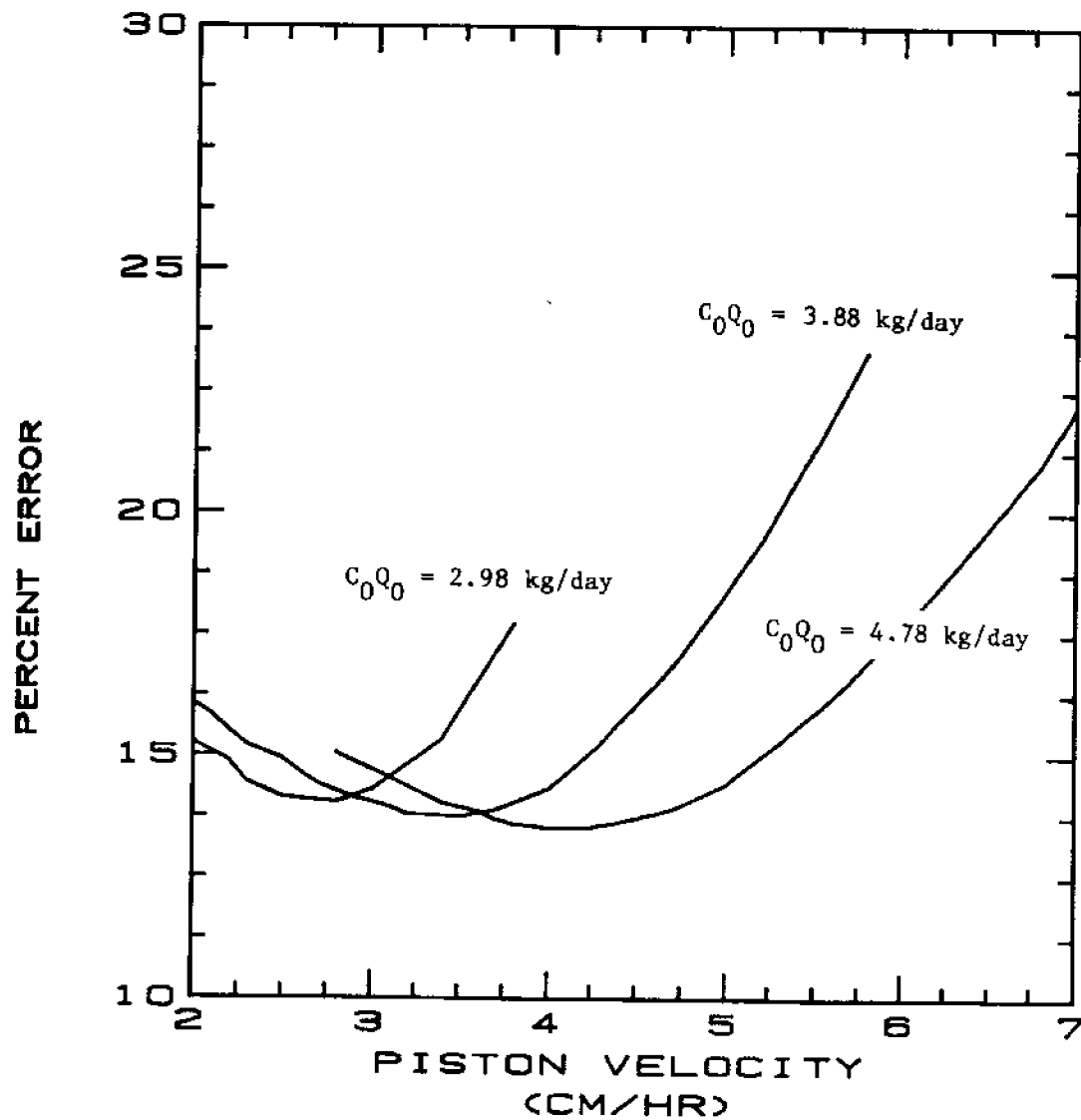
Figure 6.13   Calibration Results for CHClBr$_2$ on April 25, 1985

dates appears to fall within the range from 1 to 8 cm/hr, with the most likely value (based on effluent observations and calibration fitting errors) being 2 to 5 cm/hr. This corresponds to a stagnant film layer thickness (see Chapter 2) ranging between 50 and 400 μm, with the most likely value being 80 to 200 μm. Emerson (1975) reported values of 600 μm for small lakes, while open ocean values as low as 20 to 30 μm have been reported (e.g., Peng et al., 1974; Peng et al., 1979). Our coastal water values fall between these two extremes. Since a coastal embayment can be considered to be intermediate between these two regimes (with respect to fetch, windspeed, waves, etc.), this is an intuitively pleasing result. In addition, these values agree well with empirical relationships that relate windspeed to piston velocity. The empirical equations of Wolff and van der Heijde (1982) require a wind speed of 8 to 13 knots to produce piston velocities of 2 to 5 cm/hr for our compounds. This corresponds well to the actual wind speeds observed (Figure 6.11).

It was discussed in some detail in Chapter 2 that by simultaneously examining the piston velocites of two compounds volatilizing at different rates, the mechanism of volatilization can be inferred. This approach consists of comparing the observed ratios of piston velocities to the ratios predicted by various volatilization theories.

Unfortunately, in light of previous results, it appears that it may be difficult to distinguish different piston velocities from compound to compound. In fact, this conclusion can be reached by simply considering the chemical observations without the aid of the model calibrations. Figures 6.14 through 6.16 present the observed ratio of $CHCl_2Br$ to $CHClBr_2$

October 30, 1984

1.58

2.24

1.87

1.97

1.93

1.66

1 km
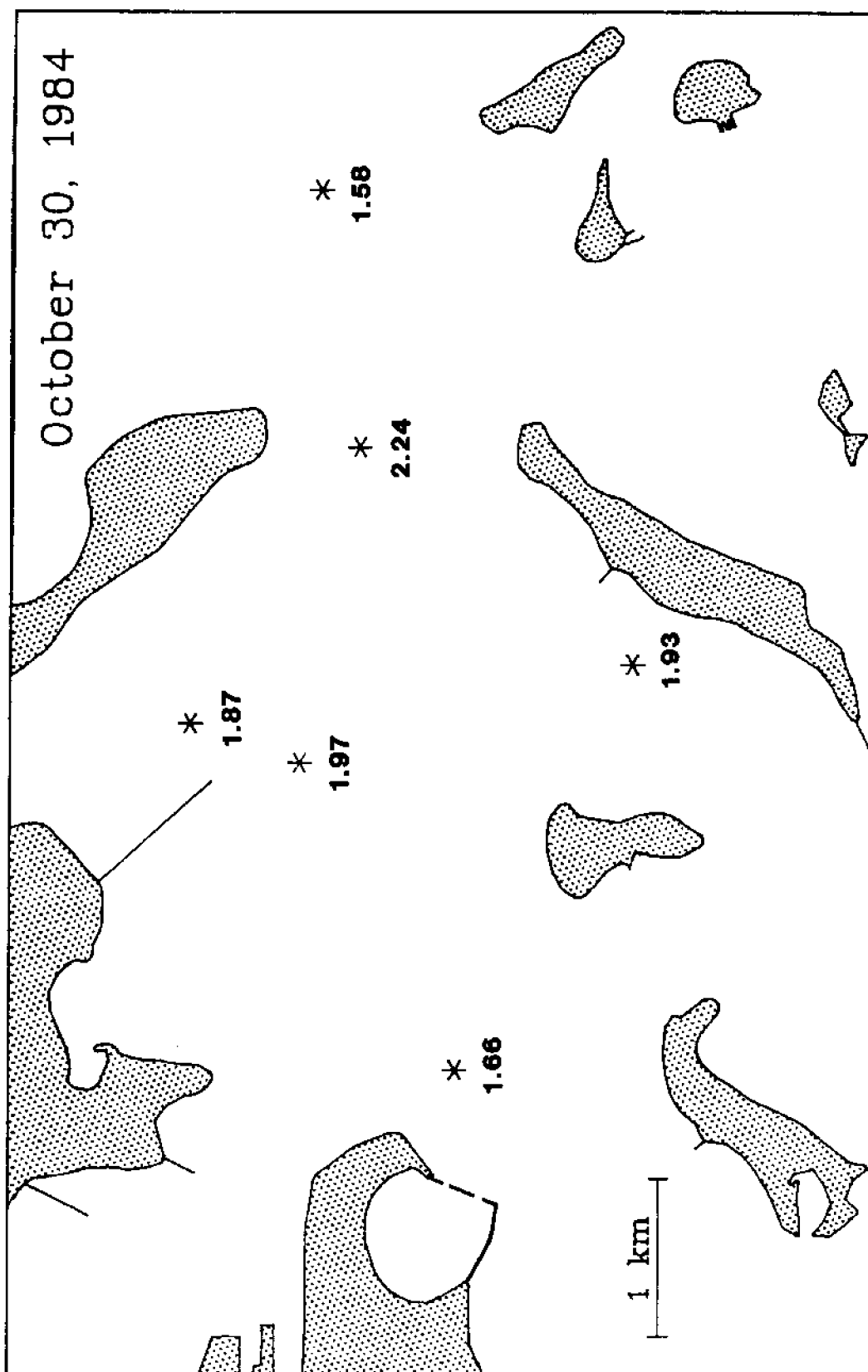
Figure 6.14 Concentration Ratios of $CHCl_2Br$ to $CHClBr_2$, in Boston Harbor at High Water Slack
(mean of surface and deep water samples) on October 30, 1984
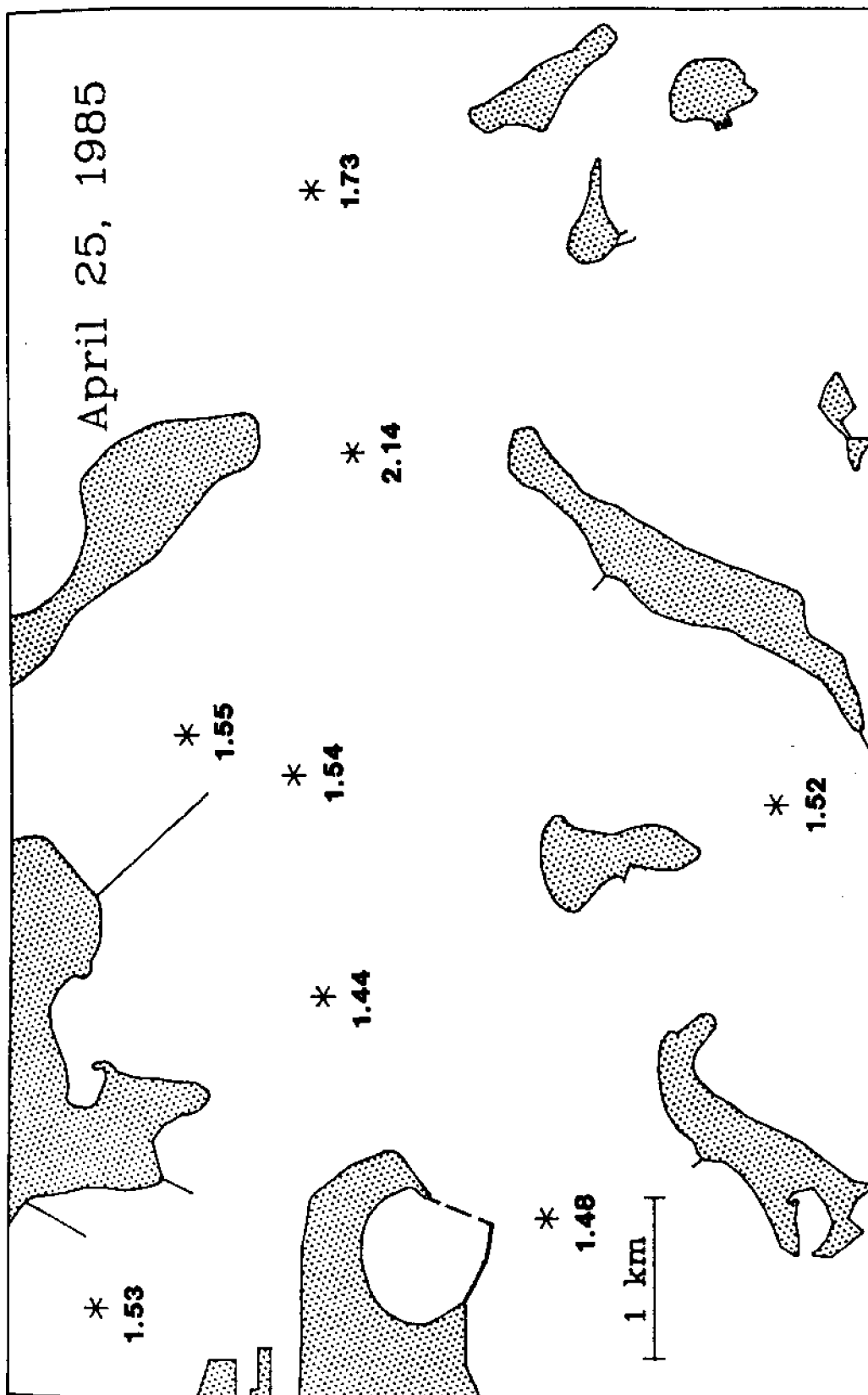
Figure 6.15   Concentration Ratios of $CHCl_2Br$ to $CHClBr_2$ in Boston Harbor at High Water Slack (mean of surface and deep water samples) on April 25, 1985

July 2, 1985

1.84

1.75

2.20

1.43

1.77

1.68

1.69

1.60

1 km
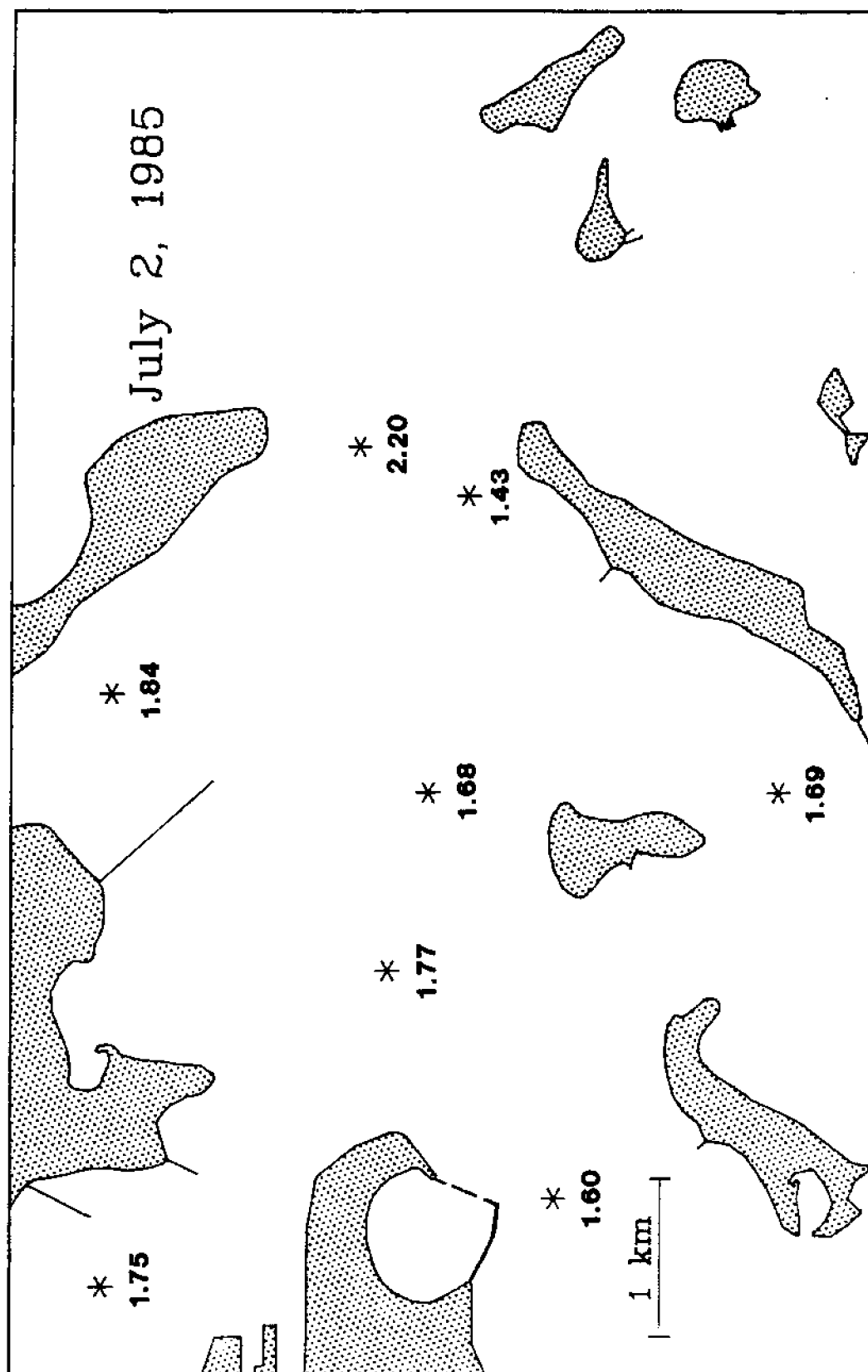
Figure 6.16   Concentration Ratios of $CHCl_2Br$ to $CHClBr_2$ in Boston Harbor at High Water Slack
(mean of surface and deep water samples) on July 2, 1985

at various points in the harbor. These ratios vary from 1.4 to 2.2. By comparing these values to the values observed in the effluent, one can evaluate whether or not the compounds are lost (i.e., through volatilization) at different rates once they are introduced into the harbor. If the ratio of these compounds in the effluent was signficantly different from that observed in the harbor, one could conclude that they volatilize differentially.

A preliminary examination of Figures 6.14 through 6.16 may lead one to suspect significant differential volatilization is occuring since the ratio in the plume at Deer Island is significantly higher than at other locations. However this is misleading since at that particular location, the observed ratio is extremely sensitive to the instantaneous effluent ratio, which is highly variable. In fact, the effluent ratio varies from 0.89 to 2.39 (± one standard deviation from the mean of 54 observations). Clearly, because of the variability of this source function, it is not possible to distinguish whether or not the effluent ratios and harbor ratios are significantly different.

Calibration results illustrate the same point. In Figures 6.17 through 6.19 the ratio of $k(CHCl_2Br)$ to $k(CHClBr_2)$ is contoured (solid lines) as a function of $C_0(CHCl_2Br)$ and $C_0(CHClBr_2)$. These curves were generated by choosing values of C_0 and minimizing the fitting error with respect to $k(CHCl_2Br)$, $k(CHClBr_2)$, and D (which was forced to be the same for both compounds). Error contours (dashed lines) are superimposed on the ratio contours. Clearly, the error minima are very shallow and cannot be used as a criterion for determining the piston velocity ratio.

OCTOBER 30, 1984
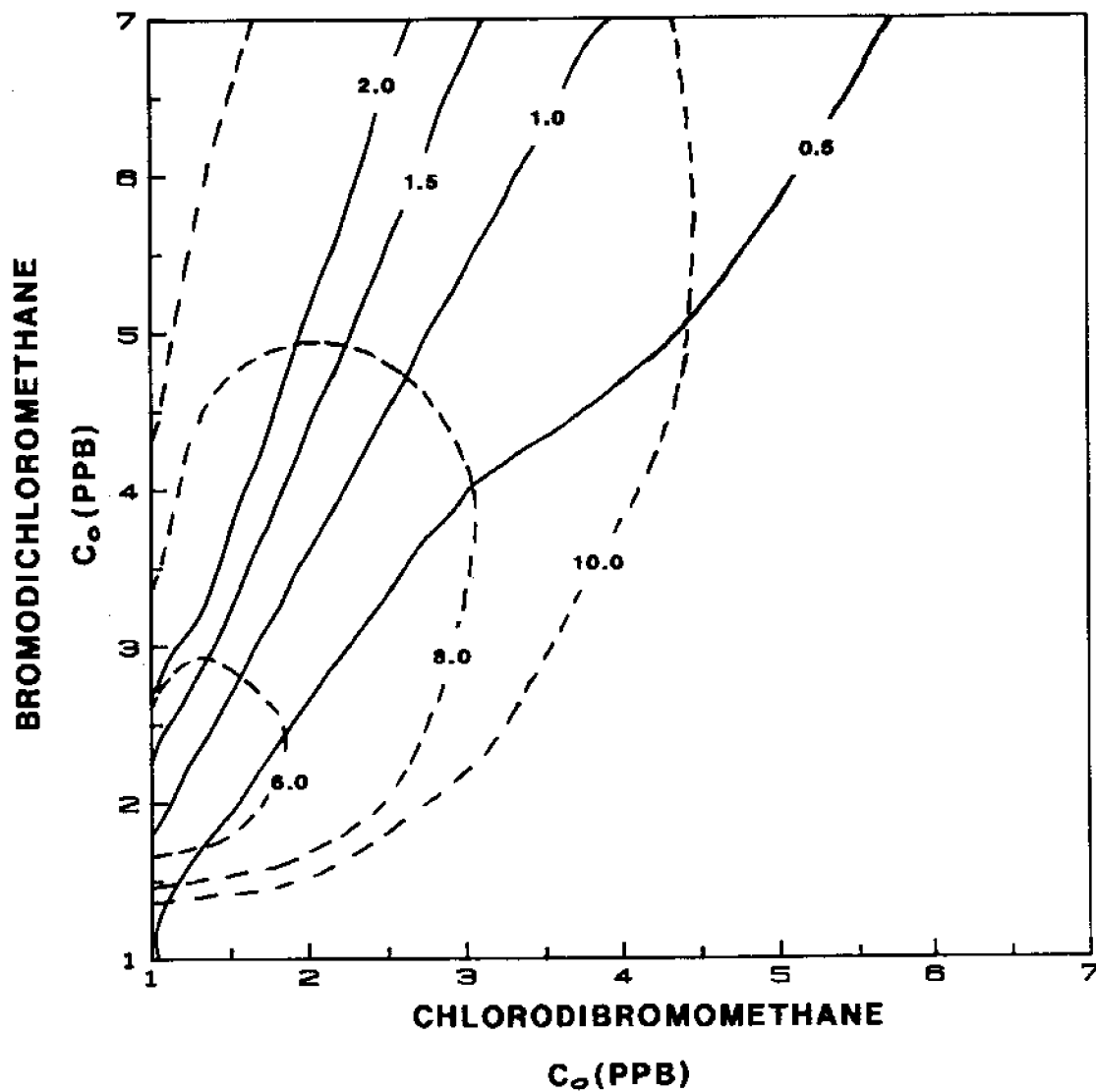
Figure 6.17 Ratio Contours of $k(CHCl_2Br)$ to $k(CHClBr_2)$ (solid lines) and Contours of % Fitting Error (dashed lines) as a Function of $C_0(CHCl_2Br)$ and $C_0(CHClBr_2)$ on October 30, 1984

APRIL 25, 1985

Figure axes: BROMODICHLOROMETHANE C_o (PPB) (vertical), CHLORODIBROMOMETHANE C_o (PPB) (horizontal)

Contour labels: 1.5, 1.0, 2.0, 0.5, 10.0, 10.5, 11.0
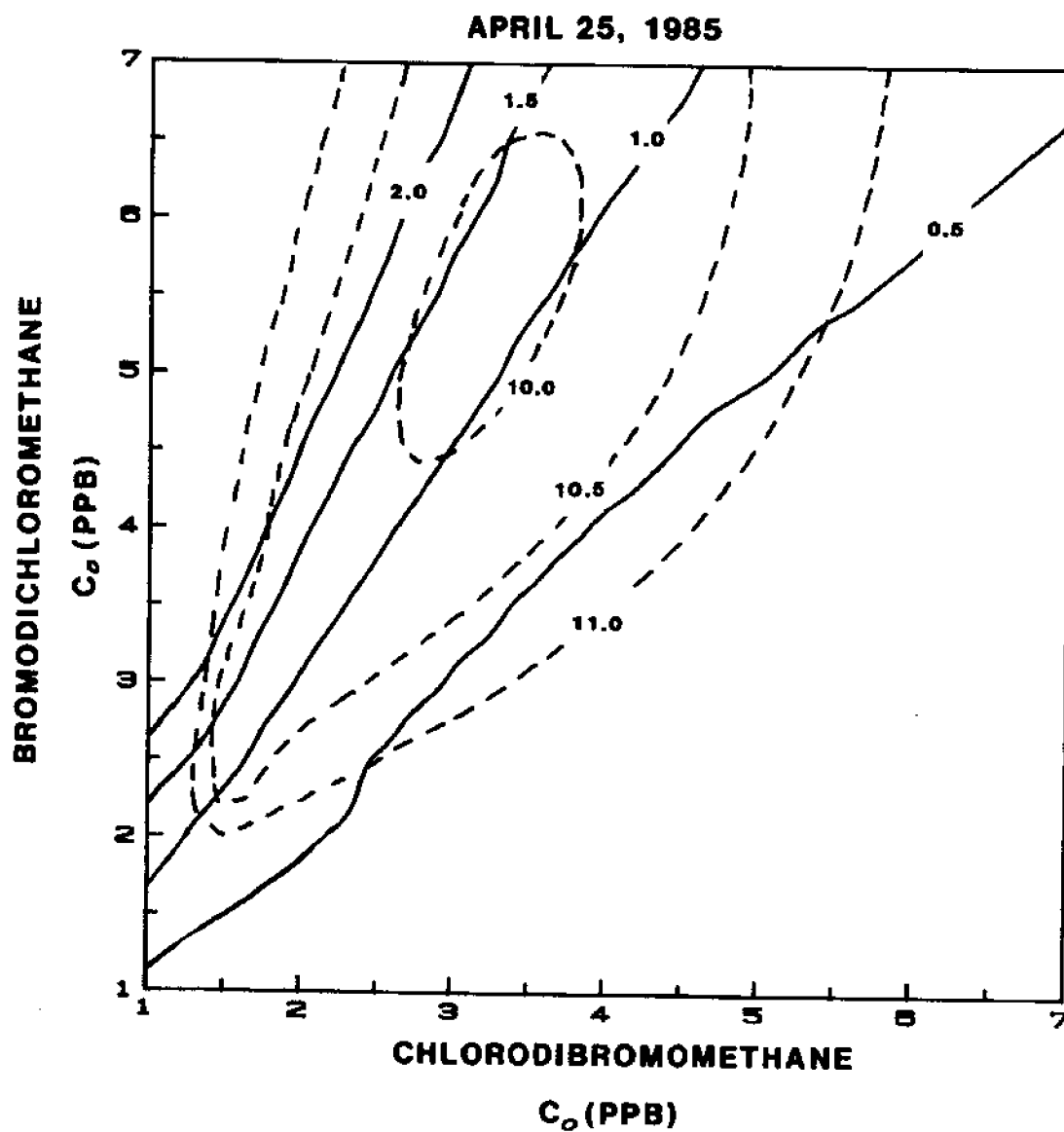
Figure 6.18 Ratio Contours of $k(CHCl_2Br)$ to $k(CHClBr_2)$ (solid lines) and Contours of % Fitting Error (dashed lines) as a Function of $C_0(CHCl_2Br)$ and $C_0(CHClBr_2)$ on April 25, 1985
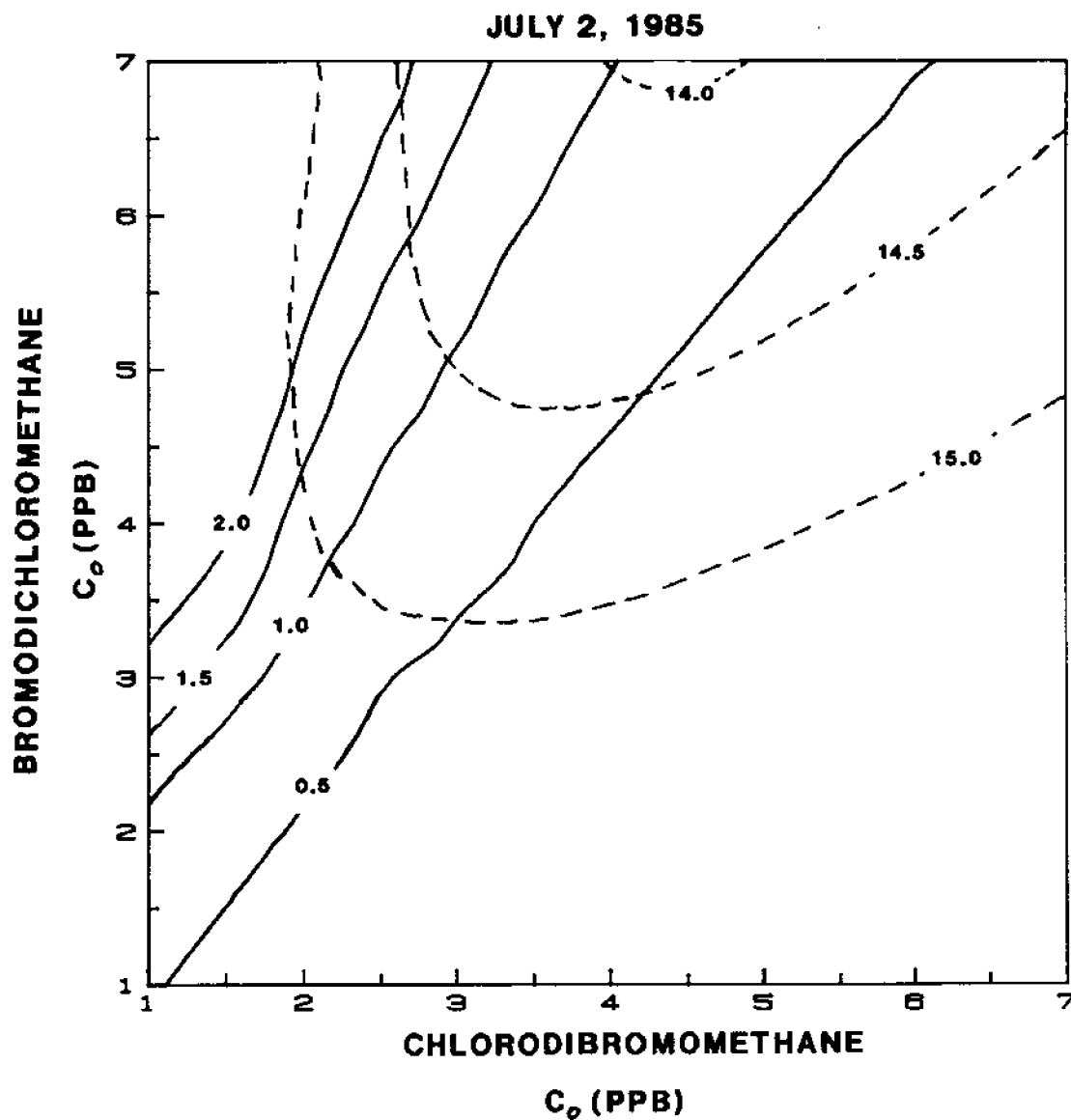
JULY 2, 1985

Figure 6.19   Ratio Contours of $k(CHCl_2Br)$ to $k(CHClBr_2)$ (solid lines) and Contours of % Fitting Error (dashed lines) as a Function of $C_0(CHCl_2Br)$ and $C_0(CHClBr_2)$ on July 2, 1985

Hence, in order to determine the piston velocity ratio, the ratio of source strengths must be constrained. However, as was illustrated in Figure 4.10 and pointed out above, this concentration ratio is highly variable, ranging from 0.89 to 2.39. Since Figures 6.17 through 6.19 indicate that the piston velocity ratio is quite sensitive to these source strengths, it is impossible to determine whether the ratio of piston velocities is significantly greater than one (implying bubble injection) and additional calibration data and/or source characterization data are needed before any statement can be made regarding the mechanism of volatilization.

Although the results regarding volatilization rates are imprecise and those regarding volatilization mechanisms are inconclusive, this is due to a lack of data, not an inadequate technique. The fact that the volatilization rates as determined by the calibrations clearly fall within the expected range indicates that, given adequate data, this technique could be used as a valuable tool for investigating volatilization rates and mechanisms in regions that cannot be studied using traditional methods. This type of approach has not been previously attempted, and this preliminary effort has served to illustrate the technique, demonstrate its applicability to a complex system, and identify data requirements.

6.4.2 Flushing Time for Boston Harbor

In Chapters 4 and 5, model simulations and tracer experiments suggested that harbor flushing was inefficient. By using the model simulations in conjunction with the tracer experiments, the flushing time of the harbor can be quantified.

A minimum theoretical tidal flushing time can be defined as:

$$t_f^m \approx \frac{V}{F} \qquad\qquad (6.4.1)$$

where t_f^m is the minimum theoretical tidal flushing time, V is the total volume of the harbor at high tide, and F is the average daily tidal flow leaving on outgoing tides. Using values of 680×10^6 m³ for V and 550×10^6 m³/day for F (Metcalf and Eddy, 1979b), the tidal flushing time is ~1.2 days. The actual flushing time will be much greater than this since most of the water that leaves on the ebb returns on the flood.

The flushing efficiency of a tidal embayment such as Boston Harbor depends not on the mean tidal circulation, but on the residual circulation. In this study, residual circulation was represented by a calibrated dispersion coefficient. Hence, the magnitude of D should be related to the flushing time of the harbor: large values of D should correspond to small flushing times.

Using dimensional analysis, a flushing time for the harbor, t_f, can be defined as

$$t_f = \frac{(L)^2}{D} \qquad\qquad (6.4.2)$$

where t_f is the harbor flushing time, L is the characteristic length scale of the harbor, and D is the calibrated dispersion coefficient. Taking a characteristic harbor length scale of 8 km and a typical calibrated dispersion coefficient ranging from 50 m²/sec to 100 m²/sec, the flushing time

for the harbor is from one to two weeks. This value agrees well with previous estimates (Ketchum, 1951a; Ketchum, 1951b; Metcalf and Eddy, 1984).

Chapter 7

Conclusion

7.1 Summary

The harmonic finite element circulation model TEA and the Eulerian-Lagrangian transport model ELA were modified and applied with high spatial resolution to Boston Harbor. In addition, complementary tracer experiments were carried out. The transport model was then calibrated to the tracer measurements in order to evaluate model behavior and investigate physical and chemical transport processes in the harbor.

Model simulations agree well with measurements, and calibrated parameters have physically realistic values. Comparisons with observations indicate that the models adequately represent the major processes acting in the system and further validation efforts are justified.

The applicabilty of a number of volatile halogenated organic compounds as tracers in coastal waters was investigated. Chemical measurements and model simulations indicate that the source functions of the chlorinated solvents are too complicated to facilitate the use of these compounds as tracers. On the other hand, two of the trihalomethanes, $CHCl_2Br$ and $CHClBr_2$, appear well suited to served as tracers. Bromoform, although possessing a somewhat more complicated source function, may also prove useful.

The use of multiple nonconservative tracers in conjunction with modeling efforts in order to study volatilization processes in natural waters

was discussed. Solution of the inverse problem to determine piston veloci-
ties in the harbor was limited by inadequate calibration data. As a re-
sult, piston velocities could only be determined to within a factor of 2 or
3. The values for $CHCl_2Br$ and $CHClBr_2$ appear to range from 2 to 5 cm/hr,
corresponding to stagnant film thicknesses of approximately 80 to 200 μm.
These values fall between those found for open-ocean sites and small lakes.
In addition, the values agree well with empirical equations relating piston
velocity to wind speed.

Due to a lack of calibration data, results regarding piston velocty
ratios (and hence volatilization mechanisms) were inconclusive. Neverthe-
less, this general technique for investigating volatilization rates and
mechanisms in natural waters (through model calibration) has been
illustrated here and shown to be applicable to complex systems that cannot
be studied using traditional methods. Effective use of this method will
require synoptic observations in both the intermediate and far fields, as
well as a detailed knowledge of the source strength.

The tracer experiments and model simulations were used to evaluate
physical mixing in the harbor. Both approaches suggested that harbor
flushing was inefficient. Model calibrations indicate a harbor flushing
time of one to two weeks.

7.2 Areas for Future Work and Improvements

Future research must focus on both the modeling and measurement as-
pects of this work. In terms of modeling, an effort should be made to
obtain a better understanding of low frequency forcings. In addition,

nonlinear dynamics should be included by applying the nonlinear version of TEA to the harbor. This can only be justified by obtaining complementary hydrodynamic measurements against which TEA-NL can be validated. Such measurements must include both Eulerian (current meters) and Lagrangian (drifters) data.

If the circulation model could be properly validated, one could then take full advantage of ELA's ability to model dispersion processes (without introducing significant numerical diffusion). At that point it may be useful to allow both the dispersion coefficient and the decay rate (piston velocity) to be spatially and temporally variable.

In terms of chemical measurements, clearly an effort should be made to better quantify the source strength at the treatment plants. This may entail sampling the source continuously for several weeks prior to a sampling trip. In addition, quantification of bromoform in power plant cooling water effluents is necessary to enable one to use this compound as an effective tracer.

Finally, and perhaps most importantly, future calibrations must be based on many measurements made throughout the computational domain. Hence, the tracer experiments must consist of numerous observations (perhaps 50 to 100) made synoptically, near the source, in the backwater regions of the harbor, and well offshore into Massachusetts Bay.

REFERENCES

Baptista, A.M. 1984. "The Solution of the 2-D Unsteady, Convective Diffusion Equation by the Combined Use of the FE Method and the Method of Characteristics." S.M. Thesis, Department of Civil Engineering, Massachusetts Institute of Technology.

Baptista, A.M., E.E. Adams, and K.D. Stolzenbach. 1984. "The Solution of the 2-D Unsteady Convection Diffusion Equation by the Combined Use of the FE Method and the Method of Characteristics," presented at the 5th International Conference on Finite Elements in Water Resources, University of Vermont, June 1984.

Baptista, A.M. 1985. Personal communication, Massachusetts Institute of Technology.

Battelle. 1982. "Analysis of Organohalogen and Other Organic Chemicals in Cooling Waters Discharged From Redondo Generating Station." Research Report Prepared for Southern California Edison Company. Battelle Pacific Northwest Laboratories, Richland, Washington.

Blanchard, D.C. and A.H. Woodcock. 1957. "Bubble Formation and Modification in the Sea and its Meterological Significance," Tellus, Vol. 9, 145-158.

Bowden, K.F. and R.E. Lewis. 1973. "Dispersion in Flow From a Continuous Source at Sea." Water Research, Vol. 7, 1705-1722.

Broecker, H.C., J. Petermann, and W. Siems. 1978. "The Influence of Wind on CO_2 Exchange in a Wind-Wave Tunnel, Including the Effects of Monolayers," J. Marine Res., Vol. 36, 595-610.

Broecker, H.C. and W. Siems. 1984. "The Role of Bubbles for Gas Transfer From Water to Air at Higher Windspeeds. Experiments in the Wind-Wave Facility in Hamburg." In Gas Transfer at Water Surfaces (eds. W. Brutsaert and G.H. Jirka), pp. 229-236. D. Reidel, Dordrecht, Holland.

Broecker, W.S. and T.H. Peng. 1974. "Gas Exchange Rates Between Air and Sea," Tellus, Vol. 26, 21-35.

Broecker, W.S. and T.H. Peng. 1984. "Gas Exchange Measurements in Natural Systems." In Gas Transfer at Water Surfaces (eds. W. Brutsaert and G.H. Jirka), pp. 479-493. D. Reidel, Dordrecht, Holland.

Brutsaert, W. and G.H. Jirka, eds. 1985. Gas Transfer at Water Surfaces. D. Reidel, Dordrecht, Holland.

Cheng, T.C. and V. Casulli. 1982. "On Lagrangian Residual Currents With Applications in South San Francisco Bay, California," Water Resouces Res., Vol. 18, No. 6, 1652-1662.

Chiou, C. T. and V.H. Freed. 1977. "Chemodynamic Studies on Bench Mark Industrial Chemicals." Report No. NSF/RA-770286, National Science Foundation, Washington, D.C

Christodoulou, G.C., J.J. Connor, and B.R. Pearce. 1976. "Mathematical Modeling of Dispersion in Stratified Waters." Report No. 219, R.M. Parsons Laboratory For Water Resources and Hydrodynamics, MIT, Cambridge, MA.

Connor, J.J. and J.D. Wang. 1973. "Mathematical Models of the Massachusetts Bay, Part I: Finite Element Modeling of Two-Dimensioal Hydrodynamic Circulation." Report No. 172, R.M. Parsons Laboratory for Water Resources and Hydrodynamics, MIT, Cambridge, MA.

Daily, J.W. and D.R.F. Harleman. 1966. Fluid Dynamics. Addison Wesley, Reading, MA.

Danckwerts, P.V. 1970. Gas-Liquid Reactions. McGraw-Hill, New York.

Deacon, E.L. 1977. "Gas Transfer to and Across an Air-Water Interface," Tellus, Vol. 29, 363-374.

Dronkers, J.J. 1964. Tidal Computations in Rivers and Coastal Waters. North Holland Publ. Co., Amsterdam.

Duran, A.P. and H.F. Hemond. 1984. "Dichlorodifluoromethane (Freon-12) as a Tracer for Nitrous Oxide Release From a Nitrogen-Enriched River." In Gas Transfer at Water Surfaces (eds. W. Brutsaert and G.H. Jirka), pp. 421-429. D. Reidel, Dordrecht, Holland.

Dyrssen, D. and E. Fogelquist. 1981. "Bromoform Concentrations of the Arctic Ocean in the Svalbard Area," Oceanol. Acta, Vol. 4, No. 3, 313-317.

EG&G. 1984a. "Oceanographic Study of Various Outfall Siting Options for the Deer Island Treatment Plant." Prepared for Havens & Emerson/Parsons Brinckerhoff, Boston, MA.

EG&G. 1984b. "Data Summary and Documentation for Field Studies in Boston Harbor, June through October, 1983." Prepared for Havens & Emerson/Parsons Brinckerhoff, Boston, MA.

Emerson, S. 1975. "Gas Exchange Rates in Small Canadian Shield Lakes," Limnol. Oceanog., Vol. 20, No. 5, 754-761.

Ewing, B.R., E.S. Chian, and J.C. Cook. 1977. "Monitoring to Detect Previously Unrecognized Pollutants in Surface Waters." Report No. EPA-560-6-77-015, U.S. Environmental Protection Agency, Washington, D.C.

Gould, J.P., L.E. Fitchhorn and E. Urheim. 1983. "Formation of Brominated Trihalomethanes: Extent and Kinetics." In Water Chlorination - Environmental Impact and Health Effects, Vol. 4 (ed. R.L. Jolley et al.), pp. 297-310. Ann Arbor Publ., Inc., Ann Arbor, MI.

Gschwend, P.M., J.K. MacFarlane, and K.A. Newman. 1985. "Volatile Halogenated Organic Compounds Released to Seawater from Temperate Marine Macroalgae," Science, Vol. 227, 1033-1035.

Gurol, M.D., A. Wowk, S. Myers, and I.H. Suffet. 1983. "Kinetics and Mechanism of Haloform Formation: Chloroform Formation from Trichloroacetone." In Water Chlorination - Environmental Impact and Health Effects, Vol. 4 (ed. R.L. Jolley et al.), pp. 269-283. Ann Arbor Publ., Inc., Ann Arbor, MI.

Harleman, D.R.F. 1980. "Transport Processes in Water Quality Control." Class Notes, R.M. Parsons Laboratory for Water Resources and Hydrodynamics, MIT, Cambridge, MA.

Hansch, C. and A.J. Leo. 1979. Substituent Constants for Correlation Analysis in Chemistry and Biology. John Wiley, New York.

Hasse, L. and P.S. Liss. 1980. "Gas Exchange Across the Air-Sea Interface," Tellus, Vol. 32, 470-481.

Hayduck, W. and H. Laudie. 1974. "Prediction of Diffusion Coefficients for Non-Electrolytes in Dilute Aqueous Solution," Am. Ind. Chem. Eng. J., Vol. 20, 611-615.

Helz, G.R. 1980. "Anthropogenic C_1 and C_2 Halocarbons: Potential Applications as Coastal Water-Mass Tracers." In Hydrocarbons and Halogenated Hydrocarbons in the Aquatic Environment (eds. B.K. Afghan and D. MacKay), pp. 435-443. Plenum Press, New York.

Helz, G.R. and R.Y. Hsu. 1978. "Volatile Chloro- and Bromocarbons in Coastal Waters," Limnol. Oceanog., Vol. 23, No. 5, 858-869.

Helz, G.R., R.Y. Hsu and R.M. Block. 1978. "Bromoform Production by Oxidative Biocides in Marine Waters." In Ozone/Chlorine Dioxide Oxidation Products of Organic Materials (eds. R.G. Rice and J.A. Cotruvo), pp. 68-76. International Ozone Institute, Inc.

Hesslein, R., W.S. Broecker, P.D. Quay and D.W. Schinder. 1980. "Whole Lake Radiocarbon Experiment in an Oligotrophic Lake at the Experimental Lakes Area, Northwestern Ontario," Canadian J. Fish. Aquatic Sci., Vol. 37, 454-463.

Higbie, R. 1935. "The Rate of Absorption of a Pure Gas into a Still Liquid During Short Periods of Exposure," Trans. A. I. Ch. E., Vol 35, 365-389.

Hsu, Y.H.L., P.A. Hwang, and J. Wu. 1984. "Bubbles Produced by Breaking Wind Waves." In Gas Transfer at Water Surfaces (eds. W. Brutsaert and G.H. Jirka), pp. 221-227. D. Reidel, Dordrecht, Holland.

Huang, J.C.K. 1971. "Eddy Diffusivity in Lake Michigan," J. Geophys. Res., Vol. 76, No. 33, 8147-8152.

Hunter-Smith, R.J., P.W. Balls, and P.S. Liss. 1983. "Henry's Law Constants and the Air-Sea Exchange of Various Low Molecular Weight Halocarbon Gases," Tellus, Vol. 35B, 170-176.

Hydroscience, Inc. 1971. "Development of Water Quality Models of Boston Harbor." Prepared for the Massachusetts Water Resources Commission, Boston, MA.

Hydroscience, Inc. 1973. "Development of Hydrodynamic and Time Variable Water Quality Models of Boston Harbor." Prepared for the Massachusetts Water Resources Commission, Boston, MA.

Jahne, B., K.O. Munnich, and V. Siegenthaler,. 1979. "Gas Exchange and Momentum Transfer in a Circular Wind-Water Tunnel," Tellus, Vol. 31, 321-329.

Jahne, B., W. Huber, A. Dutzi, T. Wais and J. Ilmberger. 1984a. "Wind/Wave-Tunnel Experiment on the Schmidt Number and Wave Field Dependence of Air-Water Exchange." In Gas Transfer at Water Surfaces (eds. W. Brutsaert and G.H. Jirka), pp. 303-309. D. Reidel, Dordrecht, Holland.

Jahne, B., T. Wais, and M. Barabas. 1984b. "A New Optical Bubble Measuring Device; a Simple Model for Bubble Contribution to Gas Exhange." In Gas Transfer at Water Surfaces (eds. W. Brutsaert and G.H. Jirka), pp. 237-246. D. Reidel, Dordrecht, Holland.

Johnson, B.D. and R.C. Cooke. 1979. "Bubble Populations and Spectra in Coastal Waters: A Photographic Approach," J. Geophys. Res., Vol. 84, 3761-3766.

Jolley, R.L., ed. 1978. Water Chlorination - Environmental Impact and Health Effects, Vol. 1. Ann Arbor Publ., Inc., Ann Arbor, MI.

Jolley, R.L. et al., eds. 1978. Water Chlorination - Environmental Impact and Health Effects, Vol. 2. Ann Arbor Publ., Inc., Ann Arbor, MI.

Jolley, R.L. et al., eds. 1980. Water Chlorination - Environmental Impact and Health Effects, Vol. 3. Ann Arbor Publ., Inc., Ann Arbor, MI.

Jolley, R.L. et al., eds. 1983. Water Chlorination - Environmental Impact and Health Effects, Vol. 4. Ann Arbor Publ., Inc., Ann Arbor, MI.

Kaltofen, M. and J. Lax. 1985. "Report on Toxic Discharges into Boston Harbor and Tributaries." Greenpeace New England, Cambridge, MA.

Kanwisher, J. 1963. "On the Exchange of Gases Between the Atmosphere and the Sea," Deep Sea Res., Vol. 10, 195-207.

Kavanaugh, M., A. Trussel, and J. Cromer. 1978. "Empirical Kinetic Model of Trihalomethane (THM) Formation: Applications to Meet the Proposed THM Standard." Proceedings of the American Water Works Association's 98th Annual Conference, June 1978.

Kerman, B.R. 1984. "A Model of Interfacial Gas Transfer for a Well-Roughened Sea." In Gas Transfer at Water Surfaces (eds. W. Brutsaert and G.H. Jirka), pp. 311-320. D. Reidel, Dordrecht, Holland.

Ketchum, D.H. 1951a. "The Flushing of Tidal Estuaries," Sewage and Industrial Waste, Vol. 23, 189-209.

Ketchum, D.H. 1951b. "The Exchanges of Fresh and Salt Waters in Tidal Estuaries," J. Marine Res., Vol. 10, 18-37.

Kolovayev, D.A. 1976. "Investigation of the Concentration and Statistical Size Distribution of Wind-Produced Bubbles in the Near-Surface Ocean," Oceanology, Engl. Transl., Vol. 15, 659-661.

Kossik, R.F. et al. 1986. "Users Manual For ELA, a Two-Dimensional Eulerian-Lagrangian Transport Model." In preparation. R.M. Parsons Laboratory for Water Resources and Hydrodynamics, MIT, Cambridge, MA.

Ledwell, J.R. 1980. "Gas Exchange Across the Air-Water Interface." Ph.D. Thesis, Harvard Unviersity.

Leimkuhler, W. 1974. "A Two-Dimensional Finite Element Dispersion Model." S.M. Thesis, Department of Civil Engineering, Massachusetts Institute of Technology.

Lewis, W.K. and W.C. Whitman. 1924. "Principles of Gas Absorption," Ind. Eng. Chem., Vol. 17, 1215-1220.

Liss, P.S. 1973. "Processes of Gas Exchange Across the Air-Sea Interface," Deep Sea Res., Vol. 20, 221-238.

Liss, P.S., P.W. Balls, F.N. Martinelli, and M. Coantic. 1981. "The Effect of Evaporation and Condensation on Gas Transfer Across an Air-Water Interface," Oceanol. Acta., Vol. 4, 129-138.

Liss, P.S. and P.G. Slater. 1974. "Flux of Gases Across the Air-Sea Interface," Nature, Vol. 247, 181-184.

Mackay, D. and W.Y. Shiu. 1981. "A Critical Review of Henry's Law Constants for Chemicals of Environmental Interest," J. Phys. Chem. Ref. Data, Vol. 10, 1175-1199

Mackay, D. and T.K. Yeun. 1983. "Mass Transfer Coefficient Correlations for Volatilization of Organic Solutes From Water," Environ. Sci. Technol., Vol. 17, No. 4, 211-217.

Medwin, H. 1977. "In Situ Acoustic Measurements of Microbubbles at Sea," J. Geophys. Res., Vol. 82, 971-975.

Memery, L. and Merlivat, L. 1984. "Contribution of Bubbles to Gas Transfer Across an Air-Water Interface." In Gas Transfer at Water Surfaces (eds. W. Brutsaert and G.H. Jirka), pp. 247-253. D. Reidel, Dordrecht, Holland.

Merlivat, L. and Memery, L. 1983. "Gas Exchange Across an Air-Water Interface: Experimental Results and Modeling of Bubble Contribution to Transfer," J. Geophys. Res., Vol. 88, 707-724.

Metcalf & Eddy, Inc. 1979a. Wastewater Engineering: Treatment, Disposal, Reuse. McGraw-Hill, New York.

Metcalf & Eddy, Inc. 1979b. "Application for Modification of Secondary Treatment Requirements for its Deer Island and Nut Island Effluent Discharges into Marine Waters." Prepared for the Metropolitan District Commission, Boston, MA.

Metcalf & Eddy, Inc. 1982. "Report on the Nut Island Wastewater Treatment Plant Facilities Planning Project: Phase I, Site Options Study." Prepared for the Metropolitan District Commission, Boston, MA.

Metcalf & Eddy, Inc. 1984. "Application for a Waiver of Secondary Treatment for the Nut Island and Deer Island Treatment Plants." Prepared for the Metropolitan District Commission, Boston, MA.

Minear, R.A. and J.C. Bird. 1980. "Trihalomethanes: Impact of Bromide Ion Concentration on Yield, Species Distribution, Rate of Formation and Influence of Other Variables." In Water Chlorination - Environmental Impact and Health Effects, Vol. 3, (eds. R.J. Jolley et al.), pp. 151-160. Ann Arbor Publ., Inc., Ann Arbor, MI.

Monahan, E.C. and M.C. Spillane. 1984. "The Role of Oceanic Whitecaps in Air-Sea Gas Exchange." In Gas Transfer at Water Surfaces (eds W. Brutsaert and G.H. Jirka), pp. 495-503. D. Reidel, Dordrecht, Holland.

Morris, J.C. 1978. "The Chemistry of Aqueous Chlorine in Relation to Water Chlorination." In Water Chlorination - Environmental Impact and Health Effects, Vol. 1 (ed. R.J. Jolley), pp. 21-33. Ann Arbor Publ., Inc., Ann Arbor, MI.

Morris, J.C. and B. Baum. 1978. "Precursors and Mechanisms of Haloform Formation in the Chlorination of Water Supplies." In Water Chlorination - Environmental Impact and Health Effects, Vol. 2 (eds. R.J. Jolley et al.), pp. 29-48. Ann Arbor Publ., Inc., Ann Arbor, MI.

Murthy, C.R. 1974. "Simulated Outfall Diffussion Experiments in Coastal Currents of a Lake," Water Research, Vol. 8, 961-967.

NAS. 1978. "Chloroform, Carbon Tetrachloride and Other Halomethanes: an Environmental Assessment." National Academy of Sciences, Washington, D.C.

Nelson, N. and B. Van Durren. 1975. "Final Report of NSF Workshop Panel to Select Organic Compounds Hazardous to the Environment." New York University Medical Center, New York.

Nicholson, B.C., B.P. Maguire, and D.B. Bursill. 1984. "Henry's Law Constants for the Trihalomethanes: Effects of Water Composition and Temperature," _Environ. Sci. Technol._, Vol. 18, 518-521.

NOAA. 1974. _Boston Harbor Tidal Current Charts._ U.S. Dept. of Commerce, Washington, D.C.

NOAA. 1984. _Tide Tables 1985 - East Coast of North and South America._ U.S. Dept. of Commerce, Washington, D.C.

O'Connor, D.J. 1984. "Turbulent Transfer Across Smooth and Rough Surfaces." In _Gas Transfer at Water Surfaces_ (eds. W. Brutsaert and G.H. Jirka), pp. 321-331. D. Reidel, Dordrecht, Holland.

Oliver, B.C. 1980. "Effect of Temperature, pH, and Bromide Concentration on the Trihalomethane Reaction of Chlorine with Aquatic Humic Material." In _Water Chlorination - Environmental Impact and Health Effects, Vol. 3._ (eds R.J. Jolley et al.), pp. 141-149. Ann Arbor Publ., Inc., Ann Arbor, MI.

Pagenkopf, J.R., G.C. Christodoulou, B.R. Pearce, and J.J. Connor. 1976. "Circulation and Dispersion Studies at the Pilgrim Nuclear Power Station, Rocky Point, Mass." Report No. 210, R.M. Parsons Laboratory for Water Resources and Hydrodynamics, MIT, Cambridge, MA.

Pearson, C.R. and G. McConnell. 1975. "Chlorinated C_1 and C_2 Hydrocarbons in the Marine Environment," _Proc. R. Soc. Lond. B._, Vol. 189, 305-332.

Peng, T.H., T. Takahashi, and W.S. Broecker. 1974. "Surface Radon Measurements in the North Pacific Ocean Station Papa." _J. Geophys. Res._ Vol. 79, 1772-1780.

Peng, T.H., W.S. Broecker, G.G. Mathieu, and Y.H. Li. 1979. "Radon Evasion Rates in the Atlantic and Pacific Oceans as Determined during the GEOSECS Progam," _J. Geophys. Res._, Vol. 84, 2471-2486.

Rook, J. 1974. "Formation of Haloforms During Chlorination of Natural Waters," _Water Treatment Exam._, Vol. 23, 234.

Rook, J. 1975. "Formation and Occurrence of Haloforms in Drinking Water." Proceedings of the American Water Works Association's 95th Annual Conference, June 1975.

Rook, J. 1977. "Chlorination Reactions of Fulvic Acids in Natural Waters," _Environ. Sci. Technol._, Vol. 11, No. 5, 478-482.

Schwarzenbach, R.P., E. Molnar-Kubica, W. Giger, and S.G. Wakeham. 1979. "Distribution, Residence Time, and Fluxes of Tetrachloroethylene and 1,4-Dichlorobenzene in Lake Zurich, Switzerland," Environ. Sci. Technol., Vol. 13, No. 11, 1367-1373.

Sittig, M. 1979. Hazardous and Toxic Effects of Industrial Chemicals. Noyes Data Corp., Park Ridge, N.J.

Stewart, R.E., H.D. Putnam, R.H. Jones, and T.N. Lee. 1971. "Diffusion of Sewage Effluent From Ocean Outfall," J. San. Eng. Div., ASCE, Vol. 97, No. SA4, 485-503.

Verschueren., K. 1977. Handbook of Environmental Data on Organic Chemicals. Van Nostrand Reinhold Co., New York.

Wang, J.D. and J.J. Connor. 1975. "Mathematical Modeling of Near Coastal Circulation." Report No. 200, R.M. Parsons Laboratory for Water Resources and Hydrodynamics, MIT, Cambridge, MA.

Weast, R.C., ed. 1975. CRC Handbook of Chemistry and Physics. CRC Press, Cleveland, Ohio.

Westerink, J.J. 1984a. "A Frequency Domain Model for Tidal Circulation." Ph.D. Thesis, Department of Civil Engineering, Massachusetts Institute of Technology.

Westerink, J.J. 1984b. Personal communication, Massachusetts Institute of Technology.

Westerink, J.J., et al. 1984. "Users Manual for TEA-LINEAR, a Linearized Harmonic Finite Element Circulation Model." Report No. 84-012, MIT Energy Laboratory, Cambridge, MA.

Westerink, J.J., K.D. Stolzenbach and J.J. Connor. 1985. "A Frequency Domain Finite Element Model for Tidal Circulation." Report No. 85-006. MIT Energy Laboratory, Cambridge, MA.

Whittemore, R.C. and J.S. Hovis. 1984. "An Assessment of the Radiotracer Technique For Measuring Reaeration Rates in Large River Systems." In Gas Transfer at Water Surfaces (eds. W. Brutsaert and G.H. Jirka), pp. 431-436. D. Reidel, Dordrecht, Holland.

Witting, J. 1971. "Effects of Plane Progressive Irrotational Wave on the Thermal Boundary Layers," J. Fluid Mech., Vol. 50, 311-334.

Wolff, C.J.M. and H.B. van der Heijde. 1982. "A Model to Assess the Rate of Evaporation of Chemical Compounds from Surface Waters," Chemosphere, Vol. 11, No. 2, 103-117.

APPENDIX I

SOURCE REPRESENTATION IN A NUMERICAL TRANSPORT MODEL

E. Eric Adams, Richard Kossik, and A. Melo Baptista

SOURCE REPRESENTATION IN A NUMERICAL TRANSPORT MODEL

E. Eric Adams, Richard Kossik, and A. Melo Baptista

Dept. of Civil Engineering, Massachusetts Institute of Technology
Cambridge, Massachusetts, USA

INTRODUCTION

Numerical models are routinely used to solve the advection diffusion equation for purposes of simulating pollutant transport in surface waters. A common difficulty in most such applications is to adequately represent concentrations in regions of high concentration gradient. For surface water calculations, strong gradients are found primarily near sources (e.g., pollutant outfalls).

One procedure for handling such problems is to represent the continuous plume near the source as the superposition of discrete puffs that are advected forward in time until they are of sufficient size to be adequately resolved with the numerical grid. Such a procedure is well suited to Lagrangian Transport Models or Eulerian-Lagrangian models in which the advection part of the advection-diffusion equation is simulated by a (Lagrangian) tracking technique.

This approach has been incorporated into the 2-D (depth-averaged) transport model ELA (Baptista et al., 1984a, b). ELA uses a split operator approach solving advection with a backwards method of characteristics using quadratic Lagrange polynomials for interpolation and using an implicit Galerkin Finite Element method for diffusion. Transformation processes such as volatilization are treated separately in a third operation. The technique is illustrated in a simulation of halocarbon concentration distributions resulting from sewage discharges into Boston Harbor.

PROBLEM DESCRIPTION

Figure 1 illustrates a typical problem involving an outfall pipe discharging into a coastal environment discretized with a relatively uniform grid. For purposes of discussion, the near field is defined as that region over which discharge momentum and buoyancy significantly influence local flow patterns. For a typical sewage outfall this dimension may be of order 10-100 m and no attempt is made to resolve concentrations within this region. However, it is desired to simulate realistic distributions as close to the near field as possible.

Theoretical analyses (e.g., Fourier analysis) and numerical experiments by a number of researchers have shown that the ability to successfully advect a pollutant source improves as the dimensionless source size (i.e., characteristic source size divided by characteristic grid dimension) increases. The minimum acceptable source size will depend on the numerical procedure and such parameters as Peclet and Courant number and total simulation time, but will fall in the general range of 3 to 10 (Gray and Pinder, 1976; Baptista et al., 1985). This criterion is not met, in general, for typical grid sizes of order 100-1000 m. As a result, artificial

diffusion is introduced, either by the scheme itself, or by the model user who artificially introduces the mass over a larger-than-realistic region. In effect, the concentration distribution becomes artificially and instantaneously spread until it is wide enough to be advected satisfactorily. The result is erroneous prediction over an intermediate region at least as large as that required for physical processes to provide similar mixing. For tidal applications, this intermediate region can easily extend for a distance of one tidal excursion or more. For regions of strong tidal currents such as Boston Harbor, this can represent several kilometers or a significant fraction of the computational domain.

Figure 1 suggests three possible procedures for improving resolution up to the point at which physical processes have spread the pollutant enough to be resolved (i.e., the intermediate field): a) local grid refinement, b) stochastic particle tracking, and c) use of puffs.

With finite element models, grid refinement is conceptually straight-forward. However, when the affected area is substantial, and multiple sources are involved, matrix size and bandwidth may increase substantially resulting in a significant increase in computational cost.

Particle tracking has been proposed as a way to resolve strong concentration gradients in Eulerian-Lagrangian models of groundwater transport (Newman, 1984). Using this approach, particles would be released at a rate corresponding to their effluent concentrations and advected by the known flow field. Diffusion can be handled by assigning a random or pseudo velocity component to the advected flow. The process is continued until the particles have diffused over sufficient elements that a smooth concentration field can be computed for subsequent discretized calculation. A major drawback with this approach is that, in order to accurately convert particle density to concentration, a large number of particles must be tracked in relation to the number of grid points.

A third option involves the use of puffs as suggested by Adams et al. (1975) and used by Holly and Usseglio-Polatera (1984). In such an approach, the intermediate field plume is represented by a number of discrete puffs, released one at a time, with a size proportional to the near field mixing zone. As with particles, each puff is tracked forward in time. However, dispersion is handled by dispersing the puffs in accordance with a prescribed dispersion law, e.g., as determined by a tracer study or as estimated from the literature (Okubo, 1971). In contrast with particles, this may involve as little as one tracking per unit of time thus reducing costs. As illustrated below, the present approach is really a hybrid, using up to five trackings per puff in order to better define puff spreading. Nonetheless, the savings should still be substantial.

DETAILS

Figure 2 illustrates, schematically, puff placement for the simple case of a constant current. The elapsed time depicted is $T = N\Delta t$ where Δt is the basic computational time step between alternate advection and diffusion calculations with ELA. ($\Delta t = 3.1$ hours is used in the following calculations.)

Assume $M\Delta t$ is the minimum duration required for the puffs to mature to full size. ($M = 1$ has been used in our calculations.) As indicated by the

overlapping circular distributions, puffs are placed around the source corresponding to mass which is physically discharged during the period $(N-M-1)\Delta t < \tau < N\Delta t$. The most recently discharged mass is positioned first (adjacent to the source) and subsequent puffs are created to allow sufficient overlap.

Puffs created during the period of duration Δt from $(N-M-1)\Delta t < \tau < (N-M)\Delta t$ are mapped onto the finite element grid at the beginning of the advection step. Younger puffs, created between $(N-M)\Delta t < \tau < N\Delta t$, are discarded unless a concentration printout is desired, in which case they are mapped onto a highly resolved local grid created only for contouring.

For the illustrative calculations below, symmetrical Gaussian puffs have been used implying isotropic dispersion. (However, different distributions could readily be used.) For each puff, the concentration distribution is thus

$$C = \frac{\dot{m}(t)\Delta\tau}{2\pi h\ \sigma^2}\ \exp\{-[(x-x_i)^2 + (y-y_i)^2]/2\sigma^2\} \tag{1}$$

where h is the local depth, $\dot{m}$ is the mass loading rate, $\Delta\tau$ is the time interval associated with the puff (see Figure 2), (x_i, y_i) is the center of mass, and σ is the standard deviation. Puff centers are tracked forward in time by reversing the fourth-order Runge-Kutta integration scheme used by ELA in the backward tracking of characteristics, along with the known space and time dependent variation in current speed. Thus

$$x_i(T) = x_0 + \int_\tau^T u\ dt$$

$$\tag{2}$$

$$y_i(T) = y_0 + \int_\tau^T v\ dt$$

In principle, puff spreading can be computed from a relationship such as

$$\sigma^2(T) = \sigma_0^2(\tau) + 2\int_\tau^T D\ dt \tag{3}$$

where E is an empirical (dispersion) coefficient and σ_0 is the initial standard deviation at the edge of the near field. σ_0 is determined from the near field mixing as

$$\sigma_0 = \frac{SQ_0}{\sqrt{12}\ |u|\ h} \tag{4}$$

where Q_0 = effluent flow rate, $|u|$ = instantaneous current speed, and S = near field volumetric dilution (determined from measurements or a model as a function of $|u|$ and h).

In a depth-integrated model, D represents physical mixing (dispersion associated with horizontal and vertical current shear as well as turbulent diffusion) plus fluid convergence/divergence effects associated with changing bottom and free surface elevation. Hence D would be expected to change with spatial position and time.

To help separate these effects, and render the intermediate field spreading of puffs similar to the far field mixing handled by finite element, an equivalent "diffusionless" puff distribution at time T can be computed by tracking $n - 1$ additional particles. These particles are distributed initially at a distance of σ_0 from the source center (x_0, y_0) and are tracked along with the puff center. The equivalent σ is then approximated as the geometric mean of the distances between particles i and the center of mass:

$$\sigma^2 = \prod_{i=2}^{n} [(x_i - x_1)^2 + (y_i - y_1)^2]^{1/(n-1)}$$

(5)

If puffs are to be tracked over a long period of time, Equations (5) and (3) can be used sequentially over a number of time steps, with the first term on the right-hand side of Equation (3) taken to be the last value of σ^2 from Equation (5). It is apparent that the major difference between this hybrid method and one using exclusively particles (i.e., Figure 2b) is the way in which diffusion is calculated.

APPLICATION

The above technique has been used to simulate the fate of treated sewage effluent discharged into Boston Harbor on the western shore of Massachusetts Bay. Boston Harbor has approximate mean width and depth of 10 km and 10 m, and is characterized by numerous islands and complicated bottom topography. Flow is primarily tidally driven with mean amplitude of about 1.4 m.

Figure 3 sketches the finite element grids that are used. The largest grid (Figure 3a) includes 888 triangular elements with linear basis functions used to compute circulation with the harmonic circulation model TEA (Westerink et al., 1985). Transport calculations are made with the inner grid (Figure 3b) comprised of triangles with quadratic interpolation functions used for the finite element (diffusion) calculations and for the interpolation component of the advection calculations. The two major effluent sources are indicated (as black dots) on Figure 3b: the Deer Island Treatment Plant (to the north) and the Nut Island Treatment plant (to the south) discharging respectively 18.4 m^3/s and 5.9 m^3/s.

Field measurements indicate that near field dilution is a strong function of tidal phase obeying the following approximate relations:

$S = 50.5|u| + 6.5$ (Deer Is.)

$S = 31.7|u| + 5.5$ (Nut Is.)

(6)

where $|u|$ is in m/s. For the Deer Is. outfall, $|u|$ varies from about 0.07 to 0.61 m/s between slack tide and maximum flood resulting in almost a factor of four variation in dilution ($10 < S < 37$). For Nut Is., $0.04 < |u| < 0.25$ m/s resulting in a factor of two variation in dilution ($7 < S < 13$).

Figure 4 illustrates computed concentration contours for the compound 1,1,1-trichloroethane, an industrial solvent discharged through both outfalls at a concentration of approximately 6.7 ppb. Simulations are shown at high tide under conditions of periodic steady-state due to M_2 tidal forcing (period = 12.4 hours), no wind stress (resulting in minimal residual circulation), an ambient diffusion coefficient of 10 m^2/s, and a piston velocity of 10 cm/hr describing volatilization. Measurements of halocarbon concentrations have also been taken in the harbor and substantiate the 2-D assumption. Parallel efforts are now under way aimed at a) model validation, b) establishing the viability of halocarbons as sewage tracers, and c) exploring the process of volatilization by comparing the geochemical fractionation of several related compounds both discharged and measured simultaneously. However, for present purposes, Figure 4 is presented to illustrate the sensitivity of predicted concentrations to the source representation. In particular, note the area of high concentrations west of the discharge from Deer Island and southwest of the discharge from Nut Island. These high concentrations represent effluent that was discharged during low tide when near field dilution is low and that has been advected toward shore during flood tide. Preliminary field measurements have confirmed this phenomenon. Figure 5a depicts corresponding high tide concentrations resulting from only the puffs released near the Deer Island outfall during the most recent 6.2 hours ($M = 1$, $\Delta t = 3.1$ hours) and Figure 5b shows the local grid. The factor of approximately 2.5 between concentrations at the western and eastern edges of the plume (representing discharge at low and high tide respectively) and those in the center (representing discharge during flood tide) is apparent.

The above calculations were made with a time step of 3.1 hours or one-fourth of a tidal period. As such, substantial computational savings were possible by saving, for each of the four tidal phases, both 1) the feet of the characteristic lines emanating backwards from each grid point necessary for computing far field concentration and 2) the intermediate field puff statistics ($\Delta \tau$, x_1, y_1, σ). Using this procedure it is estimated that the CPU time required for a two-week simulation (27 tidal cycles and the approximate time required to reach periodic steady state) is about two times that required for a single tidal cycle. While more accurate calculations would use additional tidal components, with longer repeating intervals, it is likely in many instances that transport calculations would still be required for multiple cycles, hence justifying the storage.

CONCLUSIONS

The above description and application illustrate how puffs can be used efficiently to provide increased resolution near effluent sources in pollutant transport models. Outfall configurations, model parameters (e.g., diffusion coefficients), and puff representation have been kept simple for illustration, but more sophistication can be employed if desired and warranted by available data.

REFERENCES

Adams, E. E.; Stolzenbach, K. D.; and Harleman, D. R. F. (1975) Near and Far Field Analysis of Buoyant Surface Discharges into Large Bodies of Water. Report No. 205, R. M. Parsons Laboratory for Water Resources and Hydrodynamics, M.I.T., Cambridge, Mass.

Baptista, A.; Adams, E. E.; and Stolzenbach, K. D. (1984a) Eulerian-Lagrangian Analysis of Pollutant Transport in Shallow Water. Report No. 296, R. M. Parsons Laboratory for Water Resources and Hydrodynamics, M.I.T., Cambridge, Mass.

Baptista, A. M.; Adams, E. E., and Stolzenbach, K. D. (1984b) The 2-D Unsteady Transport Equation Solved by the Combined Use of the Finite Element Method and the Method of Characteristics. Proc. 5th Int'l Conf. on Finite Elements in Water Resources, U. of Vermont, Burlington, Vt.

Baptista, A. M.; Adams, E. E.; and Stolzenbach, K. D. (1985) Comparison of Several Eulerian-Lagrangian Models to Solve the Advection-Diffusion Equation. Proc. 2nd Int'l Symp. on Refined Flow Modeling and Turbulence Measurements, U. of Iowa, Iowa City, Iowa.

Gray, W. G.; and Pinder, G. F. (1976) An Analysis of the Numerical Solution of the Transport Equation. Water Resources Research, 12:547-555.

Holly, F. M., Jr.; and Usseglio-Polatera, J.-M. (1984) Dispersion Simulation in Two-Dimensional Tidal Flow. Journal of Hydraulic Engineering, 110:905-926.

Neuman, S. P. (1984) Adaptive Eulerian-Lagrangian Finite Element Method for Advection-Dispersion. Int'l Journal for Numerical Methods in Engineering, 20:321-337.

Okubo, A. (1971) Oceanic Diffusion Diagrams. Deep Sea Research, 18:789-802.

Westerink, J. J.; Stolzenbach, K. D.; and Connor, J. J. (1985) A Frequency Domain Finite Element Model for Tidal Circulation. Report No. MIT-EL 85-006, M.I.T. Energy Laboratory, Cambridge, Mass.
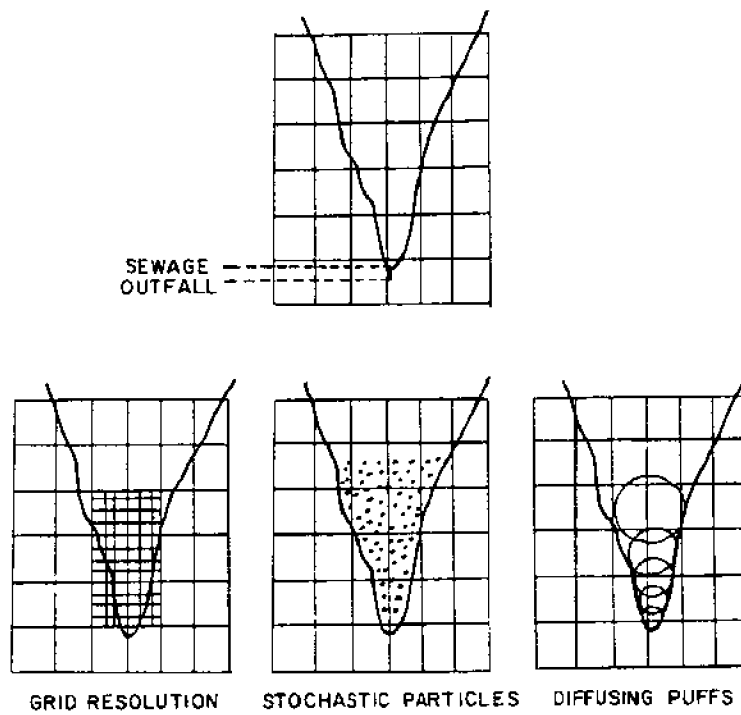
Figure 1. Techniques to Improve Near Source Resolution
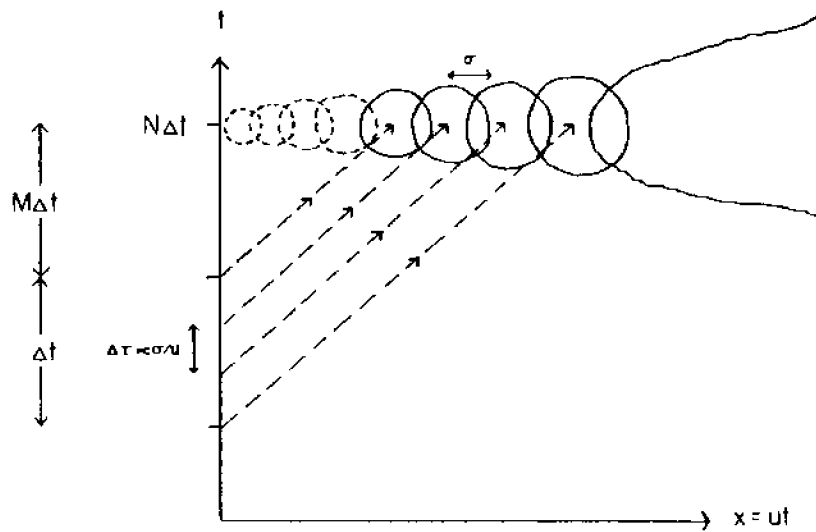
Figure 2. Schematic of Puff Placement
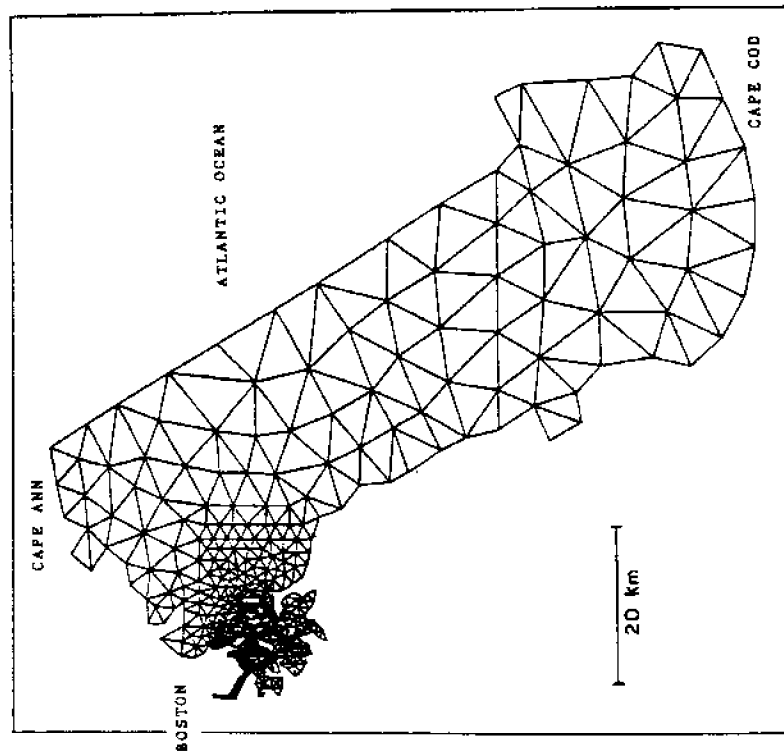
Figure 3a. Finite Element Grid
of Massachusetts Bay
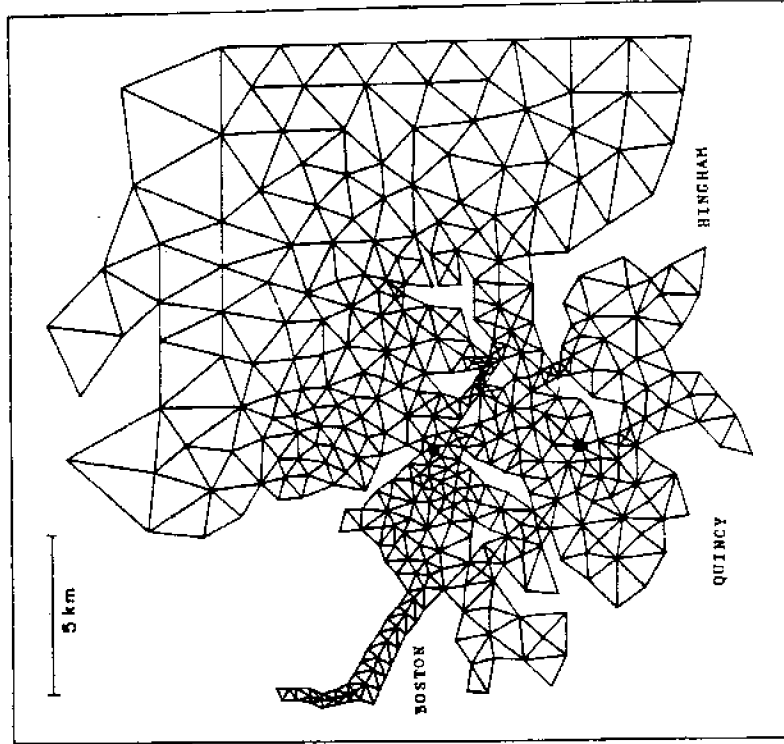
Figure 3b. Finite Element Grid –
Detail of Boston Harbor
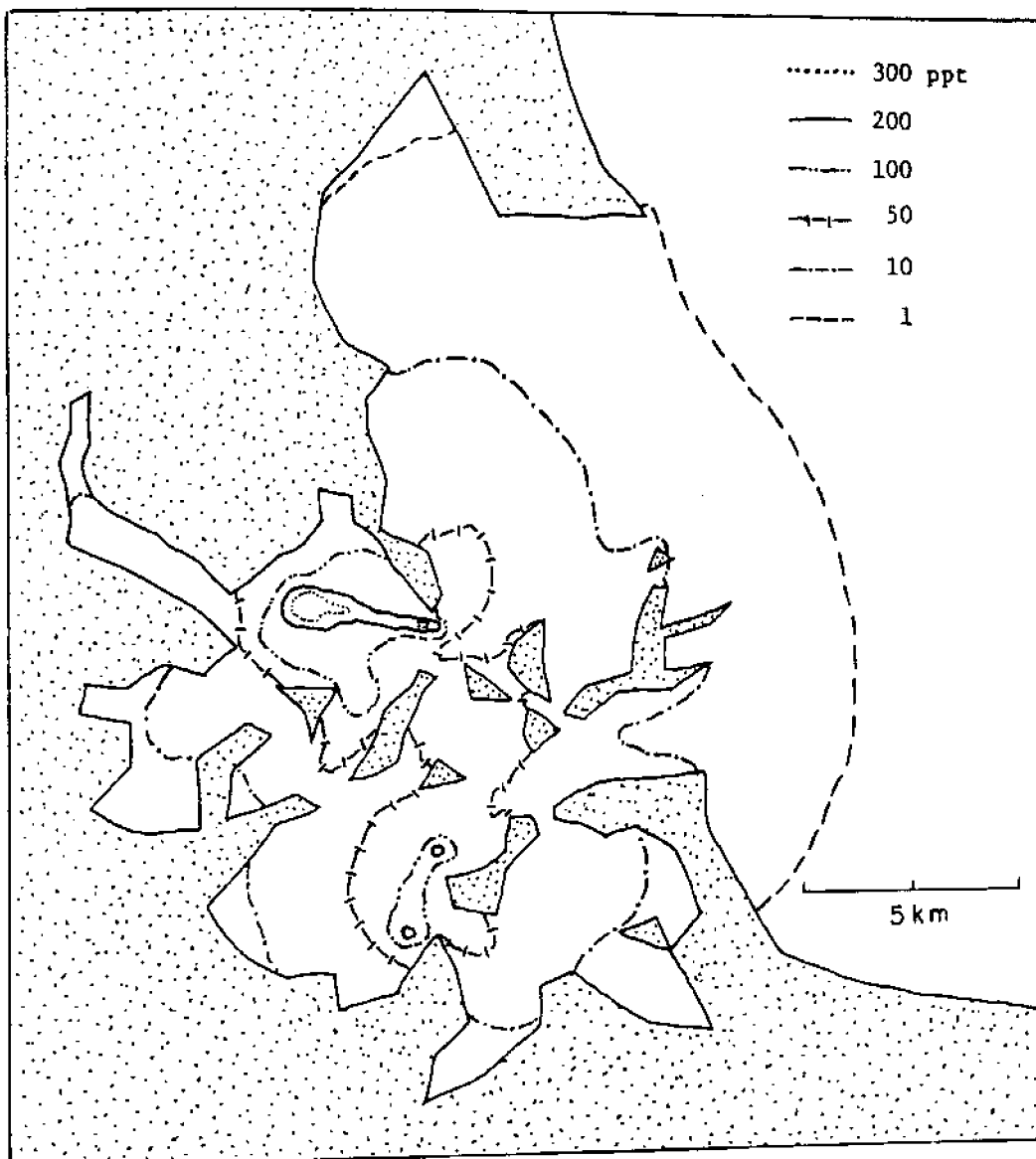
Figure 4. Simulated Intermediate and Far Field Concentration Distribution at High Tide for $Q_0 = 24.7$ m^3/sec, $C_0 = 6.7$ pbb, $k = 10$ cm/hr, and $D = 10$ m^2/sec

Figure 5a. Simulated Intermediate Field Concentration Distribution
at High Tide (Elapsed Time = 6 hrs) Corresponding to
Conditions of Figure 4

Figure 5b. Detail of Grid Within Border Shown in Figure 5a

APPENDIX II

MEASUREMENTS OF VHOCs IN SEWAGE EFFLUENT

CONCENTRATION (PARTS PER BILLION)*

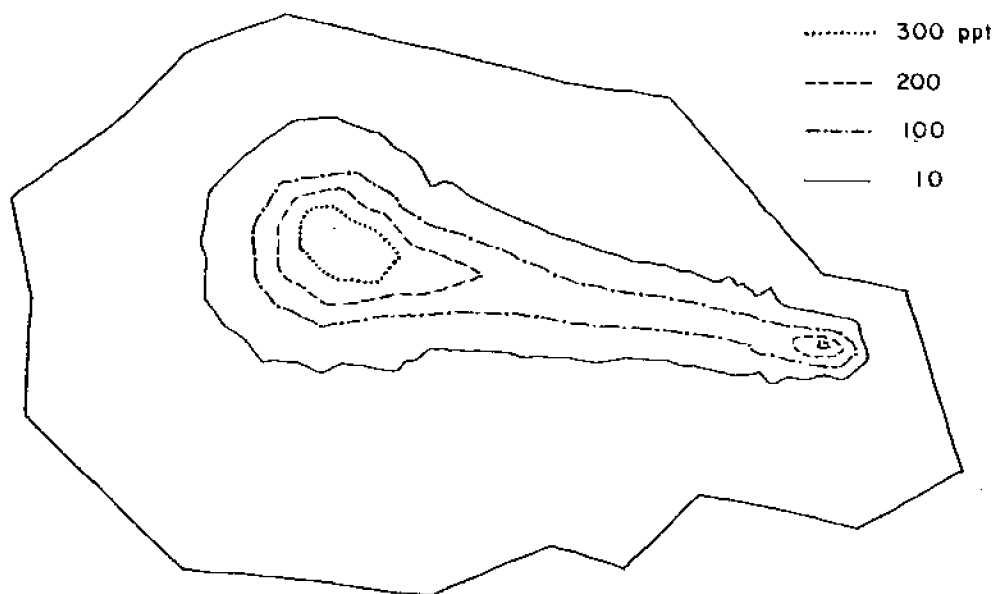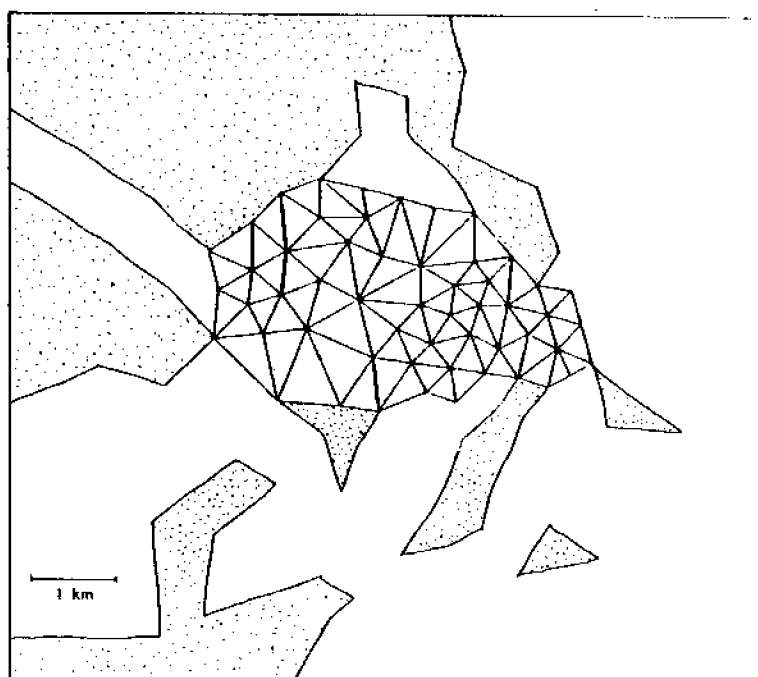| DATE/TIME		CH_3CCl_3	$CHCl=CCl_2$	$CHCl_2Br$	$CHClBr_2$	$CCl_2=CCl_2$	$CHBr_3$	flow rate (m³/sec)
1984								
8-16	10:00 AM	7.23	6.74	2.01	1.32	3.01	0.46	9.7
9-26	8:00 AM	6.37±.11	3.06±.10	2.71±.10	3.26±.11	2.96±.02	1.71±.11	12.3
9-26	9:00 AM	7.84±.21	2.91±0	1.70±.09	2.00±.13	2.91±0	1.12±.08	10.6
10-29	9:00 AM	10.08±.45	6.83±.09	6.78±.07	5.51±.18	6.92±.12	1.76±0	13.2
10-30	9:00 AM	17.79±.60	9.44±.52	3.86±.11	1.49±.07	11.26±.44	0.29±.07	11.0
1985								
4-24	10:35 AM	18.55±.12	13.85±.81	2.71±.06	2.91±0	27.03	1.36±.06	12.1
4-25	7:25 AM	15.00±1.32	11.78±1.47	2.71±.36	1.59±.23	25.20±2.59	0.24±.08	10.1
4-25	8:10 AM	15.76±.24	18.80±.33	3.14±.06	2.33±0	30.81±.52	0.79±0	11.0
4-25	9:00 AM	14.92±0	20.41±.65	2.61±0	2.50±0	26.18±.86	1.18±.02	10.6
4-25	10:00 AM	15.68±.84	16.04±.98	2.08±0	2.09±.12	25.81	0.96±.02	11.0
4-25	11:00 AM	16.44±.72	13.97±.98	2.10±.10	1.88±.06	22.64±1.38	0.53±.06	15.4
6-7	10:10 AM	17.12±.77	14.30±0	3.97±.96	3.40±.61	20.95±.49	1.86±.18	10.6
6-7	10:40 AM	16.16±1.75	13.39±1.80	3.41±.36	2.58±.27	19.76±2.76	1.13±.18	11.4
6-13	6:25 AM	14.68±.84	8.23±.33	6.77±.09	4.21±.07	18.86±1.07	1.13±0	7.0
6-13	6:40 AM	13.99±1.34	7.38±.86	5.81±.41	3.61±.27	17.59±2.15	0.83±.13	7.0
6-13	6:55 AM	15.45±2.40	9.56±2.57	7.24±1.61	4.46±1.18	21.13±3.50	1.32±.54	7.0
6-13	7:10 AM	16.32±.24	10.05±.17	7.07±.17	4.46±.13	21.76±.17	1.32±0	7.0
6-13	7:25 AM	13.73±1.95	6.65±2.57	4.92±.84	2.96±.52	16.83±3.90	0.54±.27	7.5
6-17	7:50 AM	6.71±0	6.52±.08	4.31±.12	2.80±.08	18.56±.74	ND	15.0
6-17	8:10 AM	8.85	7.35	4.26	2.43	20.33	ND	15.0
6-17	8:30 AM	6.81±.89	7.64±.17	3.97±.40	2.36±.07	18.55	ND	14.5
6-17	8:50 AM	6.66±0	6.96±.19	4.59±.20	2.43±.16	20.85±.32	ND	14.1
6-17	9:10 AM	8.67±.18	6.82±.17	4.83±.09	2.72±.28	21.69±.08	ND	14.1
6-17	9:30 AM	11.94±.57	6.00±.40	5.07±.22	2.34±.18	20.31±.93	ND	14.5
6-17	9:50 AM	7.55±.40	3.37±.21	3.67±.23	1.99±.04	13.24±.37	ND	15.0

* effluent concentrations at Deer Island; mean and standard deviation of duplicates

CONCENTRATION (PARTS PER BILLION)

DATE/TIME	CH₃CCl₃	CHCl=CCl₂	CHCl₂Br	CHClBr₂	CCl₂=CCl₂	CHBr₃	flow rate (m³/sec)
6-17 10:10 AM	8.21±.38	4.21±.38	2.91±.39	1.07±.14	16.84±.89	ND	15.0
6-17 10:30 AM	7.33±.87	4.18±.68	2.53±.36	0.81±.07	16.45±2.57	ND	15.4
6-17 10:50 AM	6.41±.42	4.36±.23	2.39±.09	0.80±0	16.97±.52	ND	15.8
6-17 11:10 AM	6.19±.05	4.36±.35	2.81±.37	1.27±.07	16.49±1.70	ND	15.8
6-24 9:40 AM	7.31±.09	5.84±.27	3.14±.04	1.59±.02	6.62±.36	0.07±0	10.8
6-24 10:00 AM	7.45±.42	5.37±.20	3.26±.09	1.97±.16	6.38±.02	0.39±.03	10.6
6-24 10:30 AM	6.31	5.23	3.06	2.74	6.12	0.80	10.8
6-24 11:00 AM	6.21±.14	5.12±.22	3.44±.04	2.81±.10	6.08±.77	1.17±.07	11.0
6-24 11:30 AM	5.60	5.23	2.78	2.17	9.97	0.52	11.2
6-24 12:00 PM	5.76±.31	5.07±.57	1.10±.16	0.71±.11	14.10±.36	ND	11.4
6-24 12:30 PM	5.73±.47	5.14±.12	1.12±.28	0.30±.09	18.40±1.70	ND	11.7
6-24 1:00 PM	6.22±.02	5.20±.03	0.96±.04	0.20±.07	16.20±.19	ND	11.9
7-2 6:00 AM	4.90±.26	6.18±.31	9.01	7.21±12	11.02±1.07	3.18±.14	7.9
7-2 6:30 AM	6.64±0	6.77±.18	8.04±.07	6.86±.08	10.01±.09	3.17±0	7.9
7-2 7:00 AM	8.04±.26	6.89±0	8.74±.38	7.43±.08	10.27±.40	3.33±.08	7.9
7-2 7:30 AM	7.51±.22	7.03±.20	7.69±.12	6.63±.10	9.96±.43	3.22±.09	9.2
7-2 8:00 AM	7.22±.20	7.17±.01	7.68±.19	6.81±.37	9.03±.49	3.47±.26	10.6
7-2 8:52 AM	6.24±.30	6.89±.38	6.99±.04	6.24±.09	8.89±.08	3.22±.26	9.7
7-2 9:00 AM	6.45±.25	7.46±.03	6.96±.61	5.72±.62	9.27±.35	2.91±.34	9.7
7-2 9:30 AM	6.68±.20	7.45±.38	6.64±.49	5.66±.53	9.81±.35	2.60±.60	9.7
7-2 10:00 AM	6.77±.07	7.95±.24	6.57±.66	4.27±.16	10.30±.47	1.47±.14	9.7
7-2 10:30 AM	6.87±.08	8.70±.05	5.57±.08	3.43±.02	10.30±.05	1.07±.03	11.4
8-28 10:00 AM	28.50±.20	18.53±.42	2.13±.18	0.77±.08	10.30±.33	0.31±.02	11.9
8-29 10:00 AM	16.46±.79	7.76±.62	2.41±.24	1.47±.21	14.66±1.21	0.54±.06	11.4
8-30 10:00 AM	13.87±.63	6.81±.54	5.78±.18	4.84±.21	8.61±.10	2.00±.27	10.6
8-31 10:00 AM	10.58±.86	5.12±.77	5.51±.66	3.01±.63	19.92	0.62±.04	13.2
9-1 10:00 AM	4.38±.29	5.18±.35	10.33±.42	12.16±.63	11.96±.69	6.88±.37	9.2
9-2 10:00 AM	3.73±.08	6.20±0	8.10±.12	8.82±.21	7.16±.18	4.69±.28	9.7
9-3 10:00 AM	4.86±.21	5.59±0	5.08±.07	4.93±.14	5.81±.18	2.56±.31	10.6